Approche multi-échelle de la formation des particules secondaires

Julien Boulon

UNIVERSITÉ BLAISE PASCAL
CLERMONT-FERRAND

GRADUATE SCHOOL OF FUNDAMENTAL SCIENCES

PhD. Thesis

in partial fulfillment of the requirements for the degree of

Doctor of Philosophy

of the Université Blaise Pascal

Speciality: Atmospheric Physics

Submitted and presented by

Julien Boulon

Multi-scale approach of the atmospheric new secondary particle formation

defended the 20th of september 2011

PhD. Committee:

Chair:	Pr. Alfons Schwarzenboeck, LaMP CNRS, Clermont-Ferrand
PhD. Examinators:	Pr. Markku Kulmala, University of Helsinki
	Dr. Ernest Weingartner, Paul Scherrer Institut, Villigen
PhD. Reviewers:	Pr. Stephane Alfaro, LISA, CNRS, Paris
	Dr. Abdelwahid Mellouki, ICARE CNRS, Orléans
PhD. Supervisors:	Dr. Karine Sellegri, LaMP CNRS, Clermont-Ferrand
	Pr. Paolo Laj, LGGE CNRS, Grenoble.

Acknowledgements

First of all... STOP !!

Maintenant, place à ma langue maternelle. Déjà que personne ne va plus loin que ces quelques pages... En plus, ça permettra à ma famille de lire au moins une de mes productions sans utiliser de dictionnaire ou *"Google translate"*...

LES PRÉLUDES

Eh bien ça y est ! L'heure est à la gratitude et à la rédaction de la partie la plus lue d'une thèse. Section parfois larmoyante mais souvent d'un intérêt ethnologique majeur pour le futur thésard préparant son entrée dans un laboratoire, la célèbre rubrique des "Re...".

Par où commencer... Ce qui a rendu cette épopée possible... Une recherche internet : plutôt vague et un peu impersonnelle. Retour en 2008, cité mondiale du vin, Bordeaux. Première rencontre avec un de mes directeurs de thèse : Paolo Laj. Quelques slides des travaux d'Hervé Venzac, futur collègue et initiateur au traitement des données instrumentales. Ça parle d'Everest et de feux rouges, de pollution et de particules. Je repars convaincu, une encyclopédie sous le bras droit et un aspirateur dans l'autre : il est fort ce Paolo. Savoir donner autant d'entrain et de sympathie en moins de cinq minutes n'est pas donné à tout le monde, c'est une des nombreuses (je présume) qualités de Monsieur Laj.

Le marketing à l'italienne ayant fait son œuvre, deuxième rendez-vous. Cette fois c'est à Toulouse durant les AEI Météo France que je rencontre Karine, celle qui allait encadrer jour après jour ce travail. J'aurai l'occasion de parler d'elle plus tard.

L'INTRODUCTION

Une thèse c'est aussi l'entrée dans un nouveau laboratoire avec ses acteurs, ses traditions et son histoire. Ici ce sont les acteurs auxquels je pense. Les premiers sont ceux qui m'ont permis d'atterrir sereinement dans le bureau 8220 du bâtiment B8, j'ai nommé Wolfram Wobrock et Andrea Flossmann. Sans eux cet atterrissage n'aurait pu s'être fait dans de si bonnes conditions. Pour ça ils méritent entièrement leur place dans cet étalage aux souvenirs "avec sourire en coin". Si leur consentement fut pour moi le deuxième top départ de cette course de fond doctorale, mes collègues et amis du laboratoire ont construit cette course, l'ont nourrit jour après jour. Dans un premier lieu, les "anciens" pas tant par l'age – je mets un point d'honneur à confirmer ma nature de sage devant ces jeunes freluquets – mais parce que maintenant on les appelle "Dr." : Hervé, Vincent et Guillaume. Entre deux vannes sur Matlab, Python et autres "geekeries", ils leur arrivaient de ne pas parler de football et c'est dans ces moments-là que leur humanité me permettait de me sentir soutenu au sein d'une équipe. C'est une

composante essentielle du bonheur que j'ai pu éprouver durant les premiers mois de ce travail et leur contribution est loin d'être négligeable. Aussi par ce texte, qu'ils trouvent l'expression de mon amitié et de ma sincère gratitude.

DÉCORS & ANALYSE FAUNISTIQUE

Comprendre ici le décor comme l'ensemble des éléments formant un cadre à l'action de la thèse. Ces éléments peuvent donc être organiques ou inorganiques.

Le "8220" a petit à petit été colonisé par la "nouvelle vague", je veux dire la nouvelle génération dont je fais partie. Nous nous sommes rapidement approprié l'espace : Boris à ma gauche un peu en arrière, Emmanuel juste en face de moi avec à sa droite Maxime lui-même à gauche de Boris. Ces deux derniers étant orientés au Nord, perpendiculairement à mon orientation qui, vous l'aurez deviné se situe sur l'axe Est-Ouest. Cet îlot constitue la zone masculine de bureau. Dans le coin fenêtre opposé au mien, la sage Elise poursuit son travail.
En dehors de ce hâvre, le laboratoire est peuplé d'autres gens (il paraît même qu'il y a un autre bâtiment !), des gens qui ont un poste, souvent, un post-doc, parfois. Ces gens sont doués de compétences dont le thésard est dépourvu. Alors ces gens, d'une patience remarquable, nous aident pour ainsi dire tout le temps. Pour ma part, cette aide s'est étendue du relevé de données à la réparation d'instruments sauvages, des questionnements intimes sur la nature de la chimie aux bases de l'electronique, en passant par la réponse à ma question favorite : "Dans quel sens on tourne pour dévisser déjà ?". Quelle patience ! Tout ces gens, David, Mickaël, Jean-Marc, Christophe, Aurélie, Lætitia, Christian, Cécile (sans qui mes nombreuses missions du Mt. Fuji à San Francisco n'auraient pus être possibles), lui, elle et aussi les autres, j'espère bien pouvoir vous rendre la pareille. Sachez que sans vous je serais peut-être mort électrocuté vingt fois ou de désespoir à force de visser sans fin, que de nombreuses données et résultats n'auraient pu émerger de mon ordinateur et que le plaisir que j'ai eu à travailler ici n'aurait pas pu être aussi complet. Votre présence et votre accueil à chacune de mes apparitions en chaussettes dans votre bureau resteront bien gravés dans mon expérience de thésard. J'espère que ces quelques mots vous feront comprendre que je vous exprime, à ma manière et encore en chaussettes, ma plus profonde reconaissance. Il y a aussi mes amis "sportifs" et festifs. Comment les oublier ? Nous avons tellement souffert ensemble, gladiateur du soccer en lutte pour la survie. Les décompressions amicales qu'ils m'ont offertes ont largement contribuées à mon équilibre durant ces trois ans. Une heure de soccer contre deux heures de bla-bla et de glou-glou. Je garderai un souvenir ému de mes nombreuses victoires (et pan ! ici j'ai le dernier mot !!). Alors Olivier, Fred, Yahya, Guillaume et tous les autres, je vous dis "bien joué !" et on peut dire que ce que vous m'avez apporté, c'est une belle victoire (une fois n'est pas coutume...).

LES CERISES

Chaque partie du tout est essentielle dans une thèse. La forme impacte directement sur le fond. Aussi certaines personnes ont occupé une place tout à fait spéciale durant ces trois années. Bien sûr mes amis, mes bons vieux potes qui à l'occasion d'un coup de fil, d'un mariage, d'une naissance ou je ne sais quels autres évènements ont toujours su me témoigner un soutient inconditionnel moral quand je venais m'étendre sur leurs épaules comme un vison mort autour du coup d'une bourgeoise du XIX^{e} siècle. Quand je venais m'étendre disais-je, pour leurs raconter mes doutes et mes peurs laissant de côté la science car qui comprend quelque chose à la nucléation de nos jours. Ces amis-là, j'ai la chance d'en avoir et je souhaite qu'ils trouvent ici une embrassade chaleureuse et émue. Alors Seb, Hugues, Panda, Jérémy, Paco ne vous déplaise vous devez lire cette thèse pour comprendre à quel point vous m'avez été essentiels pour en arriver à bout. Mais il n'y a pas que les vieux de la vieille. Cette expérience clermontoise m'a aussi donnée l'occasion de rencontrer des gens exceptionnels qui par leur présence au quotidien m'ont permis de surmonter mes échecs et de continuer d'avancer. Boris, Élodie, Laura, Marie, Antoine, Yaurick, Baptiste, mon barman André, mes colocs' Gab (le maraicher du temps libre) et Seb (l'exquis, le chercheur du bon), je vous adresse sur ces pages l'expression de mes bières distinguées et me permets de vous dire que vous comptez beaucoup pour moi. J'espère que l'avenir viendra consolider notre amitié et que le chemin parcouru ne sera qu'enrichi par nos échanges.

Maintenant vient le temps des caractères spéciaux.

En trois ans, elle n'a pas montré un seul signe de faiblesse. Elle n'a rien lâché. Toujours présente, les week-ends, le soir, le matin, le jour, en vacances, en congés maternité, en mission. Bref, toujours. Sa patience et sa constance, sa bonne humeur et sa sympathie ainsi que son imbattable volonté pour fêter nos articles ont fait que rien au monde n'aurait pu se substituer à elle dans l'accomplissement de ce travail. Vous l'aurez deviné, il s'agit de ma directrice de thèse, Karine. Si j'ai pu apprendre quoi que ce soit sur l'aérosol durant ces trois ans, c'est grâce à toi et à la pédagogie dont tu as fait preuve pour m'expliquer les fondamentaux et développements de cette science que tu affectionnes. J'espère exprimer ici l'estime profonde que j'ai à ton égard.

Enfin, il y a ma famille. Incroyable, unique, d'une richesse sans pareil. Ma soeur et Jérémy évidemment, et bien sûr Igor le petit filou, dernier né du clan. Tout les trois vous avez toujours répondu présent quand je débarquais chez vous avec un petit sac contenant une brosse à dents, parfois, mon ordinateur, tout le temps, et de l'aspirine pour faire face aux soirées bordelaises. Par chance Igor tu ne lis pas encore l'anglais mais mon heure viendra... Puis dans une famille il y a les parents. Et c'est à mes parents que je dédie ce manuscrit, bien maigre compensation au regard de ce que vous m'avez

apporté durant ces 30 ans. Malgré les difficultés à me fixer, je passe les 50 sports que j'ai dû essayer dans ma jeunesse ainsi que les études à rallonges ("Je serai virologue"... "Je serai paléo-antropologue"... "Je serai medecin"... "Je serai physicien"... Bon je serai étudiant quoi !), votre soutient n'a jamais fait défaut. Nous en avons traversé des choses et sachez, vous deux, que notre relation constitue ma plus grande fierté.

Il faut bien s'arrêter. Alors je termine par un clin d'œil à cette fille que j'ai "croisé", "recroisé" durant ces cinq dernières années. Une affaire de trajectoire donc. Une trajectoire de Bordeaux au Middle West. Minneapolis. Affaire à suivre.

P.S.: Je ne l'ai pas dit, na !

Contents

Chapter 1

Introduction

Contents

Aerosols, although not always named as such, have been the subject of many researches for centuries. To all aerosol scientists, the investigations of J. Aitken on condensation nuclei in the 1880s, are well known. But in the early seventeenth century, Rafinesque (1819) already postulated that "dusty particles may be formed in the great chemical laboratory of our atmosphere". Both Aitken and Rafinesque used the term "dust" for aerosol particles. But this nomenclature is even much older: in 1666, the french astronomer Adrien Auzout argued in a discussion to Abbe Charles in the scientific journal "Le Journal des Savants" (Auzout, 1666) that the bigger telescopes are not much better than the small ones since "[...] they magnify the vapors, the dust, and the other small objects, of which the air is always full. [...]". Besides being a completely correct statement this shows that the scientists even more than 300 years ago i- were aware of the existence of aerosol particles and ii- they had at least some information on their effects. But it still was a long way to go to systematic aerosol research. In this introductory chapter, I will present the birth and the evolution of aerosol sciences, contemporary issues and future directions of this very active research field of atmospheric sciences.

1.1 A brief history of aerosol science

1.1.1 The first considerations

Atmospheric aerosol science history is closely related to air pollution issues. The existence of unpleasant and harmful particles in outdoor and indoor atmospheres was mentioned in the very early literature. For example, the Romans complained of the foul air in ancient Rome. Serious particulate air pollution led to the prohibition of coal burning in London in 1273, followed by a Royal Proclamation by Edward I in 1306 which definitely banned coal burning in England. In 1661, John Evelyn submitted the first major tract regarding particulate air pollution to Charles II. Despite those preoccupations, the birth of aerosol science and aerosol measurement methodology did not occur until the second half of the nineteenth century.

Atmospheric aerosol science (i.e. the explanations of the origin, pattern and properties of atmospheric particulate matter) has emerged in a theoretically point of view in the age of Enlightenment ($1700 - 1800$) in parallel with the rapid growth natural sciences in general. The main issue addressed by the pioneers of modern atmospheric aerosol science was the origin of atmospheric aerosols. Theories on the origin of regional atmospheric aerosols could be grouped into six categories: busts of vapor emission from the Earth during earthquakes, formation from electrical discharges during thunderstorms, production from meteoric burns up in the upper atmosphere, volcanic emissions, windblown dust and combustion process (a detailed description of those theories can be found in Husar, 2000). One major paper during this early period is the one from Rafinesque (1819) published in the *American Journal of Science* called "Thoughts on atmospheric dust". In this dissertation, Rafinesque postulated that "Dust exists even on the tops of the highest mountains" and he also states that atmospheric particles are mixed along the whole lower layer of the atmospheric column and intuits the roles of dry and wet removal processes: "It settles slowly in clear weather but is quickly washed down by rain and snow". Furthermore, he also discussed two mechanisms of formation, distinguishing primary and secondary emissions: "Some dust is from the pulverization of road and filed surface" and "A portion is formed chemically in the atmosphere by combination of gases and elementary particles dissolved in air". But all of those assumptions are theoretical and the end of the nineteenth century will be the period of transition from theory-driven to observation-based atmospheric aerosol sciences. The application of simple physico-chemical principles allowed for the consolidation or the rejection of theories. In particular, earthquakes, lightnings and meteoritic origins of atmospheric particles were eliminated as significant contributors.

1.1.2 The experimental period

The first experimental aerosol research efforts were closely associated with initial developments in colloid chemistry (Spurny, 1998). The first observations were made on fine particles dispersed in the atmosphere, and some early experiments were performed in the laboratory. According to McMurry's review (2000), as early as 1841, J. P. Espy built a "nephelescope" with which he was able to observe cloud water formation under laboratory conditions. But he was not aware that condensation occurred on the particles. According

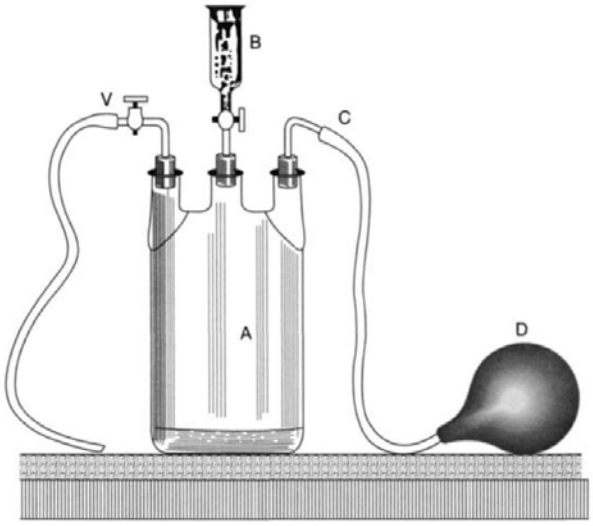

Figure 1.1: Experimental device used by Coulier for the detection of the condensation activity of dust particles. *A. Transparent flask; B. Burette; C. Connection; D. Rubber ball; V. Valve.*

to Podzimek's review (1989), in 1847, H. Becquerel hypothesized about the existence of fine particles in the air, now called *condensation nuclei*. Their existence was confirmed about 30 years later with the experiments of Coulier (1875), who was the first to publish a work showing that when air is expanded adiabatically, condensation occurs more readily in unfiltered air than in filtered air. The apparatus of Coulier was in principle the first condensation nuclei detector (Fig. 1.1). It consisted of a transparent flask (A) with a rubber bulb (D) for compressing the air in the flask. By opening the valve (V) the air could expand and condensation on aerosol particles could occur, which was qualitatively determined by the turbidity within the chamber. The same year Coulier published his results on the condensation activity, John Aitken began his research on condensation. First results were obtained five years later (Aitken, 1880a,b) and then he developed and used the first portable instruments for counting dust particles in the atmosphere (Aitken, 1889, 1891a) which allowed him to published the first paper reporting i- the condensation activity in the real atmosphere and ii- the number concentration of airborne particles in a given environment (Aitken (1888); the original scheme of the first portable *condensation particle counter* is reported figure 1.2). Based on his experiments he concluded: "(1) when water vapor condenses in the atmosphere, it always does so on some solid nucleus; (2) the dust particles in the air form the nuclei on which it condenses; (3) if there was no

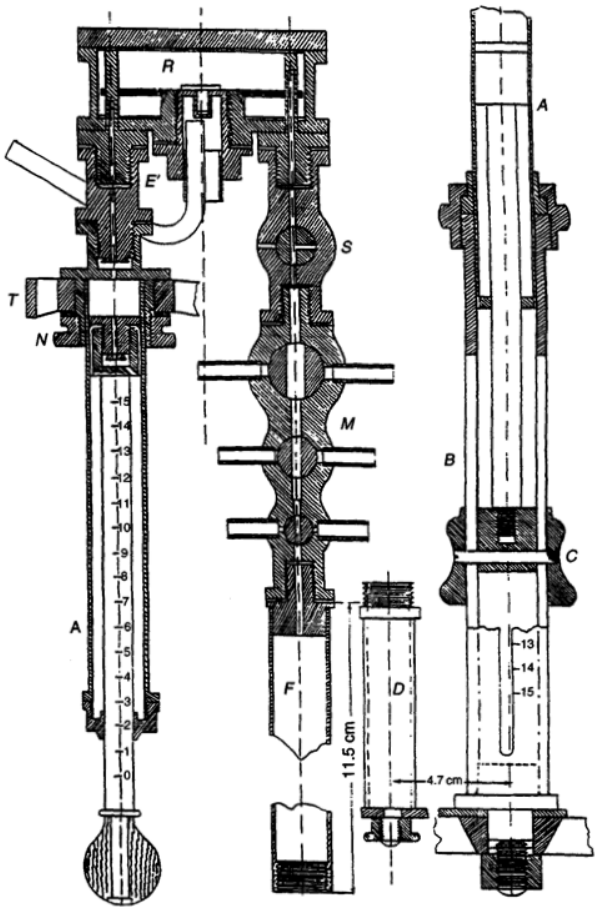

Figure 1.2: Schematic representation of the Aitken portable "dust counter" adapted from Baron and Willeke (2001). *A. Air-pump; B. Receiver; S. Stopcock; M. Apparatus for measuring air to be tested; F. filter; T. Head of tripod; N. nut; B. Metal support; D. End of tube.* The air being tested was drawn through pipe A and passed into receiver R, where it was mixed with a certain quantity of dustless air and saturated with water. The air in R was then expanded by the pump, which produced a shower of rain. The number of drops that fell on a measured area were then counted.

dust in the air there would be no fogs, no clouds, no mists, and probably no rain." Using this new instrument, Aitken provided the first experimental verification of Rafinesque's theories on secondary atmospheric aerosol formation, eighty years later its formulation. In a long series of studies, John Aitken (e.g. Aitken, 1885, 1888, 1891b) has observed that on cloudy days the nuclei count remained low. The nuclei number concentration has increased in proportion to the sunshine. Aitken concluded that "sunshine may produce some change in the (photochemically active) constituents of the atmosphere which gives rise to nuclei formation in saturated air". He also observed that the high nuclei days were not hazy which suggested to him that the nuclei were of "molecular dimensions", below the visible size range. In fact, John Aitken had formulated the precept of the first new particle formation theory. It was more than one hundred years ago.

From the work of Aitken, the aerosol science entered in a new period (the "classical period") characterized by the use and exploitation of measurements and experimental

techniques. The classical period of aerosol science research lasted approximately until the middle of the twentieth century and ended with the publication of *Mechanics of Aerosols* by Fuchs (1964). No lasers, no computers, and no spectroscopic analytical tools were available during this period.

The term *aerosol* was first used at this time and is attributed to the physical chemist E. G. Donnan in about 1918 and then introduced into the meteorological literature in 1920 by A. Schmauss, the director of the Meteorological Central Station in Munich, Germany (see references in Baron and Willeke, 2001). Schmauss worked on the comparison between the colloidal chemical processes and the processes in a cloudy atmosphere and found that those two distinct topics present strong similarities. Hence, by analogy to the term *hydrosol* (from the Greek word combination "water particle") used in atmospheric sciences, he used the term *aerosol* to describe clouds of particles and droplets dispersed in air. The broader development of aerosol measurement methods and equipment occurred after 1900, and primarily after 1920. During this period, the negative health effects of industrial aerosols and dusts were recognized.

1.1.3 The contemporary period: the birth of the climate change preoccupation

In 1965, when the U.S. President Lyndon Johnson asked the members of his President's Science Advisory Committee (PSAC) to report on the potential problems of environmental pollution, climate change was not yet a priority. The polluting effects of detergents and municipal sewage, the chronic problems associated with urban air pollution, and the risks associated with pesticides dominated public discourse about humanity's impact on the environment. However, in a 23-page appendix, which today appears prescient, the committee's Environmental Pollution Panel proposed carefully the following scenario: emissions of carbon dioxide from the burning of fossil fuels could rapidly reshape Earth's climate (see references in Peterson et al., 2008). Using new data, the first up-to-date global temperature reconstructions and carbon dioxide data that Charles David Keeling and his colleagues had been collecting since 1957 on Mauna Loa, Hawaii, and in Antarctica (Pales and Keeling, 1965; Brown and Keeling, 1965), the panel concluded that atmospheric carbon was "clearly and conclusively" rising as a result of fossil fuel burning. From this report, numerous studies and efforts were conducted to characterize the actual and past climates and their changes through the study of physical and chemical properties of the atmosphere including particulate matter in suspension in the atmosphere.

From the publication of the report of the PSAC, the effect of atmospheric aerosols was the subject of strong controversies since it was found that aerosols could have the opposite effect than CO_2: according to the paper of McCormick and Ludwig published in *Science* in 1967 they cool the climate.

In December 1968, a group of scientists convened in Dallas, Texas, for a "Symposium on Global Effects of Environmental Pollution". The goal of this meeting was to analyze the potential impact of an increasing of greenhouse gases and atmospheric aerosols amount on the climatic system. If the warming role of greenhouse gases was clearly established since the work of Pales and Keeling and (Brown and Keeling, 1965), the effect of aerosols on the Earth's radiative balance was unclear. Unfortunately, no satisfying answers were pointed out during this symposium. But the problem was submitted and fed a strong debate during 10 years: what is/are the impact(s) of aerosols on the Earth's radiative balance and the global climate ?

During this period many studies were conducted to answer this fundamental question. Some authors suggest that aerosols, through their radiative properties could cool the climate enough to overtake the warming caused by the greenhouse gases (e.g. Mitchell, 1970; Rasool and Schneider, 1971) but critics quickly pointed out some errors on radiative effect estimations both on aerosols and greenhouse gases (Charlson et al., 1972; Rasool and Schneider, 1972; Schneider and Mass, 1975). Adding to this confusion some authors advanced that aerosols may have a warming effect (Reck, 1975; Idso and Brazel, 1977, 1978). It was Hansen et al. (1978) and his colleagues who found what seemed to be the right balance between the two competing forces by modelling the aerosols emitted during the Mount Agung eruption in Bali in 1963. By 1978, the question of the relative role of aerosol cooling and greenhouse warming had been sorted out. Greenhouse warming, the researchers concluded, had become the dominant forcing (Hansen et al., 1978).

The aerosol cooling effect could be separated into two distinct phenomena. One of the most famous paper of this prolific period was the discovery of Twomey (1974). He found that aerosols, by acting as cloud condensation nuclei, could increase the number of cloud droplets "which will have higher cross-sectional areas typically hundred thousand times that of the nucleating particles". The resulting effect is the formation of numerous cloud droplets which in fact consist, in a way, in "a great magnification of the light scattering power" of the cloud condensation nuclei, leading to an increase of the albedo and thus a global cooling effect. This phenomenon is commonly named the *aerosol indirect effect*. The other component of the cooling effect was found few years later by Charlson et al. in 1991 who showed that sulfate aerosols could have a direct radiative forcing because they scatter and absorb solar and infrared radiation in the atmosphere.

1.1.4 From 1978 to present days: the explosion of organics in climate sciences

From the intensive period that was the 70's, aerosol research efforts started an exponential growth. The need to link aerosol to both chemical and physical processes is clearly

announced in the Prospero et al.'s review in 1983 "[...] our ability to assess these possible impacts [Aerosols impacts on climate but also health, author's note] is constrained by our limited knowledge of the physical and chemical properties of aerosols, both anthropogenic and natural". In his review he also pointed out the necessity to better understand the role of atmospheric condensable vapors such as H_2SO_4 or NH_3 but also organics in aerosol properties and secondary formation. Almost one hundred years after Aitken's pioneer works, the gas-to-particle conversion was re-introduced in the scientific debate. At the end of the 80's, a major event changed definitely the face of atmospheric sciences. Under the supervision of the World Meteorological Organization and the United Nations Environment Program, the *Intergovernmental Panel on Climate Change* (IPCC) was created in 1988 as an effort by the United Nations to provide the governments of the world with a clear scientific view of what is happening to the world's climate. The initial task for the IPCC was "to prepare a comprehensive review and recommendations with respect to the state of knowledge of the science of climate change; social and economic impact of climate change, possible response strategies and elements for inclusion in a possible future international convention on climate" (complete informations and references could be found at `http://www.ipcc.ch/index.htm`). The creation of such international instance led to an increase of the research effort in all environmental sciences and of course in atmospheric and aerosol sciences.
Ten years after the creation of the IPCC, i.e. the creation of a world wide preoccupation, the review on organic atmospheric aerosols made by Jacobson et al. (1998) give the first state-of-the-art of science on organic aerosols. What were at the state of projects in the work of Prospero et al. in 1983, was (partly !) explored fifteen years later and reported in the Jacobson et al.'s review. The main purpose of his review was "[...] not to quantitatively describe the importance of organic aerosols in environmental issues, but rather to present a basis for defining what data are needed." and of course what have been done.
A relevant way to provide some information on environmental and geophysical effects of a given *object* (e.g. a type of aerosol, a particular gas-phase transformation, an integrated process, etc...) could be a bottom-up approach defined as follow:

- To isolate from observations what we consider as the main object and study its properties.
- To quantify the amount of this object in the natural medium and its spatial variability.
- To create/feed a model based either on processes or on empirical data, able to reproduce observations.
- To connect this object to another one and restart the process of study described above.

The object of the Jacobson et al.'s review is defined: the organic aerosol. Properties of such aerosols arisen from isolated research groups looking for specific compounds or class of compounds for specific reasons, e.g. carcinogenic compounds to study human health effects (see for example Brushby et al., 1993) but considering the high diversity of such aerosols, data are still very sparse in 1998.

After this rapid historic introduction to aerosol science, I will present a state-of-the-art of the current knowledge on aerosols, their effect on the global climate and their formation processes.

1.2 Atmospheric aerosols and their role in the "climate factory"

As previously seen, aerosols have a direct radiative effect because they scatter and absorb solar and infrared radiations in the atmosphere. Aerosols also alter the formation and precipitation efficiency of liquid-water, ice and mixed-phase clouds, thereby causing an indirect radiative effect associated with these changes in cloud properties. The quantification of aerosol radiative forcings is more complex than the quantification of radiative forcing by greenhouse gases because aerosol mass and particle number concentrations are highly variable in space and time. This variability is largely due to the much shorter atmospheric lifetime of aerosols compared to greenhouse gases (Fig. 1.3). Spatially and temporally resolved information on the atmospheric burden and radiative properties of aerosols are needed to estimate radiative forcings. Important parameters are size distribution, change in size with relative humidity (i.e. hygroscopic properties) and aerosols chemical properties (related to complex refractive index and solubility).

1.2.1 The direct radiative effect

This effect discovered by Charlson et al. (1991) is based on the absorption-emission processes of the aerosol particle. Knowledge of a set of four quantities as a function of wavelength is necessary to translate aerosol burdens into i- aerosol optical depths, and ii- a radiative perturbation: the mass light-scattering efficiency, the functional dependence of light-scattering on relative humidity, the single-scattering albedo, and the asymmetry parameter (see in Charlson et al., 1992). All of those variables are functions of the chemical properties of the particle. Furthermore, radiative properties can change depending on whether different chemicals are in the same particles (internal mixtures) or different particles (external mixtures). In the last report of the IPCC, the estimation of the total direct radiative forcing due to aerosol particle is -0.50 ± 0.40 W.m^{-2} (IPCC, 2007).

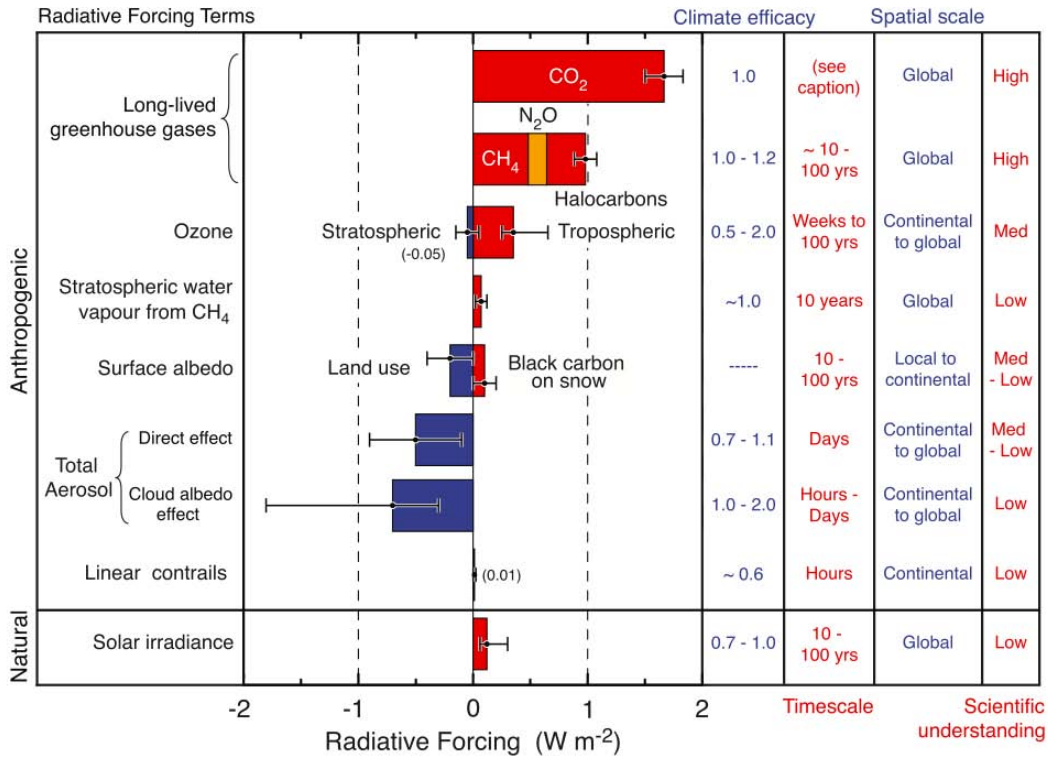

Figure 1.3: Global mean radiative forcings grouped by agent types (from IPCC, 2007). *No* CO_2 *time scale is given, as its removal from the atmosphere involves a range of processes that can span long time scales, and thus cannot be expressed accurately with a narrow range of lifetime values.*

1.2.2 The indirect radiative effect: the aerosol-cloud interactions

Indirect forcing by aerosols is roughly defined as the overall process by which aerosols perturb the Earth-atmosphere radiation balance by modulating the cloud albedo and cloud cover amount. It can be decomposed in a series of processes linking various intermediate variables such as the aerosol mass, the cloud condensation nuclei (CCN) concentration, the ice nuclei (IN) concentration, the water phase partitioning, the cloud optical depth, and many others, which connect emissions of aerosols (or their precursors) to the top of the atmosphere radiative forcing due to clouds.

The effectiveness of an aerosol particle to act as a CCN depends i- on its size and ii- on its hygroscopic properties. This last property is strongly linked to the chemical composition of the particle. CCN activity of insoluble aerosol such as dusts is still not well understood and quantified yet but it has been shown that particles with some water-soluble species contribute significantly for the indirect forcing (e.g. Kulmala et al., 1996; Eichel et al., 1996). However, there are many water-soluble compounds in the atmospheric aerosol with widely varying degrees of solubility. Accumulation mode aerosols, i.e. particles with a diameter between 0.1 and 1 µm, form the majority of CCN. The more the CCN concentration is high, the more cloud droplets are formed. From this phenomenon, two

different but related effects are identified. The first one is that the increase of the cloud droplet number associated to the decrease of their geometric diameter modify the cloud albedo: this is the "first indirect effect" discovered by Twomey (1974). Moreover, as the cloud droplet sizes decrease for a given water vapor amount, the cloud precipitation potential decrease as well. This process, highlighted by Albrecht (1989) and defined as the "second" or "semi-indirect effect", prolongates the cloud lifetime and thus enhances the radiative effect due to the cloud (Twomey, 1974). The last estimation of the indirect radiative effect was found to be between in the range of $[-1.1; +0.4]$ with a mean of -0.70 W.m^{-2} (IPCC, 2007).

Those two radiative effects, direct and indirect, are largely linked to the size of the particle but also to the chemical composition of the aerosol. For example, mineral dusts do not have the same radiative effect than soot. Those latter particles belong to the wide family of the carbonaceous aerosols composed by two main class of materials: the *elemental* carbon which is emitted from the incomplete combustion of fossil fuels and biomass (i.e. soot) and *organic* carbon. The organic class is the most important carbonaceous species in term of abundance but also the class which present the higher diversity in term of compositions and sizes. The impact of the organic composition of particulate matter on its radiative properties is not well documented and given the ubiquity of carbonaceous aerosols, the understanding of the radiative impact of aerosols on climate is certainly incomplete. Understanding how aerosols are formed and how their size and composition evolve in the atmosphere is necessary to better constrain models and thus better simulate their impact on the Earth radiative budget.

1.3 The aerosol sources: primary *versus* secondary

Aerosols result from both natural and anthropogenic sources and several different classifications exist according to either their origin (anthropogenic, biogenic, marine or volcanic), or their production mechanism opposing primary *versus* secondary aerosols. This latter classification seems to be the most appropriate since understanding how particles are formed is understanding from what they are formed which is strongly linked to the origin.

1.3.1 The primary sources

Primary particles are defined as particles that are emitted in the atmosphere directly in a solid or liquid phase. Examples are soot particles produced from uncomplete combustion processes, primary organic aerosols emitted by plant or dust particles generated by the erosion of surface soils by the wind or sea spray issued from wave breaking over the oceans. Primary particles are generated through a momentum transfer thus their emission is

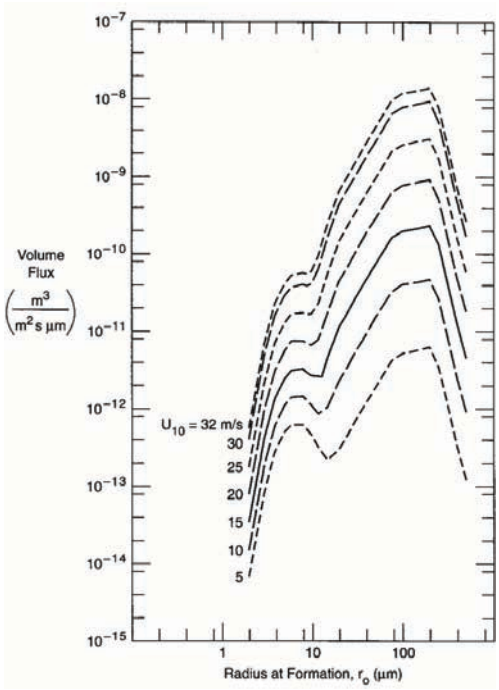

Figure 1.4: A sea spray generation function linking the size distribution of generated particles to the wind speed (from Andreas, 1998).

directly linked to the intensity of this momentum transfer. For example Andreas (1998) have developed a sea-spray generation function which is dependent of the wind speed (Fig. 1.4).

1.3.2 The secondary sources

The secondary particles are generated i- from the conversion of gases to particles and ii- the condensation of gases on pre-existing particles. The first process leads to the formation of new particles thus increasing the total number of particles and the second process leads will increase the mass of the total particle but with number conservation. In the following we will focus on the new particle formation through the nucleation process. Mechanisms which lead to the new secondary particles are complex and different theories are developed in the chapter 2 of this thesis. However, the formation of secondary atmospheric aerosols could be split into two different main steps:

1. The formation of thermodynamically stable "clusters" (i.e. an aggregate of molecules). This first phase is the nucleation phase (Fig. 1.5).

2. The growth of those clusters by i- condensation of organic and/or inorganic vapors and ii- coagulation. (Fig. 1.5).

It is important to note that during the first steps of aerosol growth, condensation and coagulation are antagonist processes. If large particles exist prior the onset of the new particle formation and growth then the vapors will condense on the larger surface

available i.e. on pre-existing particles rather than contribute to the formation and growth of new particles. Knowledge on the exact processes governing atmospheric new particle formation and the vapors participating in them is the key to quantify the global aerosol number source issued from secondary formation.

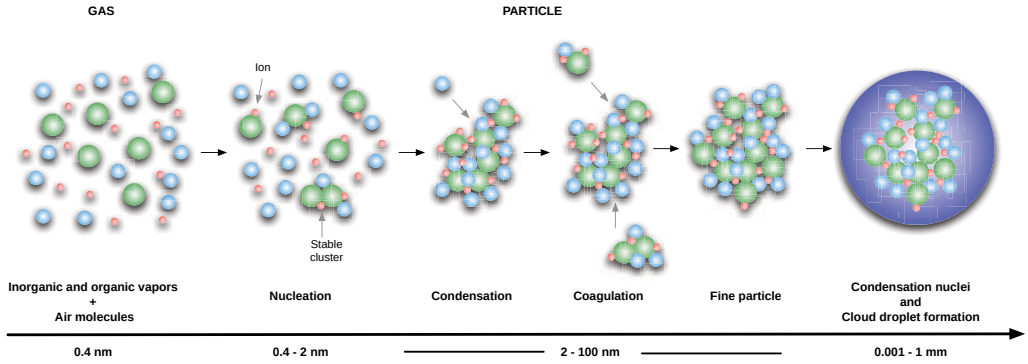

Figure 1.5: Secondary aerosol formation and growth, from nucleation to the cloud droplet formation.

1.4 Aim of this doctoral thesis

One of the actual challenges in aerosol science is to describe accurately how new particles are formed from gaseous precursors. The formation of secondary new particles have now been studied for several decades, but the degree of our knowledge on the theoretical mechanism (gas – particle conversion) is not sufficient to accurately predict where, when and with which intensity new secondary aerosol generation will take place in the atmosphere. New particle formation events have been observed in various environments (see for a review Kulmala et al., 2004b) from polluted area (Hämeri et al., 1996; Harrison et al., 2000; Woo et al., 2001; Stanier et al., 2004; Dunn et al., 2004) to clean or rural sites (Weber et al., 1997; Mäkelä et al., 1997; O'Dowd et al., 1998; Suni et al., 2008), polar areas (Weber et al., 2003; Asmi et al., 2010) and high altitude sites (Weber et al., 1995; Venzac et al., 2007; Shaw, 2007; Nishita et al., 2008; Rodriguez et al., 2009). Most recently, it has been proposed by researcher of our group that nucleation may be promoted at high altitudes (Venzac et al., 2009). This hypothesis was a suggestion based on a few examples of measurements performed simultaneously at different altitudes, but it potentially has important implications for the atmospheric science. Indeed, the vertical extend of nucleation has only been studied episodically during airborne measurements, while models need statistically reliable information on the occurrence of nucleation over the whole atmospheric column. In this thesis, I have analyzed continuous measurements over long time periods (more than a year) for two European high altitude sites (Jungfraujoch, Switzerland, Puy de Dôme France) (see chapter 4). For the puy de Dôme site, two different altitudes were instrumented to test the hypothesis according to

which nucleation is promoted at high altitudes. These studies allowed the investigation of i- the nucleation process in clean environment (frequency, condensable vapors, role of ions...), ii- the vertical extent of the new secondary aerosol formation. Results of this work are reported chapter 4. Furthermore, during the Eyjafjallajokull volcanic crisis, in spring 2010, the volcanic plume was detected at the puy de Dôme research station providing a unique chance to characterized aerosol processes within a volcanic plume. The first observation of a nucleation of new particles in such plume is also reported chapter 4.

In a more process-based approach, some authors investigated the phenomenon under controlled conditions in smog chambers in order to identify key parameters or chemical species involved in the nucleation (Griffin et al., 1999; Koch et al., 2000; Bonn et al., 2002; Bonn and Moortgat, 2002; Rohr et al., 2003; Hao et al., 2009; Metzger et al., 2010; Duplissy et al., 2010). However, the mechanisms involved in the formation of a new particle are numerous, extremely rapid and complex. One major difficulty to understand them is linked to the size of the new particles when they are formed. When nucleation occurs, clusters of the nanometer scale have intermediate properties between gases and particles, and observations are difficult due to instrumental limitation. Hence, the process-based modelling is necessary to test some hypothesis. Many models have been built to simulate the nucleation and growth processes observed in the atmosphere and to predict the climatic impact of such aerosols. The first ones only consider the formation of new sulfuric acid-water droplets under atmospheric conditions (e.g. Kulmala et al., 1995) but authors rapidly improved these models by adding more processes. For example, the AEROFOR model (Pirjola et al., 1999), includes gas-phase chemistry, nucleation (binary homogeneous nucleation of the sulfuric acid-water system), condensation and coagulation growth and dry deposition of large particles. The main limitation of such models is that ions-induced nucleation, ternary and nano-Köhler theories are not taken into account. This gap in the processes representation is filled in by the last generation of models (e.g. Tammet and Kulmala, 2005; Korhonen et al., 2004; Leppä et al., 2009). Consequently, understanding the nucleation process implicates that the first steps of cluster formation and growth are adequately detected. Lately, instruments that allow to detect clusters down to less than 1 nm and to follow their growth to higher sizes were introduced in the aerosol research field. The first one is the *Air Ion Spectrometers* series which allow the detection of atmospheric ions (AIS) and total particles (NAIS) in the mobility range 3.16 to 0.0013 $cm^2.V^{-1}.s^{-1}$ (See chap. 3). The use of this novel instrumentation, completed with a Scanning Mobility Particle Sizer (SMPS) which allow the measurement of particle from 15 nm to 800 nm, we were able to conduct many smog chamber experiments in collaboration with the "Laboratoire des Systèmes Atmosphériques" of Créteil for atmospheric relevant studies and with the "Institut de Recherche sur la Catalyse et l'Environement" of Lyon within

the PIREP project for studies of new particle formation associated with diesel engine processes. Combining results obtained from those experimental works and numerical simulations using a simple model of aerosol growth, we provide a new parametrization of the organic nucleation and highlight the role of the chemical structure of the father organic compound on the first steps of the new particle formation process (See chapter 5).

This doctoral thesis was conducted within the frame of different European and french projects (EUCAARI, EUSAAR, PIREP, LEFE-Chat, LEFE-Aerosol) and its main objective was to provide a multi-scale approach of the nucleation process form the field to the laboratory. Some parts of the work presented in the chapter 4 has been already published in the journal *Atmospheric Chemistry and Physics* and many results of the chapter 5 will be submit ted to publication soon.

Chapter 2

Theoretical approaches of the nucleation and growth of new particles

Contents

Atmospheric new particle formation consists in a complicated set of processes that includes the production of nanometer-size clusters from gaseous vapors, the growth of these clusters to detectable sizes, in competition with their simultaneous removal by coagulation with the pre-existing aerosol particle population. While new particle formation was found to be ubiquitous in various environments (Kulmala et al., 2004b, see for a review of observations) several gaps in our understanding of this phenomenon still exist especially on the basic process-level of the new particle formation. To introduce the complexity of the nucleation, the most relevant theories of the nucleation will be presented in this chapter. This will constitute a basis for the analysis of various nucleation events in the chapters 4 and 5.

As already mentioned above, the anatomy of a nucleation events could be described in two steps: 1- The formation of the thermodynamically stable clusters and 2- The growth of those clusters. In the following, I will present the different theories that have been developed to explain the new particle formation events and then those theories will be discussed through a comparison to field measurements.

Nucleation can be either homogeneous (when the nucleation probability is homogeneous

thorough the system, i.e., it takes place inside of an uniform medium) or heterogeneous (when the probability of nucleation is much higher around some foreign substance or surface such an ion or a solid particle than in the rest of the system). Furthermore, the nucleation process can involve only one chemical species (homomolecular nucleation) or more (heteromolecular nucleation). The combination of all those possible mechanism lead to at least four different nucleation processes:

- Homogeneous - homomolecular nucleation such as the nucleation of pure water,
- Homogeneous - heteromolecular nucleation such as the nucleation of the $H_2SO_4-H_2O$ binary system or the $H_2SO_4-NH_3-H_2O$ ternary system,
- Heterogeneous - homomolecular nucleation such as the nucleation of sulfuric acid on a sulfuric acid pre-existing seed,
- Heterogeneous - heteromolecular nucleation such as the nucleation of organic vapors on a sulfuric acid pre-existing seed.

2.1 Homogeneous nucleation

2.1.1 The unary system model

Homogeneous - homomolecular nucleation (HHN) is strongly dependent on the vapor saturation ratio which is defined as follow:

$$S = \frac{P_X}{P_{sat,X}(T)} \tag{2.1}$$

where P_X is partial pressure of the species X and $P_{sat,X}(T)$ the saturation vapor pressure of X in equilibrium with its liquid phase at temperature T. $S < 1$ for unsaturated vapor, $S = 1$ for saturated vapor and $S > 1$ for supersaturated vapor.
Furthermore, from the thermodynamical point of view, the change in the Gibbs free energy budget$\Delta\ G$ must be negative to allow the droplet formation, meaning that the energy is minimized when forming a droplet of a radius r. The variation of the Gibbs free energy is defined by Eq. 2.2:

$$\Delta G = \frac{4\pi r^3}{3v_{drop.}} \times (g_{drop.} - g_{vap.}) + 4\pi\sigma r^2 \tag{2.2}$$

where $\frac{4\pi r^3}{3v_{drop.}}$ is the number of molecule X in the droplet (r is the droplet radius and $v_{drop.}$ is the volume of a molecule X in the droplet), $g_{vap.}$ and $g_{drop.}$ are respectively the Gibbs free energy for a molecule X is the gas phase and in the droplet. The term $4\pi\sigma r^2$ is the free energy associated with an interface with radius of curvature r and surface tension σ (Seinfeld and Pandis, 1998).

The term $(g_{drop.} - g_{vap.})$ is linked to the surface formation and can be expressed as follows:

$$(g_{drop.} - g_{vap.}) = -k_b T \ln(S) \tag{2.3}$$

where k_b is the Boltzman constant, T is the absolute temperature and S the saturation ratio (Eq. 2.1). By combining Eq. 2.2 and Eq. 2.3, the Gibbs free energy change can be expressed as follows:

$$\Delta G = 4\pi\sigma r^2 - \frac{4\pi}{3} \times \frac{k_b T \ln(S)}{v_{drop}} r^3 \tag{2.4}$$

As an example, the variation of$\Delta\ G$ as a function of the radius of the droplet for pure water and for different values of the saturation ratio S is reported on the figure 2.1.

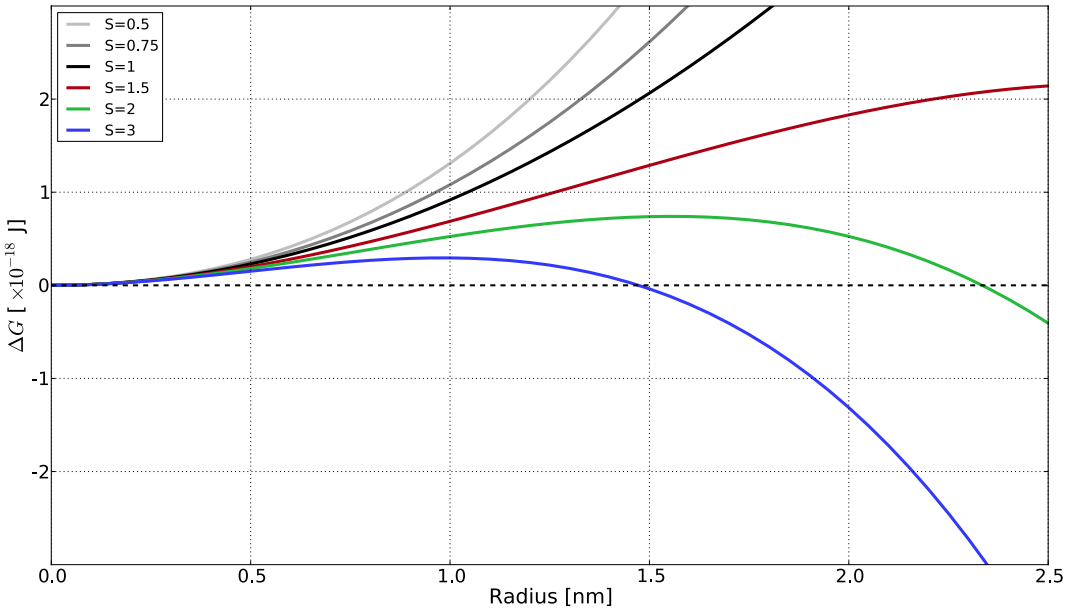

Figure 2.1: Pure water homogeneous nucleation computations for different saturation ratios ($T = 293$ K).

The critical radius $r^\star$ is the radius for which the condensation of any additional molecule will lead to a larger diameter which has a lower δG which in turn will lead to the condensation of more molecules and hence a spontaneous growth. $r^\star$ is defined by Eq. 2.5:

$$r^\star \text{ for } \frac{\partial(\Delta G)}{\partial r} = 0 \Longleftrightarrow r^\star = \frac{2\sigma v_{drop.}}{k_b T \ln(S)} \tag{2.5}$$

The number of monomer contained in the critical cluster $i^\star$ and the nucleation rate J can be determined from the kinetic approach of the homogeneous - homomolecular nucleation theory (Seinfeld and Pandis, 1998):

Table 2.1: Homogeneous nucleation calculation of pure water at $T = 293$ K. $v_{drop.} = 2.989 \times 10^{-29}$ m^3, $\sigma = 73 \times 10^{-03}$ N.m^{-1} and $P_{sat,H_2O} = 2336,96$ Pa.

S [∅]	$r^\star$ [nm]	$i^\star$ [#]	N_1 [#.m^{-3}]	J [cm^{-3}.s^{-1}]
0.5	–	–	$2.88 \times 10^{+23}$	0.0
0.75	–	–	$4.33 \times 10^{+23}$	0.0
1.0	∞	∞	$5.78 \times 10^{+23}$	0.0
1.5	2.66	2639	$8.66 \times 10^{+23}$	7.9×10^{-208}
2	1.56	528	$1.15 \times 10^{+24}$	7.63×10^{-55}
3	0.98	133	$1.73 \times 10^{+24}$	8.31×10^{-07}

$$i^\star = \frac{32\pi}{3} \times \frac{v_{drop.}^2 \sigma^3}{(k_b T)^3 \ln(S)^3} \tag{2.6}$$

$$J = \sqrt{\frac{2\sigma}{\pi m_{drop.}}} \frac{v_{drop.} N_1^2}{S} \times \exp\left[-i^\star \frac{\ln(S)}{2}\right] \tag{2.7}$$

An example of homogeneous calculation for pure water is reported on table 2.1. Those calculations show that the HHN requires a high degree of supersaturation to be triggered. Moreover, the HHN rates of the unary water system are still low even for 300% of saturation ($S = 3$).
Those results suggest that the HHN mechanism can not be predominant in the atmosphere and can only occur in very specific conditions. For example, strong turbulence could enhance the formation of highly supersaturated zones where the HHN could be triggered or during a brutal cooling of an organic vapor.

The homogeneous - homomolecular nucleation theory had been extend to describe the case when two or more different species are engaged hence building a new theory: the homogeneous - heteromolecular (HHeN) nucleation theory. In the following, two main HHeN of interest in atmospheric aerosol science will be presented, the homogeneous - heteromolecular nucleation of the $H_2SO_4-H_2O$ binary system and of the $H_2SO_4-NH_3-H_2O$ ternary system.

2.1.2 The $H_2SO_4-H_2O$ binary system

The heteromolecular nucleation process was first studied by Flood but its atmospheric implications was introduced by Doyle in 1961 who computed the nucleation rate of sulfate particles (see references in Kulmala and Laaksonen, 1990). This mechanism appears to be the most important binary homogeneous nucleation (BHN) system in the atmosphere. Contrarily to the HHN, in the BHN theory none of the vapor species must be supersaturated in the gas phase but with the respect to a liquid solution droplet (Kulmala and

Laaksonen, 1990).
In the H_2SO_4−H_2O binary system, the variation of the Gibbs free energy during the formation of a mixed cluster of sulfuric acid (A) and water (W) is described by the following equation:

$$\Delta G = n_A(\mu_{A,drop.} - \mu_{A,vap.}) + n_W(\mu_{W,drop.} - \mu_{W,vap.}) + 4\pi\sigma r^2 \tag{2.8}$$

where r is the radius of the droplet, and $\mu_{A,drop.}$, $\mu_{W,drop.}$ and $\mu_{A,vap.}$, $\mu_{W,vap.}$ are the chemical potentials of each species respectively in the mixed droplet (*drop.*) and the gas phase(*vap.*). For a given chemical species, the variation of the chemical potential from liquid to gas phase is described by the Eq. 2.9:

$$\mu_{drop.} - \mu_{vap.} = -k_b T \ln\left(\frac{p}{p_{sol.}}\right) \tag{2.9}$$

where p is the partial pressure of the considered chemical species if the gas phase and $p_{sol.}$ is the vapor pressure of the considered component over a flat solution of the same composition as the droplet. If we consider that i- in the droplet, water is the solvent (i.e. $[H_2O] >> [H_2SO_4]$), and that ii- in the gas phase, the total pressure due to all species is low compared to the pressure of the system then chemical activities of a given species for each phase could be defined as follow:

$$a_{i,vap.} = \frac{p_i}{P_{sat,i}} \equiv S_i \text{ and } a_{i,drop.} = \frac{p_{sol.,i}}{P_{sat,i}}$$

Hence, from Eq. 2.8 and Eq. 2.9, ΔG can be expressed as

$$\Delta G = 4\pi\sigma r^2 - k_b T\left(n_A \ln\left(\frac{S_A}{a_{A,drop}}\right) + n_W \ln\left(\frac{S_W}{a_{W,drop}}\right)\right) \tag{2.10}$$

In this expression of the Gibbs free energy, the radius of the droplet do not appear except in the positive term due to the surface formation $4\pi\sigma r^2$. The radius r is given by the relation 2.11:

$$\frac{4}{3}\pi r^3 \rho_{drop.} = n_A m_A + n_W m_W \tag{2.11}$$

ΔG is now a function of two variables n_A and n_W. The energy barrier$\Delta\ G^\star$ is defined by the solution of the system. On the energy surface defined by the space (n_A,n_W), the $\Delta G^\star$ is characterized by a saddle point.

$$\left.\frac{\partial \Delta G}{\partial n_A}\right|_{n_W} = \left.\frac{\partial \Delta G}{\partial n_W}\right|_{n_A} = 0 \tag{2.12}$$

An example of the$\Delta\ G$ calculation in case of the sulphuric acid - water binary system is shown figure 2.2. The calculation was made from the paper of Kulmala and Laaksonen (1990) and data could be found in Seinfeld and Pandis (1998). The calculation of J

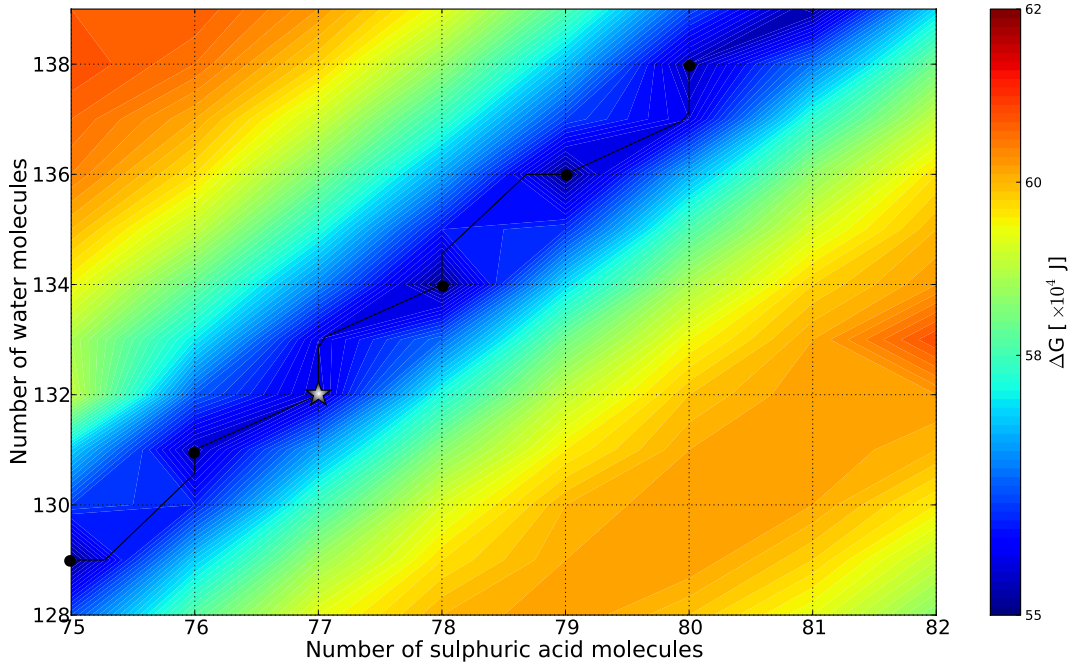

Figure 2.2: Evolution of$\Delta\ G$ according to the number of H_2O and H_2SO_4 in the cluster. Partial pressure for each species are $p_A = 153.3 \times 10^{-11}$ Pa and $p_W = 2 \times 10^4$ Pa (from Seinfeld and Pandis, 1998). The black dots represent local minima of the Gibbs free energy surface and the star represents a saddle point$\Delta\ G^\star(n_A^\star, n_W^\star)$ ($n_A^\star = 77$ and $n_W^\star = 132$).

is much more complicated than in the case of the HHN theory and requires numerous thermodynamic data. But since the J is strongly linearly dependent to the relative humidity and to the temperature, some authors developed an empirical relation (Eq. 2.13) to estimate the critical sulfuric acid concentration that produces a nucleation rate of 1 $cm^{-3}.s^{-1}$ (Jaecker-Voirol and Mirabel (1989) and Wexler et al. (1994) in Seinfeld and Pandis (1998)).

$$C_{crit.} = 0.16 \exp[0.1T - 3. \times 10^{-2} RH - 27.7] \tag{2.13}$$

where T is the absolute temperature, RH is the relative humidity and $C_{crit.}$ is expressed in $\mu g.m^{-3}$. This simple relation provides a way to check if the BHN involving the sulfuric acid - water system can occur in a given set of (T, RH) conditions.

The evolution of $C_{crit.}$ according to T and RH is plotted on figure 2.3. From this graphic, we can deduce that this nucleation mechanism can not describe accurately nucleation in low tropospheric conditions since the sulfuric acid critical concentrations required to nucleation at typical temperatures is quite elevated. However, this mechanism could occur in higher atmospheric layers where temperature are much lower than in the low troposphere. The fact the binary nucleation scheme is not adapted to nucleation in the low troposphere is confirmed by several observations. Many studies of nucleation events report higher values of the particle formation rates than the ones expected on the basis of binary H_2SO_4−H_2O nucleation alone (see for examples Covert et al. (1992); Hoppel

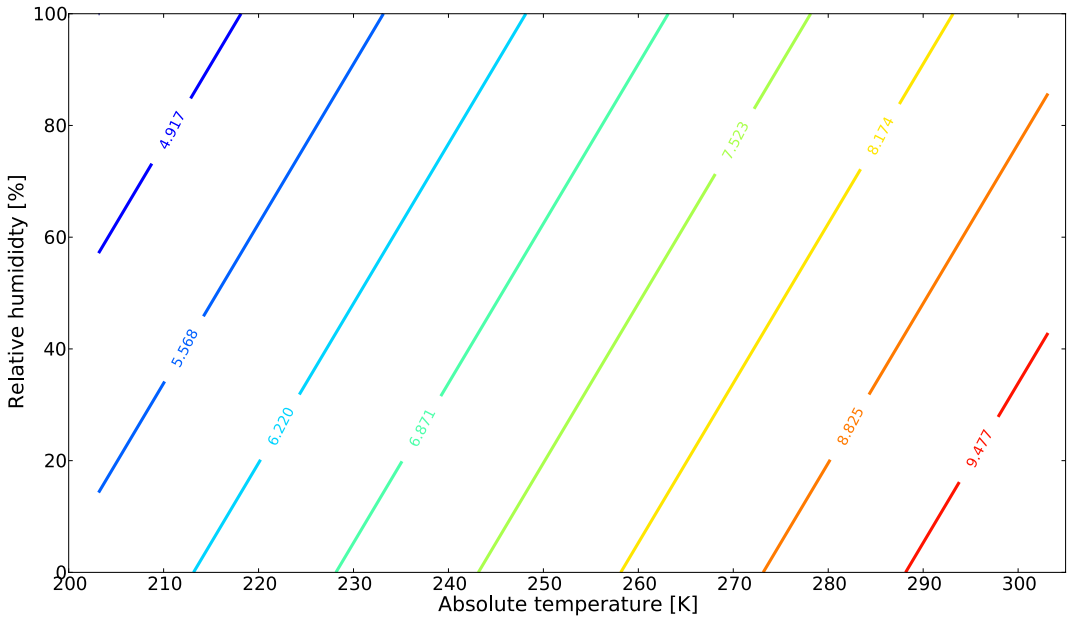

Figure 2.3: Evolution of the $C_{crit.}$ for different temperature and relative humidity conditions. Iso-contours are $\log(C_{crit.})$ values with concentration in [molec.cm^{-3}].

et al. (1994) for marine boundary layer, O'Dowd et al. (1999) for coastal environment or Kulmala et al. (2001b) for boreal forest. Several explanations were proposed to explain the enhanced observed particle production. The following sections will present the most relevant theories: the participation of a third chemical compound (formation of a ternary system), the contribution of ions to stabilize the cluster (ion-induced nucleation) and the heterogeneous nucleation.

2.1.3 The $H_2SO_4-NH_3-H_2O$ ternary system

The equations and physics that describe the ternary homogeneous nucleation (THN) are the same than the ones used for the BHN except that three species are involved in the cluster formation. The first classical ternary theory of nucleation was built by Korhonen et al. (1999) using the $H_2SO_4-NH_3-H_2O$ system based on the fact that i- ammonia, NH_3, is ubiquitous in the atmosphere and ii- this species reduce the vapor pressure of the sulfuric acid above the solution ($p_{A,sol.}$ in the term $a_{A,drop}$ of the Eq. 2.10) hence enhancing the cluster formation (see references in Korhonen et al., 1999). As for the BHN, nucleation rate parameterizations were developed (Napari et al., 2002; Merikanto et al., 2007) but only few studies have confronted the model predictions to laboratory of field measurements.

In 2002, during an intensive coastal environment field campaign at Mace Head, Kulmala et al. have shown that the i- measured sulfuric acid and ammonia concentrations were sufficiently high to onset THN and ii- the classical BHN theory could not explain the observed particle formation rate. Authors concluded that the detected particle formation events could be initiated by the homogeneous nucleation of the ternary system formed

by $H_2SO_4-NH_3-H_2O$. But if the nucleation of new particles could be explained by this nucleation mechanism, the growth to detectable sizes (> 3 nm) could not be explained by the low concentration of sulfuric acid and other condensable vapors had to be involve at least in the growth process.

Homogeneous nucleation theories provide a first description of the nucleation process. These theories assume that the system is only composed of gases. The introduction of pre-existing particles in the system lead to the scavenging of monomers and growing clusters because of the lower energy barrier needed to condense or coagulate on particles than form a new one. Therefore, if the pre-existing particle (or cluster) concentration is high enough, the homogeneous nucleation can be quenched. Those processes are described by the heterogenous nucleation theory.

2.2 Heterogeneous nucleation

An important characteristic of the atmosphere is the ubiquitous presence of particles. This implies that seed are permanently available for the onset of heterogeneous nucleation. On the other hand, those pre-exiting particles provide surface area on which vapors can condense leading to a depletion of condensable species that are necessary for the homogeneous nucleation processes. The condensation of vapors on such pre-existing clusters previously formed by homogeneous nucleation could help to cross the nucleation barrier of energy to reach the critical cluster size, hence onset the growth process. Such a phenomenon is called an activation process and was described for atmospheric binary system by Lazaridis et al. (1992). Later, Kulmala et al. (2004a) have adapted the results obtained by Lazaridis et al. to build the "nano-Köhler" theory of nucleation to explain the formation of organic aerosol. Since the main process of this theory is the condensation of vapor on pre-existing seeds, I will first introduce the condensation phenomenon before going further in the nano-Köhler theory and its implications for aerosol formations.

2.2.1 The condensation process

The condensation is the phase change of a given vapor into a condensed phase. As previously seen, when the phenomenon occurs in a system strictly composed by a gas phase, it leads to the formation of new particles through homogeneous nucleation process. If particles are introduced in the system, vapors can condense on them instead of forming new particles. When a vapor condenses on a particle population, the particle diameters increase, $n(dp, t)$, while the total concentration remains the same.
The aerosol particle size distribution (PSD) can be describe by a sum of log-normal

distributions (Eq 2.14):

$$n(dp,t) = \sum_{i=1}^{n} \frac{N_i}{\log(\sigma)\sqrt{2\pi}} \times \exp\left(-\frac{\left(\log(dp) - \log(\bar{dp_i})\right)^2}{2\log^2(\sigma)}\right) \tag{2.14}$$

where N_i is the aerosol number concentration, $\bar{dp_i}$ is the mean diameter and σ_i is the standard deviation of the i^{th} log-normal mode.

The condensation growth rate $GR_{cond.}$ is defined as the rate at which the volume v (or diameter) of a particle increases. For particles composed of only one species i, in a homogenous gaseous system, $GR_{cond.,i}$ is defined by Eq. 2.15 (Seinfeld and Pandis, 1998):

$$GR_{cond.,i} = \frac{dv}{dt} = \frac{2\pi^{2/3}(6v)^{1/3} D_i M_i}{\rho_{part.} RT} \times f(Kn,\alpha,\beta,\gamma)(p_i - p_{eq.}) \tag{2.15}$$

or for the particle diameter variation:

$$GR_{cond.,i} = \frac{d\ dp}{dt} = \frac{4 D_i M_i}{RT\ dp\rho_{\ part.}} \times f(Kn,\alpha,\beta,\gamma)(p_i - p_{eq.}) \tag{2.16}$$

where D_i is the diffusion coefficient of the vapor, M_i the molecular weight of the vapor and $f(Kn,\alpha,\beta,\gamma)$ is the correction due to non continuum effects and imperfect surface accommodation and $(p_i - p_{eq.})$ represents the difference between the partial pressure of the species i far from the particle (p_i) and the equilibrium vapor pressure $(p_{eq.})$. This latter term is the driving parameter for of the condensation process. $f(Kn,\alpha,\beta,\gamma)$ is defined by the following relations:

$$Kn(r) = \frac{\lambda}{r}$$

$$f(Kn,\alpha,\beta,\gamma) = 1 + Kn(r)\left(\alpha + \beta\exp\left[-\frac{\gamma}{Kn(r)}\right]\right)$$

where α, β and γ are empirical parameters. For $Kn(r) << 1$, the system is in the continuum regime, in free molecular regime for $Kn(r) >> 1$ and in slip regime for $0.4 < Kn(r) < 20$. In the particular case of nucleation studies, it is commonly assumed that the system is in the free molecular regime, i.e. particles are affected by the motion of individual gas molecules. Particles larger than 100 nm are treated as being submersed in a continuous gaseous medium characterized by a Knudson number $Kn(r) > 1$, then $f(Kn,\alpha,\beta,\gamma)$ is assumed to be equal to the unity.

If we assume an excess of the saturated vapor, the first result of the equation 2.16 is that the condensation growth rate is inversely proportional to the diameter (Eq. 2.17).

$$GR_{cond.} = \frac{A}{dp} \Longrightarrow GR_{cond.} \propto \frac{1}{dp} \tag{2.17}$$

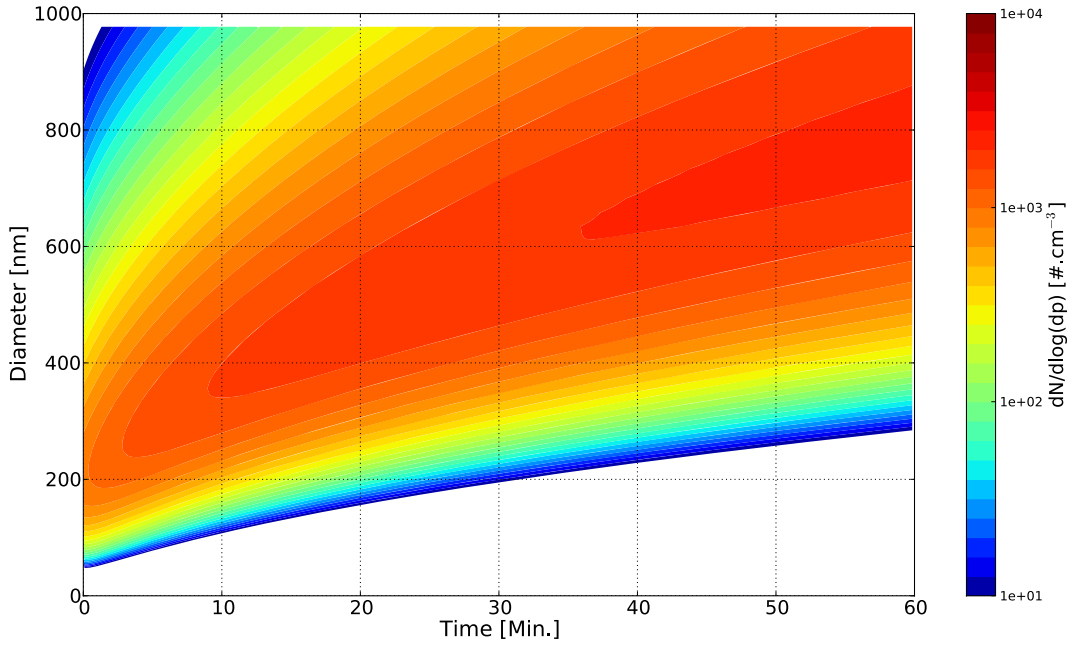

Figure 2.4: Evolution of sulfate particle size distribution in an homogeneous gaseous system. Conditions are $T = 298$ K, $P = 1013.25$ hPa and 1 ppbv of sulfuric acid.

where A is a constant equal to $\frac{4D_i M_i}{\rho_{part.}}(p_i - p_{eq.})$.
It is now possible to estimate the PSD modification by the condensation process. For an initial monodisperse aerosol population $n_0(dp_0, t = 0)$ (Eq. 2.14 with n=1), the new PSD $n(dp, t)$ is given by the equation 2.18.

$$n(dp, t) = \frac{dp}{\sqrt{dp^2 - 2At}} \times n_0\left(\sqrt{dp^2 - 2At}\right) \tag{2.18}$$

An example of the evolution of a sulfate aerosol size distribution in a gaseous media is represented on figure 2.4. As seen on figure 2.4, the condensation process can strongly impact the aerosol size distribution. For nucleation studies, pre-existing particles act as a sink for the condensable vapors, hence quenching the new particle formation process. The potential for gazes to condense on pre-existing particles can be characterized by a parameter defined as the condensation sink (CS) which is equivalent to a velocity. This parameter determines how rapidly molecules of a given species (usually sulfuric acid) will condense onto pre-existing aerosols. The CS strongly depends on the shape of the PSD and is defined by the Eq. 2.19 (Pirjola et al., 1999).

$$CS = 4\pi D_{vap.} \int_0^\infty r\beta_M(r)N(r)dr \tag{2.19}$$

where $\beta_M(r)$ is the transitional correction factor, r the radius of the particle and $N(r)$ the particle concentration of radius r. The transitional correction factor was introduced by Fuchs and Sutugin (1971) to take into account the difference between the kinetic, free molecular and slip regimes defined by the Knudsen number (see above). This factor is

defined by the equation 2.20:

$$\beta_M(r) = \frac{1 + Kn(r)}{1 + (\frac{4}{3\alpha} + 0.337)Kn(r) + \frac{4}{3\alpha}Kn(r)^2} \tag{2.20}$$

where α is the sticking coefficient usually assumed to equal to the unity. Consequently, in the free molecular regim ($Kn(r) >> 1$), the $CS \propto r^2$ while in the continuum regime ($Kn(r) << 1$), $CS \propto r$. In a more general point of view, condensation sink for tropospheric aerosol is $CS \propto r^a$, where $1 < a < 2$.

Another process can significantly change the PSD shape: coagulation. The aerosol particles form a dynamic system, hence each particle is animated by a motion due to the temperature (Brownian motion) and external forces, leading to collisions between particles. Some of those collisions can lead to the formation of a "new" particle composed by the two parent particles. In case of heterogeneous nucleation, the parent particles have the same size (intra-modal coagulation) but can have different compositions. The growth of nucleated particles induced by coagulation was found to be anecdotic in the atmosphere: for a growth rate of 1 nm.h^{-1}, the concentration of parent particles with a diameter lower than 5 nm should be around $1 \times 10^{+06}$ #/cm^{-3} (Kulmala et al., 2004a). However, inter-modal coagulation of small particles onto larger particles can strongly impact the PSD, shifting the mean diameter to larger sizes and inducing a decrease of the total particle number concentration. Large pre-existing particle will act as a sink of small particles and can therefore interrupt the nucleation process. The coagulation sink ($CoagS$) determines how rapidly nm-size aerosols are removed through coagulation process, it is consequently equivalent to a velocity. For a particle of a diameter i, $CoagS$ can be calculated using the relation 2.21 (Kulmala et al., 2001a):

$$CoagS_i = \sum_j K_{ij} Nj \tag{2.21}$$

where K_{ij} is the coagulation coefficient between particles of the diameter i and j (Fuchs and Sutugin, 1971) and N_j is the particle number concentration of diameter j.

2.2.2 The nano-Köhler theory of the new particle formation

The traditional Köhler theory (Köhler, 1936) describes the nucleation of cloud drops on water soluble aerosol nuclei. However, in contrast to the traditional Köhler theory, the nano-Köhler theory describes a thermodynamic equilibrium between a nanometer-size cluster, water and an organic compound that is fully soluble in water (Laaksonen et al., 1998), i.e., it does not form a separate solid phase but is totally dissolved into the mixed solution. A complete description of the theory can be found in Kulmala et al. (2004a, 2006).

Unlike in homogeneous nucleation, the nucleation rate in heterogeneous nucleation is in

many cases either very difficult to measure experimentally due the instrumental limitations which not allow the accurate measurement of seed particles. Easier to measure is the proportion of activated aerosol within the total aerosol population, i.e. the nucleation probability (see chapter 5). As noted earlier, an aerosol particle is able to grow via further condensation. The evolution of the number of *non-activated* particles is defined by:

$$\frac{dN_{non-act.}(t)}{dt} = -\frac{N_{non-act.}(t)}{N_{seed}} \times J_{HeN} dt \tag{2.22}$$

where N_{seed} is the number concentration of pre-existing aerosol seeds (i.e. cluster) and J_{HeN} is the maximum value of the heterogeneous particle formation rate. The solution of the Eq. 2.22 is given by:

$$N_{non-act.}(t) = N_{non-ac.}(t=0) \times \exp\left(-\frac{J_{HeN} t}{N_{seed}}\right) \tag{2.23}$$

The nucleation probability can be defined from the previous relation.

$$P(t) = 1 - \frac{N_{non-act.}(t)}{N_{non-act.}(t=0)} \Longleftrightarrow P(t) = 1 - \exp\left(-\frac{J_{HeN} t}{N_{seed}}\right) \tag{2.24}$$

The threshold value $P(t^\star) = 0.5$ usually defines the onset of the nucleation process. Using the relation 2.24, it is possible to estimate experimentally J_{HeN} since its formulation and theoretical calculation is much more tricky than it is for homogeneous nucleation. A detailed theoretical study of heterogeneous nucleation can be found in the PhD. thesis of Lauri (2006).

The nano-Köhler activation presents a lower energetic barrier to trigger the nucleation and growth process than homogeneous nucleation no matter if the condensable vapor is soluble or insoluble in the seeds (Petersen et al., 2001). This theory does not constitute a self complete theory since it cannot explain the seed formation but, in association with homogeneous theories, it provides a more complete description of the new particle formation process which could be split into two different steps: i- the formation of stable clusters from homogeneous nucleation and ii- the activation and growth of such stable clusters by condensation of vapors.

2.3 The ion-induced nucleation

The ion-induced nucleation (IIN) is a nucleation theory that involves the formation of charged clusters. In this particular case, the attractive potential between ions and ions, and between, ions and the dipole moment (induced or not) of the condensable vapor reduces the thermodynamic barrier for nucleation and hence, enhances the condensational growth (e.g. Lovejoy et al., 2004; Nadykto and Yu, 2004). This theory is based on

the fact that ions are generated continuously, and ubiquitously, by galactic cosmic rays (as a function of altitude and latitude) and local sources such as radioactive decay or lightning. Mechanisms involved in this theory are not different than the ones that have been developed in the previous paragraphs. The main difference is that an electrical term due to the charge state of each component. Nucleation mechanisms involving ions have been proposed to be important for aerosol formation in the atmosphere (e.g. Arnold, 1980; Yu and Turco, 2001).

2.4 Formulations of nucleation parametrizations

In order to include the nucleation into large scale model, calculation procedures of the particle formation rate must be simplify to reduce the computational burden. Consequently to this need, different parametrizations of the nucleation process based either empirically from laboratory and field measurements, or, from the classical and kinetic nucleation models derived from BHN or THN theories has been developed (e.g. Harrington and Kreidenweis, 1998; Vehkamäki et al., 2002; Sihto et al., 2006; Yu, 2006, 2008; Kuang et al., 2008). A comparison of 12 nucleation parametrizations have been conducted by Zhang et al. (2010). This study highlights that predicted nucleation rates differ by many order of magnitude depending on the used parametrization. In general best agreement were found for parametrizations derived from field measurements (e.g. Sihto et al., 2006; Kuang et al., 2008) which were developed under specific atmospheric conditions dependent of the measurement site. Furthermore, those empirical give much higher nucleation rates than reference laboratory measurements and do not include T and RH consideration in their power law formulations. On the other hand, parametrizations developed from the BHN/THN theories (e.g. Yu, 2006; Merikanto et al., 2007, 2009; Yu, 2008) tend to underpredict the observed nucleation rates but are the closest to laboratory measurements and could be adapted to various conditions since they explicitly include T and RH. Consequently, those latter parametrizations are the closest representations of the BHN/THN theories compared to Harrington and Kreidenweis (1998); Vehkamäki et al. (2002). Parametrizations proposed by Sihto et al. (2006) and Kuang et al. (2008) represent respectively the activation (i.e. activation of small clusters via heterogeneous nucleation) and kinetic (i.e. new cluster formation from sulfuric acid or sulfuric acid derived molecules) type nucleation.

Chapter 3

Tools for the new particle formation event detection and analysis

Contents

The detection and the analysis of new secondary particle formation events in the atmosphere is based on the measurement of the particle number size distribution and the charge state of those particles. Different types of instruments exist, always based on the selection of particles from their mobility with a Differential Mobility Analyzer (DMA), but with different particle detection devices (e.g. electrical or optical). In this chapter, neutral and charged particle size distribution measurement devices will be presented, as the key tools of this thesis.
Moreover, a LIDAR instrument (LIght Detection And Ranging) was used to characterize the vertical structure of the atmosphere, useful for nucleation studies, and will hence be also described.

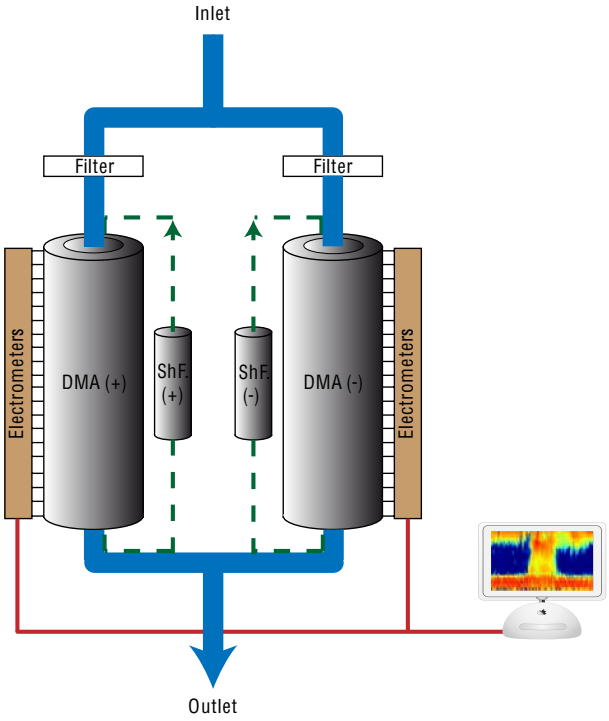

Figure 3.1: Schema of an AIS. ShF. are the sheath-air filter, the green dot line represents the offset loop.

3.1 Particle size distribution measurement devices

3.1.1 The Air Ion Spectrometer family

Air Ion Spectrometer (AIS) is developed by Airel Ltd, Estonia, for in-situ high time resolution measurements of ions and charged particles. The measured mobility range extends from 3.2 to 0.0013 $cm^2.V^{-1}.s^{-1}$, corresponding to Stokes-Millikan mobility diameters (Mäkelä et al., 1996) between 0.8 and 42 nm in NTP-conditions. The AIS has two identical differential mobility analyzers (DMA) functioning in parallel: one for negatively charged particles and the other for positively charged particles (Fig. 3.2). Each analyzer has a flow rate of 90 litres per minute (lpm): 30 lpm of sample flow, and 60 lpm of closed loop sheath air flow. The high flow rate is necessary to minimize the ion diffusion losses so that low concentrations of smaller ions can be detected with a reasonable signal to noise ratio. The inner cylinder of the analyzer is divided into 4 isolated sections and their voltages are kept unaltered during the whole measurement cycle. Measurable ions move towards the outer cylinder due to the radial electric field. The outer cylinder is divided into 21 isolated sections forming, together with their own electrometers, the 21 measuring channels of the analyzer. The ions precipitate onto these sections according to their electrical mobility, and the electrometers measure the currents induced by the ions. Before and after each ion measurement, an offset measurement is performed.

An unipolar corona charger having a polarity opposite to that of the analyzer, together with the subsequent electric filter, eliminates all charged particles from the input air.

Thus the zero drift of the electrometers and the parasitic currents of the section isolators are continuously measured. These parasitic currents are subtracted from the measured total currents and the corrected electrometer signals form the instrument record. Via the parasitic current dispersions the measurement random uncertainties are assessed. Using the mathematical model (instrument equation) of the AIS and the transfer functions of the measurement channels, determined by the analyzer geometry, flows, voltages, and ion losses, the instrument record is converted to mobility spectrum of the particles, which is a distribution density vector with 28 elements (Mirme et al., 2007). Time resolution is user defined, but the minimum for one ion spectrum is in the order of one minute, depending on the level of noise.

An improved version of the AIS is the Neutral cluster and Air Ion Spectrometer (NAIS). The NAIS has an additional charger-filter section in the inlet after the offset section providing a possibility to measure neutral particles as well. The first assumption is that the measurable particles are in charge equilibrium. They are further charged using an unipolar corona charger with ion currents of -22 nA (negative polarity) and +25 nA (positive polarity). The charging probability of particles then basically depends on the particle size, corona ion current and sample flow (exposure time). The charged fraction of particles induced to the sampled air is known for all sizes (estimated from Fuchs theory). The corona ions (generally < 2 nm depending on concentration, air composition, polarity, etc.) are removed by the electrical filters, leaving a confidence size range between 2 and 42 nm (Asmi et al., 2009). However, especially the smallest aerosol particles might not have reached the equilibrium state. The NAIS measures, in turn, the mobility distribution of particles (from negative and positive DMAs, particle measurements), and of naturally negatively and positively charged particles and ions (ion measurements), and the background (offset measurements, green dot line on Fig. 3.2). The NAIS has thus an additional operation mode, where prior to charging, the measured particles are exposed to corona ions of opposite sign. The purpose is to bring the particles closer to the equilibrium charge distribution. The ion and offset modes are measured in the NAIS as in the AIS.

3.1.2 The Scanning Mobility Particle Sizer

We used a custom SMPS made by Hervé Venzac during his Master thesis research. The SMPS (Fig. 3.1) is composed by a DMA and a Condensation Particle Counter (CPC, TSI model 3010). Before entering the DMA, the whole particle distribution is charged to equilibrium by the neutralizer (^{63}Ni or a corona discharge). The number of charge of each particle is well known (Wiedensohler, 1988). Once charged, the particles are selected according to their electrical mobility by the DMA. Contrarily to the AIS/NAIS, the current in the DMA is constant along the whole DMA and variable in time. For a given current, the DMA select one electrical mobility hence only particles which have the corresponding

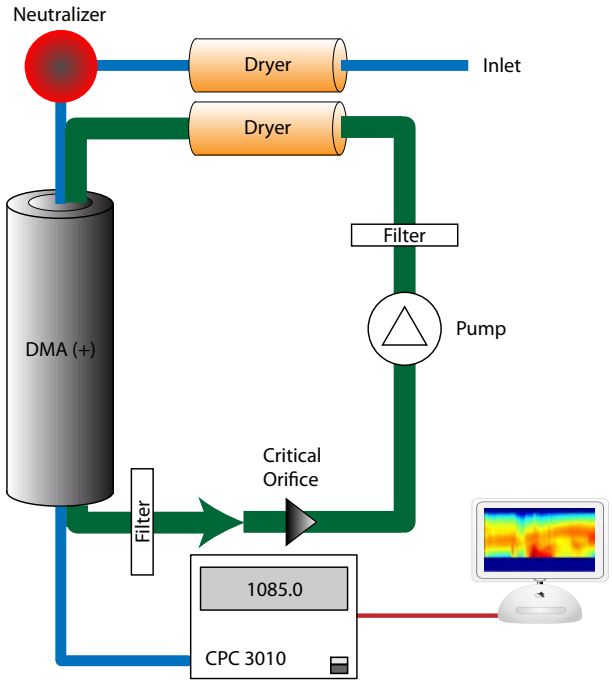

Figure 3.2: Schema of the SMPS. The green line represents the excess & sheath-air loop.

electrical mobility will be counted by the CPC, the others are carried outside the DMA with the excess flow. To measure the PSD, the voltage oscillates between two boundary values of current which set the minimum and the maximum electrical mobility diameter which can be measured. The SMPS we used allow the detection of particles between 10 and 700 nm (Venzac et al., 2008).

3.1.3 Instrument calibrations and intercomparison

SMPS and AIS/NAIS are regularly calibrated and intercompared. The SMPS calibration was organized in the frame of the integrated european project EUSAAR (EUropean Supersites for Atmospheric Aerosol Research) at the Institute of Tropospheric Research of Leipzig. The goal of such a project is to ensure harmonization, validation and data diffusion of SMPS data of the 20 European ground-based supersites involve in the project (more details on EUSAAR and the intercalibration workshops can be found in Venzac, 2008).

Two AIS/NAIS calibration and intercomparison workshops were organized in 2008 (Asmi et al., 2009) and between May and June 2009 (see in Annexe Gagné et al., 2011) in the frame of the EUCAARI project (EUropean integrated project on Aerosol-Cloud-Climate & Air quality Interactions). The objectives were to insure that instruments were performing in a comparable way prior and after the intensive observation period of the project that was planned during the 2008 year. During the 2009 workshop, the goals were in particular i-to discuss results for mobility and concentration results compared to the first calibration workshop, ii- to compare AIS/NAIS with three other reference

instruments: a balanced scanning mobility analyzer (number size distribution of cluster ions in the size range 0.7 and 7 nm in diameters), a Differential Mobility Particle Sizer (DMPS) which a provide a measurement of the PSD between 10 and 300 nm in diameter and an Ion-DMPS. The latter one is identical to a DMPS, with the exception that its bipolar charger can be switched on or off and the voltage applied to the DMA can be either positive or negative, thus allowing PSD of neutral and charged aerosols. During the intercomparison, the Ion-DMPS was measuring particles between 2.2 and 11.5 in diameter.
Measurement were conducted in indoor and outdoor air, during a provoked new particle formation event by peeling citrus fruits in a room. Charged and total PSD, concentrations and mean diameter were compared between 11 AIS/NAIS and the 3 references. This workshop provided a list of considerations and advices to keep in mind while performing analysis of AIS/NAIS data. The most important one are listed below (for more details, see Gagné et al., 2011 in the appendice section):

- The mobility detection can be trusted for AISs and NAISs, provided that the instrument is clean and the flows are not obstructed.
- The concentration can vary from one individual instrument to the other by up to 10% within the same instrument type.
- The NAISs can overestimate the total particle concentration by a factor 2 to 3 and to a lesser extent the ion concentration (based on calibration results and comparison with DMPS and ion-DMPS).

Those three major points have to be taken into account for the AIS/NAIS measurement interpretations and comparison with other instruments (e.g. SMPS).

3.2 LIDAR measurements

LIght Detection And Ranging (LIDAR) is, along with RAdiowave Detection And Ranging (RADAR), one of the main technique of the vertical profiling of the atmosphere. The LIDAR is based on the interactions of a light beam with the atmospheric constituents. These interactions depend on the considered constituent, it goes from elastic (Rayleigh and Mie diffusion) to inelastic backscattering (Raman diffusion) but also absorption, fluorescence or doppler processes.
The LIDAR used at the Laboratoire de Météorologie Physique is a Raymetrics Rayleigh-Mie LIDAR emitting at 355 nm, with parallel and perpendicular polarization channels. The instrument provides profiles of volume backscatter and extinction coefficients of aerosol particles, the depolarization ratio, and water-vapor-to-dry-air mixing ratio. The LIDAR returns signals strongly dependent on height z (in the case of a ground-based,

vertically pointing lidar) and decreasing with z^2 (Eq. 3.1). Correcting the signal with z^2 thus removes the height dependence.

$$P(z) = K\frac{O(z)}{z^2} \times \beta(z,\lambda)\exp\left[-2\int_{Z_0}^{Z}\alpha(z,\lambda)dz\right] \tag{3.1}$$

where K summarizes the performance of the lidar system, $\frac{O(z)}{z^2}$ describes the altitude-dependent measurement geometry. These two factors are completely determined by the lidar setup and can thus be controlled by the experimentalist. $\beta(z)$ is the backscatter coefficient at the altitude z and α is the extinction coefficient. Both depend on the wavelength of the laser light. This wavelength dependence is determined by the size, the refractive index, and the shape of the scattering particles.
Using the LIDAR equation (Eq. 3.1) and assuming that particles are spherical and that their composition are known (i.e. the refractive index is known), it is possible to determine a vertical profile of the backscattering profile hence a vertical profile of atmospheric aerosols. In the present work, we only used the LIDAR signal to retrieve a Planetary Boundary Layer (PBL) height.

3.3 Data processing for nucleation event characterization

A new particle formation event (NPF), as previously described by Dal Maso et al. (2005), must present four criteria: "1.- A distinctly new mode of particles must appear in the size distribution, 2.- the mode must start in the nucleation mode, 3.- the mode must prevail over a time span of hours and 4.- the new mode must show signs of growth". The classification of event days was performed visually using the daily contour plot of the ion size distribution evolution. Data were first categorized into three main classes : undefined, non-event and nucleation event days. Since different types of nucleation can be observed, event days were classified into different classes (Ia, Ib, II and Bump) according to their quality and their applicability to a growth rate analysis (Hirsikko et al., 2007) :

- Ia : Continuous growth of clusters (< 3 nm) to large particle (≥ 20 nm).
- Ib : These events are not as strong as class Ia events and sometimes cluster or intermediate growth are not clearly visible on the size distribution but the growth rate calculation remains possible.
- II : A clear event is identified but the growth from clusters to large particles is not regular and the shape of the size distribution is unclear. A further analysis of the new particle formation event characteristics is complex.

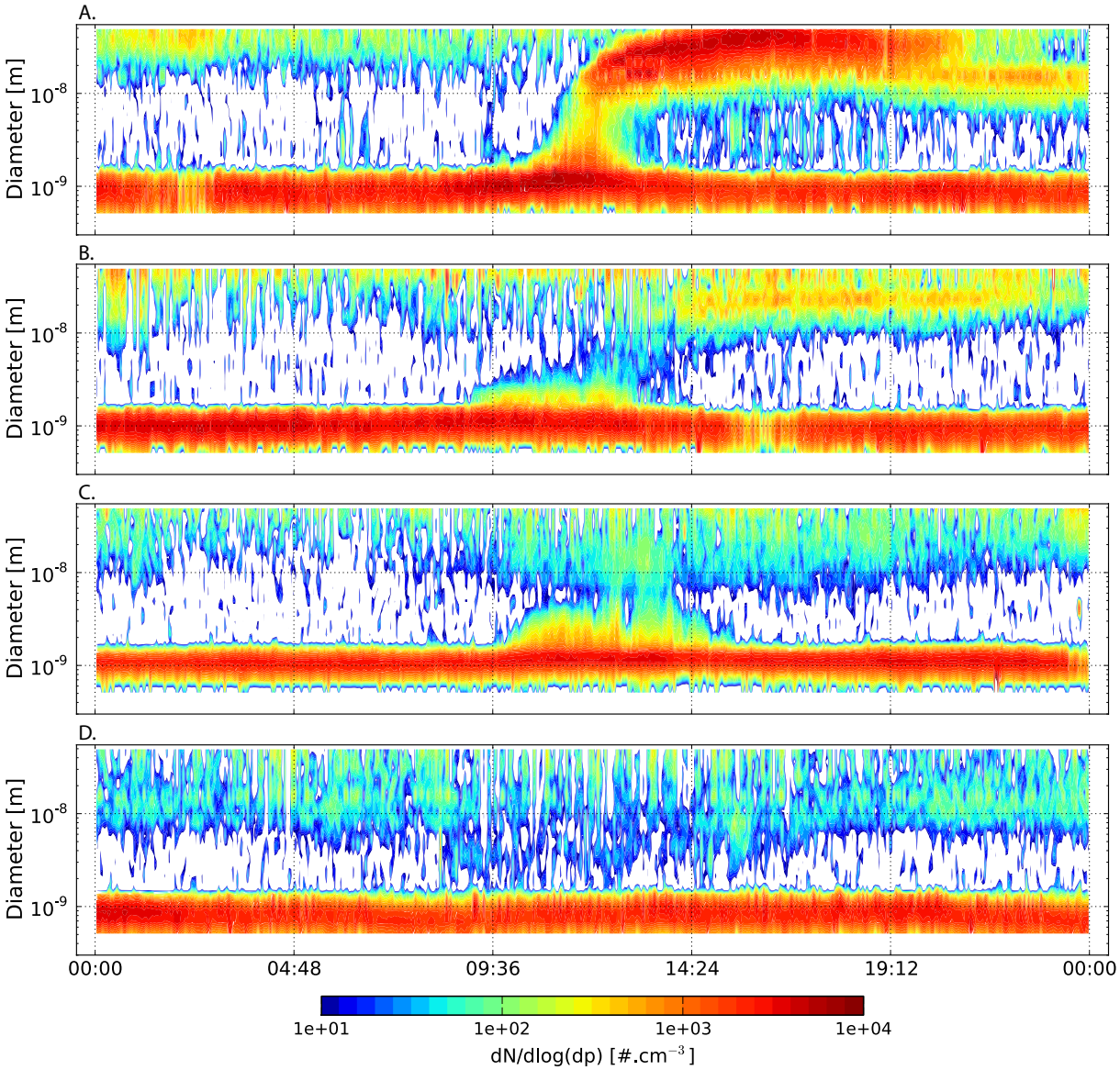

Figure 3.3: Different type of event days: Ia (A.), II (B.) and Bump (C.) and a non-event day (D.)

- Bump : A burst of clusters is detected but it is not followed by a significant growth and particle formation. Different explanations are possible such as the total consumption of the condensing vapors or a change in the air mass type.

Examples of a non-event day and different type of event days are reported on figure 3.3).

3.3.1 Nucleation rates calculations

3.3.1.1 The growth rate

The NPF process can be segregated into different steps. Four different boundary diameters (1.3, 3, 7 and 20 nm) were determined as representative of different growth steps, as usually chosen for growth rate (GR) calculations (Hirsikko et al., 2005). This allow

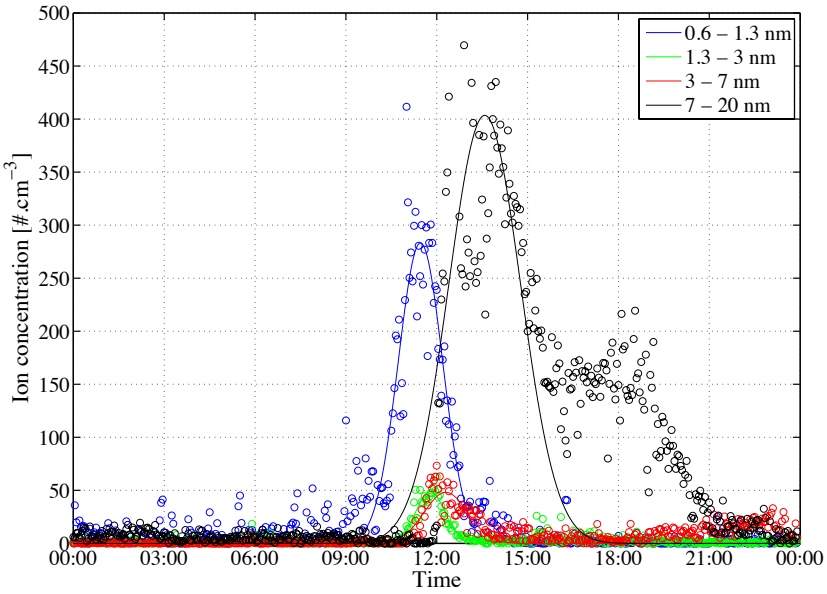

Figure 3.4: Fitting procedure to estimate the growth rate.

the study of the temporal variation of the GR and its dependence to the particle diameter. The growth can be described as follows: First, the smallest particles (1.3 nm) concentration increases until a local maximum, then it decreases following a gaussian shape. While the first population concentration decreases, the next one (3 nm) starts to increase until reaching a local maximum etc... The growth rate between two size classes were computed by calculating the time needed to switch from the lower size class local maximum concentration to the nearest higher size class local maximum concentration, as proposed by Hirsikko et al. (2005). In the present work, a normal distribution is fitted to the different size class concentration maxima using a trust-region algorithm (Byrd et al., 1987) by minimizing the least square residues (Fig. 3.4). Thus the growth rate was computed using the fitted parameters as follows:

$$GR_{dp_x - dp_y} = \frac{dp_y - dp_x}{t_{max(dp_y)} - t_{max(dp_x)}} \tag{3.2}$$

where $t_{max(dp)}$ is the time when the particle population of diameter dp is maximal. The GRs were computed for class Ia and Ib NPF classes. However, for some class Ib days, the GRs calculation was not possible due to local pollution events, changes in air mass types or NPF interruption by clouds. Those days were not taken into account in the growth rate analysis. Furthermore, the effect of coagulation on the size evolution was not included in the GR calculation since its effect is negligible when the new particle formation is onset. The growth rate is directly linked to the condensable vapor concentration through the equation 3.3. Thus, the minimal vapor concentration necessary to produce a given

growth rate can be calculated as follows (Dal Maso et al., 2002):

$$GR = \frac{ddp}{dt} = \frac{4m_{vap.}\beta_M[Vapor]}{\rho dp} \tag{3.3}$$

where $m_{vap.}$ is the masse of a vapor molecule, β_M is the transitional correction factor for the mass flux (see Eq. 2.20), $[Vapor]$ is the condensable vapor concentration, ρ is the aerosol density and dp is the particle diameter.

3.3.1.2 The formation rates

Formation rates of charged ($J_2^{\pm}$) and neutral (J_2) for 2 nm-aerosols were computed according to Eq. 3.4 and 3.5 (from Kulmala et al., 2007):

$$J_2 = \frac{dN_{2-3}}{dt} + CoagS_2 \times N_{2-3} + \frac{f}{1\text{nm}} GR_{1.3-3} N_{2-3} \tag{3.4}$$

$$\begin{aligned} J_2^{\pm} &= \frac{dN_{2-3}^{\pm}}{dt} + CoagS_2 \times N_{2-3}^{\pm} + \frac{f}{1\text{nm}} GR_{1.3-3} N_{2-3}^{\pm} \\ &\quad + \alpha \times N_{2-3}^{\pm} N_{<3}^{\mp} - \beta \times N_{2-3} N_{<2}^{\pm} \end{aligned} \tag{3.5}$$

where $N_{2-3}^{\pm}$ is the ion number concentration (positive or negative ions) [#.cm^{-3}] in diameter range from 2 to 3 nm and $N_{<x}^{\pm}$ is the ion number concentration below x nm. $CoagS_2$ is the coagulation sink of 2 nm particles [s^{-1}]. α and β are respectively the ion-ion recombination coefficient and the ion-neutral attachment coefficient and were assumed to be equal respectively to 1.6×10^{-6} cm^3.s^{-1} and 1×10^{-8} cm^3.s^{-1} (Tammet and Kulmala, 2005). The factor f represents the fraction of the aerosol population in a size range from 2 to 3 nm which is activated for the growth. We assumed this factor to be equal to unity. The time derivative of N_{2-3} is directly obtained from the NAIS measurements. $CoagS_2$ is derived from SMPS and/or NAIS data.

It is also possible to derivate the J_2 from J_{20} calculated from SMPS following a similar relation than Eq. 3.4. The method was firstly introduced by (Kerminen and Kulmala, 2002) and then improved by Lehtinen et al. (2007).

$$J_x = J^{\star} \exp\left[-\gamma\ dp^{\star} \frac{CoagS(dp^{\star})}{GR}\right] \tag{3.6}$$

where

$$\begin{aligned} \gamma &= \frac{-1}{m+1}\left[\left(\frac{dp_x}{dp^{\star}}\right)^{m+1} - 1\right] \\ m &= \frac{\log\big(CoagS(dp_x)\big) - \log\big(CoagS(dp^{\star})\big)}{\log(dp_x) - \log(dp^{\star})} \end{aligned}$$

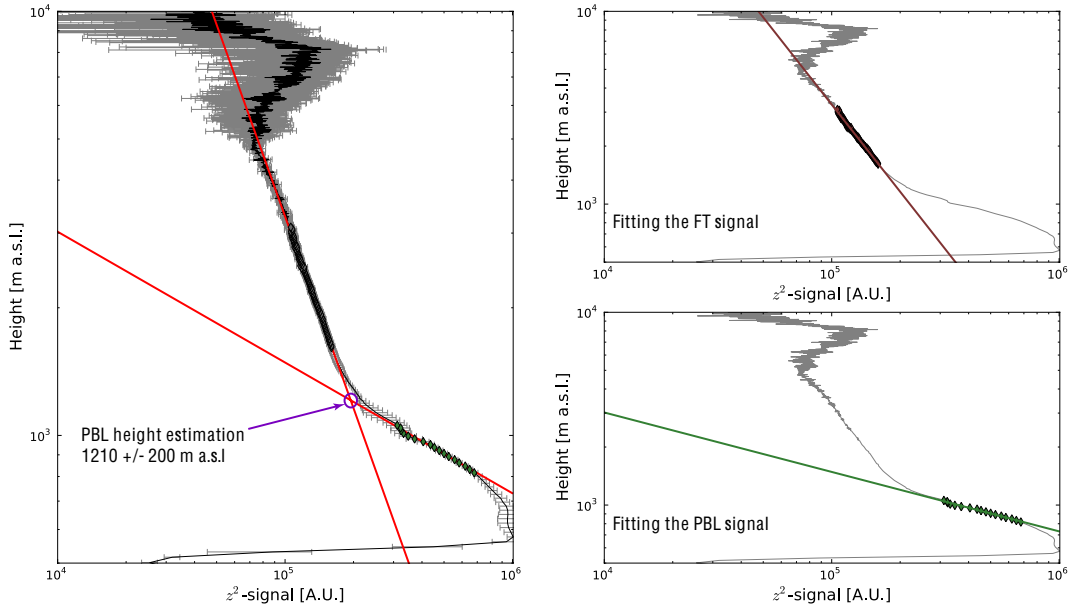

Figure 3.5: Planetary boundary layer estimation procedure.

$J^\star$ in the equation 3.6 if the nucleation formation rate and $dp^\star$ the diameter of the stable clusters freshly formed by nucleation. Assuming the $dp^\star \in [1.5; 2]$ nm, it is possible to estimate J_2 from SMPS data.

3.3.2 Characterization of atmospheric layers

It is well known that aerosol particles are more numerous within the PBL than in the FT, so we assume that the summit of the PBL is characterized by a modification of the light diffusion regime. Hence, the height of the planetary boundary layer is estimated by the inflexion point between the back-scattering signal dominated by Rayleigh diffusion and the back-scattering signal dominated by the Mie diffusion (strongly linked to the decrease of the particle concentration in this part of the atmosphere). An example is presented on figure 3.5. The position of the inflexion point is determined using fitting two different parts of the profile, assuming that the PBL upper boundary is located at the slope rupture point ("I-Fi" algorithm). We also estimate the height of the injection layer, i.e. the interface between the PBL and the FT, using the divergence between the fit of the Rayleigh regime and the measurements assuming that its width is the height where $abs(Fit - Measurement) > (mean(Measurement) - std(Measurement))$. This method was compared to the wavelet covariance transform algorithm (WCT) proposed by Brooks (2003), initially developed for marine boundary layer height retrievals.

The calculated PBL height was found to be 32.2% higher on average when it was computed using our method (Table 3.1). The difference between the two methods is found to be maximal when i- the PBL is strongly polluted and stratified and ii- the PBL is relatively clean and has a low vertical extend. The best agreement is found when the PBL is well mixed and polluted while large discrepancies appear when the PBL is

Table 3.1: Comparison between the WCT and I-Fi algorithms between 09:00 and 11:00, during nucleation events. P events is for a nucleation events only detected at the PdD station and D events are for events detected at the PdD and at a low altitude station.

Date	I-Fi	WCT	Relative Error to WCT
26/02/2009	1376 ± 350	1015 ± 165	35.6
28/02/2009	1244 ± 813	1075 ± 90	15.7
13/03/2009	1215 ± 198	850 ± 142.5	42.9
17/03/2009	1275 ± 193	910 ± 82.5	40.1
18/03/2009	984 ± 126	865 ± 27.5	13.7
27/04/2010	1640 ± 621	1570 ± 97.5	4.4
28/04/2010	1594 ± 1119	1585 ± 570	0.6
29/04/2010	1126 ± 892	1225 ± 225	-8.1
17/05/2010	3143 ± 692	2680 ± 45	17.3
19/05/2010	2701 ± 869	N.D.	N.D.
20/05/2010	N.D.	N.D.	N.D.
21/05/2010	1735 ± 857	1570 ± 22.5	10.5
08/03/2010	1443 ± 379	1180 ± 105	22.3
05/03/2010	2446 ± 20417	1075 ± 135	127.5
02/03/2010	2077 ± 939	1675 ± 30	24.0
22/03/2009	1842 ± 800	1000 ± 120	84.2
21/03/2009	1318 ± 286	910 ± 172	44.8
20/03/2009	1362 ± 244	910 ± 135	49.7
19/03/2009	1094 ± 129	895 ± 82.5	22.2

stratified or clean. Those patterns come from the fact that the WCT method tries to find the upper limit of the main aerosol layer (i.e. the start of the decrease of the Mie regime) whereas the I-Fi method was build to find the transition from Mie diffusion regime to Rayleigh diffusion regime i.e. the transition from planetary boundary layer influenced layers to free tropospheric influenced layers. Compared to WCT and based on the shape analysis of the time evolution of the LIDAR signal, this procedure seems to be better adapted to the calculation of the PBL height in mountainous area such as puy de Dôme.

3.4 Modelling the new particle formation events

3.4.1 All roads lead to Rome...

A powerful tool to test hypothesis on nucleation and new particle formation processes is the process-based modelling. If the aerosol measurements provide new information, theories and modelling activities help to understand them and identify which processes and parameters play a key role in the observations. Different types of new secondary particle formation models, depending of the scientific community, have been developed. The community of chemists developed models based on the particle chemical composition thermodynamically related to the gas phase composition and its evolution through homogeneous/heterogenous chemical reactions (e.g. Aumont et al., 2005; Camredon et al., 2010; Lane et al., 2008; Tsimpidi et al., 2010) while the community of physicists have built some models based on the particle size distribution evolution related to the physical properties of condensable vapors (e.g. Lehtinen and Kulmala, 2003; Korhonen et al., 2004; Leppä et al., 2009). In the later type, the time evolution of the particle size dis-

tribution (PSD) is driven by four main processes: i- the nucleation of new clusters, ii- condensation, iii- coagulation and iv- deposition. If the early steps of the new particle formation are only considered, the deposition processes (dry and wet) can be neglected. Considering the numerical point of view, the key element is the representation of the PSD. The two main approaches are the sectional and the modal representation (Fig. 3.6).

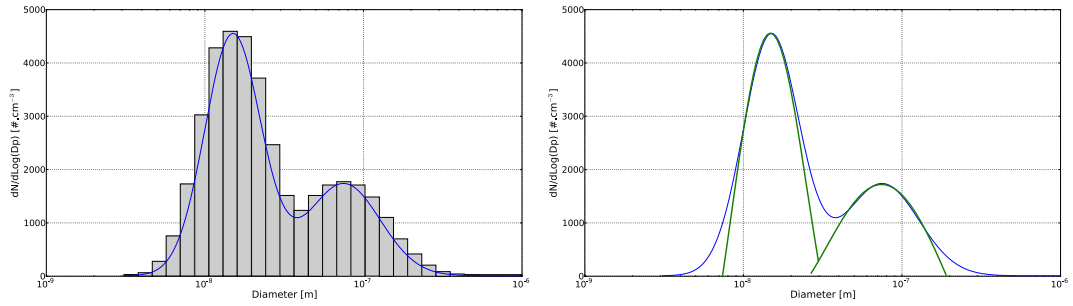

Figure 3.6: Sectional and modal (respectively left and right subplot) description of a particle size distribution (blue).

In the sectional approach, the PSD is approximated by a discrete number of size sections or bins. A bin is usually composed by a number of all-equivalent-particles, i.e. monodisperse population with a flat distribution and errors due to this assumption increase with the size of the bins. Hence the sectional representation efficiency strongly depends on the number of bins (up to thousands), which can rapidly increase the computational burden. Furthermore, the evolution of particles from one bin to another leads to numerical diffusion problems, which increase errors in the model outputs. This latter point could be avoided by using a modal representation in which the particle growth is represented by the motion of modes in the size space. Hence the PSD is represented as a sum of analytical functions (or modes, in general log-normal distributions and typically more than 2). This simple representation is very efficient to compute the growth of a given particle population by condensation but it cannot describe the input of new clusters by nucleation (for a comparison between the different approaches, see Whitby and McMurry, 1997; Zhang et al., 1999)

3.4.2 Adaptation of an existing code for new particle formation purpose: From M7 to M4-NPF

In this work, we adapted in collaboration with the Max Plank Institute of Hamburg, an existing size-resolved aerosol microphysics module (M7 aerosol model, Vignati et al., 2004) primarily developed to be coupled to general circulation models and chemistry transport models (REMOTE, Vignati et al., 2004). In this model, the PSD is represented using an mixed approach between the sectional and the modal descriptions, i.e. the pseudomodal approach. In this representation, the PSD is segmented in different bins which are individually described as a log-normal mode with a fixed geometric standard

deviation σ. Each mode is described by total particle number and mass concentrations. The average particle radius is derived from number and masses concentrations. The M7 model use 7 modes to describe the PSD:

- Four modes are defined for mixed aerosols (i.e. water-soluble mixture of insoluble and soluble material): nucleation (sulfate particles), Aïtken (black carbon (BC) and organic carbon (OC) in an internal mixture with sulfate), accumulation and coarse modes (which can be composed of the same species than the other modes, plus sea salt and dust).
- And three modes are used to describe insoluble particles: an Aïtken mode composed by an internally mixed of BC/OC, an accumulation and coarse mode containing dust.

The separation of the total PSD into two sub-PSDs allows the evolution of the initially insoluble compounds to evolve into compounds with different hygroscopic properties. Properties of each modes are summarized in the table 3.2.

Table 3.2: Properties of the modes implemented in the M7 model (from Vignati et al., 2004).

Aerosol property	Modes	Geometric standard deviation σ	Dry radius size interval nm
Soluble	Nucleation	1.59	$0-5$
	Aïtken	1.59	$5-50$
	Accumulation	1.59	$50-500$
	Coarse	2.0	>500
Insoluble	Aïtken	1.59	$5-50$
	Accumulation	1.59	$50-500$
	Coarse	2.0	>500

This 7-pseudomodal description is not relevant for new particle formation modelling since the two smaller bins overlap the whole size range of the nucleation and subsequently growth process. For the purpose of our studies, we created a simplified version of M7, named M4-NPF, in which the PSD is composed of a single component aerosol divided in 4 size sections with a fixed geometric standard deviation. This later parameter was estimated for each size classes from AIS and NAIS measurements and from the literature (see Tab. 3.3).

3.4.2.1 Implemented processes et their representations

Processes considered in the simplified version M4-NPF are a selection of relevant processes implemented in the original model M7. For nucleation and growth in the size range of interest for new particle formation simulation issues, represented processes are: i- the nucleation of new clusters from sulphuric acid homogeneous nucleation, ii- the condensation of vapors onto pre-existing particles and iii- the coagulation. However, to avoid

Table 3.3: Properties of the modes implemented in the M4-NPF model. ⋆ values for Aïtken and accumulation modes are taken from Venzac et al. (2009).

Aerosol property	Modes	Geometric standard deviation σ (⋆)	Dry radius size interval nm
Soluble	Cluster	1.2	$0-3$
	Nucleation	1.35	$3-10$
	Aïtken	1.75	$10-30$
	Accumulation	2.0	$30-100$
	Coarse	2.0	>100

uncertainties link the unknown clusters' composition and to the sulphuric acid production from sulfate radical oxidation, the nucleation mode population is given as a parameter (see section "Thermodynamic, chemical and aerosol physical inputs").

The condensation process The condensation rate of the condensable vapor for the mode i is described by the formulation proposed by Fuchs (1964):

$$C_i = \frac{4\pi D_{vapor}\bar{r}_i}{\frac{4D_{vapor}}{\alpha v_{th}\bar{r}_i} + \frac{\bar{r}_i}{\bar{r}_i+\lambda}} \tag{3.7}$$

where D_{vapor} is the diffusion coefficient of the condensable vapor, $\bar{r}_i$ is the geometric mean diameter of the mode i, α is an accommodation coefficient assumed to be equal to the unity, v_{th} is the thermal velocity and λ is the mean free path of a vapor molecule. Hence the variation of condensable vapor concentration is defined by the differential equation 3.8.

$$\frac{d[Vapor]}{dt} = K_{in} - \sum_{i=1} 4N_i C_i [Vapor] \tag{3.8}$$

where K_{in} is the condensable vapor input parametrization, N_i is the particle number in the mode i and $[Vapor]$ the concentration of condensable vapor available (see Eq. 3.3).

The coagulation process The loss of particle number concentration of diameter i due to self-coagulation and coagulation onto larger particle of diameter j is given by Eq. (3.9):

$$\frac{dN_i}{dt} = -\left(\frac{1}{2}K_{ii}Ni^2 + \sum_i K_{ij}N_iN_j\right) \tag{3.9}$$

where K_{ii} and K_{ij} are respectively the intra-modal and inter-modal coagulation coefficient determined from Fuchs (1964) as:

$$K_{ij} = \frac{16\pi \bar{D}_{ij}\bar{r}_{ij}}{\frac{4\bar{D}_{ij}}{\bar{v}_{th,ij}\bar{r}_{ij}} + \frac{\bar{r}_{ij}}{\bar{r}_{ij}+\bar{\lambda}_{ij}}} \tag{3.10}$$

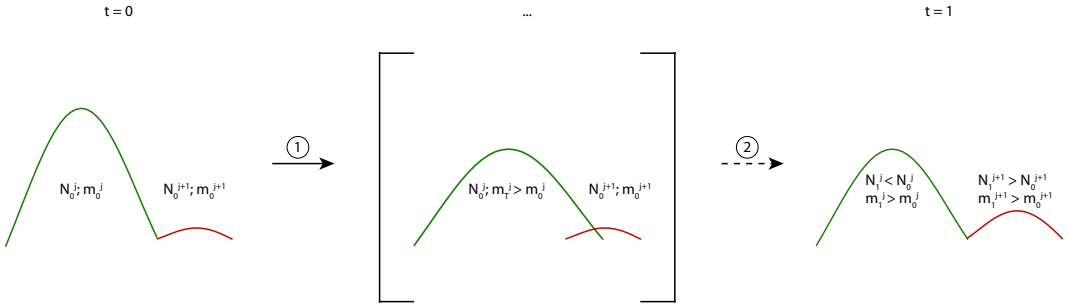

Figure 3.7: Evolution on the represented size distribution in case of condensation and coagulation on the green mode only. The first arrow (1) illustrates the condensation and coagulation processes on the green mode, the second arrow (2) represents the particle number and mass reallocation process from the green to the red mode.

where $\bar{D}_{ij}$, $\bar{v}_{th,ij}$ and $\bar{\lambda}_{ij}$ are respectively the diffusion coefficient, thermal velocity, and mean free path length for an aerosol with radius $\bar{r}_{ij}$, the mean of the geometric mean radii of the modes i and j.

The evolution of the aerosol population Condensation and coagulation processes affect the particle population of each size sections at each time step. They increase the mean radius of each particle, and particles in a given bin will growth into the adjacent larger size domain. The way particles move from one bin to another play a central role in the accuracy of the model predictions. This problem, called the *numerical diffusion*, results in the fact that each mode is allowed to growth in a restricted fixed size domain (Tab. 3.3). Since the modes are defined by a log-normal distribution, the number and mass concentration distribution within the mode can be calculated using the cumulative log-normal distribution function. The procedure for mass and number transfer is represented on the figure 3.7. The reallocation process is represented by the dot line arrow and it occurs only if the mass m_T^j is greater than the theoretical mass of the mode i if all particles have the diameter $r_T = \exp\left(\frac{\log(r_{min,j})+\log(r_{max,j})}{2}\right)$. Then all particles with a radius greater than the upper limit $r_{max,j}$ of the mode j, are transferred with their corresponding mass to the mode $j+1$.

3.4.2.2 Thermodynamic, chemical and aerosol physical inputs

The M4-NPF model is a box-model, which does not require many inputs. Furthermore, those inputs depend on the complexity of the modelled phenomenon. In its present version, only one chemical species is represented so parameters such as vapor diffusion coefficient or particle density must be adjusted depending on the considered chemical component. The table 3.4 summarizes the inputs of the model.

Table 3.4: Inputs of the model M4-NPF

Input	Variable / Parametrization
Time of simulation	from 1 second to the day scale
Thermodynamics	T, P, RH values or time-dependant evolution
Gas & Particle	Diffusion coefficient, density, molecular mass
Condensable vapors	Punctual *versus* time-dependant source
Pre-existing particle	Particle mass distribution & Source rates

Chapter 4

Field studies of new particle formation events at different altitude stations

Contents

4.1 New particle formation at high altitude locations: Study at a high alpine site in Switzerland

This section has been published under the reference:

Boulon, J., Sellegri, K., Venzac, H., Picard, D., Weingartner, E., Werhle, G., Collaud Coen, M., Bütikofer, R., Flückiger, E., Baltensperger, U. and Laj, P.: New

particle formation events and ultrafine charged aerosol climatology at a high alpine site (Jungfraujoch, 3580 m a.s.l), *Atmospheric Chemistry and Physics*, 10, 9333-9349, doi:10.5194/acp-10-9333-2010, 2010.

Nucleation and new particle formation events at high altitude locations is still poorly documented compared to PBL locations. The study conducted by Venzac et al. (2008) showed that the nucleation could be enhanced by the altitude. Furthermore, the role of ions is suspected to be more important at high altitude locations since the galactic cosmic ray flux should be less attenuated (see for example Yu, 2002; Kazil and Lovejoy, 2004). During the EUropean Integrated project on Aerosol Cloud Climate and Air Quality Interactions (EUCAARI), a NAIS was installed from April 2008 to May 2009 at the Sphinx research laboratory located on the Jungfraujoch, a Swiss Alpine mountain which culminate at 3580 m above the sea level. The goal was i- to detect and characterized nucleation events (frequency, seasonality, GR and J) and ii- to quantify the role of ions in the new particle formation process a this high altitude site.

4.1.1 Measurements

The Jungfraujoch is situated on the Northerly crest in a saddle between the mountains Mönch (4099 m a.s.l.) and Jungfrau (4158 m a.s.l.), and belong to the glacier accumulation zone. Aerosol measurements were performed at the Sphinx laboratory located on the southern side of the Jungfraujoch at 3580 m a.s.l. (46°32'51" N, 7°59'6" E), Switzerland, 100 m below the main crest of the Bernese Alps. Jungfraujoch is a station of the Global Atmosphere Watch (GAW) program. Therefore, among other parameters, the total aerosol number concentration, light absorption and scattering coefficient at various wavelength are routinely measured at the site (Collaud Coen et al., 2007). Additionally, the size distribution between 16 and 570 nm is measured by a custom built SMPS. Meteorological parameters are monitored at the Swiss National Monitoring Network for Air Pollution (NABEL), located within a horizontal distance of 150 m, at the top of the crest (3580 m a.s.l.). The monitored parameters include thirty minute averaged concentrations of NO, NO_2, NO_x and O_3, and daily averaged concentrations of SO_2, aerosol sulfur, and particulate matter with aerodynamic diameter below 10 µm (PM10). Neutron measurements were performed on the terrace of the Sphinx laboratory with an IGY neutron monitor which is composed by 18 counter tubes (Flückiger and Bütikofer, 2009). The campaign dataset is composed of 309 days starting from the 9th April 2008 to the 5th May 2009 with 83 days of interruption due to instrumental failures. The measurements are performed with an instrument which classifies total particles (charged and neutral), and negative and positive atmospheric ions according to their electrical mobility.

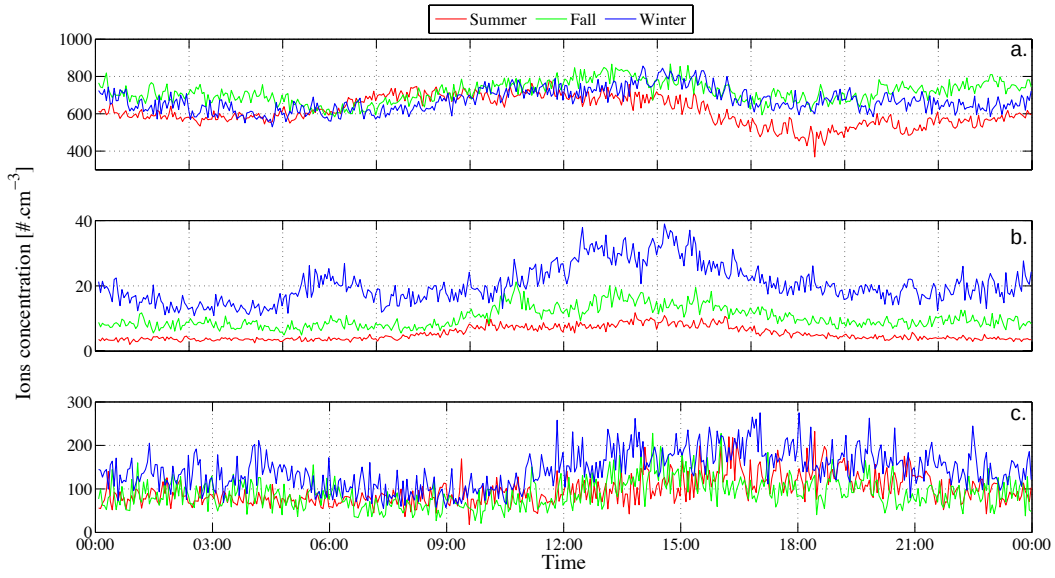

Figure 4.1: Median diurnal variation of positive ion size class concentrations from July 2008 to April 2009. a. Cluster ions, b. Intermediate ions and c. Large ions. *Summer: Jul - Sep 2008, Fall: Oct - Dec 2008, Winter: Jan - Mar 2009.*

4.1.2 Air mass analysis

The impact of the air mass origin and trajectory on the charged aerosol concentration and on the potential of nucleation is studied after calculation of three days air mass back trajectories using the HYSPLIT transport and dispersion model (Draxler and Rolph, 2003). Three days prior sampling were chosen based on the turnover time of aerosol particles, evaluated to be from $1.6 - 1.7$ days for nuclei size ranges, to 2.4 days for 200 nm particles Tunved et al. (2005). The calculation is performed over the whole field campaign period every 12 hours at 00:00 and 12:00 Local Time (LT).

4.1.3 Results

4.1.3.1 Ultrafine charged aerosol climatology

The yearly median total ion concentration (Fig. 4.1) presents a diurnal variation pattern. During the night, the concentration of ions is quite stable with a mean concentration of 678 #.cm^{-3} for negative ions and 709 #.cm^{-3} for positive ones. From 06:00 LT, the concentration of both polarities increase until reaching a maximum of 825 #.cm^{-3} and 875 #.cm^{-3} respectively for negative and positive ions at 13:00 LT. Then the concentrations decrease rapidly from 15:00 to 18:00 LT to reach the level of night time.

Baltensperger et al. (1997) showed that diurnal variations of aerosol parameters such as surface area are due to thermally driven vertical exchange. In their article, Lugauer et al. (2000) have demonstrated that during winter the Jungfraujoch is most of time decoupled from the PBL and, during the summer, air from the PBL is transported to the site by thermally driven convection. Zellweger et al. (2000) were more restrictive and

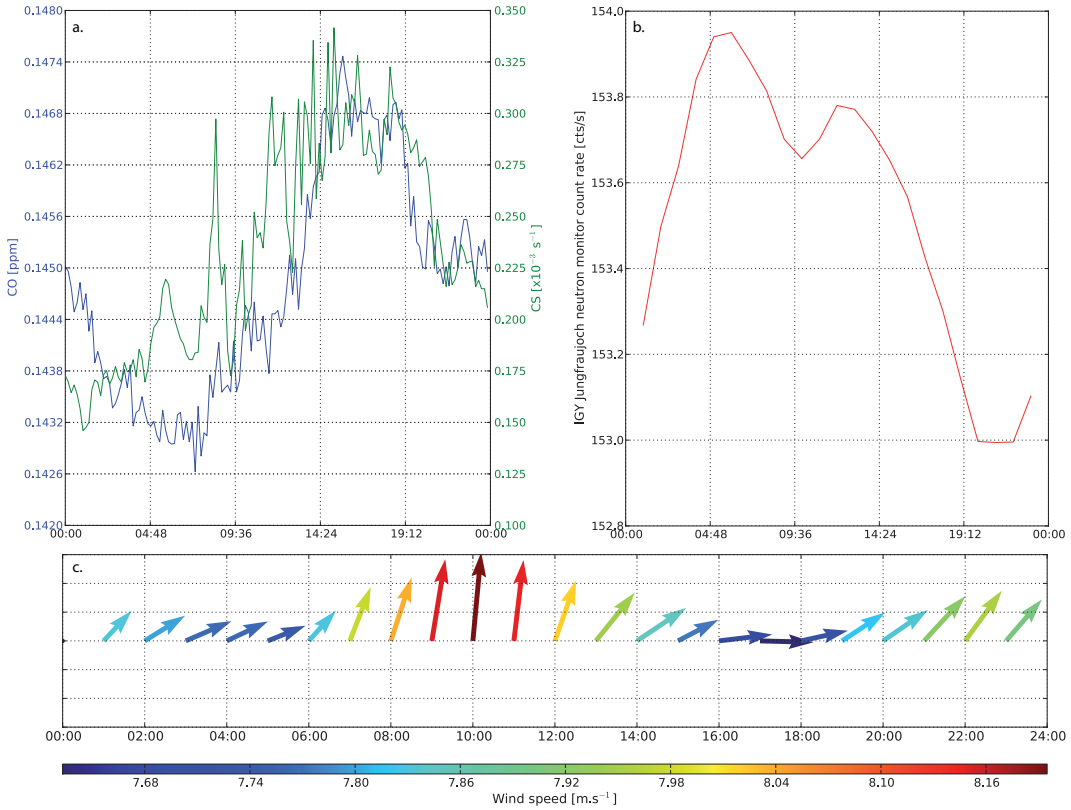

Figure 4.2: a. Mean diurnal variation of carbon monoxide (blue) and condensational sink (green) (*left panel*), b. neutron monitor count rate (red) (*right panel*) and c. wind direction and speed (*bottom panel*).

showed that during summertime, night time measurements with northwesterly advection are considered to represent FT conditions according to the NO_y speciation. Another study made by Forrer et al. (2000) confirms the transportation of some gases (e.g. CO) is made by thermally driven vertical transport which occurs during daytime. Finally, night time measurements from 03:00 to 09:00 were considered representative of FT conditions for Jungfraujoch (Weingartner et al., 1999) but also for other high altitude sites in Europe (puy de Dôme, Venzac et al., 2007) and high altitude Himalaya (Venzac et al., 2008). Here, we calculated the diurnal variation of CO, CS, neutron flux and wind direction and speed averaged over the measurement period (Fig. 4.2). The clear diurnal variation of the CO concentrations and CS with a maximum at mid-afternoon and the positive correlation between these two variables ($r = 0.7373$) confirms the influence of the PBL at the measurement site during the day. This is also confirmed by the typical wind pattern of valley breezes shown on Fig. 4.2 c. Considering the pre-cited studies and the diurnal variation of aerosol and CO concentrations, CS and wind direction observed at Jungfraujoch over the measurement period, the data set has been segregated into two sub data sets composed of night time measurements on one hand, and day time measurements (from 09:00 to 18:00 LT) on the other hand.

The total ion concentration measured at night (Fig. 4.1) can be considered as a FT

ion nighttime background, while the increase of ion concentrations during the day is likely due to advection of ions or ion sources from the planetary boundary layer. Ions are classified in three different size classes: the cluster ions from 0.5 to 1.8 nm, intermediate ions from 2.1 to 6.8 nm, and large ions from 8 to 47 nm.

Clusters are considered as embryos for new particle formation and growth, they are found to be ubiquitous in the atmosphere (Kulmala and Kerminen, 2008), intermediate ions concentrations usually increase only when a NPF is occurring (see Venzac et al., 2007, 2008), lastly large ions can be disconnected from the new particle formation events and be linked to external incoming of polluted air parcels. Total ion concentrations are dominated by the cluster ions concentrations, which drive the observed diurnal variations. The known sources of ions are either radioactive species such as radon, or cosmic rays (CR). Due to the local cosmic rays anisotropy, regular daily variations of the CR flux is estimated to be on average 1% (Usoskin and Kosvaltsov, 2008). Other variations of CR fluxes could be more important but on timescales larger than the day. As a proxy of atmospheric ionization and CR flux, the neutron flux was analyzed using neutron counter measurements (Aplin et al., 2005). The observed diurnal variation of neutron flux during this field campaign was 0.16%. Since the observed diurnal variation of charged cluster concentrations (average 22.5%) is higher than the one of CR flux proposed by Usoskin and Kosvaltsov and higher than the diurnal variation of neutron flux measured during the field campaign, it can be concluded that the cosmic rays are not the major ion source at the measurement site and that radioactive species such as radon is mainly responsible of the ion production at this altitude. In the PBL, previous studies of ion diurnal variations showed that radon is the main ionizing agent responsible of the cluster ion formation (Hõrrak et al., 2003). Gäggeler et al. (1995) showed that radon concentration at Jungfraujoch is dominated by transport and not by local production since the ground is most of time covered by snow. According to those previous results and to the diurnal PBL injection of air parcels at the measurement site (Fig. 4.1 and 4.2), it is assumed that the diurnal variation of the cluster ions concentration is mainly due to the vertical transport of high radon concentration air parcels from the planetary boundary layer during the day and to atmospheric ionization from GCR or residual radon during the night. However, a deeper study is needed to investigate the respective role of radon and GCR in ions formation at this site using direct correlations.

A weak seasonality of total ions concentration, largely dominated by clusters, was found, opposing high concentrations during fall and winter (no significant difference between them) to low concentrations during summer (Fig. 1). This result is in agreement with the analysis performed by Weingartner et al. (1999) who pointed out that $10 - 18$ nm total particles concentrations showed a maximum during wintertime. A closer look at the diurnal variation of cluster ions shows that summertime cluster ions are lower than winter time cluster ion concentrations especially during the $15:00 - 24:00$ time range. Hence, it is likely that the high concentrations of larger particles drifted up the station

during summertime around this time of the day represent a significant condensational sink for the cluster ions.
The seasonal variation of intermediate ions is also showing a minimum for summer time. During winter, intermediate ions strongly peak between 12:00 and 15:00. This peak could be linked to the presence of clouds, which effects will be studied in the following section.

4.1.3.2 Cloud effects

Clouds are known to have a significant effect on ion clusters and intermediate ion concentrations and on NPF occurrence (Venzac et al., 2007; Lihavainen et al., 2007). Consequently, we chose to further separate potential cloudiness conditions from clear sky conditions and analyze them separately to better characterize the cloud effect on aerosol. Unfortunately, LWC measurements were not available during the field campaign, so RH data were used to segregated in-cloud from out-of-cloud conditions. The limit value of RH used to distinguish out-of-cloud and in-cloud conditions (i.e. $RH \geq 96\%$) was validated using LWC data for the puy de Dôme station and Nepal station (unpublished data). Mean and median ion concentration variations are reported on figure 4.3. In order to determine if differences are statistically significant between our sub-classes (nighttime/daytime, in-cloud/out-of-cloud, positive/negative polarity), a T-test was performed on the data set. For the cluster size classes, ion concentrations decrease by a factor of 1.5 to 2.5 when the conditions change from out-of-cloud to in-cloud (Fig. 4.3, a). Intermediate ions concentrations are, on the contrary, surprisingly increased by the presence of a cloud, especially for the negative ions. The observed effect of clouds on cluster ions is in agreement with the results reported by Venzac et al. at the puy de Dôme station (Venzac et al., 2007) and Lihavainen et al. (2007), who argue that the cloud is a powerful scavenger for cluster ions. Cloud effects on intermediate ions, however, are different according to the measurement site : in clouds, the intermediate ion concentrations decrease at the PBL forest site of Hyytiälä (Lihavainen et al., 2007), but remain unchanged at the altitude site of puy de Dôme (Venzac et al., 2007) and increase at the high altitude site of Jungfraujoch (this study). Further studies are necessary to understand this phenomenon especially the role of cloud microphysics, which should be investigate deeper.
Concerning the large ion mode, as expected for this size, negative and positive ion population are close to equilibrium under clear sky conditions. In the presence of a cloud, the two populations are increased by a factor 1.4 (41%) and 1.2 (20%) respectively for positive and negative ions. Figure 4.3 (b) is showing the mean ion concentrations (as opposed to the median ion concentrations shown figure 3a). The mean out-of-cloud concentrations are not significantly different from the median concentrations. However, the in-cloud mean ion concentrations are different from median in-cloud ion concentrations, indicating that intense sporadic events are taking place under cloudy conditions. From

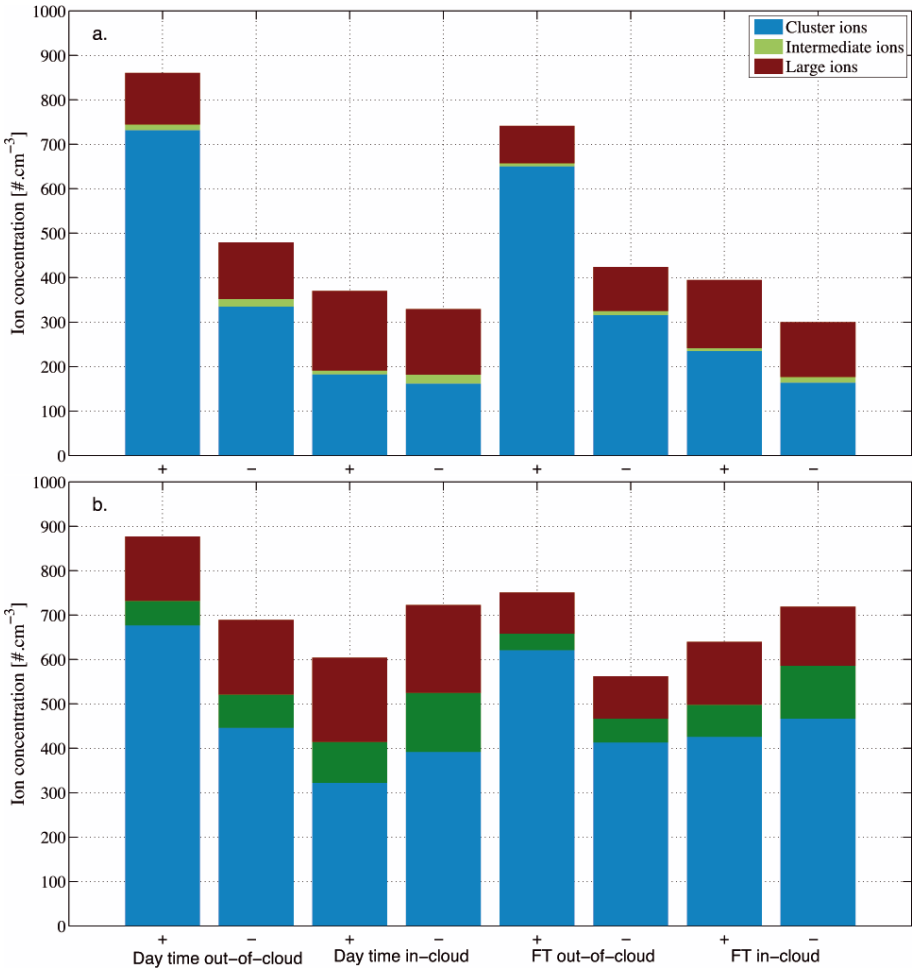

Figure 4.3: Yearly median (*top panel*) and mean (*bottom panel*) concentration cluster (blue), intermediate (green) and large (red) ion concentrations from July 2008 to April 2009 on daytime and nighttime under clear sky and cloudy conditions.

the comparison between median and mean ion concentrations in cloud, we conclude that cloud conditions favor the production of sporadic high concentrations of cluster and intermediate ion positive and especially negative ions.

Clouds have a complex effect on ions, particles and gas concentrations. Consequently, in order to understand the impact of other parameters on nucleation and NPF, it is important to segregate in-cloud from out-of-cloud conditions at altitude sites. This will be done in the following sections.

4.1.3.3 New particle formation event analysis

Event statistics The 309 days of data were analyzed and classified into event, non-event and undefined days. Undefined days (25 days) represent only 8.1% of the data, 73.8% of observed days were classified as non-event days (228 days) and among those days, 59% (135 days) were classified as "in cloud" conditions. NPF events were observed on 17.5% of days (i.e. 54 days). Monthly statistics are shown on Fig. 4.4 and class occurrence of NPF event as defined chapter 3, section 3.3.1. are presented Table 4.1. New particle

Table 4.1: Nucleation event statistics.

Class of nucleation	Occurrence
Ia	3
Ib	14
II	17
Bump	16
Featureless	4

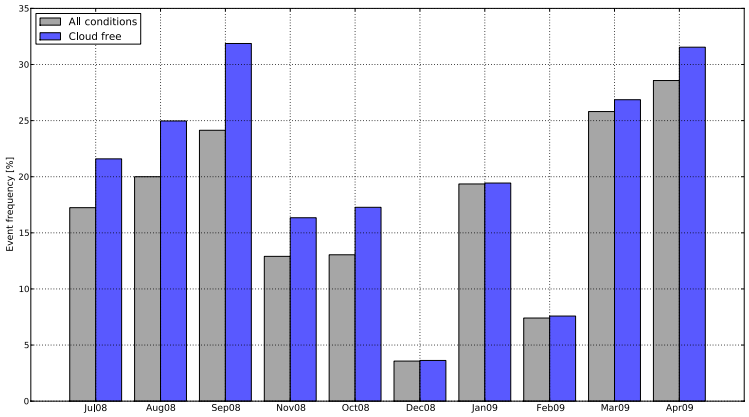

Figure 4.4: Monthly frequencies of nucleation/new particle formation events. *Grey bars : events according to the total number of days ; Blue bars : events according to the number of clear sky days.*

formation frequencies present a clear seasonality with a minimum of events during winter and maximum from spring to autumn. The maximum of events occurred in April 2009 (28.6% of observed days present an event) and the minimum during December 2008 (3.6% of observed days). An especially high frequency of nucleation event (highest number of Ib events) was observed during January 2009. Meteorological parameters and air mass origin analysis do not show significant differences compared to other months. A longer study of nucleation events at Jungfraujoch is needed to statistically characterize this seasonality. At other sites where a NPF events seasonal variation could be studied, the maximal occurrence was usually observed during the spring and autumn seasons as well (Manninen et al., 2010), and during the summer season for altitude sites (Venzac et al., 2008) while the minimal occurrence frequency is always observed during winter (Venzac et al., 2008; Manninen et al., 2010; Boulon et al., 2011). The seasonal variation of the frequency of NPF events is opposite to the seasonal variation of ion cluster concentrations previously mentioned. Hence, the concentration of preexisting cluster ions is not necessarily linked to NPF events at the Jungfraujoch station.

The presence / absence of a cloud during NPF days was checked for all the NPF days and it appears that clouds reach the measurement site during the NPF process for only 4 days (7.1% of NPF observed days). Furthermore, when a cloud occurs during the event

the nucleation / growing process is stopped. Considering the low frequency of nucleation during cloudy conditions and the fact that clouds interrupt the NPF process, the hypothesis that cloudy conditions inhibit the new particle formation process is confirmed. This phenomenon has to be linked with 1.- the lack of production of condensable species by photochemical processes, 2.- the scavenging property of cloud droplets which could remove clusters or/and condensable vapors from the atmosphere (Baltensperger et al., 1998) and 3.- the significant increase of the CS (due to the high surface area droplets offer for condensing). However, even though clouds seem to affect the frequency of NPF events, they do not drive their seasonal variation. Indeed, the maximum of cloud frequency is observed during summer. Hence, the seasonal variation of the frequency of NPF events is even more pronounced when considering only out-of-clouds conditions (Fig. 4.4).
Parameters influencing the new particle formation frequency was further investigated considering different atmospheric components such as H_2SO_4 concentration, H_2SO_4/CS, UV radiation and UV/CS (Fig. 4.5). Since no H_2SO_4 direct measurements were conducted during the field campaign, the sulfuric acid proxy proposed by (Petäjä et al., 2009) was used with Hyytiälä's parameters (Eq. 4.1 where $k = 8.8 \times 10^{-7}$ $m^2.W^{-1}.s^{-1}$). Hence H_2SO_4 real concentrations could be very different from our calculations, but their time variations should be respected.

$$Proxy([H_2SO_4]) = k \times \frac{[SO_2] \times UVB}{CS} \tag{4.1}$$

Even if a slight positive correlation between H_2SO_4 concentrations and nucleation frequency exists ($r = 0.067$), the proxy cannot explain the observed nucleation frequency. Furthermore, the nucleation frequency is anti-correlated with H_2SO_4/CS and UV/CS ($r = -0.419$ and $r = -0.227$ respectively) and hence positively correlated with the CS ($r = 0.471$). In fact, the strongest correlation is found to be the one with UV radiation alone ($r = 0.552$). Those results suggest that 1- other compounds than H_2SO_4 such as VOCs must be involved in the new particle formation process as previously shown by Laaksonen et al. (2008) and Paasonen et al. (2009) respectively in the boreal forest environment and at a forest high elevation site (Hohenpeissenberg, 980 m a.s.l.), and in smog chambers by (Metzger et al., 2010), and, 2- the new particle formation process at Jungfraujoch is linked to polluted air parcels incoming since the events are positively correlated with the condensational sink.

Charged and neutral particle formation rates and the role of ions in nucleation at Jungfraujoch Ions significantly contribute to new particle formation events, as previously shown by Arnold (1980); Yu and Turco (2001). In order to quantify the role of ions in the nucleation process at Jungfraujoch, the charged and cluster formation rate and the ion-mediated fraction were calculated for 2 nm particles.
The analysis of the 2 nm charged particle formation rates ($J_2^{\pm}$, Table 4.2) shows that neg-

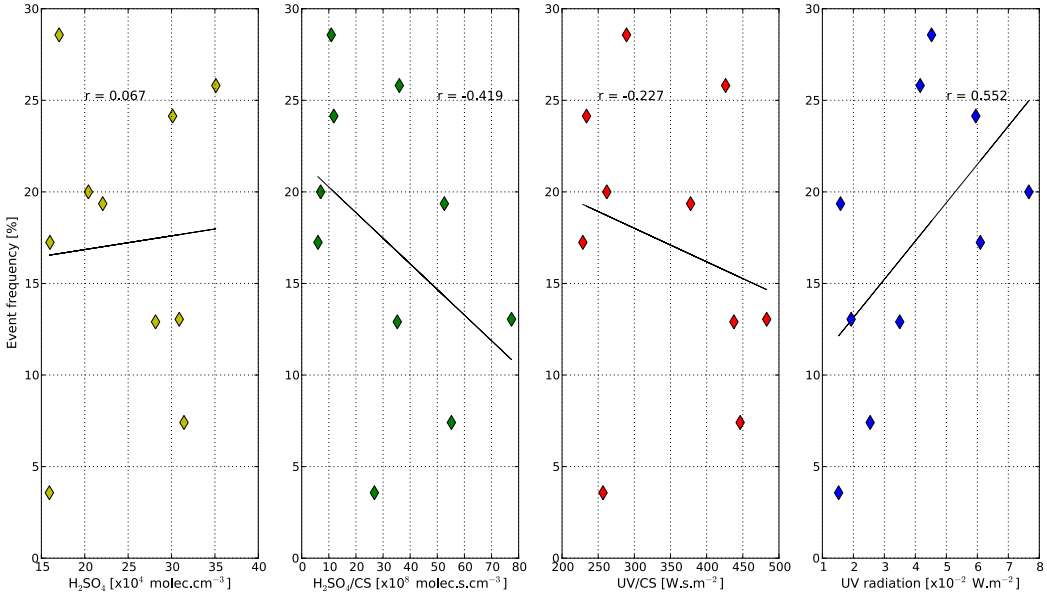

Figure 4.5: Relation between events frequency and atmospheric components.

atively charged particle formation rate is always higher than the one of positive particles whatever the class of event (Ia or Ib). Within the accuracy of the method, the total particle formation rates J_2 (Eq. 3.4) were estimated from the data provided by the particle mode of measurement of the NAIS. This was done in order to quantify the importance of the ion-mediated nucleation in this environment. The median J_2 was found to be 8.8 times bigger than the median $J_2^{\pm}$ (Table 4.2). In other environments such as the boreal forest, J_2 is at least one order of magnitude bigger than the charged particle formation rate (Manninen et al., 2009). This indicates that ion-mediated nucleation (IMN) is relatively important at Jungfraujoch. In order to investigate the role of ions in nucleation, the IMN fraction is calculated according to Eq. 4.2:

$$\begin{aligned} IMN &= \frac{J_2^+ + J_2^- + J_{2,rec}}{J_2} \\ \text{where} \quad J_{2,rec} &= \delta \times \alpha \times N_i^+ \times N_i^- \end{aligned} \tag{4.2}$$

where δ is the probability that a collision between two ions of both polarities leads to the formation of a stable neutral cluster (here it is assumed that $\delta = 1$), α is the ion-ion recombination coefficient, $N_i^{\pm}$ is the concentration of ions which size range were selected in order that the diameter of the resulting neutral diameter was in size range $2-3$ nm. IMN shows a large range of values depending of the event day with a median value of 22.3%. Manninen et al. (2010) have computed ion-induced nucleation rate (IIN) which can be derived from Eq. 4.2, assuming $J_{2,rec} = 0$ cm^{-3}.s-1. IIN contribution to nucleation event at Jungfraujoch is 21.8%. This value is higher than the one computed by Manninen et al. (2009) for the boreal environment suggesting that IIN is more important for nucleation events at Jungfraujoch than at lower altitude sites. The median value of J_2^+, J_2^- and J_2 at

Table 4.2: Details of nucleation characteristics. *Atl. is for Atlantic and EaE. for Eastern Europe.*

Date	Class of event	$GR_{1.3-3}$ [nm.h^{-1}]	GR_{3-7} [nm.h^{-1}]	GR_{7-20} [nm.h^{-1}]	J_2^+ [#.cm^{-3}.s^{-1}]	J_2^- [#.cm^{-3}.s^{-1}]	J_2 [#.cm^{-3}.s^{-1}]	Air mass Origin
19/04/2008	Ib	6.8	9.1	6.3	0.17	0.21	2.09	–
10/07/2008	Ia	4.2	3.6	4.4	0.18	0.28	2.08	Atl.
06/08/2008	Ib	5.7	–	–	0.10	0.15	1.89	Atl.
30/08/2008	Ib	6.9	–	–	0.21	0.21	3.84	Atl.
23/09/2008	Ib	2.8	1.1	4.9	0.14	0.28	0.72	EaE.
26/09/2008	Ib	2.0	1.8	2.3	0.06	0.14	1.17	EaE.
13/11/2008	Ia	6.1	8	5.7	0.82	1.21	1.40	Atl.
14/11/2008	Ib	3.2	3.3	3.6	0.22	0.38	1.05	Atl.
26/12/2008	Ib	6.6	2.3	10.3	0.57	0.78	5.41	EaE.
20/01/2009	Ib	6.0	7.1	8.0	0.18	0.52	2.03	Atl.
19/03/2009	Ia	5.7	11.7	6.0	0.35	0.28	7.46	Atl.

Jungfraujoch are respectively 0.19, 0.28 and 2.03 cm^{-3}.s^{-1}. According to Manninen et al. (2010), $J_2^{\pm}$ found at Jungfraujoch is similar to the $J_2^{\pm}$ computed for many other sites in Europe, while it is the J_2 found at Jungfraujoch which is significantly lower than the J_2 found at other places in Europe. The fraction of ion-mediated nucleation is hence higher than at other sites because of the lower neutral nucleation detected at this high altitude site. This finding is conflictual with the results from Mirme et al. (2010) who found no sign of an enhance role of ion-induced nucleation toward the tropopause. It is worth mentioning that our J_2 calculation is a higher limit, since 3 nm particles concentrations detected with the SMPS technique were measured to be lower than the 3 nm particles detected from the NAIS. According to those results, ion-mediated nucleation appear to be a significant source of new particle in the troposphere as previously shown by Yu et al. (2008) for boundary layer conditions.

Growth rates analysis Growth rates were calculated for Ia and Ib events (detailed growth rates and formation rates are reported Table 4.2).

GR can vary over different size ranges of nanometer sized particles because 1- the condensable surface do not grow linearly with size and 2- the condensable gases concentrations vary with time (with the intensity of photochemistry for instance). These reasons usually lead the analysis of nanoparticle growth rates to be split in several size ranges. In fact, given the uncertainty on the calculated GRs. The mean growth rate values for class I events in each size class are [5.1±1.7, 5.3±3.5, 5.7±2.2] respectively for $1.3-3$, $3-7$ and $7-20$ nm size classes, showing that the growth was rather constant from 1.3 to 20 nm. No significant differences were found between the class Ia and class Ib regarding the mean growth rates.

Concentrations of condensable vapors and source rates were calculated from GRs values according to Dal Maso et al. (2002). Gaseous source rates at Jungfraujoch are relatively low (5.12 ± 3.8 $\times 10^3$cm^{-3}.s^{-1}) compared to those observed in the boreal forest or in coastal environment (from 1.1 to 52 $\times 10^5$cm^{-3}.s^{-1}). This difference is not surprising

since boreal forests and coastal environments are known to house high biological sources of condensable vapors, such as VOC emitted from the vegetation or iodine compounds emitted from exposed sea weed fields.

In Hyytiälä, growth rates are respectively 1.9, 3.6 and 4.2 nm.h^{-1} for the size classes $1.3-3$, $3-7$ and $7-20$ nm (Manninen et al., 2009). It is surprising that the Jungfraujoch GRs are higher than at a high volatile organic compound (VOC) concentration sites such as the boreal forest. On another hand, the condensational sink ($\bar{CS} = 2.39 \pm 1.56$ $\times 10^{-4}$s^{-1} for all days, and for out-of-cloud conditions $\bar{CS}_{events} = 2.90 \pm 1.12$ $\times 10^{-4}$s^{-1} and $\bar{CS}_{non-events} = 2.54 \pm 1.52$ $\times 10^{-4}$s^{-1}) at Jungfraujoch is so low that even limited concentration of condensable vapors can trigger new particle formation easily. To compare to other sites, this CS value is lower than the one computed by Venzac et al. (2007) for the puy de Dôme altitude station ($\bar{CS} = 58 \times 10^{-4} s^{-1}$) or for the NPO-P station (Venzac et al., 2008; $\bar{CS} = 15.6 \pm 3.6 \times 10^{-4} s^{-1}$), and according to Manninen et al. (2010), the Jungfraujoch CS value is the lowest of the 12 european EUCAARI measurement sites. The GRs calculated in this work differs slightly form the one computed in Manninen et al., 2010 (i.e. $GR_{1.3-3} = 3.7$ nm.h^{-1}), due to differences in the calculation methods and to some subjectivity on the choice of the time lap over which the growth is calculated. The difference between the GRs calculated in this work and the ones given in Manninen et al. gives an idea of the uncertainty associated to this parameter. Mean values of growth rates for mountain sites present a large scale of variation due to local biogeography. Venzac et al. (2008) have detected NPF events on Everest (5079 m a.s.l.) with an AIS during February−March 2007 and the mean GR value was estimated at 1.8 ± 0.7 nm.h^{-1}. Mean value for puy de Dôme is 5 ± 3.5 nm.h^{-1} for the period between March 2006 and December 2007 (Venzac, 2008). An extended study made by Boulon et al. (2011) provides more accurate mean values: 3.22 ± 0.25, 6.52 ± 0.20 and 8.85 ± 0.14 nm.h^{-1} for $1.3-3$, $3-7$ and $7-20$ nm size classes. The mean GR for the entire nucleation mode ($1.3-20$ nm) is 6.20 ± 0.12 nm.h^{-1}. At Mt. Norikura, Japan (2770 m a.s.l.), Nishita et al. (2008) have calculated a mean GR of $2.6-3.1$ nm.h^{-1} between September 2001 and August − September 2002 measurement period. Shaw (2007) reports higher GR from 10 to 23 nm.h^{-1}, at Mt. Lemmon, Arizona (2790 ma.s.l.). Those last high values of growth rate are explained by the authors as the result of high organic vapor concentration from desert vegetation associated with high UV-A radiation.

4.1.3.4 Air mass origin analysis

In this subsection, the impact of the air mass origin on the occurrence of the new particle formation process is investigated. Air masses were classified according to their geographical origin with a resolution of $10° \times 10°$ (Fig. 4.6).

According to the Hysplit model, all air masses originate from more than 2500 m a.s.l. but since this model uses as input data meteorological variables with 10° of resolution, it cannot describe local air mass motion such as topographical effects or convection. As-

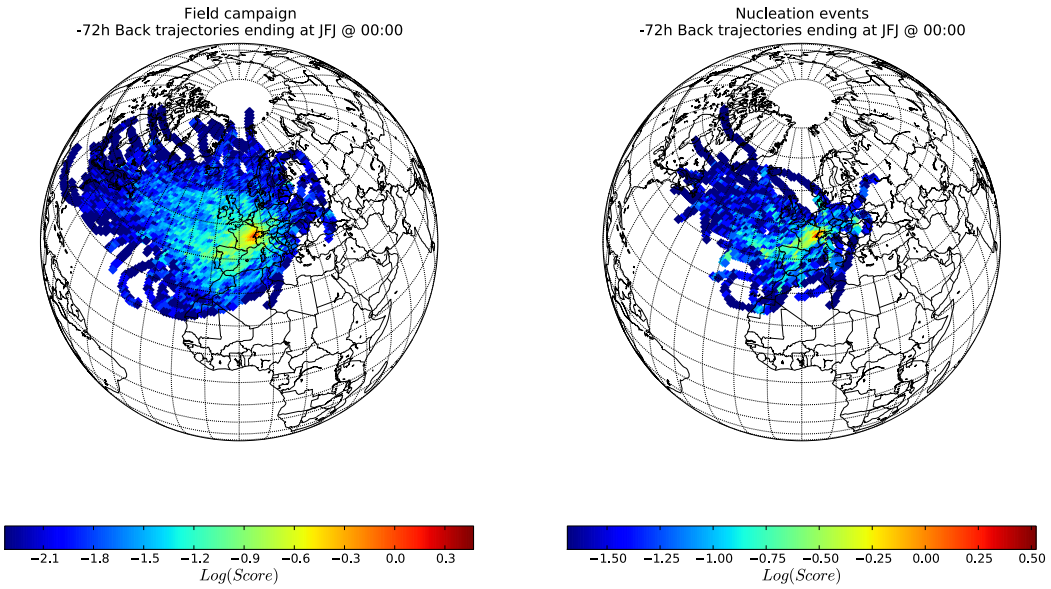

Figure 4.6: Three days air mass backtrajectories ending at the measurement site at 00:00 LT for all the field campaign (*right panel*) and for new particle formation events (*left panel*). The score is the number of occurrence of a given geographical position.

suming that, altitude outputs are overestimated for high altitude sites and will not be discussed further. Five different classes were created depending of the air mass' origin: Atlantic, African, Nordic, Eastern and Western European air masses. Atlantic (68.5%) and European continental origin (respectively 6.4% and 14.2% for eastern and western Europe origin) represent the highest proportion of air mass origin ending at Jungfraujoch (89.1%) followed by african (7.5%) and nordic (3.4%) air masses. The new particle formation event frequency for each air mass type is reported on Table 4.3 and it appears that air mass from Eastern Europe (latitude:]40N; 70N[and longitude: [20W and more]) have the highest probability to lead to a NPF event, while the lowest probabilities of new particle formation events are found in the air masses from Western Europe (latitude:]40N; 70N[, longitude:]10W;20W[if latitude $<$ 60N, else longitude]0;20W[) and Nordic area (latitude $\geq$ 70N). This is rather different from the air mass dependencies found in the boreal forest, where nordic air masses were found to favor NPF event as shown by Sogacheva et al. (2005). In the boreal forest where high concentrations of condensable species are emitted from the vegetation, the absence of a preexisting condensational sink seems to be a strong condition for the occurrence of NPF events.

In the case of the Jungfraujoch, which can be described as a low preexisting condensational sink environment, the presence of condensable vapors from polluted areas (typically from Eastern Europe which is known to be an hotspot of non-methane volatile organic compounds as shown by Lanz et al., 2009) seems to prevail in the occurrence of NPF events. Eastern Europe air masses show the highest CS on NPF event days (Table 4.3), confirming this hypothesis. The new particle formation mechanism can also be partly

Table 4.3: New particle formation events according to air mass origin.

Air mass origin	Nucleation from air mass origin [%]	Nucleation frequency of the air mass [%]
Atlantic	58.3	15.4
Africa	12.5	16.2
Nordic	2.1	10
Eastern europe	20.8	33.3
Western europe	6.3	8.6

examined by studying the dependency of preexisting clusters on the air mass origin, for event and non-event days. Mean size distributions are calculated before nucleation occurs (03:00-06:00 LT), and during the NPF events (09:00-12:00 LT), again under clear sky conditions, in order to exclude air mass related to cloud effects (Fig. 4.7, a and b).

Non event days We clearly observe from figure 7a, that while the cluster mode does not experience any variation according to the air mass origin, the intermediate ion mode shows a stronger variability. In fact, in Nordic air masses, the intermediate ions concentrations are highest (see Table 4.3) whereas in air masses from Eastern Europe, concentrations are the lowest. In other air masses, concentrations are similar one to the other. During non-event days, the size distribution of charged aerosol particles (Fig. 4.7, top panel) show a weak diurnal variation in all air mass types, with higher concentrations of intermediate and large ion size classes during the afternoon compared to night. This pattern permits to quantify the increase of concentrations solely due to the updraft of charged particles or ion sources (i.e. radon) form the valley by thermally driven convection. The situation is very different for event days.

Event days During the new particle formation event days, size distributions of ions and charged particles are very different from those of non event days even before nucleation occurs (between 03:00 and 06:00 LT, Fig. 4.7, bottom panel), but, based on a T-test analysis, considering all events, the cluster concentration does not differ from event to non-event days prior to NPF so differences are observed for intermediate and large size classes. For atlantic and african origin the main difference is observed for intermediate ions concentration which is four times lower for event days. The situation is completely different for air masses from eastern and western europe which present a higher intermediate ions concentration for events days (respectively 13.1 and 2.6 times more). Finally, nordic air masses present a high concentration of intermediate ions compared to others origins for both event and non-event days. This is probably due to the fact that nucleation has already occur in these air masses which is consistent with previous work which have shown that nordic air masses favor NPF event and hence present the highest nucleation mode concentration (Sogacheva et al., 2005). Those air masses, contrarily to the other,

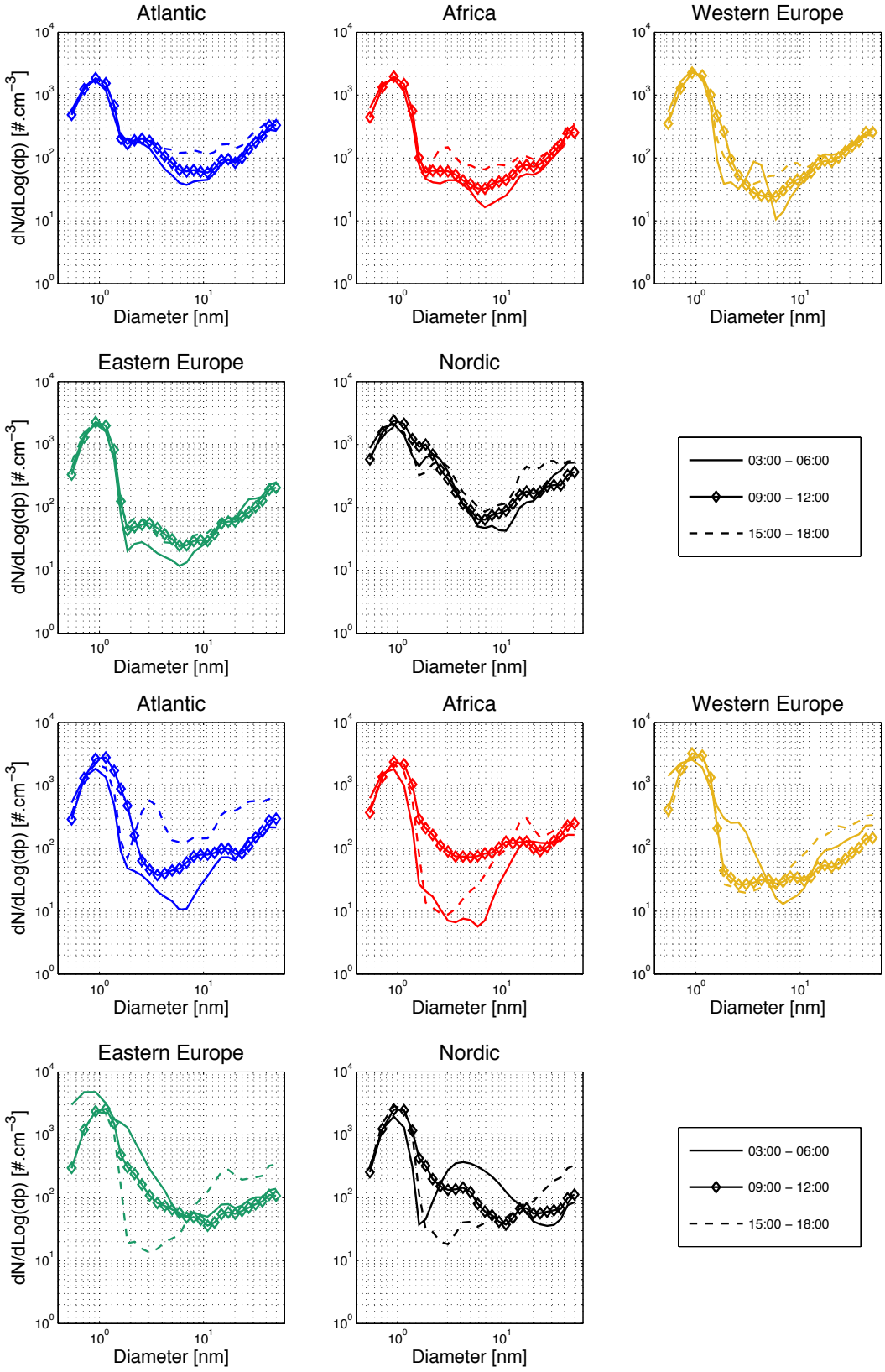

Figure 4.7: Positively charged aerosol distribution of different types of air mass origin endings at Jungfraujoch at 00:00 LT for non event days (*top panel*) and event days (*bottom panel*).

present variation for the large ions concentration which is 2.4 times lower during event days prior to NPF.

During the new particle formation process (between 09:00 and 12:00) though, the cluster mode concentration increases by a factor 1.5 ± 0.3 and its geometric mean diameter shifts to larger diameters (typically from 0.8 nm to 1 nm or more) in all air masses but the Eastern Europe air masses. This result indicates that in most air masses, the formation of new clusters does occur during a NPF event.

In Eastern air masses, the pre-existing cluster concentrations are more than three times higher on event days compared to non event days, and during the NPF event no more cluster ions are formed, showing that it might be predominantly the growth of pre-existing clusters rather than nucleation of new clusters which contribute to the NPF events in eastern Europe air masses.

These observations agree with the conclusion of the study of Lehtipalo et al. (2010), in which it is shown that in some environments, NPF are driven by condensation of condensable gazes onto preexisting clusters rather than by nucleation of new clusters. Furthermore, this result can be linked to results obtained by Metzger et al. (2010) who show that the concentration of condensable vapors plays a key role in the nucleation and growth process as predicted by Kulmala et al. (2000, 2006).

After the NPF event, the intermediate ion concentrations decrease by growing to sizes beyond the upper diameter bound of the instrument. The impact of NPF on the size distribution can be evaluated by comparing the increase of large ion (which diameter is higher than 8 nm) number concentration from 03:00−06:00 to 15:00−18:00 for non event days with the same increase during event days (Table 4.4). The increase of large ions concentrations is significantly higher (by a factor 2.3 ± 1.0) on event days than on non event days except when air masses come from the Nordic areas (Table 4.4). This is probably due to the fact that NPF linked to nordic air masses are not type I events i.e. not intense or not complete. This result reveals that new particle formation events could significantly increase the number concentration of particles in the free troposphere as already suggested by Sellegri et al. (2010). At the NCO-P station (5079 ma.s.l., Nepal), it was shown that new particle formation events occur with a frequency close to 50% of observed days and that upper free troposphere residual layer aerosol composition could be strongly influenced by NPF events.

4.1.4 Summary of this study

The ultrafine charged aerosol concentration variability and new particle formation events were studied using a Neutral cluster and Air ion Spectrometer within the EUCAARI field campaign 2008 − 2009 at the Jungfraujoch research station in the Swiss Alps. Within this campaign, 309 days starting from the 9th April 2008 to the 5th May 2009 were analyzed.

Table 4.4: Comparison of positive ion concentrations for event and non event days. Concentrations are given in [#/cm^{-3}], ΔClusters and ΔLarge ions are computed respectively between (09:00−12:00) and (03:00−06:00), and, (15:00−18:00) and (03:00−06:00) LT. CS values are given for clear sky days.

	Atlantic	Africa	Western Europe	Eastern Europe	Nordic
			Event days		
Clusters (03:00−06:00)	573 ± 46	578 ± 76	978 ± 281	2005 ± 708	524 ± 109
ΔClusters	344 ± 57	196 ± 97	-15 ± 292	-1193 ± 710	262 ± 140
ΔLarge ions	245 ± 268	68 ± 129	68 ± 140	102 ± 26	41 ± 33
CS [$\times 10^{-4}$ s^{-1}]	2.39 ± 1.32	2.35 ± 2.33	3.07 ± 3.54	3.80 ± 0.67	ND.
			Non event days		
Clusters (03:00−06:00)	567 ± 68	573 ± 71	730 ± 55	619 ± 56	779 ± 278
Δ Clusters	36 ± 76	21 ± 81	-3 ± 63	52 ± 76	121 ± 342
Δ Large ions	66 ± 68	41 ± 74	15 ± 184	0 ± 219	136 ± 260
CS [$\times 10^{-4}$ s^{-1}]	2.28 ± 2.48	3.43 ± 4.34	1.78 ± 1.06	2.69 ± 2.45	ND.

A diurnal pattern of the total ions concentration, dominated by cluster ions, was found with a maximum during the day and a minimum during the night. This diurnal variation was related to the updraft of surface layer air parcels rich in preexisting particles and ion sources such as radon from the valley during the day. Cluster ion concentrations were found to be predominantly driven by radon rather than cosmic rays. The charged cluster concentration also shows a weak seasonality with minimum concentrations observed during summer, due to lower afternoon concentrations compared to winter time. This finding is likely due to the high condensational sink due to the updraft of large particles during this season and time of the day.

The statistical analysis of new particle formation events occurrence reveals that event days represent 17.5% of measured days and a seasonality pattern was pointed out with maximum of event frequency during spring and autumn and minimum during winter. This seasonality is opposite to the one of cluster ion concentrations. This is an indication that, on average, the preexisting cluster concentration is not a driving parameter for NPF events occurrence. The NPF frequency is quite low compared to other sites, including high altitude sites. The site is often under cloudy conditions, which inhibit nucleation and new particle formation events, even if they promote sporadic high concentrations of cluster and intermediate ion positive and especially negative ions. When the measurement site is in cloudy conditions, we showed that the cluster ion concentrations are decreased by a factor 1.5 to 2.5. Because cloud droplets efficiently scavenge ions and particles, and presumably because photochemistry is inhibited, NPF were observed to occur only 7.1% of the time under cloudy conditions. However, even though clouds seem to affect the frequency of NPF events, they do not drive their seasonal variation. Indeed, the seasonal variation of the frequency of NPF events is even more pronounced when considering only out-of-clouds conditions.

The ion-mediated nucleation seems to play an important role in the new particle formation process at this measurement site since ions and recombination products

explain 22.3% of the particle formation.
Dependence of the event frequency on atmospheric conditions were investigated and a positive correlation was found between the NPF event occurrence and UV radiation. A weaker positive correlation was also found between nucleation event and H_2SO_4 concentration. Those results suggest that other compounds than H_2SO_4, such as organic vapors, are involved in the nucleation and subsequently growth process. A positive correlation between the NPF events frequency and the condensational sink indicates that these species are likely linked to polluted conditions and that, at Jungfraujoch, the presence of condensing vapors is a more important parameter for NPF to occur than a low CS. NPF were also studied as a function of air mass origins according to the HYSPLIT model and we found that NPF event frequency is strongly linked to the origin of the air mass. Furthermore, two different new particle formation process were observed according to the air mass origin. For all air masses except those from Eastern Europe, event days pre-existing cluster concentrations are not significantly different from non-event days concentrations, but new clusters are formed during the NPF event. On the contrary, in air masses from Eastern europe, the pre-existing cluster concentrations on event days are more than three times higher than the concentrations observed for non-event days, and during the NPF event no more cluster ions are formed, showing that it might be predominantly the growth of pre-existing clusters rather than nucleation of new clusters which contribute to the NPF events.

It has been shown that the nucleation is linked (i) to the origin of the air mass arriving at the sampling site and (ii) to polluted air parcels incoming from the valley to the sampling site. Here the question is "Does the nucleation occur in the whole air mass/air parcel or does it occur because of the ascension of the air mass/ air parcel ?". In other words, what is the vertical scale of the phenomenon, is this constrained by particular parameters at the sampling site such as a low temperature of is it homogeneous along the whole atmospheric column ? Multiple measurements of the aerosol size distribution along the vertical gradient are needed to explore such phenomenon. Such instrumental deployment have been set-up in the puy de Dôme area, central France, and results a long term study at two different nearly located altitude stations are reported in the following section.

4.2 The vertical extent of nucleation events

This section has been published under the reference:

Boulon, J., Sellegri, K., Picard, D., Pichon, J.-M., Fréville, P. and Laj, P.: Investigation of nucleation events vertical extent: a long term study at two different altitude sites, *Atmospheric Chemistry and Physics*, 11, 5625-5639, 2011.

If the nucleation of new ultrafine particles from the gas phase has been observed in various continental and marine locations indicates that nucleation followed by new particle formation (NPF) events is an ubiquitous phenomenon in the planetary boundary layer (PBL), up to which altitude these NPF events take place, and where they are initiated is still under debate. Crumeyrolle et al. (2010) observed during airborne measurements that NPF events was limited to the PBL vertical extent while Hamburger et al. (2010) have evidenced high concentrations of ultrafine particles in the upper free troposphere. Several studies show that atmospheric dynamics such as turbulence or boundary layer mixing could trigger the nucleation process (i.e. Nilsson and Kulmala, 1998; Nilsson et al., 2001). In longer term study, Komppula et al. (2003) have shown that the new particle formation was occurring at two different medium altitude sites (340 and 560 m a.s.l.). During the intensive field campaign SATURN, Stratmann et al. (2003) showed that nucleation could take place inside the residual layer and that it could be induced by the break-up of the nocturnal inversion. Furthermore, they explained the ultrafine particle concentration at a ground-based measurement site as a result of the mixing down of the freshly formed particles within the residual layer. A recent intensive field campaign using LIDAR soundings coupled with 12 helicopter particle measurement flights confirm that the new particle formation process is enhanced in layers of high turbulent mixing such as the residual layer (Wehner et al., 2010). Wehner and co workers also showed that the NPF reported to occur in the residual layer are connected to peaks of ultrafine particle number concentrations at the ground level (Cabauw, Netherlands). Those previous studies are based on few cases (less than twenty) and most of them use particle measurement devices which size cut is no lower than 3 nm. Atmospheric research station located at mountain sites may lay at the interface between the low and the high troposphere. Although there might be some bias at mountain sites due to the distortion of the air flow because of the topography, they provide statistical information that can not be obtained from airborne studies. The bias due to the topography can however be indirectly evaluated by analyzing the LIDAR vertical profile in regard to the in situ measurements. In the following, we propose the first long term study of the vertical extent of the new particle formation process based on a 4-yr measurement period at two different altitudes: The puy de Dôme station (1465 m a.s.l.) and the Opme station (660 m a.s.l.). Both sites were equipped with AIS or NAIS to track the nucleation process. Such an observational set-up allows the tracking of in situ nucleation versus transport from one site to the other. In addition to particle measurement devices, the atmospheric vertical structure and the boundary layer evolution was investigated using LIDAR measurements that were operated at about 11 km of each measurement sites, from the roof of the laboratory.

4.2.1 Measurement sites

Measurements were conducted at two nearly located mid-altitude sites: the puy de Dôme station (mountain site) and Opme station (rural site).
The puy de Dôme research station (PdD) is located at 1465 m a.s.l. in central France (45°46′ N, 2°57′ E). The station is surrounded mainly by a protected area where fields and forests are predominant, the agglomeration of Clermont-Ferrand (300 000 inhabitants) being located 16 km East of the station. Meteorological parameters, including the wind speed and direction, temperature, pressure, relative humidity and radiation (global, UV and diffuse), atmospheric trace gases (O_3, NO_x, SO_2, CO_2) and particulate black carbon (BC) are monitored continuously throughout the year. Winter and summer temperatures vary typically from −10 to +10 °C and 5 to 25 °C respectively. Westerly and northerly winds are dominant. During the November–April period, the access road to the station is restricted preventing from local contamination.
The Opme station is located around 12 km South-East of the PdD station (45°42′ N, 3°05′ E, 660 m a.s.l.) in a rural area dominated by agricultural fields and forest. At this station the ultrafine aerosol and/or ion size distribution are/is monitored with an AIS or a NAIS depending on the period of the year. Basic meteorological parameters such as temperature, relative humidity and pressure are continuously measured. The geographical area of the two measurement sites is represented in the figure 4.8 (photography). As seen, the two sites are not separated by any topographical barrier (see the 3D plots and the topographical profile, Fig. 4.8) so that air parcels can move free of constraint between the two sites (Fig. 4.8).

4.2.2 Instrumentation

4.2.2.1 Particle measurement devices

Because the PdD station is more than 50% of the time in-cloud, the aerosol sampling is performed through a whole air inlet (WAI) which ensures efficient sampling of both cloud droplets and interstitial aerosol in ”in-cloud” conditions. The WAI samples air at 12 m above the ground through a heated inlet that avoids ice formation. Wind velocity around the inlet head is lowered by a wind-shield to ensure efficient sampling even at elevated wind speeds. Air is sucked into a 12-cm-diameter PVC tube at a flow rate of 30 m^3 h^{-1} subsequently sub-sampled inside the PVC tube with a 5-cm-diameter stainless-steel tube ensuring iso-kinetic sub-sampling. The stainless-steel section of the inlet is equipped with a heated section to evaporate cloud droplets and to maintain the relative humidity of sampled air at about 50%. Interstitial aerosols and evaporated cloud residues are sampled simultaneously at a constant relative humidity and can be compared in size regardless of the environmental conditions. Temperature never exceeded 25 °C to limit aerosol volatilization. A SMPS (Scanning Mobility Particle Sizer), measured the particle number size distribution (10–400 nm) at the top of the puy de Dôme station through the

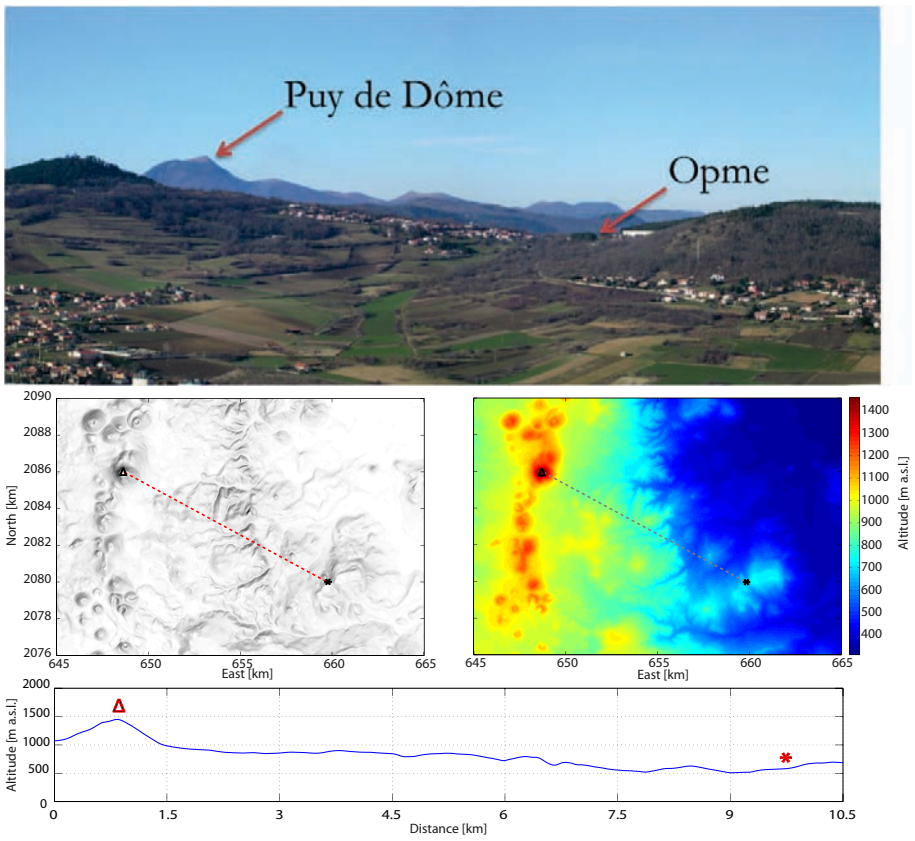

Figure 4.8: Topographical view of the two measurement sites.

WAI continuously since May 2005, with a two-minute resolution. The SMPS is composed of a condensation particle counter TSI 3010 and a Differential Mobility Analyzer (DMA) columns TSI-3081. The instrument data evaluation and the seasonal variation of the aerosol size distribution are described in details in Venzac et al. (2009).

A separate short inlet was used for the AIS and NAIS sampling, directly through the station front facade, in order to avoid the re-combination of ions in the sampling line. The upper size-cut of large ions sampled through the AIS inlet is 10 µm for a wind speed of 2 m s^{-1} and 2 µm for; a wind speed of 5 m s^{-1} wind speed. As a result, few droplets should enter the inlet, except at wind speeds smaller than 5 m s^{-1} which is rare at the station (Venzac et al., 2007). The mobility distributions of atmospheric positive and negative ions are measured with the AIS (Airel Ltd., Mirme et al., 2007), providing the ion size distribution in the diameter range 0.8–42 nm for NTP-conditions (mobility range: 3.162–0.0013 cm^2 V^{-1} s^{-1}). The AIS sampling alternated with NAIS (Neutral clusters and Air Ion Spectrometer) sampling (see chapter 3 for instrumentation detailed description).

The data discussed in the following are based on samplings achieved during more than three years from February 2007 to June 2010 for puy de Dôme site (AIS/NAIS & SMPS) and from October 2008 up to June 2010 for Opme site (AIS/NAIS). Within this period, 952 days are available for the PdD station and 437 days for Opme station.

4.2.2.2 LIDAR measurements

In addition to in-situ measurements and in order to characterize the atmospheric layers structure, LIDAR measurements were performed from the roof of the Laboratoire de Météorologie Physique (45°45′ N, 3°6′ E, 410 m a.s.l.). Atmospheric layers characterization procedure could be found in the chapter 3, in the section *Characterization of atmospheric layers*.

4.2.3 Results

4.2.3.1 Nucleation events at the puy de Dôme station

Events classification The classification of event days was performed visually using the daily contour plot of the ion size distribution evolution using the classes previously detailed in the chapter 3, in the section *Data processing for nucleation event characterization*.

Based on the long term continuous measurements, the seasonal variation of the nucleation events frequency at the PdD station is presented Fig. 4.9. Nucleation occurs around one third of the time at the PdD (30.8%) which is in agreement with the previous study made by Venzac et al. (2007). Unfortunately, due to many discontinuities in the measurements, we cannot perform such an analysis for the Opme station. The observed seasonal variation (Fig. 4.9) is not very pronounced but we can distinguish two maxima (one during early spring and the other one during the early autumn). At other sites where the frequency of nucleation events show a seasonal variation the maximal occurrence was usually observed during the spring and autumn seasons as well (Manninen et al., 2010) except for the Mt. Everest station (Venzac et al., 2008) where the maximal occurrence of nucleation events is during the summer. At Mt. Everest, authors explain this phenomenon as a result of the strong upslope wind that occurs during daytime in the summer and brings condensable vapors to the measurement site. The minimal occurrence frequency is always observed during winter months partly due to a lower photochemical activity (Venzac et al., 2008; Manninen et al., 2010; Boulon et al., 2010).

Nucleation rates Total and charged particle formation rates were calculated using Eq. 3.4 and Eq. 3.5, and the growth rates were computed using the method presented illustrated on fig. 3.4, in the chapter 3, section *Nucleation rates calculations*. The mean formation rates of charged and neutral particles are 0.07 ± 0.09 respectively for positive ions, 0.07 ± 0.08 for negative ions, and 1.38 ± 0.19 for neutral species. From those results, the ion-induced nucleation (IIN) fraction was computed and the mean contribution of ions to the total formation rate was found to be in average $12.5 \pm 2.0\%$. However, to estimate the error in formation rate calculation we compared the computed J_2 value with the one that can be derived from SMPS measurement and J_{15} calculation using the relation given

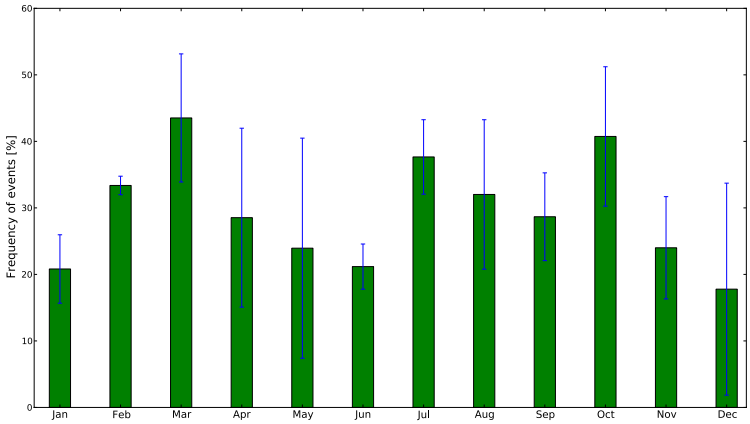

Figure 4.9: Monthly mean nucleation frequencies at the puy de Dôme station.

by (Lehtinen et al., 2007). The J_2 computed using the NAIS was found to be on average 2.4 ± 1.7 times higher than the ones derived from SMPS data. Thus the IIN fraction could be underestimated by the same factor, so the value provided is a lower limit of the IIN. At other continental high elevation sites, a high IIN contribution to the nucleation process was also pointed out: 21.8% for the Jungfraujoch high altitude station (3580 m a.s.l., Switzerland, Boulon et al., 2010) and 5% for Hohenpeissenberg (980 m a.s.l, Germany, Manninen et al., 2010) in comparison to boundary layer sites (Manninen et al., 2010 and Iida et al., 2006, 2.6 ± 2.8 % in average on both studies). These results suggest that IIN is favored at high elevations.

The role of sulfuric acid Sulfuric acid concentrations were estimated using the parametrization proposed by Petäjä et al. (2009) (see Eq. 4.1). The difference in sulfuric acid concentrations calculated during nucleation event days and non-event days was tested with the Welch's t-test (t-test for two samples with unequal variance and unequal population). We found that the null hypothesis of identical average scores could not be rejected at the threshold of 5% (i.e. sulfuric acid concentrations are not statistically different between event and non-event days). Furthermore, the correlation between sulfuric acid vapor concentration and the particle formation rate was found to be very low. Also no quadratic dependance of the formation rate, J, on the sulfuric acid concentration were found (Fig. 4.10). This result is in agreement with the analysis of the nucleation events occurring at the Jungfraujoch station (Boulon et al., 2010). It is likely that, at the puy de Dôme station and at the Jungfraujoch station, condensing compounds other than H_2SO_4, such as volatile organic compounds are involved in the new particle formation process. This assumption was also pointed out from chamber experiments by (Metzger et al., 2010). In order to test this hypothesis, we also tested different nucleation parametrizations involving sulfuric acid (Table 4.5, #1) and we found that the formation rate parametrizations do not correlate with the observed J. Other parametrizations of charged formation rate involving a preexisting cluster number concentration and (i) sul-

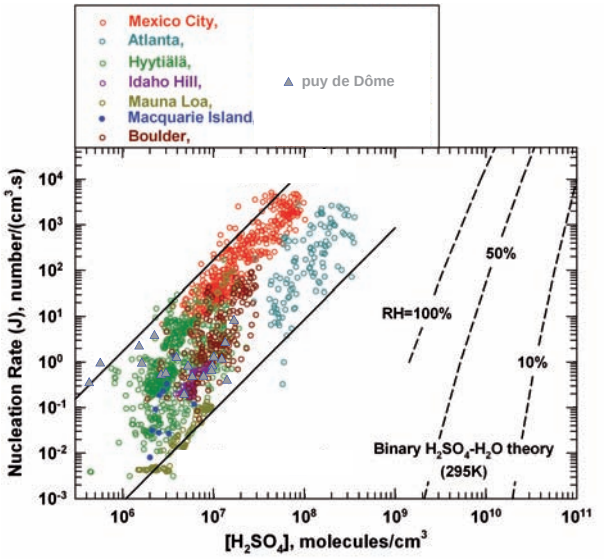

Figure 4.10: Dependence of atmospheric nucleation rates on sulfuric acid vapor concentrations at the puy de Dôme compared to diverse locations. Hyytiälä data courtesy of Kulmala et al., other data courtesy of McMurry et al.

Table 4.5: Formation rates calculated from different parametrizations. a. From Nieminen et al. (2010), b. From Kerminen et al. (2010).

ID.	Model	Pearson's r
# 1	$J_2 = 4.9 \times 10^{-07} \times \mathrm{H_2SO_4}^b$	-0.0855
# 2	$J_2^+ = 1.9 \times 10^{-10} \times N^+ GlobRad^{2,a}$	0.1434
# 3	$J_2^+ = 6.5 \times 10^{-18} \times N^+ (\mathrm{H_2SO_4})^{2,a}$	-0.1932
# 4	$J_2^- = 1.6 \times 10^{-10} \times N^- GlobRad^{2,a}$	0.2328
# 5	$J_2^- = 6.7 \times 10^{-18} \times N^- (\mathrm{H_2SO_4})^{2,a}$	-0.1877

furic acid (Table 4.5, #3 and 5) or (ii) the global radiation as a proxy of photochemically induced nucleation (Table 4.5, #2 and 4) were also tested. It appears that $J_2\pm$ models involving global radiations slightly correlate with observed $J_2\pm$. On the contrary, parametrizations that use sulfuric acid concentrations could not explain the observed charged formation rates. Those results corroborate the hypothesis that photochemical processes involving other compounds than H_2SO_4, such as organic vapor, are more relevant to describe observed particle formation rates at the puy de Dôme station.

Air mass backtrajectories influence We investigated the impact of the air mass origin on the occurrence of a nucleation event using the three days air mass back trajectories computed with the HYSPLIT transport and dispersion model (Draxler and Rolph, 2003). Since the air mass origin and path to the measurement site does not differ significantly between 00:00 and 12:00, only results for 12:00 will be included in our analysis (Fig. 4.11). The calculation was done over all sampling days common to both sites, 437 days. Air mass back-trajectories and origins are respectively reported in Fig. 4.11 and Table 4.6.

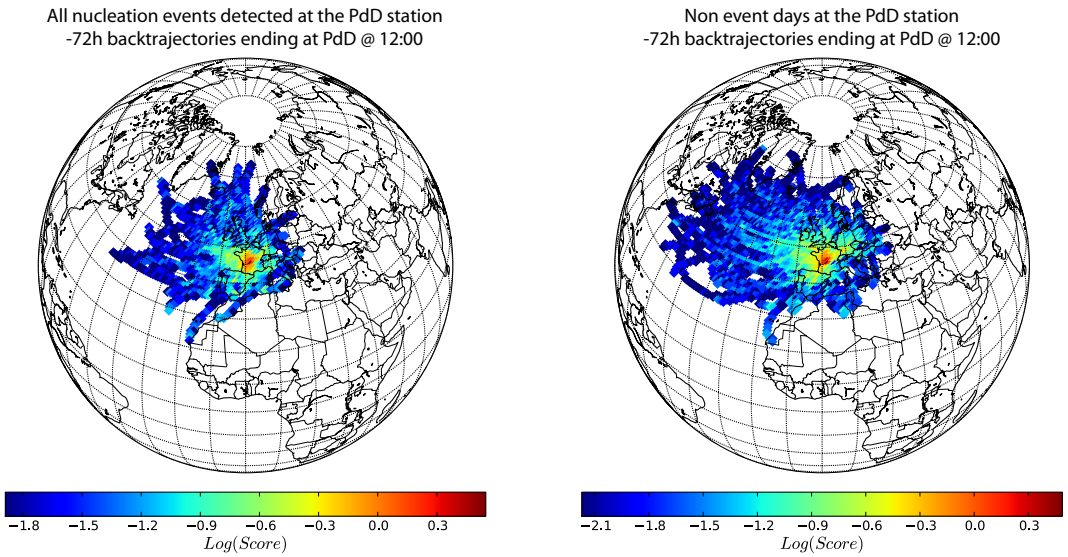

Figure 4.11: Three days prior air mass backtrajectories computed with Hysplit model.

Table 4.6: Origins of air masses reaching the puy de Dôme sampling site. *123 days could not be studied because of lack of data to run the Hysplit model.*

Air mass origin	All days	Events	Nucleating ratio
Atl.	169	59	0.35
Afr.	19	5	0.26
WE.	105	36	0.34
EE.	14	3	0.21
Pol.	7	4	0.57

The station is mainly under the influence of western air masses (i.e. from Atlantic and continental western Europe areas, Fig. 4.11). These two air mass types represent 87.3% of air masses reaching the sampling site and are associated to 88.8% of the nucleation events. Air masses from Africa and Eastern Europe represent 10.5% of total air masses and 7.5% of the total nucleation events. Polar air masses are very rare (2.2% of the total air masses and 3.7% of the observed nucleation) but have the highest nucleating ratio (Table 4.6). Those results suggest that there is no link between nucleation events and air mass origin since nucleating ratios of all air masses are not significantly different. Furthermore, the vertical transport was also computed and 77.7% of the time air masses were found to be located between 0 and 1500 m a.s.l. while 22.1% of the time above 1500 m but below 2500 m a.s.l.. This later value is slightly less important in case of nucleation events (21.3%). It can be seen that non-nucleating air masses originate from farther west suggesting they travel at high wind speed at higher altitude, and hence they could be less influenced by fresh boundary layer inputs. The seasonality of air mass types reaching the PdD station was studied by Venzac et al. (2009) who showed that western air masses reaching the puy de Dôme have travelled over longer distances during winter compared to summer. Hence another explanation for lower nucleation frequencies in more distant western air masses is because they coincide with winter conditions.

4.2.3.2 Comparison of nucleation events between the two sites

We investigated the cases when nucleation occurs (1) only at one station (puy de Dôme or Opme) and (2) at both sites. The data set was reduced to days for which data are simultaneously available at both sites. On 437 days when data was available at both sites, nucleation occurred on 161 days (i.e. 36.8% of the time). On those event days, 157 events (97.5% of detected events) were detected at the PdD station and 91 (56% of detected events) at the low elevation station of Opme. Those first results show that the nucleation process is clearly enhanced at the altitude station (see Tab. 4.7). 95.6% of events (87) detected at Opme station were also detected at the PdD station whereas only 4 events are detected at the low elevation station only, indicating that the new particle formation process usually occurs at a large vertical extent. On the contrary, considering the events detected at the elevation station of puy de Dôme, 44.5% of these events (70 events) were not detected at the lower altitude site. Based on those observations, all the nucleation events were classified into four different categories according if the event is detected (i) at the puy de Dôme station only (case "P"), (ii) at the Opme station only (case "O"), (iii) at both measurement sites and at the same time (case "D_S") or iv- at both sites but not at the same time (case "D_D"). Average contour plots of each case are presented in Fig. 4.12. In the following section, we present a closer look at few atmospheric parameters corresponding to each case, in order to investigate the factors influencing one or the other configuration.

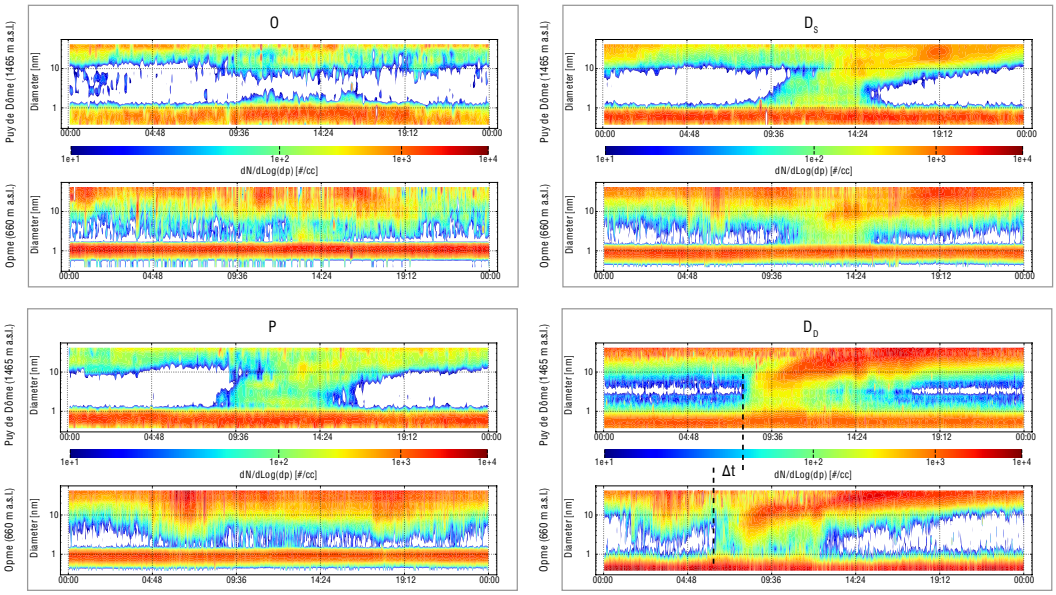

Figure 4.12: Average temporal evolution of the negatively charged particle size distribution for the puy de Dôme (upper panels of grey boxes) and Opme (lower panels of grey boxes) in case of "O" events (upper left box), "P" events (lower left box), "D_S" events (upper right panel) and "D_D" (lower left box).

Table 4.7: Statistical data of nucleation event occurrences.

	PdD & Opme	Only Opme	Only PdD
Nb. events	87	4	70
Frequency	19.9%	0.91%	16.0%

Relationship to other atmospheric parameters Figure 4.13 shows a comparison of the different atmospheric parameters detected at the PdD station, averaged over all cases of nucleation event at the PdD station (Nuc, grey bar) or over all cases of non-event at the PdD station (Nev, grey bar). Data reported are parameters averaged over the 09:00–11:00 time period, which is assumed to correspond best to the nucleation period. Furthermore, we divided the data-set into two different sub-groups, according to "in-cloud" conditions at the puy de Dôme site. This procedure allowed us to analyze the influence of various atmospheric parameters independently of the influenced of clouds, which was previously shown to be important (Venzac et al., 2007).

Studied parameters (relative humidity, global radiation, black carbon, SO_2, O_3 and NO_x) present a higher variability during nucleation event days, compared to non-event days. The negative effect of a strong relative humidity is clearly observed as previously shown by Venzac et al. (2007), presumably because of the strong condensational sink that cloud droplets offer to the nucleating/condensing species. We also point out that the average O_3 concentration is lower in case of event days compared to non-event days. The scavenging role of clouds on gases is revealed by the analysis of the B part of Fig. 4.13 where it can be seen that atmospheric concentrations of SO_2 and O_3 are two times lower during "in-cloud" conditions. Going into more specific cases, Fig. 4.13 reveals that studied atmospheric parameters are roughly the same when a nucleation event is detected at the PdD station, no matter if the event is detected or not at the Opme station simultaneously (comparison of the grey-Nuc bar and orange bar). On the contrary, we show that the situation is very different when the nucleation occurs only at the low elevation site (Fig. 4.13, yellow bar). In fact, in case of O type events, we show that all measured parameters have the same median values as during a typical non-event day at the PdD station, i.e. higher relative humidity and higher ozone concentrations.
The condensational sink (CS) represents the loss of condensable vapors due to pre-existing particles per time unit (Pirjola et al., 1999). In a recent paper, Boulon et al. (2010) have shown that nucleation at the Jungfraujoch high altitude station could be linked to an increase of the condensational sink (CS) previous to the onset of the nucleation process, suggesting that the presence of condensing vapors probably associated to these high CS are driving the NPF events. In this study the CS could only be computed for the PdD station since no SMPS were available at the Opme site. The mean CS computed before the nucleation onset (06:00–09:00 time period) and when liquid water content (LWC) is lower than $0.02\,\mathrm{g\,m^{-3}}$ ("out-of-cloud" conditions) are reported in Fig. 4.14. We found that, on average, the CS is lower for event days ($3.73 \pm 0.11 \times 10^{-3}\,\mathrm{s^{-1}}$) than for non-event days ($5.17 \pm 0.15 \times 10^{-3}\,\mathrm{s^{-1}}$) (grey bars, respectively named Nuc and Nev), illustrating the inhibiting effect of a high CS on nucleation as often found in the literature. The CS calculated when the event takes place at both stations ($3.96 \pm 0.20 \times 10^{-3}\,\mathrm{s^{-1}}$, orange bar) is slightly higher than when nucleation occurs only at the higher elevation one ($3.50 \pm 0.11 \times 10^{-3}\,\mathrm{s^{-1}}$, green bar). Again, a strong difference is observed in case of "O"

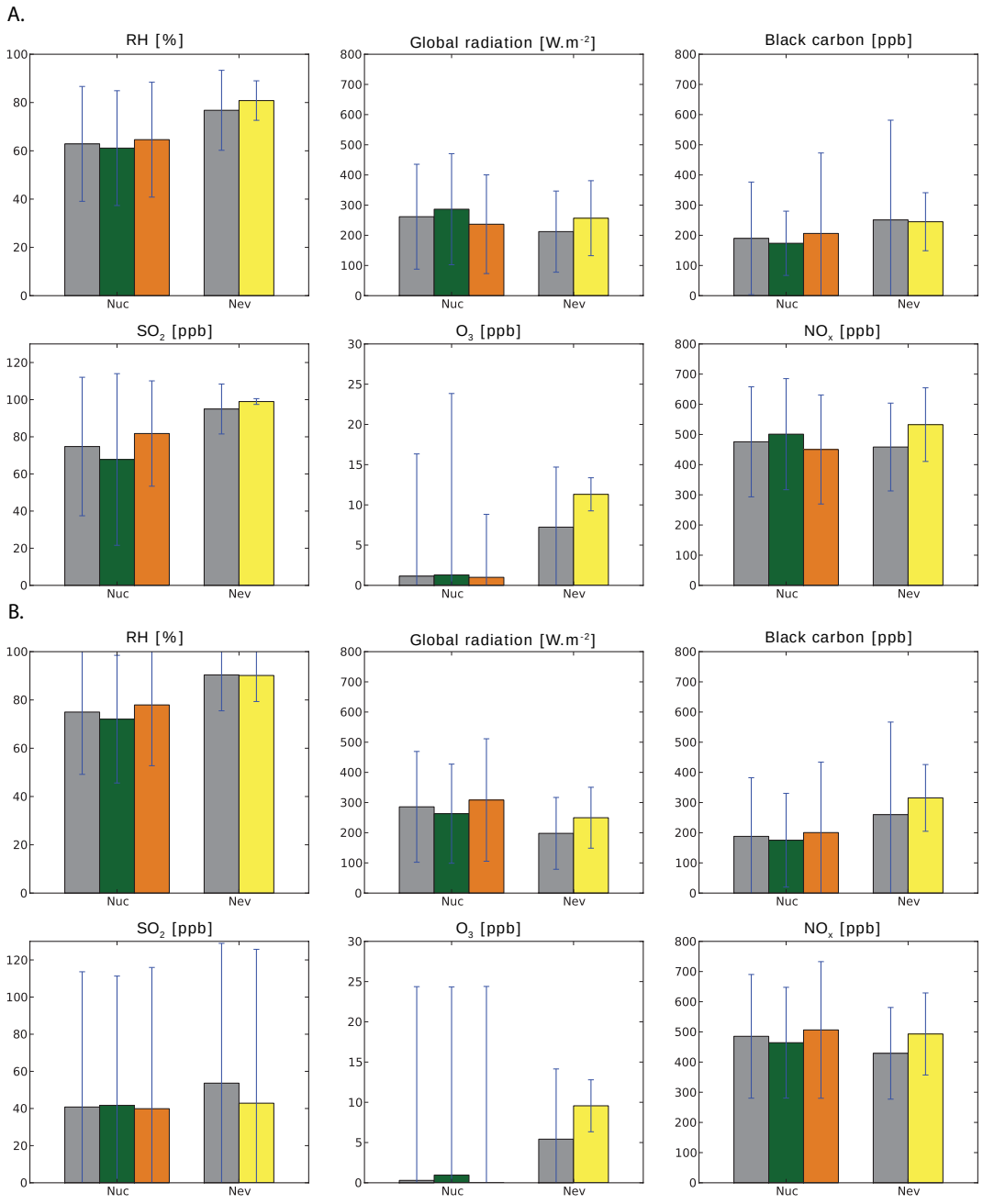

Figure 4.13: Average and standard deviation of atmospheric parameters measured at the puy de Dôme station in case of event (Nuc, N=157) or non-event (Nev, N=276) days with or without cloud events filtering (respectively A. and B.) calculated over the 9-11:00 time period. Grey bars represents the general case, when the nucleation is observed at the puy de Dôme station (Nuc) or not (Nev). The green and the orange bars are respectively for a nucleation events that occur only at the puy de Dôme station (N=70) and an event that occur at both measurement sites (N=87). The yellow bar is for events that only occur at the Opme station (N=4).

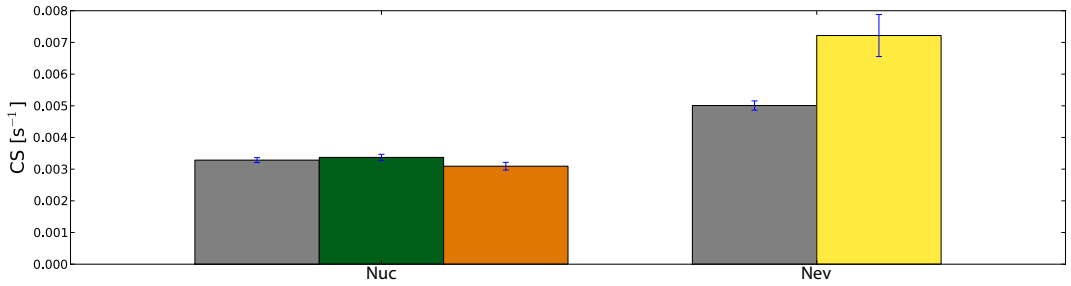

Figure 4.14: Condensational sink average values with standard deviations for event days (Nuc) and non-event days (Nev) at the puy de Dôme station when LWC < 0.02 g/m^3. Grey bars represents the general case, when the nucleation is observed at the puy de Dôme station (Nuc) or not (Nev). The green and the orange bars are respectively for a nucleation events that occur only at the puy de Dôme station (N=70) and an event that occur at both measurement sites (N=87). The yellow bar is for events that only occur at the Opme station (N=4).

type events (Fig. 4.14, yellow bar). In those cases, the CS is two times larger than the one observed in case of nucleation at the PdD station (Fig. 4.14, Nuc). Our hypothesis is that in case of "O" events, the site is in the vicinity of clouds (as it will be shown later) and aerosols might still be hydrated, shifting the distribution to higher sizes and therefore increasing the condensation surface.
To summarize, at the PdD station, high condensational sinks seem to inhibit the nucleation process. This result is opposite to what Boulon et al. found at Jungfraujoch (JFJ). The JFJ is located at a higher altitude, (3580 m a.s.l.), and surrounded by areas mainly covered by snow, thus presumably a more remote site, generally poor of condensing vapors, thus limiting nucleation. The puy de Dôme station is located at a lower altitude, surrounded by a coniferous forest and can be strongly influenced by the planetary boundary layer during the summer days (Venzac et al., 2009). As a consequence, it is likely that, at the PdD station, the condensable vapor concentration is not as a strong limiting factor to trigger the nucleation as at the JFJ station, because it is always present at relatively high concentrations due to the proximity of the vegetation. In this VOCs enriched environment, a low CS becomes the main condition for nucleation to occur. The CS calculated at the PdD station was found to be one order of magnitude higher than the at JFJ, and it is obviously limiting the occurrence of nucleation events at the site, confirming the relevance of our assumption.

In the following, each category of nucleation events (O, P, D_S and D_D) will be studied separately. For each type of events, we will report the corresponding tropospheric structure of the atmosphere using ground based LIDAR measurements and potential equivalent temperature, θ_e, calculation according to the Bolton procedure (Bolton, 1980). Over the measurement period, LIDAR data are available for 132 days. When no LIDAR data are available, two air masses or atmospheric layers will be considered the same if (i) the two θ_e temporal evolutions are strongly correlated with each other during the nucleation process,

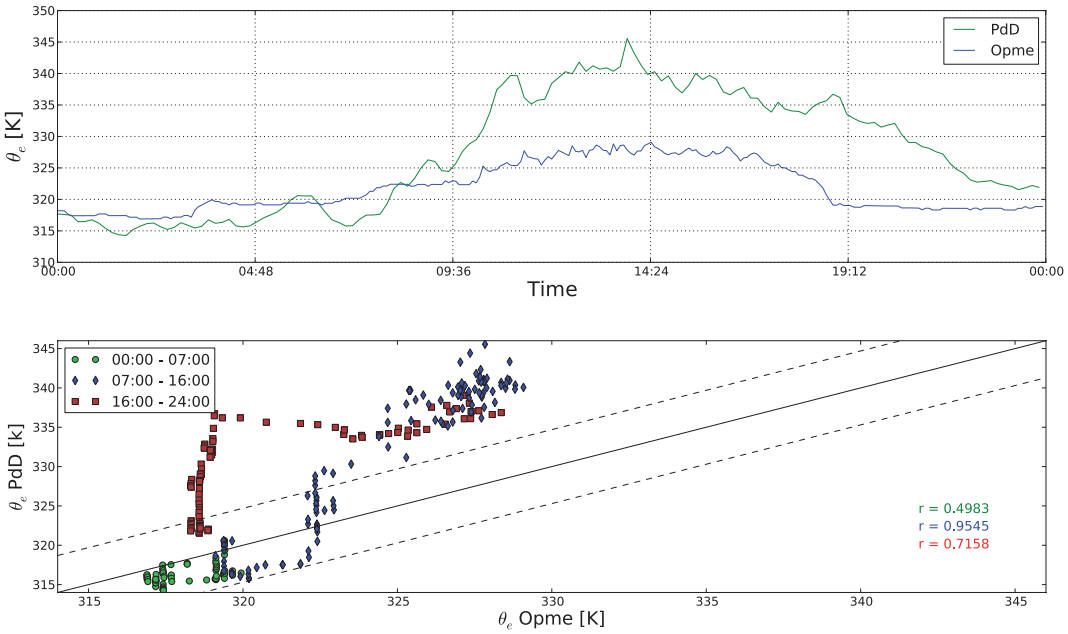

Figure 4.15: Evolution of equivalent potential temperature, θ_e at both sites (upper panel) and the correlation between the two sites (bottom panel) in case of nucleation at Opme site (12/08/2007). On the bottom panel, the lines represent the uncertainty boundaries of the θ_e (1:1) line.

and, (ii) the two equivalent potential temperatures are the same within the uncertainties of measurements. Uncertainties were computed using the classical error propagation theory, it was estimated to $\pm 4.7\,\mathrm{K}$ ($1\times\sigma$), i.e.$\Delta\ \theta_e \leq 4.7\,\mathrm{K}$.

O cases: Nucleation events at the Opme station only Nucleation events that occur only at the Opme station are very rare: only 4 events occurred on 437 observed days (4.4% of the total observed nucleation events detected at Opme). Unfortunately, no LIDAR data are available for those events. As mentioned above, those cases present all characteristics in terms of atmospheric chemical properties of a non-event day for the puy de Dôme station: high relative humidity associated with a high CS. Going further in the analysis revealed that in each O case, when the nucleation is triggered at Opme station, clouds are detected at the PdD station (Fig. 4.12, case O) and likely interrupted the nucleation process through the scavenging of condensable vapors and/or pre-existing clusters by cloud droplets (Venzac et al., 2007). During all those events, Opme was cloud free because of its low elevation.

In the following, we analyze an example but it is representative of all four "O" cases. Also in terms of boundary layer dynamics, the same pattern is always observed. In case of "O" type events, Opme and PdD seem to be both within the PBL at the beginning of the nucleation process. This assertion is based on the comparison between the temporal evolution of the equivalent potential temperature (θ_e) at puy de Dôme and Opme. Figure 4.15 shows the temporal evolution of θ_e and the correlation of this

thermodynamic tracer between the two sites at three different periods of the day (00:00 to 07:00, 07:00 to 16:00 and 16:00 to 00:00) and during the nucleation period (between 09:00 and 11:00). During the night and early morning, the two sites have the same θ_e but the low correlation ($r(\theta_e) = 0.4930$) indicates that the two sites are in different atmospheric layers. After 07:00 and until around 09:30, the two equivalent potential temperatures become equal and their evolution is strongly correlated ($r(\theta_e) = 0.8391$). After 09:30, the θ_e(PdD) $>$ θ_e(Opme) but their evolution is still strongly correlated ($r_{9:30-16:00} = 0.9545$). This could indicate that both sites are not located within the PBL unless this layer is strongly stratified thus inhomogeneous.
During the morning, the PdD station is in "in-cloud" conditions between 07:00 and 09:30, mean values of the relative humidity (RH) and liquid water content (LWC) are respectively 100% and 0.089 g m^{-3}, when the nucleation is triggered at Opme site. During the nucleation period, between 09:00 and 11:00, $RH = 100 \pm 0.04\%$ and $LWC = 0.07 \pm 0.05$g.m^{-3} in average which means that the station is mainly in "in-cloud" conditions while the nucleation is detected at the Opme site. Later during the day, the PdD station is still in "in-cloud" conditions or in the vicinity of clouds (RH and LWC between 07:00 and 16:00 are respectively 96.0% and 0.024 g m^{-3} in average). This type of event do not inform us on the spatial extent of the nucleation but two hypotheses could be formulated: (i) the spatial extent of the nucleation is very low and it occurs only within a small geographical area before all reactive and condensable species have been completely consumed, (ii) the nucleation could occur within the whole column in the PBL but condensable vapors have been scavenged by cloud droplets at the high altitude site. According to statistical analysis of the events repartition between the two sites, it is likely that the second hypothesis is the most probable. As we will show in the following, when the nucleation is triggered at Opme site, the phenomenon can usually be detected at the altitude station as well (87 events on 91 measured at Opme station).

In the following, we investigate deeper the spatial extent of the nucleation through the study of the vertical structure of the atmosphere when the nucleation occur at the altitude site (cases "P", "D_S" and "D_D").

P cases: Nucleation events at the puy de Dôme station only This case represents 43.5% of the total number of nucleation events observed in this study (70 events on the 161 events, Table 4.7). Among these nucleation events, LIDAR data are available for 10 days.
The average daily time series of the cluster and particle size distributions at both sites is shown in Fig. 4.12, case "P". As seen, no nucleation event is detected at the Opme site, the two peaks of particle concentration seen at Opme station on early morning and at the end of the afternoon are due to traffic-related emissions. In Fig. 4.16 the temporal evolution of the equivalent potential temperature at both sites, θ_e, is reported for a typical "P"

case event (13 March 2009). All "P" case event days show the same pattern. The diurnal evolution of θ_e, which is lower at the altitude site at night and early morning (unstable conditions), suddenly increased until reaching the same value as at the low elevation site, within uncertainties. This clearly indicates a change in atmospheric thermodynamical properties (T, P, RH).

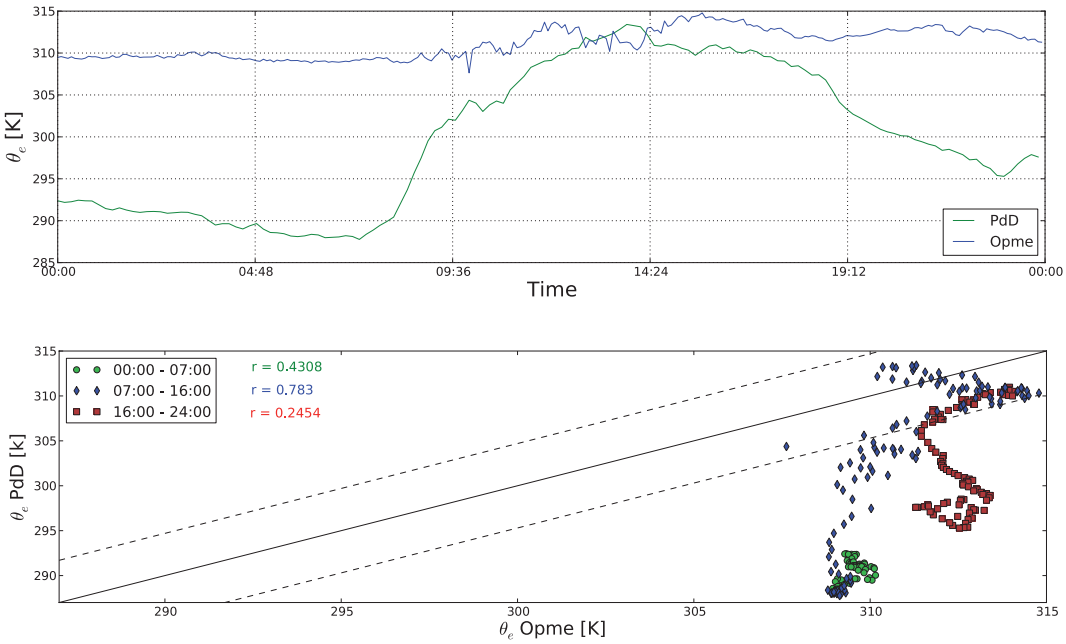

Figure 4.16: Temporal evolution of equivalent potential temperature at both sites during a high altitude event ("P", 13/03/2009).

The evolution of θ_e between the two sites associated with a non-equality between the equivalent potential temperatures highlights that air parcels of each site are very weakly connected with each other during the nucleation process (in the case of 13 March 2009, $r(\theta_e) = 0.3080$ and$\Delta\ \theta_e = -7.2532\,\mathrm{K}$). This hypothesis is confirmed by the LIDAR measurements. The z^2 LIDAR back-scattering signal (we will name it the z^2-signal in the following), reported Fig. 4.17 (left panel) is consistent with this interpretation and clearly shows that the two sites are located within different atmospheric layers. A more precise analysis of the z^2-signal was performed and is reported on the right panel of the Fig. 4.17. It confirms that the Opme site is located within the PBL while the PdD is located at between the PBL and the FT, and more precisely above the upper boundary in what we defined as the entrainment zone. The average height of the PBL computed using our procedure between 09:00 and 11:00 for "P" cases is $1220 \pm 190\,\mathrm{m}$ a.s.l., hence confirming that the PdD station is located above the PBL during the nucleation process. By the end of the afternoon the LIDAR signal shows a subsidence of atmospheric layers when the thermic convection stops, leading to an atmospheric disconnection between the two sites. This is illustrated by an increasing of$\Delta\ \theta_e$ between the two sites and a decrease of the θ_e pearson correlation between the two stations.

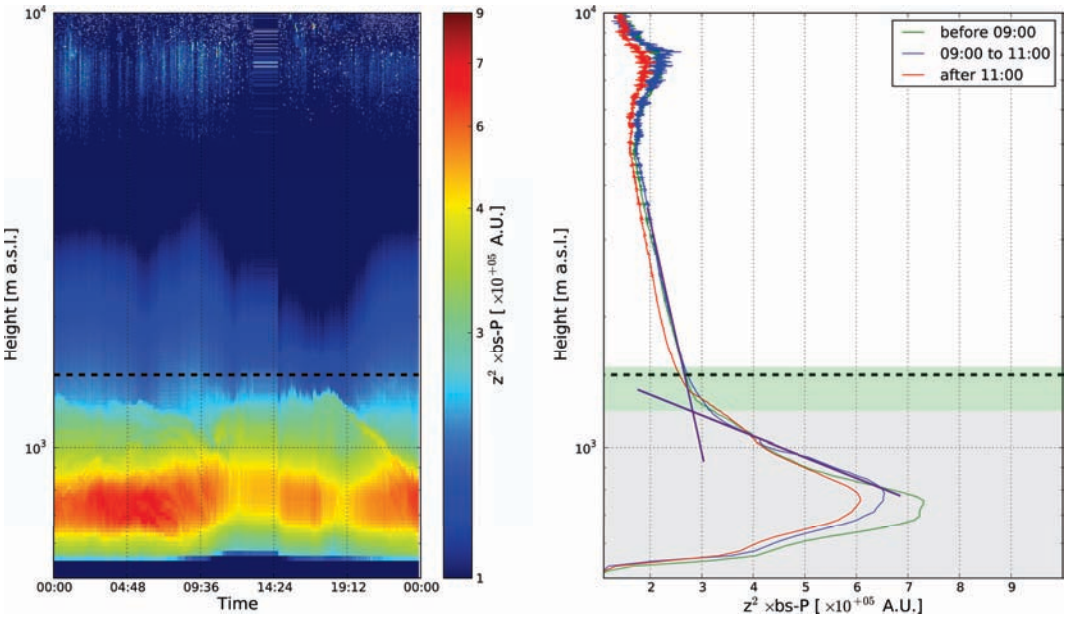

Figure 4.17: *Left panel:* LIDAR z^2-signal evolution in arbitrary units (13/03/2009). *Right panel:* Average LIDAR z^2-signal i- before 09:00 (green line), ii- between 09:00 and 11:00 (nucleation time) and iii- after 11:00. On both graphics, the black dot line represents the hight of the puy de Dôme station.

D_x cases: Nucleation events at both sites The "D_x" case represents 54% of the total number of nucleation events observed in this study (87 events on the 161 observed events, Table 4.7). Among these nucleation events, LIDAR data are available for 26 days. Two different sub-cases could be outlined: (i) the nucleation is triggered at the same time at both sites (47 events), and, (ii) the nucleation is first detected at the low elevation station (Opme) and after a variable time delay, the event is detected at the altitude site (PdD) (40 events).

- Simultaneous events (D_S): This phenomenon is observed on 47 days i.e. one third of the total nucleation events observed at the PdD station and 54% of the "both sites events". As seen on the temporal evolution of the aerosol number-size distribution (Fig. 4.12, case D_S), the two events detected at both measurement sites start at the same time and present similar shapes and characteristics. In opposition to what we observed on the previous cases, here the evolution θ_e is well correlated along the day (Fig. 4.18) and especially during the nucleation process where the median Pearson's correlation is 0.739 for all D_S events. The LIDAR signal analysis (Fig. 4.19) confirms what is deduced from the analysis of the temporal evolution of θ_e. As seen in Fig. 4.19, the air parcels at the two sites are strongly connected: the PdD station is located inside the lower part of the entrainment zone while Opme station is within the planetary boundary layer. Moreover, during those cases, the PBL is not very polluted and well mixed. The nucleation events occur during the PBL development when the PBL influence on the entrainment zone is maximal.

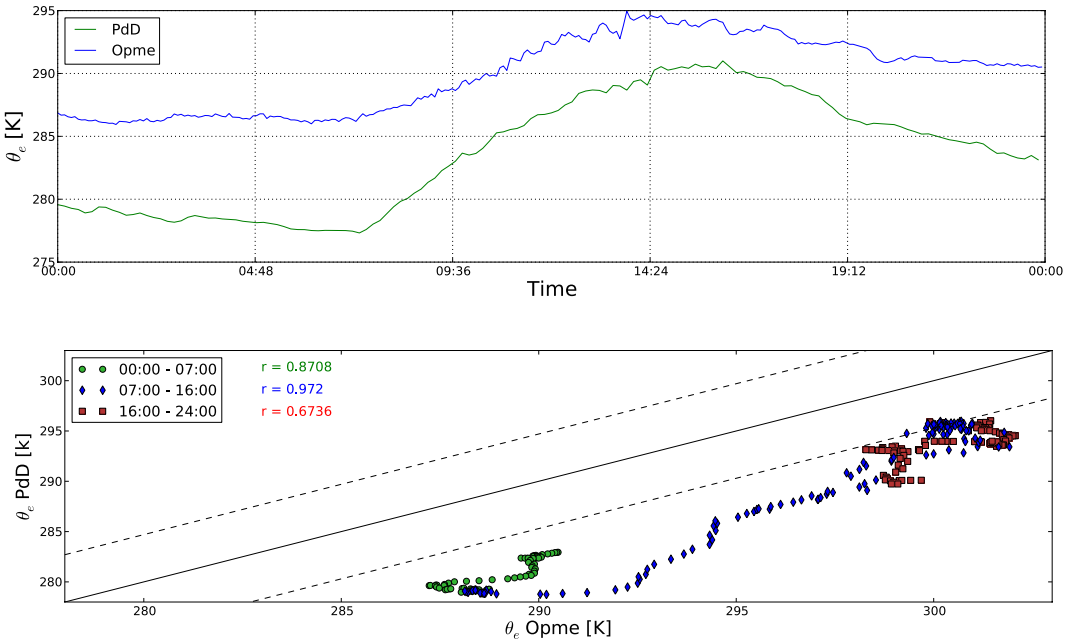

Figure 4.18: Temporal evolution of equivalent potential temperature at both sites during a simultaneous nucleation event ("D_S", 22/03/2009).

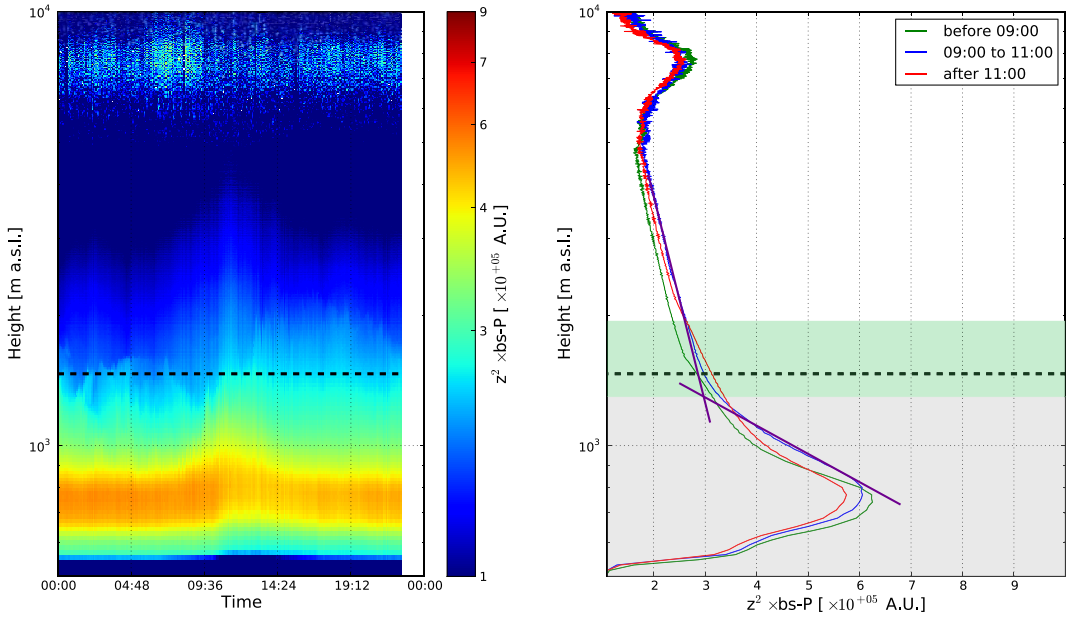

Figure 4.19: *Left panel:* LIDAR z^2-signal evolution in arbitrary units in case of simultaneous nucleation event (22/03/2009). *Right panel:* Average LIDAR z^2-signal i- before 09:00 (green line), ii- between 09:00 and 11:00 (nucleation time) and iii- after 11:00. On both graphics, the black dot line represents the hight of the puy de Dôme station.

In this case of simultaneous nucleation, we can conclude that nucleation occurs at the same time within the whole planetary boundary layer column. This means that all the elements required to trigger nucleation are homogeneously distributed within the low tropospheric column, from the entrainment zone to the ground level.

- Non simultaneous nucleation (D_D): In "D_D" cases (40 events), the nucleation process occurs at both sites but it does not start at the same time at both stations. However, the temporal evolution of aerosols distribution (Fig. 4.12, D_D) shows that the nucleation events present very similar shapes and characteristics at both sites. This observation suggests that the two events are connected. An example of the evolution of theta is given in Fig. 4.20. All "D_D" cases show the same theta evolution pattern. The non-correlated evolution of θ_e (Fig. 4.20) shows that the two sites seem to be located within two independent air parcels when the nucleation is triggered at the low elevation station ($r(\theta_e) = -0.1370$ and$\Delta\ \theta_e = -7.118 \pm 1.093$ K). The median correlation of the equivalent potential temperature during the nucleation event for all D_D events is 0.586. This value is lower compared to the one observed for D_S cases indicating that the atmospheric connection between the two sites is weaker. On the contrary, LIDAR measurements (Fig. 4.21) indicate that the two measurement sites are located within the planetary boundary layer (the upper limit, in the case of 21 May 2009, was found to be 1700 ± 515 m a.s.l.). The time delay of the nucleation at the altitude site could be due to a strong stratification of the boundary layer.

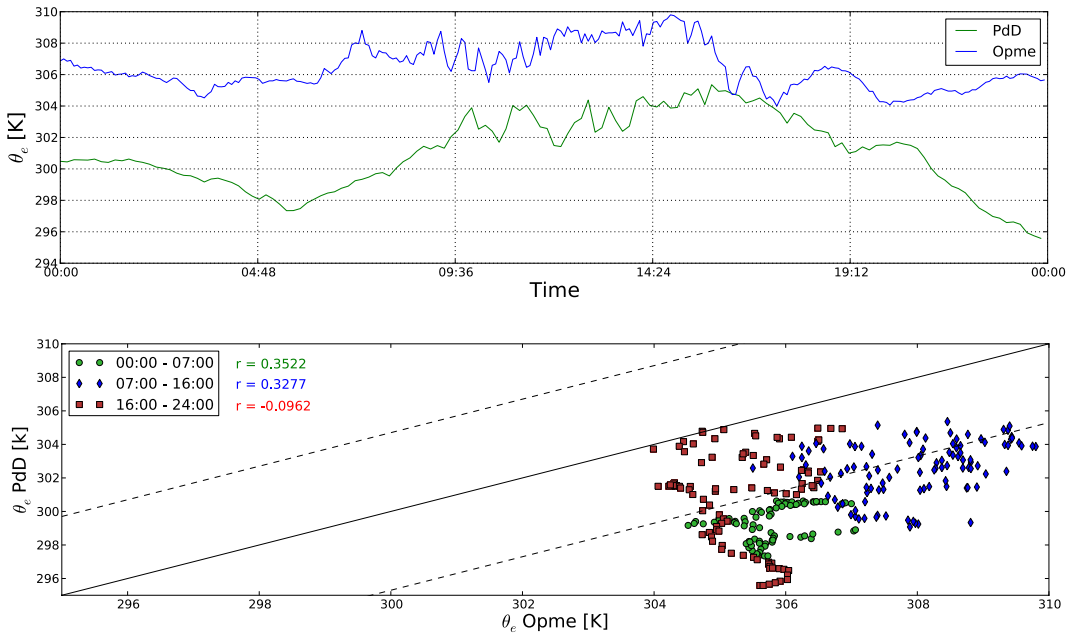

Figure 4.20: Temporal evolution of equivalent potential temperature at both sites during a non-simultaneous nucleation event ("D_D", 21/05/2010).

For all "D_D" and "D_S" events, we calculated the elevation of the top boundary of the PBL using the procedure we detailed Sect. 2.1.2. The average heights for "D_S" and "D_D" cases are respectively in average 1390 ± 280 and 2120 ± 310 m a.s.l. For the general "D_x" cases, the average PBL extent is 1760 ± 210 m a.s.l. which is significantly higher than in the "P" cases even though it shows a higher variability. The analysis of the potential tem-

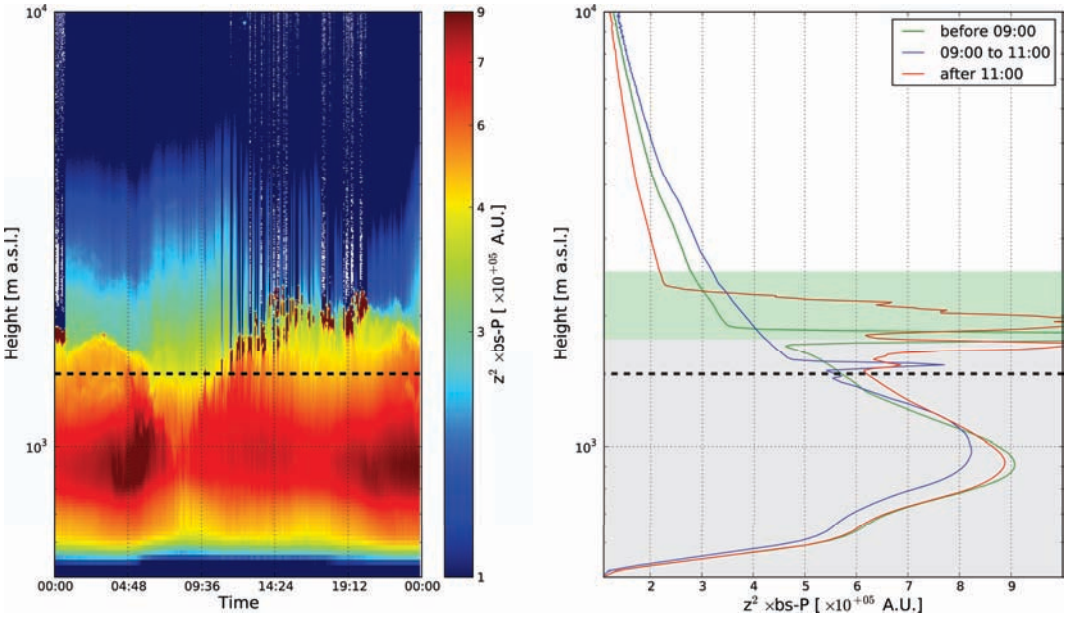

Figure 4.21: *Left panel:* LIDAR z^2-signal evolution in arbitrary units in case of non-simultaneous nucleation event (21/05/2010). *Right panel:* Average LIDAR z^2-signal i- before 09:00 (green line), ii- between 09:00 and 11:00 (nucleation time) and iii- after 11:00. On both graphics, the black dot line represents the hight of the puy de Dôme station.

perature vertical gradient $\frac{\partial\theta}{\partial z}$ indicates that in both cases (D_D and D_S), the atmosphere is vertically stable. This indicates that the turbulent convection is not well developed at the time of the nucleation onset. This observation confirms that, in case of the simultaneous nucleation, all components required to trigger nucleation are homogeneously distributed within the PBL. During the D_D cases, the PBL is much more polluted as it is revealed by the LIDAR measurements and the nucleation primarily occurs at low altitude before being detected at the high altitude suggesting a transportation of the nucleation process. In those particular cases, the nucleation process at the high altitude station is strongly linked to the PBL development because the nucleation is detected at the high altitude site when the PBL extend over the puy de Dôme measurement station. This suggests that during D_D cases, components and conditions needed for the nucleation might be transported through advective motion of air parcels from low altitude to the high altitude station. This assumption is in agreement with the θ_e evolution at both site which present a temporal shift equal to the time delay observed on the nucleation event.
In case of events at both sites (D_x events), no difference were found in GR and J values between the two sites. This result supports the fact that the nucleation process is homogenous over the two sites for D_x type of events. In case of the nucleation at the Opme station only, calculations of GR and J were not possible because of the nucleation shape (calculations are possible for Ia and Ib cases). A larger data set will allow us to analyze and compare those events in the future. However, an analysis of GR and J between P and D_x events was conducted and reported on table 4.8. The main difference between the two types of events is the contribution of neutral species to the nucleation, which ap-

pears to be more than 5 times higher during "P" events while the charged formation rates remain roughly unchanged. This result highlights the variability of nucleation processes according to the altitude and atmospheric layers and support the assumption that the role of ions in the nucleation process could increase with the elevation (Yu et al., 2008).

Table 4.8: Comparison of nucleation characteristics between D_x and P events.

	$GR_{1.3-20}$ [nm.h^1]	J_2 [s^{-1}]	IIN fraction [%]
P events	5.86 ± 2.75	0.67 ± 0.2	32.0
D_x events	6.15 ± 2.55	1.86 ± 2.32	6.2

4.2.4 Summarize and concluding remarks

We investigated the occurrence of nucleation and growth of newly formed particles at a high elevation site, (puy de Dôme, center of France), through long-term measurements of clusters and particle size distributions. We first found that the nucleation frequency is quite high (30% of observed days in average) and present a slight seasonal variation, with two maxima during early spring and autumn and a minimum during winter. From our observations, formation rates of 2 nm particles and their growth rate to larger size were computed using NAIS and AIS data. Average J_2 are respectively $\bar{J}_2 = 1.382 \pm 0.195\,\mathrm{s}^{-1}$, and average GR are $\bar{\mathrm{GR}}_{1.3-20\ \mathrm{nm}} = 6.20 \pm 0.12\,\mathrm{nm\ h}^{-1}$. No seasonal variation of GR could be outlined at both sites. Different types of nucleation events defined by their spatial location and extent were pointed out:

- The "P" type corresponds to a nucleation event which is only detected at the high altitude station of the puy de Dôme (43.5% of the total observed events).
- The "O" type is defined by an event which occurs at the low elevation station of Opme only (2.5% of the total observed events).
- The "D_x" cases represent 54% of the total observed events and are characterized by a nucleation event detected at both station at the same time ("D_S" sub-cases) or with a time delay ("D_D" sub-cases).

The analysis of the nucleation rates according to the type of event revealed that the role of neutral species decrease in case of "P" events compared to events that occur over the whole PBL (D_x events). This points out that nucleation mechanisms could be different according to the altitude or atmospheric layers. Measurements of charged and neutral particles indicate that ion induced nucleation (IIN) contributed by $\bar{\mathrm{IIN}} = 12.49 \pm 2.03\%$ to the total nucleation. Compared to other low elevation sites ($\bar{\mathrm{IIN}} = 2.6 \pm 2.8$), the IIN calculated at the puy de Dôme is quite high but close to the one computed at European altitude sites ($\bar{\mathrm{IIN}} = 15.10 \pm 6.96$) (Manninen et al., 2010; Boulon et al., 2010), suggesting

that the ion contribution to nucleation is enhanced at high altitudes.

The relationships between available atmospheric parameters and the nucleation and growth occurrence were analyzed, showing little significant difference between event and non-event days for most atmospheric parameters except for relative humidity, ozone concentration and the condensational sink. This three parameters are all significantly lower in case of nucleation event at the puy de Dôme site (e.g. $\bar{CS}_{events} = 3.73 \pm 0.11 \times 10^{-3}\,s^{-1}$ while $\bar{CS}_{non-events} = 5.17 \pm 0.15 \times 10^{-3}\,s^{-1}$). This latter observation does not corroborate the results reported from the Jungfraujoch high alpine site, where authors found that new particle formation events frequency surprisingly increases with the condensational sink (Boulon et al., 2010). Different condensable vapor/CS ratio, probably due to the local environment, are likely very different at the two stations (snow at the alpine station versus coniferous forest at the PdD station). Furthermore, we found that sulfuric acid does not seem to play a key role in the nucleation process at puy de Dôme, as also shown at the Jungfraujoch station, suggesting that at those two altitude sites, the nucleation is mainly influenced by other condensable vapors such as VOCs.

Combining the puy de Dôme measurements with measurements at the lower altitude station of Opme, we were able to investigate the vertical extent of the nucleation process in this rural mountainous area. In the puy de Dôme measurement area, the PBL development is less sharply defined than over flatlands due to complex topographic effects on atmospheric dynamics. The boundary layer development must be analyzed for each type of event: "O", "P" and "D_x". Since no LIDAR data were available for "O" type events, only "P" and "D_x" cases are analyzed. During "P" events, the puy de Dôme is located in the upper part of the entrainment zone, between the FT and the PBL, while the Opme station is located within the PBL. During those cases, the PBL is relatively clean (based on the LIDAR signal) and well mixed. The nucleation events occur during the PBL development when the PBL influence on the entrainment zone is maximal. On the contrary, it was found that in "D_S" cases both sites are likely to be located in the planetary boundary layer or in the lower part of the entrainment zone. This latter result highlights that the nucleation occurs within the whole lower tropospheric column, from the free troposphere to the ground level. During the non-simultaneous events, the D_D cases (24.8% of total observed events), the PBL is much more polluted and the nucleation primarily occurs at low altitude before being detected after a various time delay at the high altitude suggesting a transportation of the nucleation process. In those particular cases, the nucleation process at the high altitude station is strongly linked to the PBL development since the nucleation is detected at the high altitude site when the PBL extend over the puy de Dôme measurement station.

The vertical extend of nucleation and growth events observed in this study exhibit some similarities with the one detected during previous airborne studies. During the EUCAARI field campaign, Crumeyrolle et al. (2010) have shown that the vertical extension of the new particle formation events do not exceed the top of the boundary layer and that most

of the nucleated particle events observed have not been formed at the surface but must have nucleated elsewhere in the boundary layer suggesting that the nucleation process could be enhanced by the elevation. In a similar manner, during the IMPACT campaign (Wehner et al., 2010), authors have demonstrated that the nucleation likely occurs at high altitude, in turbulent zones of the residual layer. Our findings demonstrate in a statistically relevant approach that the nucleation process is more frequent at high altitude site and occurs twice as frequently as actually detected in the PBL. Different assumptions can be made in order to explain why nucleation is more frequent at the high altitude site. The lower temperatures at higher altitudes increase the saturation ratio of condensable species (for a given concentration). Furthermore, LIDAR data show that the particle concentrations and hence the condensational sink decrease with the altitude. Although we do not know about the vertical gradient of condensable vapors concentrations, the two predicted gradients tend to favor the nucleation and growth processes. Another possible reason why nucleation is more frequent at the PdD station might be mixing processes at the interface between the PBL and the FT. At this interface, turbulence might be increased due to the different properties of the two distinct atmospheric layers. As already proposed by Wehner et al. (2010), this turbulent mixing could lead to local supersaturation of condensable vapor which in turn could enhance the nucleation process. In addition to this statistical analysis, different vertical scales of nucleation have been pointed out: (i) the nucleation only occurs at high altitude above the mixed layer, between the PBL and the FT in the upper entrainment zone; (ii) the nucleation occurs at the same time along the whole the PBL and in the entrainment zone and (iii) the nucleation is triggered within the low PBL and then transported to highest altitude during the PBL development. Those observations suggest that the nucleation and subsequently growth process could have a very large vertical extent, at least up to more than 800 m. However, this work only provide a lower boundary value since no measurements were available above the puy de Dôme station. Thus complementary airborne studies are needed especially to characterize what happen in the free troposphere when the nucleation is triggered in the planetary boundary layer and in the entrainment zone. Future campaigns involving airborne measurements would allow to check if the nucleation extends over the planetary boundary layer–free troposphere limit or if the phenomenon is vertically constrained as suggested by the work of Crumeyrolle and co-workers.

4.3 A case study of an extreme event: The spring 2010 Eyjafjallajokull volcano eruption

The following work has been published and could be found under the following reference:

Boulon, J., Sellegri, K, Hervo, M. and Laj, P.: Observations of nucleation of new

particles in a volcanic plume, *Proceedings of the National Academy of Sciences of the United States of America*, 108, 12223–12226, 2011.

As seen in the two previous section, at altitude sites, the nucleation do not seem to be strongly correlated with the sulfuric acid estimated concentration. During spring 2010, an unusual events provided us a unique chance to compare different nucleation theories involving the sulfuric acid to nucleation events that occur in a naturally enriched sulfate environment.

The Eyjafjallajokull volcano located in the south of Iceland (63°38' N, 19°36' W, summit 1660 m a.s.l.) erupted on the 20th of March 2010. A major outbreak of the central crater under the covering ice cap followed on the 14th of April 2010 (Institute of Earth Sciences, 2010). A large volcanic plume composed of ashes and gases rose up to the tropopause level (∼10 km) for days and were observed by satellite and ground-based remote sensing instruments. The volcanic plume reached European altitude stations several times in the following days and until the end of the eruptive period on the 21st of May 2010. This event was a unique opportunity to characterize the volcanic ash plume after it had been photochemically aged for several days, with a sophisticated instrumentation that can only be ground-based.

The volcanic plume was first detected over Europe at the High altitude station Zugspitze (2650 m, Germany) on the night from the 17th to the 18th of April 2010 and a second time in the afternoon of the 19th of April. Both the SO_2 and the particle number concentrations (Dp > 3 nm) where detected with concentrations exceeding the 99th-percentile value (years 2000-2007), and were highly correlated with each other (Flentje et al., 2010). At the puy de Dôme station, a strong depolarization signal indicative of volcanic ash (Sassen et al., 2007) was detected using LIDAR measurements on the 18th and 19th of April 2010 and from the 18th to the 20th of May 2010. During April, the volcanic plume was only detected in the free troposphere (between 3500 and 4000 m a.s.l) above the puy de Dôme site and neither variations of SO_2 nor particles concentration compared to the mean diurnal variation level could be detected at the puy de Dôme station (1465 m a.s.l.), indicating that the volcanic plume did not reach the lower troposphere and the planetary boundary layer. On the contrary, during the May episodes, the main volcanic ash plume was first detected around 3000 m a.s.l and then mixed into the boundary layer, as witnessed by an increase of the depolarization ratio in the LIDAR signal and a peak of the SO_2 concentration at the puy de Dôme station. Hence, those particular events observed in May 2010 can be analyzed in detail with specific ground-based instrumentation.

Air masses origins and iso-baric backtrajectories were simulated using the Hysplit model and were conducted for each hour of the day for the period between the 18th and 20th of May. Results confirm that the volcanic plume arrived during the night between the 18th and the 19th May 2010 after 100h of transportation. At the puy de Dôme station, the plume was first detected between 2500 and 3000 m a.s.l. on the 18th of May at 11:45 pm

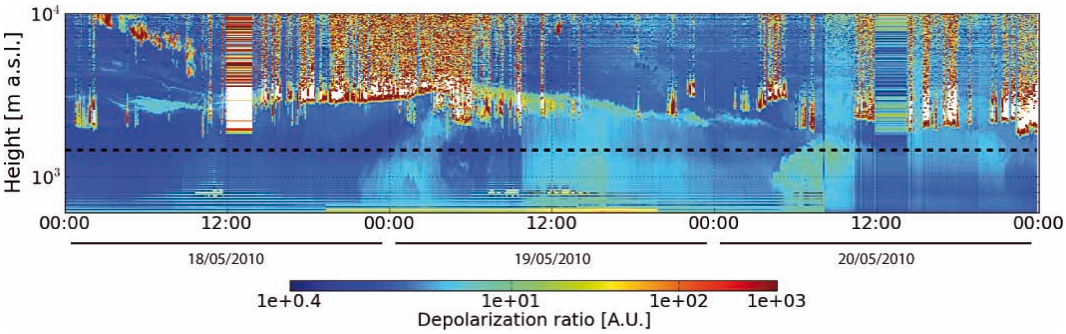

Figure 4.22: Depolarization ratio measured by LIDAR, the dotted line illustrates the height of the puy de Dôme research station.

when SO_2 concentrations peaked until reaching a maximum value of 2.25 ppbv around 4:00 pm exceeding the 99th-percentile value measured at the station from 2005 to present days (Fig. 4.23). This boundary layer intrusion is also detectable from the LIDAR signal as an increase of the depolarization ratio in the atmospheric lowest layers (Fig. 4.22).

One parameter determining if nucleation of new particles occurs in a given environment is the condensational sink (CS). If the CS is high prior to the potential onset of the nucleation event then condensable vapors condense on pre-existing particles rather than form new particles by nucleation. The evolution of the CS (Fig. 4.24, lower panel) calculated from the pre-existing particulate surface, following the method of Pirjola and co-workers (Pirjola et al., 1999), did not increase with the intrusion of the volcanic plume, hence indicating that large particles emitted by the volcano had already settled. This is confirmed by the low number concentration of supermicronic particles detected at the station (< 1 cm^{-3}). As the sun is rising, photochemical reactions lead gas-phase SO_2 to be oxidized to sulfuric acid. This chemical process was estimated using an indirect approach based on global radiation, SO_2 amount, and CS, following the work of Petäjä et al. (2009). The calculation indicates that the production of sulfuric acid reached 3.7 ppt, exceeding the 09-14:00 90th-percentile determined from long-term measurements (from 2005 to present days) using the same calculation procedure. One limitation in the reliability of this calculation procedure is linked to the fact that the oxidative capacity of the atmosphere was shown to be significantly lowered during volcanic eruptions (Pinto et al., 1989; Laj et al., 1990). However, the sulfuric acid levels that we calculate are in the same order of magnitude as the one directly measured at the Zugspitze in the Eyjafjalla plume in April 2010 (0.65 ppt) (Flentje et al., 2010).

4.3.1 Volcanic induced new particle formation events

Strongly correlated to the simulated H_2SO_4 concentrations, the particle concentration follow a clear diurnal variation, both on the 19th and on the 20th of May, with number concentrations multiplied by 2.5 at 14h compared to night time concentrations and by 5

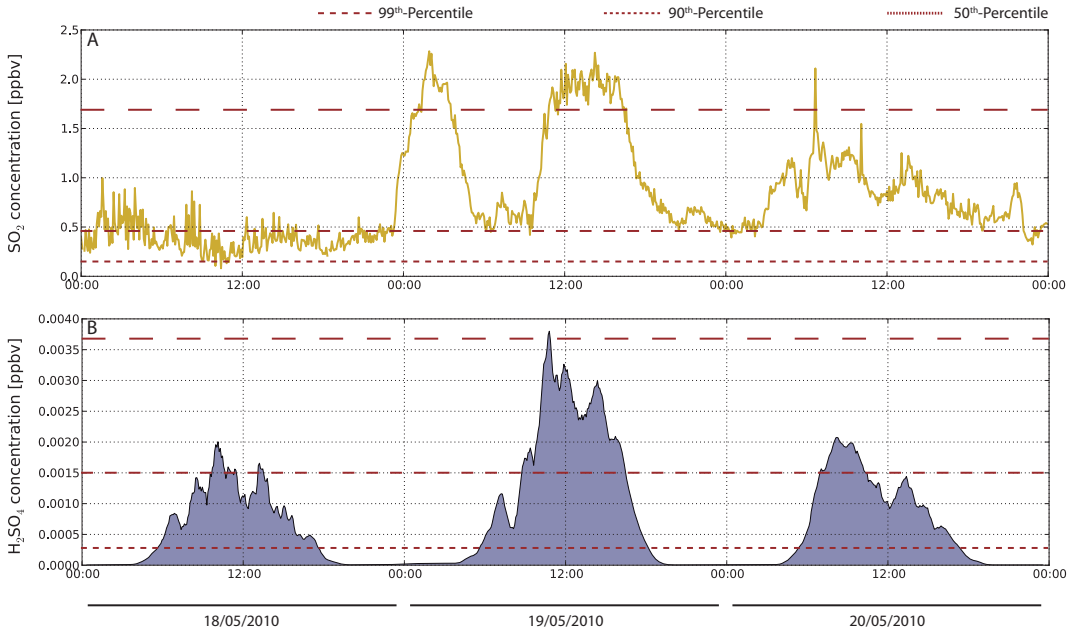

Figure 4.23: Evolution of the SO_2 concentration at the puy de Dôme station (A, upper panel) and calculated H_2SO_4 (B, lower panel).

specifically in the size range from 0.8 to 42 nm. The size distributions of aerosol particles measured with the NAIS (Fig. 4.24, upper panel) shows that these particles are formed from the nanometric scale by nucleation, and that they subsequently grow in the following hours. Events started respectively around 10:00 and 07:30 on the 19th and 20th of May, when the CS was respectively of 6.8 and 11.0 $\times 10^{-3}$ s^{-1}. These CS values are slightly higher than the average CS observed on nucleation-event days and no-nucleation-event days calculated from a long term study conducted at the site by Boulon et al. (2011) (respectively 3.73 ± 0.11 and 5.17 ± 0.15 $\times 10^{-3}$ s^{-1}), highlighting that an exceptionally high condensable vapor concentration was needed to onset the nucleation process.

The formation rate for 2-nm particles (J_2) are classically calculated to evaluate the number of particles formed per time unit (see methods). The nucleation events detected in the volcanic plume are characterized by J_2 that are four times higher ($J_2 = 4.76 \pm 2.63$ s^{-1}) than the average values computed from long-term measurements (2007-2011) at the station ($\bar{J}_2 = 1.32 \pm 0.95$ s^{-1} on 34 comparable events) and 10% higher than the J_2 99th-percentile value (3.66 s^{-1} calculated on 34 comparable events). After the observations of the presence of H_2SO_4 and water in volcanic particles during the Pinatubo eruption by Deshler et al. (1992), the majority of studies used the H_2SO_4−H_2O binary homogeneous nucleation (BHN) theory(e.g. Ramaswamy et al., 2006; Schmidt et al., 2010; Highwood and Stevenson, 2003; Zhao et al., 1995) to estimate the particle formation rates. In the same manner, we can calculate from our data the H_2SO_4−H_2O binary homogeneous nucleation rate $J_{2,BHN}$ using the Yu's procedure (Yu, 2007), which is the closest to the BHN theory according to the laboratory analysis made by Zhang

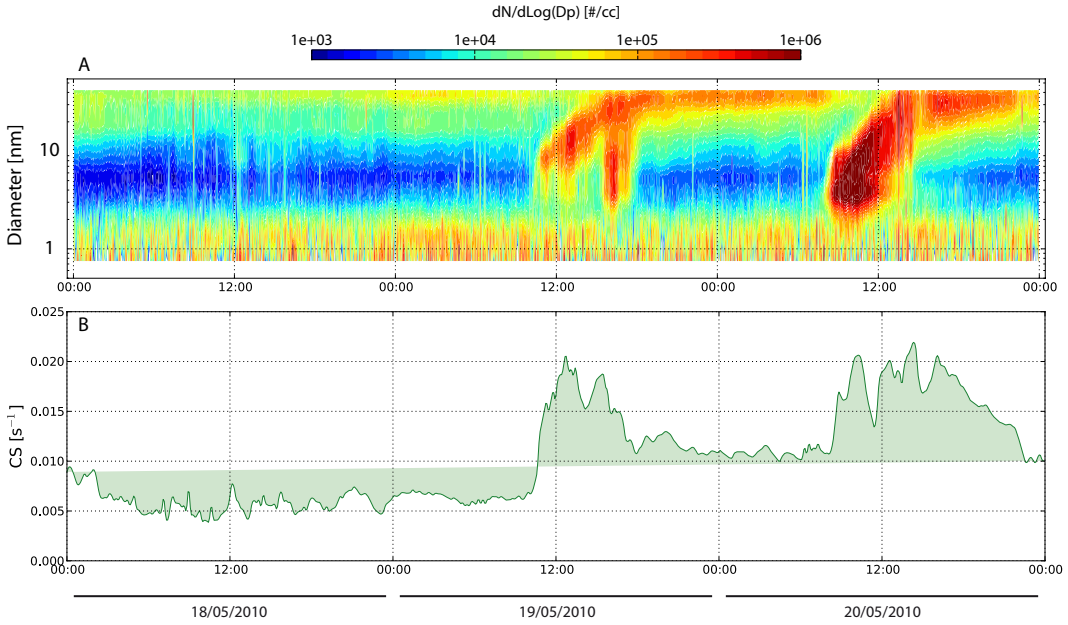

Figure 4.24: Evolutions of the total (charged and neutral) particle size distributions (A, upper panel) and condensational sink (B, lower panel) from the 18 to the 20 May 2010.

et al. (2010). The computed $J_{2,BHN}$ was found to be 7 to 8 orders of magnitude below the observed J_2, suggesting that the volcanic nucleation events could not be adequately described with the $H_2SO_4-H_2O$ binary homogeneous nucleation scheme as it was done in the previous modeling studies. Furthermore, we found that those nucleation events are characterized by an unusual low ion-induced nucleation rate ($IIN = 1.2$ %) compared to the average value computed from long-term measurements ($IIN = 12.49 \pm 2.03$ %, calculated on 34 comparable events Boulon et al., 2011), indicating that the observed nucleation should be described by a neutral nucleation and growth mechanism.

The average particle growth rate of newly formed particles calculated over the 1.3 to 20 nm size range, was 5.26 ± 0.76 nm.h^{-1} which is slightly lower than observed growth rates at the puy de Dôme station (6.20 ± 0.12 nm.h^{-1} Boulon et al., 2011). From this value, the minimal condensable vapor concentration needed to explain the particle growth velocity derived from the work of Dal Maso et al. (2002) was estimated to be $2.65 \pm 0.71 \times 10^{+07}$ molecules/cm^3. The agreement between the calculated condensable vapor concentration and calculated sulfuric acid concentrations during the nucleation process ($3.67 \pm 0.78 \times 10^{+07}$ molecules/cm^3 in average) suggests that the nucleation events observed is likely linked to the H_2SO_4 produced from the atmospheric oxidation of the volcanic emitted SO_2. As a consequence, this observation may also indicate that organic vapors do not significantly contribute to the observed new particle growth, contrary to usual nucleation and growth events in the planetary boundary layer under remote conditions (Paasonen et al., 2010). When particles grow above a certain limit, between 50 and 100 nm diameter, they can act as cloud condensation nuclei (CCN). The potential CCN concentration is classically estimated using the two ratios N50/Ntot

and N100/Ntot where N50 and N100 are respectively the particle concentration with a diameter higher than 50 nm and 100 nm, Ntot is the total concentration. From SMPS data we calculated that freshly formed particle significantly contribute to increase the number of potential CCN. After the nucleation and growth event $38.25 \pm 6.2\%$ of super-10nm particles have reach the 50 nm diameter and $15.2 \pm 3.0\%$ the 100 nm diameter and therefore could act as CCN.

The observational data and analysis presented here demonstrate that nucleation and subsequently growth can be derived from volcanic eruption gaseous released and that this new secondary particle formation event could occur within the lower troposphere at a large distance from the eruptive activity. The analysis of such events reveals that the binary $H_2SO_4-H_2O$ homogeneous nucleation scheme implemented in modelling studies is not adapted to describe the processes observed in the low troposphere, even at high sulfuric acid concentrations. The underestimation of the formation rate of new secondary particles in volcanic plumes by 7 to 8 orders of magnitude when performed from calculations based on this nucleation scheme could lead to an underestimation of the cloud condensation nuclei and the subsequent potential formation of low-level clouds. As a consequence, such results may help to revisit nucleation schemes implemented in all past simulations of the impact of volcanic eruptions on climate. Schemes involving a third specie such as ammonium (ternary nucleation theory Korhonen et al., 1999) or the nano-Köhler theory of cluster activation (Kulmala et al., 2004a) are examples of paths to explore in order to improve the representation of nucleation and particles growth to climate relevant sizes in global models. In the following, simulation of observed events were conducted using the model M4-NPF.

4.3.2 Modelling the volcanic induced nucleation at the puy de Dôme station

The new particle formation event observed during the 20th of May 2010 was simulated using the M4-NPF model. The simulation was conducted using the mean temperature, pressure and relative humidity during the nucleation events (roughly between 07:30 and 13:00). The H_2SO_4 concentration used as an input in the model was the one simulated using the proxy defined by Petäjä et al. (2009). The sub-3 nm cluster concentration is assumed to be constant and an estimated concentration, assumed to be the upper boundary value, is derived from the NAIS measurements ($\sim 23.9 \pm 5.3 \times 10^{+04}$ #.cm^{-3}). The optimal cluster source rate was optimized, within the regards of measurements, to minimize the misfit between simulated and observed particle concentration during the reaction. The best agreement between model and measurements was found for a cluster concentration of $3.3 \times 10^{+04}$ #.cm^{-3}. Model outputs are represented on the figure 4.25. As seen on Fig. 4.25, even though the simulated nucleation is triggered sooner,

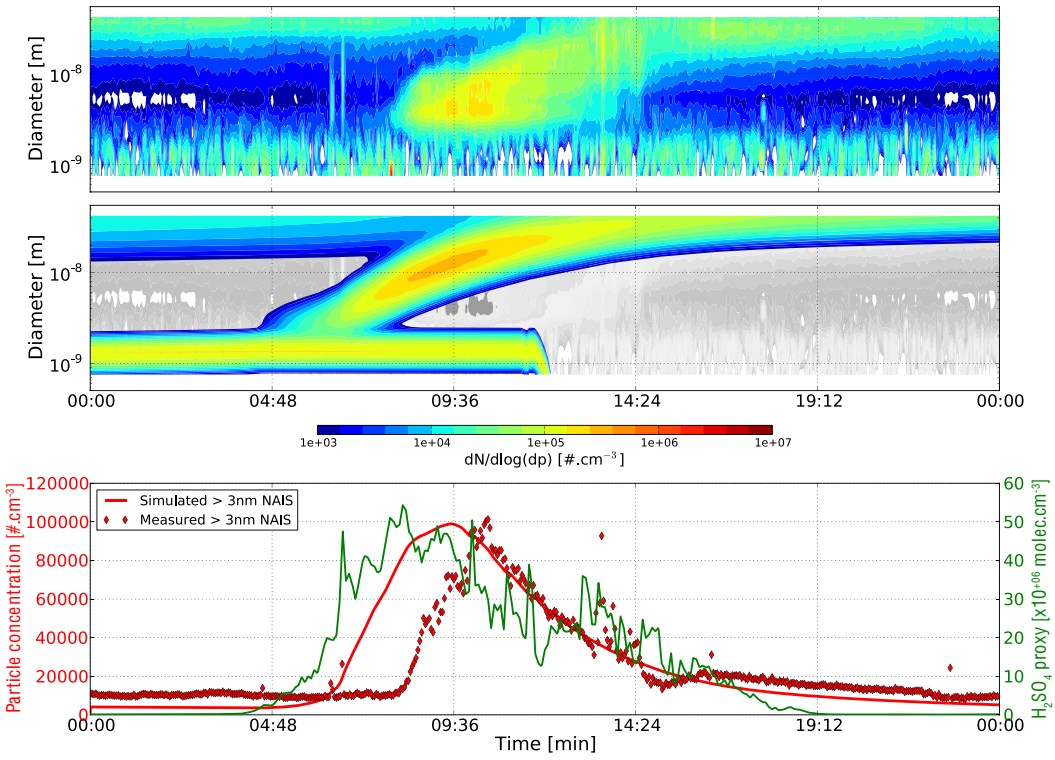

Figure 4.25: Simulation of the nucleation events observed at the puy de Dôme station the 20th of May 2010. Measured and simulated aerosol size distributions are reported respectively on the upper and the middle panel. Particle concentrations and H_2SO_4 proxy are reported in the bottom panel.

the global dynamic of the new particle formation event is well represented. The time delay between observed particle formation and the H_2SO_4 is estimated to be around 2.25 hours. A similar time shift is observed between the dynamic of the simulated and the measured particle number concentration. The comparison between observables and simulation products for the 20th of May 2010 event are reported in the table 4.9.

We first can notice that observed growth rates are larger than simulated growth rate, indicating that other condensable gases may contribute to the newly formed particles growth. However, if the growth rates are not accurately represented, 3 nm-formation rates are well described by the model suggesting that the condensation process on sub-3nm pre-existing clusters is able to explain the observed new particle formation. The

Table 4.9: Measured and M4-NPF simulated nucleation characteristic rates. The growth rates and formation rates are respectively expressed in nm.h^{-1} and in #.cm^{-3}.s^{-1}, NMB is the normalized mean bias [%].

Observables	$GR_{1.3-3}$	GR_{3-7}	GR_{7-20}	J_3
Measured	6.0	6.8	7.6	7.4
Simulated	N.D.	3.2	5.6	7.2
NMB	N.D.	-112.5	-35.7	-2.8

Table 4.10: Comparison of different nucleation parametrizations. *NMB* is for "normalized mean bias".

Type	Parametrization	Formulation	J_3 [#.cm^{-3}.s^{-1}]	NMB
Binary	Yu, 2008	$J \propto f(N_{H_2SO_4}, T, RH)$	$< 10^{-08}$	$> -10^{+08}$
Ternary	Yu, 2006	$J \propto f(N_{H_2SO_4}, T, RH)$, $F_{NH_3} = 2$	$< 10^{-08}$	$> 10^{+08}$
	Yu, 2006	Optimized NH_3 stabilization effect, $F_{NH_3} = 550$	7.4	0.0
Activation	Sihto et al., 2006	Activation type nucleation, $J = 1.7 \times 10^{-06}[H_2SO_4]$	6.1	-21.3
Kinetic	Kuang et al., 2008	Kinetic type nucleation, $J = 1.6 \times 10^{-14}\ [H_2SO_4]^{2.01}$	2.5	-66.2
	Sihto et al., 2006	Kinetic type nucleation, $J = 0.6 \times 10^{-12}[H_2SO_4]^2$	2.2×10^{-05}	$> -10^{+05}$

closer parametrization to our observation would hence to be the so-called "activation-type" nucleation, i.e. the activation of small clusters via heterogeneous nucleation, as already proposed by Sihto et al. (2006). This parametrization was tested and compared to other parametrizations (see table 4.10) and it was found that this formation rate formulation gives the best agreement with the observed nucleation rate. It also can be noticed that the ternary nucleation theory failed to explain the observed event with a laboratory measurement derived NH_3 stabilizing factor ($F_{NH_3} = 2$) and a stabilizing factor of 550 is necessary to explain the formation rate which seems to be unrealistic. There is a possibility that the activation mechanism could also explain the time delay between M4-NPF outputs and the measurements. Indeed, the M4-NPF model only account for condensation and coagulation and no activation thermodynamic are represented. An other assumption could be advanced to explain the premature onset of the modelled nucleation. The simplistic description of the pre-existing aerosol size distribution leads to an underestimation of the condensational sink, thus the critic condensable vapor concentration needed to trigger the nucleation and growth is reached sooner in the model.
In the M4-NPF, we assume that a cluster mode always exist and that its number is constant. Furthermore, when the coagulation process of cluster on Aïtken mode is activated, all the clusters are removed within few seconds whatever the source rate is. Thus we limit the coagulation of clusters to intramodal and mode+1 processes to fit to the observations. This also reveal that the cluster physics is not accurately described by the Fusch theory of coagulation. If the activation type nucleation is likely to be the most adequate mechanism to represent the observed events, the parametrization provided by Sihto et al. (2006) should be used carefully since it does not take into account for temperature and relative humidity which are known to play important role in the nucleation process. Moreover, the activation factor, here 1.7×10^{-06}, should be adapted to the considered measurement site.

Observation and modelling results highlight that the BHN as well as the THN kinetic approximation failed to represent the nucleation at a high altitude even in a natural sulfate-enriched environment. Site specific parametrization derived from activation or kinetic type nucleation mechanisms are likely to be the most adequate ones for the new

particle formation rate prediction under these conditions. However, those parametrizations are too simplistic to predict or to describe nucleation in various environments since they do not take into account for temperature and relative humidity nucleation dependency and the pre-factors in those empirical nucleation rate formulations derived from different field measurements may vary by up to 4 order of magnitude (Zhang et al., 2010). We show that a simple condensation and coagulation mechanism of a single condensable vapor, the sulfuric acid in our particular case, assuming a constant cluster source rate, could provide a good approximation of new particle formation rates in environment dominated by one type of condensable vapor.

4.4 Concluding remarks

The three different but complementary studies that were presented in this section provide new informations on the nucleation process and its spatial extent. At the Jungfraujoch and puy de Dôme stations and contrarily to what it is usually observed in the planetary boundary layer, we show that the sulfuric acid is not likely to be the central actor of the onset of the nucleation and that other vapors are needed to explain the nucleation process under classical atmospheric conditions characteristics of each station. However, we show during the Spring 2010 volcanic episode that in a sulfate-enriched environment that acitvation or kinetic type sulfuric acid nucleation parametrization could be a fairly good approximation. Consequently, we show with a more complex model that the condensation of sulfuric acid on a pre-existing cluster population can reasonably describe the observed new particle formation event dynamics and formation rates. However, in this latter case, the growth rate of freshly formed particles computed with our model were slighlty underestimated. One plausible reason is that the chemical composition of pre-existing cluster play a role in the growth process. It has been proposed that ammonia would participate to enhance atmospheric nucleation by stabilizing molecular clusters containing sulfuric acid molecules but this theory failed to explain observed nucleation rates. Recent studies conducted by Barsanti et al. (2009) and Smith et al. (2010) have shown that amines and aminium–organic acid salts contribute significantly to the first steps of nanoparticle growth. Such mechanism could explained the difference between modelled and observed growth rates. At Jungfraujoch and puy de Dôme station, parametrizations involving UV radiations and pre-existing clusters concentrations give the best agreement with observed nucleation rates suggesting that organic vapors may play an important role in ultrafine aerosol nucleation and growth. Those results are in agreement with the recent paper of Kuang et al. (2010) which reports that the contribution of sulfuric acid to the nucleation-mode particle growth rate is less than 10% at various continental sites. All those studies and results converge to the conclusion that new theoretical tools and new parametrizations are needed to represent the nucleation and subsequently growth processes, tools which take into account for organic compounds and activation mechanism, parametriza-

tions which account for temperature and relative humidity role in the nucleation process as well as the role of organics in the first steps of the new particle formation. In the following chapter, experimental studies were conducted to investigate the role of organics in the nucleation and growth processes. During those experiment no sulfuric acid were introduced in the system in order to provide an "organic nucleation parametrization".

Chapter 5

Laboratory experiments: probing the nucleation process

Contents

In the past two decades, the focus has been put on sulfuric acid, which is suspected to play a central role in nucleation processes,. More recently, a growing number of studies have been dedicated to the role of organic species as well (e.g. Bonn and Moortgat, 2002; O'Dowd et al., 2004; Kulmala et al., 2004a; Metzger et al., 2010). In the preceding chapter, we show that sulfuric acid cannot explain the whole NPF process at two European altitude locations. Other condensable vapors such as volatile organic compounds were found suspected to play a very important role in these processes. The goal of the following section is to investigate with laboratory experiments and modelling the role of such compounds.

5.1 Combustion reactor experiments: the PIREP project

Diesel is the dominant fuel used by personal and commercial transport sector. Diesel engines also power most non-road equipment including construction and agricultural equipment, marine vessels and locomotives. While the operational advantages of diesel engines are clear, diesel fuel is a major contributor to particulate matter emission. Exposure to diesel exhaust particulates is reasonably anticipated to be a human carcinogen. To date, most of the diesel particulate matter reduction efforts have focused

on either new engine replacements or retrofitting existing engines with post combustion emission control equipment. However, vehicle emission is still one of the major sources of nanoparticles in urban areas (Morh et al., 2003a,b). New particle formation in vehicular exhaust is a complex process which depends on wide range of factors such as the sulfur content in fuel and lubricating oil, the engine combustion regime as well as the exhaust after-treatment setups or the exhaust dilution. Previous studies on high sulfur-containing fuel have shown that the binary homogeneous nucleation may account for ultrafine particle formation in exhaust plumes (Du and Yu, 2006).
In many countries, the sulfur content of the diesel fuel has been drastically reduced (typically from 500 to 10 ppm and below) but recent laboratory experiments and in situ measurements have shown that number concentrations of nanoparticles emitted by vehicles running on the ultra-low sulfur fuel remain high in contradiction with the BHN theory predictions (e.g. Arnold et al., 2006; Kittelson et al., 2006). Consequently, ion-mediated nucleation has been proposed as an alternative formation mechanism of the diesel nucleation mode particle both with filter after-treatment and without exhaust after-treatment (Yu, 2001). However, Maricq (2006) have experimentally shown that diesel exhaust particles exhibit a neutral nucleation mode except without a diesel particulate trap.
Based on those results, measurements of particle size distribution were undertaken by Lähde et al. (2009) using an air ion spectrometer and a nano-SMPS. They found that a charged nucleation mode is detected in the exhaust plume but that its concentrations were too low to be explained by the IMN. Hence, because both BHN and IMN theories fail to explain the observed nucleation rates in case of low sulfur-containing fuels, it is suggested that the nucleation mode is likely formed by condensation of vapors onto non-volatile core.

In the following, secondary particle formation from engine combustion process will be studied using an experimental set-up built in the frame of the PIREP project (french acronym for "Innovative Process for Reducing Emissions of diesel Particles") and based at the IRCELyon, CNRS UMR 5256. During those experiments, the nucleation and new particle production were investigated as a function of the post-treatment and the dilution of the exhaust plume.

5.1.1 Experimental set-up

The aim of the experimental set-up is to mimic the exhaust of diesel engine by generating soot in suspension in a gaseous reactive mixture (additional gases) (Fig. 5.1). Additional gases are composed by O_2 (10%), CO (5000 ppm), CO_2 (8%), NO (500 ppm), C_3H_6 and C_3H_8 (with the ratio C_3H_6:C_3H_8 = 1). The set-up is composed by:

- a commercial combustion device (CAST HiVol),

- an oven with a diesel particle filter (DPF) support,

- and a diluting tube which length can be varied.

Particles were characterized using a Scanning Mobility Particle Sizer (SMPS), an aethalometre (Aethalo.) and an Aerosol Mass Spectrometer (AMS). Nucleation was tracked using a NAIS. Only the NAIS data will be discussed here. According to the intercalibration studies conducted by Asmi et al. (2009) and Gagné et al. (2011), NAIS mobility measurements are trustworthy but particle concentration are overestimated especially in the sub-3nm range. However when the concentration sub-3nm particles is high which is espected in exhaust plume relative error on sub-3nm particle concentration become insignificant. Therefore, in the following the whole particle size distribution measured by the NAIS will be considered.

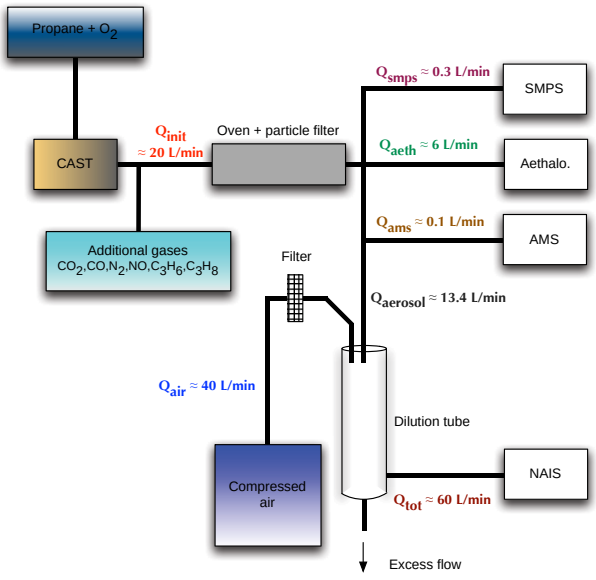

Figure 5.1: Instrumental set-up used during the PIREP experiments.

An experiment cycle is composed of 3 different phases (Fig. 5.2): i- the loading phase (*Ch.*) where particles generated by the CAST are accumulated on the DPF (increase of the ΔP and filter temperature T); ii- the purge of the system (*P.*) before regeneration (Pressured air with additional gases are injected in the system while the PF is shunted) to clean the pipes and iii- the regeneration phase during which additional gases are injected and the DPF is heated until the decrease and stabilization of the ΔP. Different combustion regimes (CR) of propane were investigated along a complete experimental cycle (Fig. 5.2) but three of them representative of O_2 excess (CR1), stoichiometric conditions (CR1) and lack of O_2 (CR1) will be presented (Tab. 5.1).

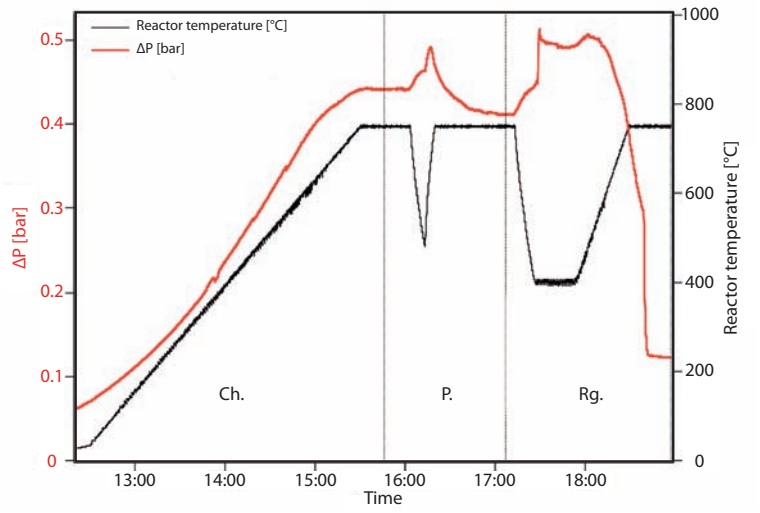

Figure 5.2: Example of an experimental cycle. *Ch.* is for the DPF loading phase, *P.* is the purge of the system and *Rg.* is the DPF regeneration phase.

5.1.2 Results

For each CR, we characterized the number distribution of particles generated during each phase of the cycle, i.e. with or without the post-treatment device.

Characterization of the generator particulate production The combustion regimes, as presented in the Table 5.1, are representative of an oxygen concentration available during the combustion process. The higher CR, the smaller oxygen concentration is injected in the generator, thus providing conditions for incomplete combustion of the propane. As shown on figures 5.3, large differences in term of concentration and

Table 5.1: Characteristics of different combustion regimes.

CR	Air [L.h^{-1}] Dilution	N_2 [L.h^{-1}] Quenching	C_3H_8 [L.h^{-1}] Fuel	N_2 [L.h^{-1}] Mixing	Air [L.h^{-1}] oxidation
1	1200	450	3.6	0	93
4	1200	450	3.6	9	90
8	1200	450	3.6	19.5	79.5

particle diameter modes exist between CR1, CR4 and CR8. Main characteristics of each CR are reported in the table 5.2. The charged fraction only represent 2.8% of the total particle concentration measured by the NAIS so in the following, we will only consider neutral particles. The NAIS measurements reveal the production of a dominant 1.2 nm diameter cluster mode. The tail of another larger mode is also detected, confirmed by the SMPS measurements, which indicate that this Aïtken mode diameter is located between 35 nm (CR8) and 80 nm (CR1). As reported in the table 5.2, the total number concentrations detected by the SMPS (10 nm$\geq$ Dp $\leq$ 400 nm) increases from CR1 to CR8. On the contrary, particles emitted during highly oxygenated combustion (CR1 and

Table 5.2: Physical properties of generated particles measured by NAIS, SMPS and AMS.

Instrument	Properties	CR1	CR4	CR8
NAIS	Modes [nm]	~ 1.2 & > 42	~ 1.2 & > 42	~ 1.2, 25 and > 42
	super-3nm [$\times 10^{+14}$#.m^{-3}]	2.9	3.1	3.0
	sub-3nm [$\times 10^{+14}$#.m^{-3}]	4.8	4.6	1
SMPS	Modes [nm]	80	70	35
	Total particle [$\times 10^{+14}$#.m^{-3}]	4.0	5.5	8.0
	Mass [mg.m^{-3}]	500	350	10
AMS	Organic mass [mg.m^{-3}]	20	10	1

4) present a higher mass than the ones produced during poorly oxygenated combustion (CR8). Organic mass spectra measured with the AMS for CR1 and 4 are in agreement with the diesel exhaust literature. For higher combustion regimes, particles are more oxidized and are enriched (relative composition) in polycyclic aromatic hydrocarbon. In the following, the discussion will be focused on the CR1 since this regime is the most representative of a classical diesel exhaust in term of ratio of oxygen content during the combustion process.

Post-combustion filtration and regeneration experiments Post-treatment devices (DPF) were either used alone or with an oxidation catalyst (DOC) introduced between the soot generator and the DPF. Filters mean porosity was 15 µm. Once a DPF was introduced in the system, the concentration of particles with a diameter larger than 20 nm was filtered by 99.9% (NAIS and the SMPS measurements) during the whole experimental cycle (Ch., P. and Rg.). An example of a DPF result is shown on figure 5.4. In the sub-20 nm size range, we still observe a cluster mode at 1.2 nm during the loading phase with an average concentration of $2 \times 10^{+04}$ #.cm^{-3} (Black curve and plot on the figure 5.4). The presence of clusters could be linked to an inefficient filtering of the DPF or due to nucleation after the DPF has filtered most of the aerosol condensational sink, but let condensable gases go through. The hypothesis of nucleation after the DPF was tested by varying the length of the dilution tube. We observed that during the loading phase, clusters grow from 0.95 nm at 16 cm from the exhaust, to 3.5 nm at 100 cm from the exhaust. The growth rate seems constant at least until 1 m after the exhaust (residence time of 0.13 s in the dilution tube). The calculated growth rate is $GR = 21.2$ nm.s^{-1} indicating that (i) measured clusters are not an intrumental artefect and (ii) under these conditions, particles would reach a climate-relevant size of 50 nm after a residence time of 2.3 seconds in the atmosphere.
When the Rg. phase starts, the temperature of the filter is lower than during the loading phase (Fig. 5.2) and only clean gases (clean air and additional gases) are injected in the system. The soot combustion is tracked through the diminution of theΔ P and it was found to occurs for $T = 555$°C. It coincides with a peak of cluster production ($\sim 10^{+06}$ #.cm^{-03}) detected with the NAIS (Rg. + 32min). Again, this can be either due to the expulsion of clusters trapped in the DPF during the loading phase, or due to nucleation

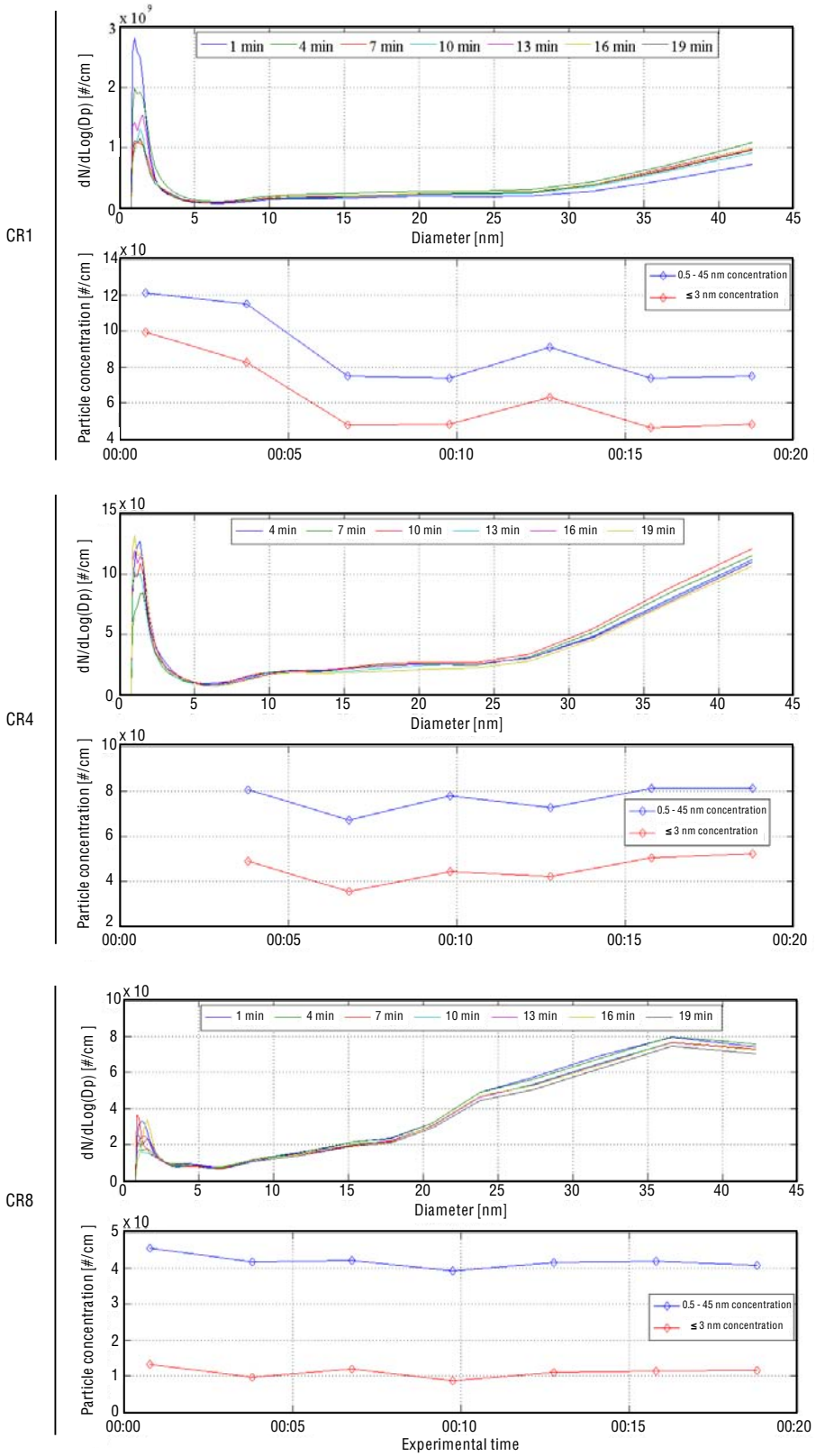

Figure 5.3: Evolution of the total particle size distribution measured with the NAIS during CR1 (top panel), CR4 (middle panel) and CR8 (bottom panel) experiments.

from gazes issued from the combustion of particles trapped on the filter during the loading phase. As the combustion occurs, the particle concentration decreases down

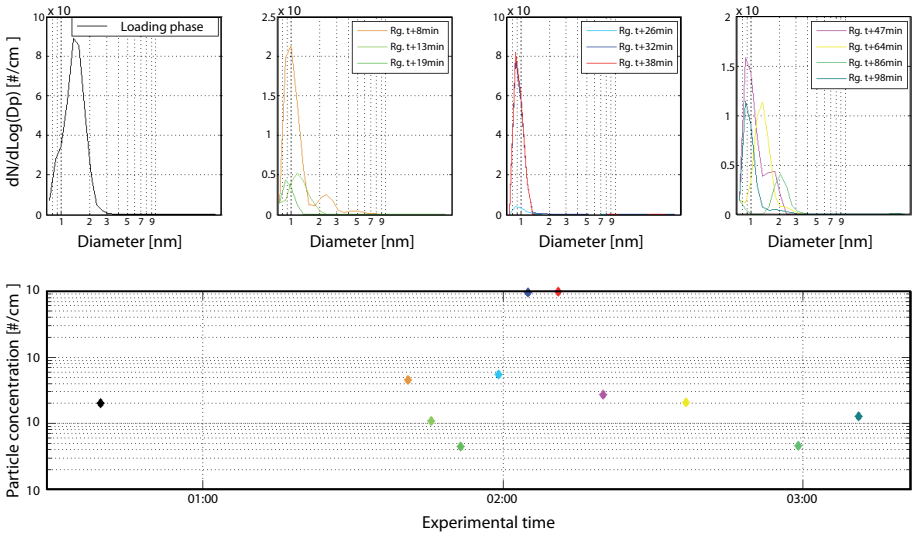

Figure 5.4: Evolution of the total particle size distribution measured with the NAIS during a full experimental cycle (CR1).

to $\sim 10^{+04}$ #.cm^{-03} in average, while the mode of emitted particles increases through condensation of combustion products (from 0.9 nm at Rg. +32 min to 2 nm at Rg. + 86 min). When a DOC is introduced before the DPF, it makes the regeneration temperature decrease down to $T = 510$°C. This effect is linked to the NO oxidation into NO_2 which is a more efficient oxidative compound than O_2 for soot combustion. However, the effect of the DOC on the ultrafine particle production during the regeneration phase was not found to be significant in term of number concentration in the size range from 0.8 to 42 nm ($\sim 10^{+12}$ #.m^{-3} with or without the DOC), but significant differences were found in the growth rates of ultrafine particles (from 2.2 to 0.3 nm.s^{-1} without and with DOC respectively). This result suggests that the condensable vapor concentration available for condensational growth has been significantly decreased by the DOC.

As a result, those experiments highlight that secondary particles are generated from condensable vapor released during i- the combustion process and ii- the particle filter regeneration. The mass spectrometry analysis of such particles reveals that those particles are composed by organics. No sulfates were detected. Consequently, those experiments point out that nucleation can occur in the exhaust of engine after a post-treatment device even in the absence of sulfuric acid.

Nucleation from organics in the absence of sulfuric acid has also been observed from biogenic compound ozonolysis under atmospheric conditions and further characterized in simulation chamber experiments. Those experiments conducted in collaboration with the Laboratoire Interuniversitaire des Systèmes Atmosphériques de Créteil are presented in the next section.

5.2 Nucleation from the ozonolysis of biogenic terpenes in a simulation chamber

Detailed mechanism of nucleation in the atmosphere remain unclear, especially the role of organics in the first steps of new particle formation. Smog chamber (e.g. Metzger et al., 2010) and field measurements (e.g. Bonn et al., 2008; Paasonen et al., 2010) show that organics, associated with sulfuric acid are involved in the condensational growth but also in the nucleation process. The parametrization proposed by Metzger et al. (Eq. 5.1) predicts that nucleation can not occur in absence of sulfuric acid.

$$J_{1.5} = k[H_2SO_4]^m[\text{NucOrg}]^n \tag{5.1}$$

where $m = 1.0 \pm 0.04$, $n = 0.8 \pm 0.04$ and $k = 7.2 \pm 4.4 \times 10^{-13}$ cm^3.s^{-1}. When m and n are constrained to unity, $k = 7.5 \pm 0.3 \times 10^{-14}$ cm^3.s^{-1}.
Furthermore, in their work, Metzger et al. used high concentrations of 1,3,5-trimethylbenzene (250 ppb) as representative of anthropogenic organics and performed photo-oxidation experiments in a 27-m^3 teflon chamber. Particles were measured using a nano-SMPS, which allows particle detection in the size range $4 - 100$ nm. Such experimental conditions do not allow for the study of charged particles since teflon act as an ion filter due to its dielectric property and the SMPS cannot reveal the first steps of the nucleation process because of its size range limits.
According to the review made by Kanakidou et al. (2005), "[...] the emissions of biogenic volatile organic compounds (BVOCs), which are emitted mainly by vegetation, are estimated to exceed those from anthropogenic emissions.". Isoprene is the BVOC which has the largest emission rate of all non-methane VOCs, estimated at 600 Tg.yr^{-1} (Guenther et al., 2006). This hemi-terpene is now well know to be a SOA precursor (see the review of Carltonn et al., 2009). However, monoterpenes and especially α-pinene, β-pinene, sabinene and limonene account for 40 to 80% of the overall terpene emission on a global scale, when isoprene is excluded. Their relevance as precursors of new particles has been proved by different studies (e.g. Koch et al., 2000; Bonn et al., 2002; Rohr et al., 2003; Bonn et al., 2008). However, no parameterization of particle formation rate due to those VOCs is available in the literature. The experiments conducted at the Interuniversitary Laboratory of Atmospheric System (LISA, CNRS UMR 7583) in the CESAM smog chamber (i.e. french acronym for Experimental Multiphasic Atmospheric Simulation Chamber – Chambre Expérimentale des Systèmes Atmosphériques Multiphasiques) were designed to fill those gaps.

5.2.1 Experimental set-up

Dark ozonolysis experiments of sabinene and α-pinene were carried out in the CESAM chamber using 100 ppb of ozone and monoterpene concentrations ranging from 10 to 100

ppb in a dry atmosphere ($RH < 1\%$).

The simulation chamber The simulation chamber (Fig. 5.5) is extensively described in Wang et al. (2011) but as opposed to the chamber used by Metzger et al., CESAM is made of stainless and its volume is more than six times lower (4.2 m^3) which allow a mixing time lower than one minute ($\sim 45s$ according to Wang et al., 2011). Those characteristics allow to work i- on charged species and ii- with small amount of reactive gases. The smog chamber is initially filled with 80% of N_2 and 20% of O_2. However the NAIS and SMPS pump from the chamber at a flow rate of about 61 lpm. In order to keep the pressure constant in the chamber, the same flow rate of N_2 is injected into the chamber. To avoid over- or under-pressure inside the chamber compared to ambient local pressure, a teflon bag (i.e. a kind of tank) is connected between the chamber and the N_2 source so that the flow rate could be adjusted visually. One of the consequences of this procedure, is that the $N_2 : O_2$ ratio is a time variable. Its evolution will be described is in the following.

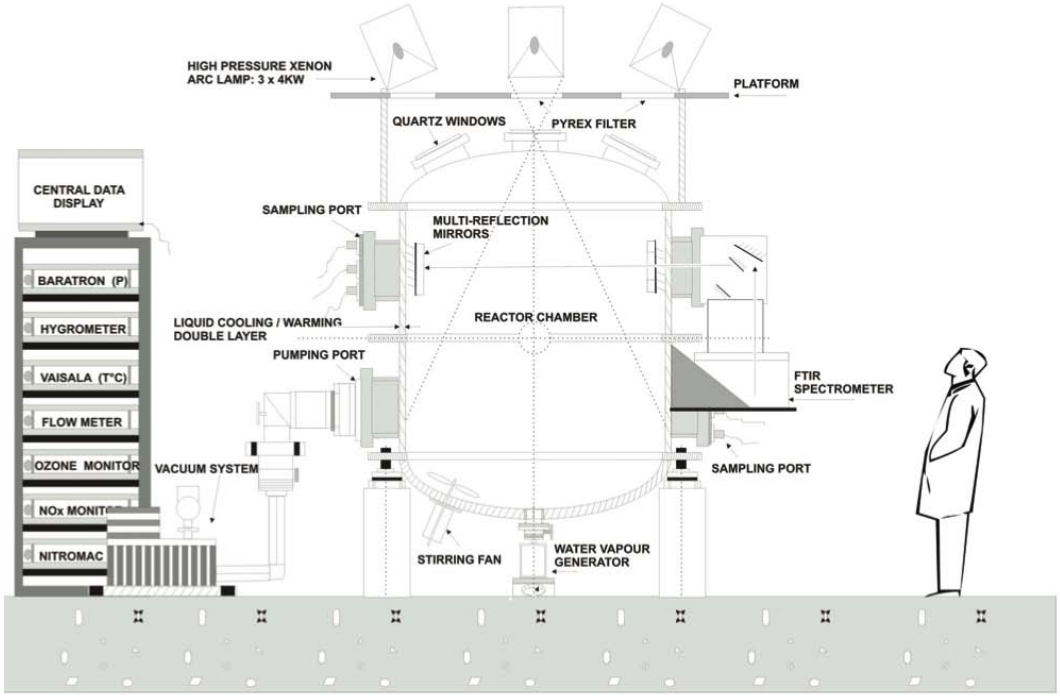

Figure 5.5: Schematic front view of the CESAM facility (from Wang et al., 2011).

Measurements Particle size distribution were measured using a combination of a NAIS and a SMPS which allow the detection of charged particle from 0.8 to 42 nm (NTP-conditions) and total particle from 0.8 to 700 nm. NO_x and O_3 measurements are respectively performed with an APNA-370 and an APOA-370 both from Horiba®. The terpene concentration is continuously monitored using a Fourier transform infra-red

spectrometer (FT-IR) Bruker© Tensor™. The FT-IR system records spectra between 500 and 4000 cm^{-1} with an optimal resolution of 0.5 cm^{-1}.

Schedule of an experiment Since the O_2 fraction in the chamber changes in time due to the N_2-refill process, experiments have been conducted according to a strict plan:

1- Filling the chamber with the 80:20-$N_2 + O_2$ mix (1 hour) $\Longrightarrow$ Characterization of the $N_2 + O_2$ chamber background (20 minutes).

2- Injection of O_3 ($\approx$ 170 ppb) $\Longrightarrow$ Characterization of the $N_2 + O_2 + O_3$ chamber background until reaching 100 ppb of O_3 (20 to 30 minutes in average).

3- Injection of the terpene (in average 48.1 ± 5.3 minutes after the beginning of the step 1).

4- Pumping of the chamber (few hours).

The effect of the lack of O_2 (i.e. high $N_2 : O_2$ ratio) was tested by increasing the time delay before the terpene injection (see Table A.2).

5.2.2 Results

5.2.2.1 Neutral cluster mode measurement characterization

According to Asmi et al. (2009), total particle measurements below 3 nm could not be relevant for low particle concentrations. Considering this result, we also conducted an experiment to characterize the NAIS neutral cluster measurement mode in our experimental conditions. Particle produced by the NAIS for a given thermodynamical condition set could be estimated by filtering the air sucked by the instrument and analyze the fraction of particle which are still detected by the instrument.
The filter was build using gas-mask filters since their porosity allows a high flow rate (maximum human breathing flow rate is approximatively 20 lpm) and was adapted to the NAIS inlet. Ambient air filtration experiment were conducted in a room of the laboratory in atmospheric conditions (Fig. 5.6).

As seen on the figure 5.6, the filter significantly impacts the particle size distribution: in average 95% of charged particles and 76.1% of the total particles (charged and neutral) are filtered. However, in the total particle mode, the NAIS produces sub-3nm ions during the neutralization phase Asmi et al. (2009), and we confirm that sub-3nm particles concentrations are over-estimated even when the filter is on (low particle concentration conditions). Assuming that the filter is not charged, no difference should exist between the filtration efficiency of super-3nm charged particles and neutral ones. Hence, for (T, P, RH) conditions of experiment (respectively 8.4 ± 0.9 °C, 945 ± 0.5 hPa and 63.7 ± 4.5 %), the sub-3nm particles generated inside the instrument was estimated to be respectively for positive and negative analyzer $\sim 2350 \pm 200$ and $\sim 5600 \pm 640$ $\#.cm^{-3}$.

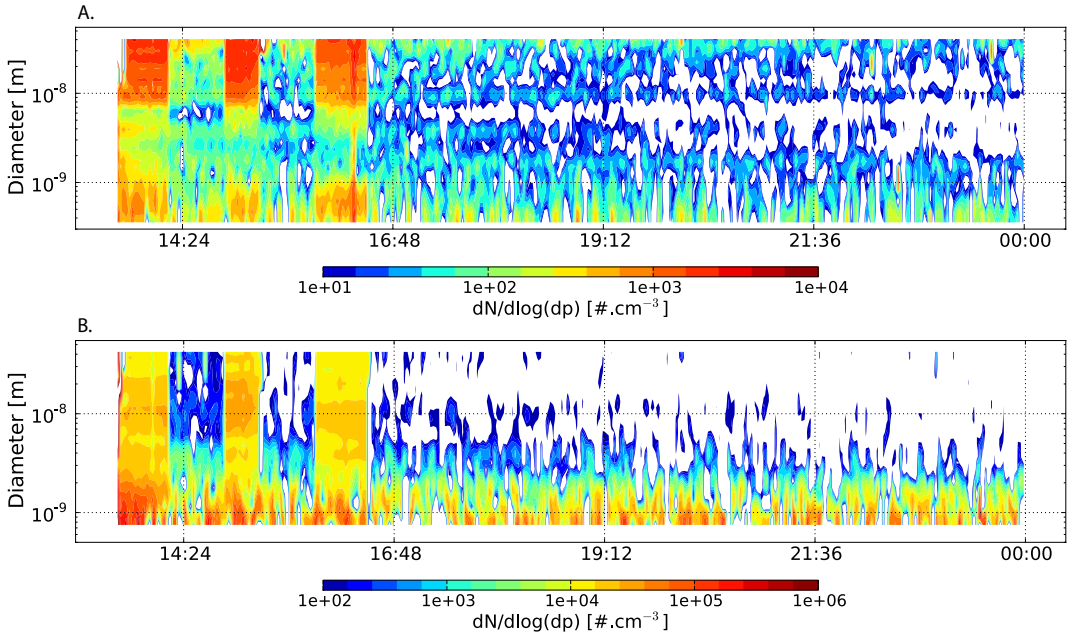

Figure 5.6: Filtration experiments. A. Negatively charged particles and B. Total particles detected by the negative analyzer.

A recent paper by Manninen et al. (2011) shows that the chemical composition of such ions are strongly influenced by the carrier gas composition, i.e. the gas compostion of the sucked air. Consequently, we chose to only consider sub-3nm concentration as an upper limit value because of the lack of quantitative knowledge on ions production due to the corona discharge and its dependence to the air composition and properties in our conditions (N_2 : O_2 ratio, RH, particle concentrations, organic vapors, etc...).

5.2.2.2 Characterization of the chamber background

The chamber background particle concentration was characterized before each experiment. The chamber was filled by N_2 until reaching 80% of the standard atmospheric pressure (P_{std} = 1000 hPa), then O_2 was added until the pressure inside the chamber equals P_{std}. Before connecting the NAIS to the simulation chamber the ratio N_2 : O_2 is 80:20. One major result was to find extremely high concentrations of sub-3nm clusters in the empty chamber (only N_2 and O_2 present). These neutral sub-3nm cluster concentrations increased with time and we found that they were mainly linked to the N_2 concentration. This result is corroborated by the recent work of Manninen et al. (2011). Measurements in the ion-mode of the NAIS revealed that less than 10^{-03}% of these clusters were charged. The evolution of the N_2 and O_2 concentration was calculated using both a discrete iterative procedure and an analytical model of dilution described by the set of equations 5.2 and 5.3. The simulated gaseous evolution in the smog chamber is reported on figure 5.7. Relative errors of the dilution model is below 0.6% for nitrogen and below 10^{-3}% for oxygen calculations after 120 minutes of simulations, thus this model is

relevant to compute the evolution of the N_2 and O_2 composition in the chamber.

$$N_2(t) = N_2(t{=}0) \times (1{-}d)^t + O(t) \quad (5.2)$$

$$O_2(t) = O_2(t{=}0) \times (1{-}d)^t \quad (5.3)$$

$$\text{where: } d = \frac{N_2^{in}}{V} \text{ and } O(t) = N_2^{in}\left(1{-}\frac{1{-}(1{-}d)^t}{\ln(1{-}d)}{-}(1{-}d)^t\right)$$

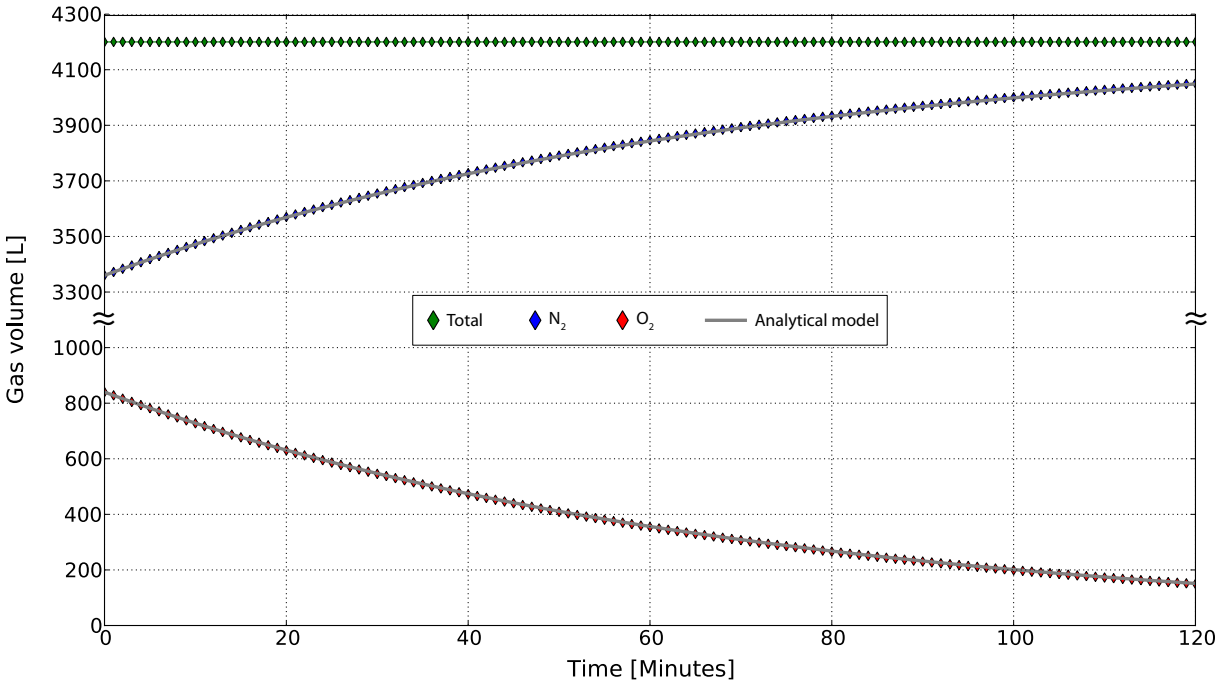

Figure 5.7: Simulation of the gas composition of the chamber.

5.2.2.3 Nucleation experiments

Nucleation experiments were conducted for two terpenes, an endo- and an exo-cyclic compound (Fig. 5.8), respectively the α-pinene and the sabinene which are two species of the top-4 highest emitted monoterpenes on a global scale when isoprene is excluded (Kanakidou et al., 2005). Those two molecules are also characterized by a very similar reaction rate with ozone, thus it allows to investigate the role of the oxidative products derived from their ozonolysis rather than the kinetic effects (Tab. 5.3).

Experiments were conducted using different concentrations of terpenes (from 10 to 80 ppb) while the chamber temperature, pressure and ozone content at the time of injection were maintained constant over the whole experiments. For all experiments (more than 40), PSD for charged and neutral particles, were obtained with a time resolution of 2 minutes both for NAIS and SMPS during a total reaction time of 40 minutes, in which the monoterpene was converted by nearly 100% (Fig. 5.10). Experimental conditions are

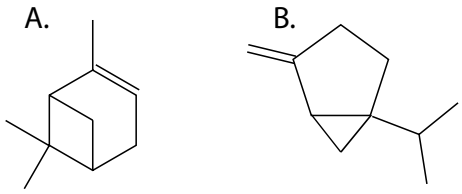

Figure 5.8: Chemical structure of the α-pinene (A., endocyclic compound) and the sabinene(B., exocyclic compound).

summarized in table A.2 reported in the appendix section.
The observed nucleation events present a similar shape than the one observed in the nature (see figure 5.9). High numbers of particles grow from the cluster size, from the cluster population already present in the chamber, or from this population plus new clusters formed after the terpene has been injected. After most of the terpene has reacted in the chamber and the particles have reached a stable size, it was calculated that the SOA yield (i.e. the particle mass produced from a given terpene mass consumption) was the same for sabinene and alpha-pinene and are in the range of 20 to 40% depending the injected concentration. However, we found that the dynamics of the new particle formation are different from one compound to the other. New particles could be observed after an induction period (Fig. 5.9 and 5.10). The time delay is due i- to the time necessary for the terpene to be mixed in the chamber and ii- to the reactivity of the terpene to produce condensable vapors. The delay was experimentally defined as the time when the increase of particles has exceeded three times the noise level (Koch et al., 2000). During the experiments, the time delay measured for the sabinene was found to be around 150 seconds while it was around 450 seconds for the α-pinene, even though the rate constant of the reaction of sabinene with ozone is lower than the one between α-pinene and ozone. From the reaction rate constant of the terpene with ozone (Atkinson and Arey, 2003), it is possible to calculate the terpene mass consumption needed to onset the nucleation. Values reported in the table 5.3 show that the calculated minimum amount of sabinene needed to trigger the nucleation and growth processes is three times smaller than the amount of α-pinene.

Table 5.3: First considerations on the new particle production dynamics.

Terpene	$k_{O_3+Terp.}$ (298 K) [$\times 10^{-17}$ molec.cm^{-3}.s^{-1}]	Time delay [s]	ΔTerpene [$\times 10^{-14}$ molec.cm^{-3}]
Sabinene	8.3	150	1.215
α-pinene	8.4	450	3.915

The analysis of the maximal particle number concentration measured with the SMPS shows that the ozonolysis of sabinene produces more numerous particles than the one with the α-pinene. At the end of the experiments, particles produced from the ozonolysis

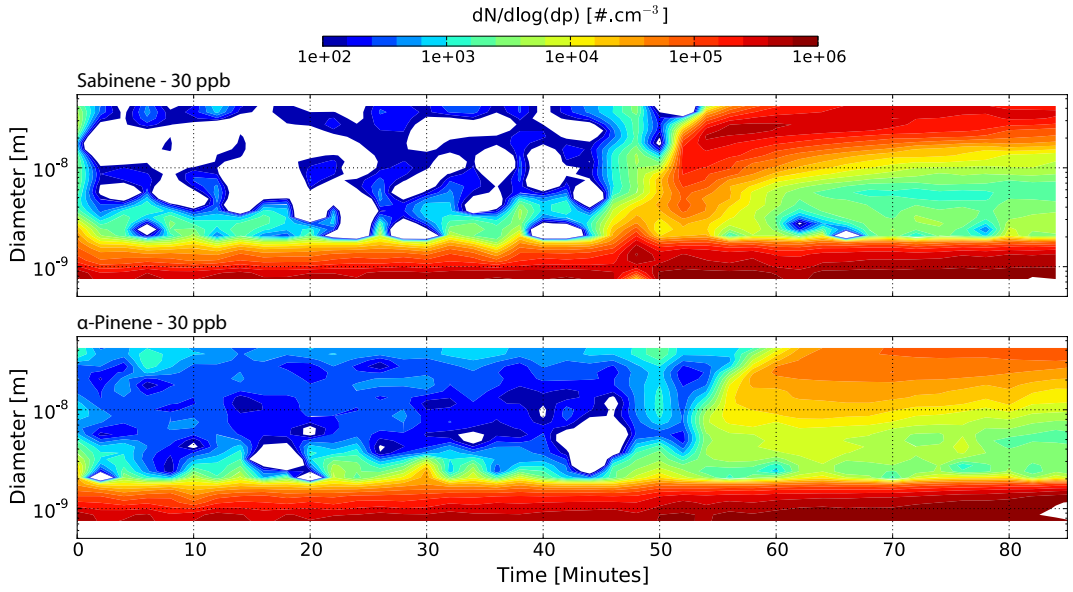

Figure 5.9: Evolution of the particle size distribution during nucleation experiments using 30 ppb of sabinene (upper panel) and 30 ppb of α-pinene with 100 ppb of ozone.

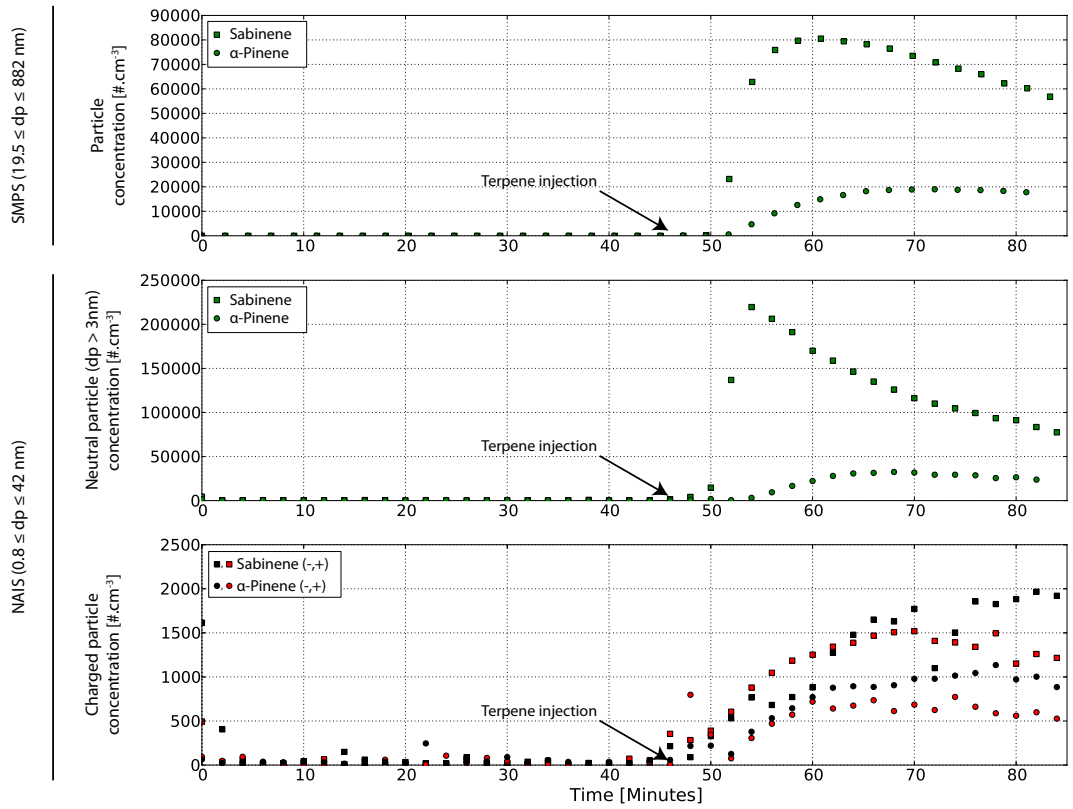

Figure 5.10: Evolution of the particle concentration during nucleation experiments using 30 ppb of sabinene and 30 ppb of α-pinene with 100 ppb of ozone.

of sabinene are smaller ($\bar{Dp}$ = 39 nm for 30 ppb after 30 minutes of reaction) than the ones produced from the ozonolysis of alpha-pinene ($\bar{Dp}$ = 45 nm for 30 ppb after 30 minutes of reaction). As expected, the particle concentration is strongly link to the terpene amount injected in the chamber (see Fig. 5.11). If we assume that 100% of the terpene reacted, it is possible to calculate the conversion ratio from gas to particle k_{part}. For the sabinene, k_{part} is 2716.8 #.cm^{-3}.ppbv^{-1}, i.e. 1.08 $\times 10^{-07}$ #.molec^{-1} while this constant was found to be 513.70 #.cm^{-3}.ppbv^{-1}, i.e. 0.20 $\times 10^{-07}$ #.molec^{-1}. Hence, the threshold concentrations of vapor needed to onset the new particle formation were estimated respectively for sabinene and α-pinene around 9.26 and 50$\times 10^{+06}$ molec.cm^{-3}. These values suggest once again that the sabinene present a higher nucleating potential (see the table A.2 reported in the appendix section).

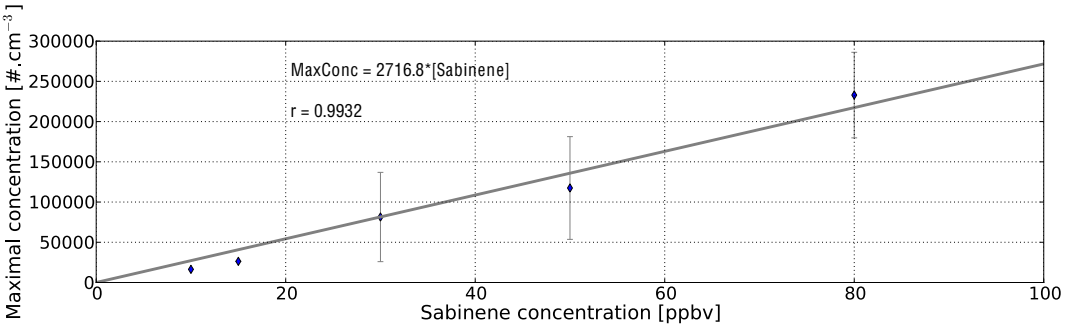

Figure 5.11: Evolution of the maximum aerosol production according to the sabinene concentration injected in the chamber.

From the measured PSD, the 3-nm particle formation rate (J_3) and the GR was calculated using the equations 3.4 and 3.5 and the method presented in the chapter 3 (see Table A.2). The power law model of formation rate established by Metzger et al. (Eq. 5.1) was modified to the following form:

$$J_3 = k_{nuc}[\mathrm{O_3}][\mathrm{Terpene}]^m \tag{5.4}$$

where k_{nuc} is a kinetic parameter and m, according to the fundamental nucleation theorem, is interpreted as the number of vapor molecules in the nucleating cluster. However, all experiment were conducted with a constant value of [O_3], then it comes:

$$J_3 = k[\mathrm{Terpene}]^m \tag{5.5}$$

where $k = k_{nuc}[\mathrm{O_3}]$ is defined. Parameters were estimated using a least-square fitting procedure on experimental results (Fig. 5.12). For sabinene $k_{Sab.} = 3.88 \pm 5.81$ ppbv.s^{-1} and $m_{Sab.} = 1.49 \pm 0.34$ ($r = 0.9624$) and for the α-pinene, $k_{\alpha P.} = 29.5 \pm 74.44$ ppbv.s^{-1} and $m_{\alpha P.} = 0.45 \pm 0.62$ ($r = 0.5232$). Furthermore, it was found in case of the sabinene experiments that the J_3 is correlated with the sub-3nm pre-existing cluster ($r = 0.8253$) while no significant correlation was found during the α-pinene experiments ($r = 0.2671$).

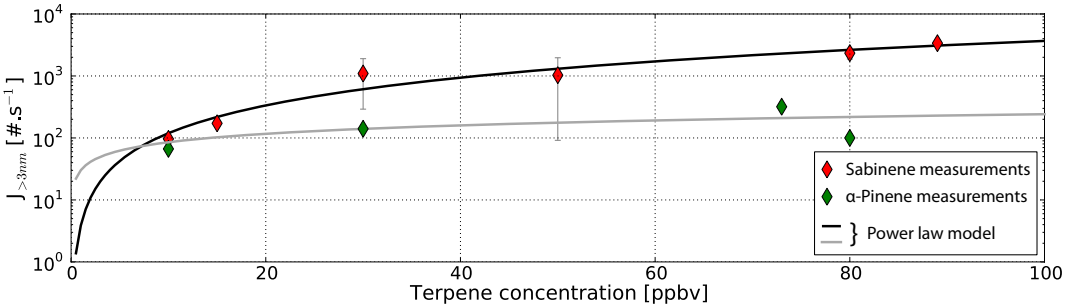

Figure 5.12: Neutral particle formation rate J_3 as a function of the terpene concentration.

As expected from previous results, the 3nm-particle formation rate during dark ozonolysis of the sabinene is much more higher than the one of the α-pinene. Furthermore, the m exponent variation between the two injected terpenes confirms that the processes leading to the new particle formation might be different according the chemical nature of the terpene. This phenomenon was previously highlighted by Bonn et al. (2002) who connected new particle formation properties in the presence of water ($RH = 30\%$) to the chemical structure of the injected terpene and its oxidative products. In the present work, the opposition between endocyclic compounds such as the α-pinene and exocyclic compounds such as sabinene (Fig. 5.8) is again pointed out.

The evolution of the growth rate during the particle formation process is reported on figure 5.13. As expected the two terpenes exhibit large differences in the growth rate evolution but if the sabinene ozonolysis produces more particles than the one of the α-pinene, α-pinene derived particles growth faster and to larger sizes. The growth rate evolution could be segmented into different phases (letters on the figure 5.13). It was found that

- $\frac{dGR}{dt} < 0$ for both terpene after the "ignition phase" (A),

- $\frac{dGR}{dt}$ increases monotonously for sabinene reactions (i.e. the GR decreases monotonously during B and C phases) while its behavior is more complex in the case of α-pinene reactions (the GR decreases during B and C phases with a slope rupture when entering C, then increases during D before decreases once again during the E phase).

In those experiments, the coagulation process can be neglected in a first approximation. Therefore, and as it has been previously discussed in chapter 2, the GR due to the condensation of one specie of a given condensable vapor in excess would evolves monotonously with the inverse of the particles mean diameter (Eq. 2.17). In our case, the nature and

concentration of the condensable vapor are not known but the GR evolution profile suggests that different vapors or concentrations are involved in the growth process. In both cases, variations of the time derivative value of the GR indicate a change in the condensable vapor concentration or volatility. This is especially true for the case of α-pinene ozonolysis. This result suggests that secondary oxidative products likely play an important role in the dynamic of the growth process (from the B phase on) while the role of the primary compounds are more important during the first steps of the nucleation process (A).

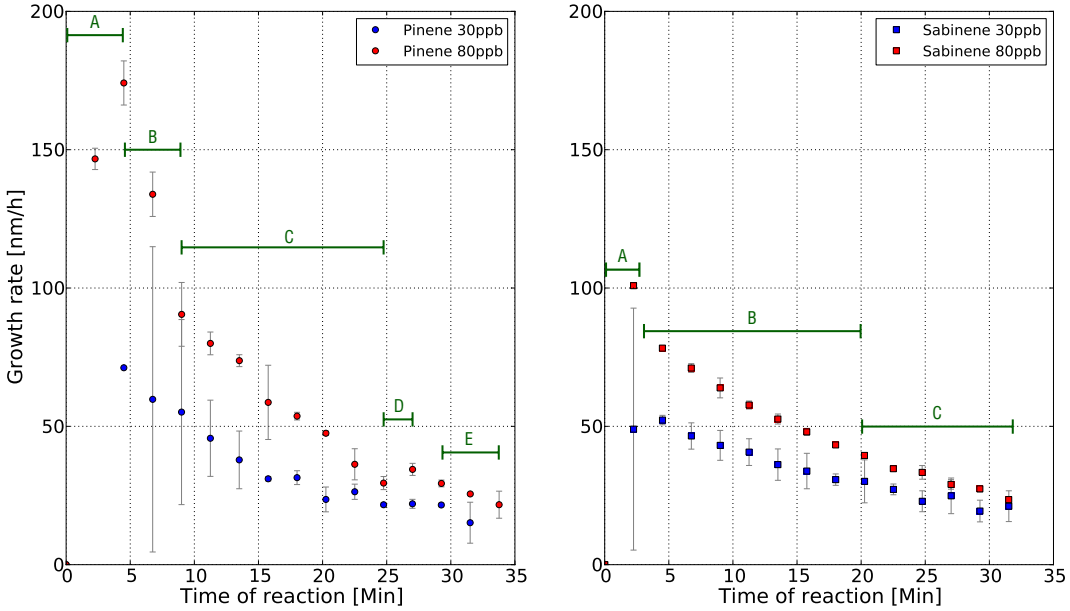

Figure 5.13: Evolution of the growth rate according to the reaction coordinate for both terpene (left panel: α-pinene; right panel: sabinene) and for 80 and 30 ppb (respectively red and blue markers). The green lines and letters represent the main zone of the GR evolution.

5.2.3 Discussion

It seems that the ozonolysis of sabinene occasionally generates new clusters contrarily to what is observed during α-pinene experiments. On the other hand, a strong correlation between the pre-existing sub-3nm particle concentrations during the sabinene experiments suggests that this terpene's oxidative products also have a strong potential for growing pre-existing clusters. A closer look at the sign of the sub-3nm particle concentration variation after the injection of the terpene ($f(\Delta) > 0$ or < 0) was analyzed. No significant pattern of $f(\Delta)$ could be found in the case of the sabinene indicating that both nucleation of new clusters and condensation are involved. On the contrary, the $f(\Delta)$ is homogeneously negative in the case of experiments based on the α-pinene which exhibits a dominant condensation behavior rather than a nucleating behavior. However these assumptions have to be used with caution since the relevance of the sub-3nm particle measurements is still at debate.

Moreover, the slight difference between the rate constants of both terpene reaction with ozone can not explains the gap of nucleation behavior of the two studied compounds (Tab. 5.3). This means that the primary terpene is not mainly involved in the nucleation and growth process but rather the oxidative products are. Different relationship between the particle formation rates and the preexisting cluster concentrations, and different growth rate time evolution between the two terpene ozonolysis that we studied indicate that the oxidative products are likely very different. Those difference in term of chemical structure and associated physical properties (e.g. partition coefficient, volatility) has to be considered to clarify our understanding of the nucleation process. It is widely admitted that the carbon number of organics can increase during monoterpene ozonolysis. Donahue et al. and coworkers (Donahue et al., 2011) have shown that the volatility of organic compound decrease with the carbon number (Fig. 5.14).

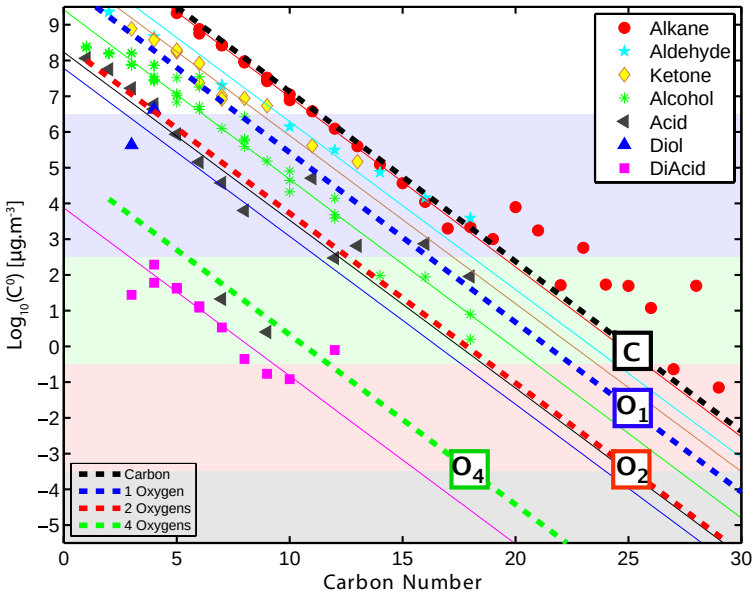

Figure 5.14: Evolution of the volatility $Log_{10}(C^0)$ *versus* carbon number (adapted from Donahue et al., 2011).

In order to investigate the role of condensation of different oxidative products, we performed numerical simulation of those ozonolysis experiments using the M4-NPF model described in chapter 3. Simulations were done as follow for both terpenes:

- A condensable vapor concentration derived from experimental data (see Eq. 3.3 in chapter 3) is injected at the same time than the terpene is injected in the chamber $\Longleftrightarrow$ Only one first generation oxidative compound is involved. The condensable vapor concentration time evolution is then fully driven by the physical processes considered in the model.

- We consider an average mixing time in the chamber of 45 seconds (Wang et al., 2011).

- The molecular mass of the oxidative products is derived from the work of Müller et al. (2009). Three different masses were tested here from the lighter (blue dot line on Fig. 5.16 and 5.18), to the heaviest one (red dot line on Fig. 5.16 and 5.18) and the average mass of oxidative products (yellow line on Fig. 5.16 and 5.18).

- The sub-3nm cluster concentration is assumed to be constant and the maximum concentration is estimated from the NAIS measurements ($\sim$ 3.35 $\pm$ 2.06 $\times 10^{+05}$#.cm^{-3}). The optimal cluster source rate was optimized to minimize the misfit between simulated and observed particle concentration during the reaction.

5.2.3.1 Sabinene experiments

Simulation results for the sabinene 30 ppb experiment is reported on the figure 5.15 and 5.16.

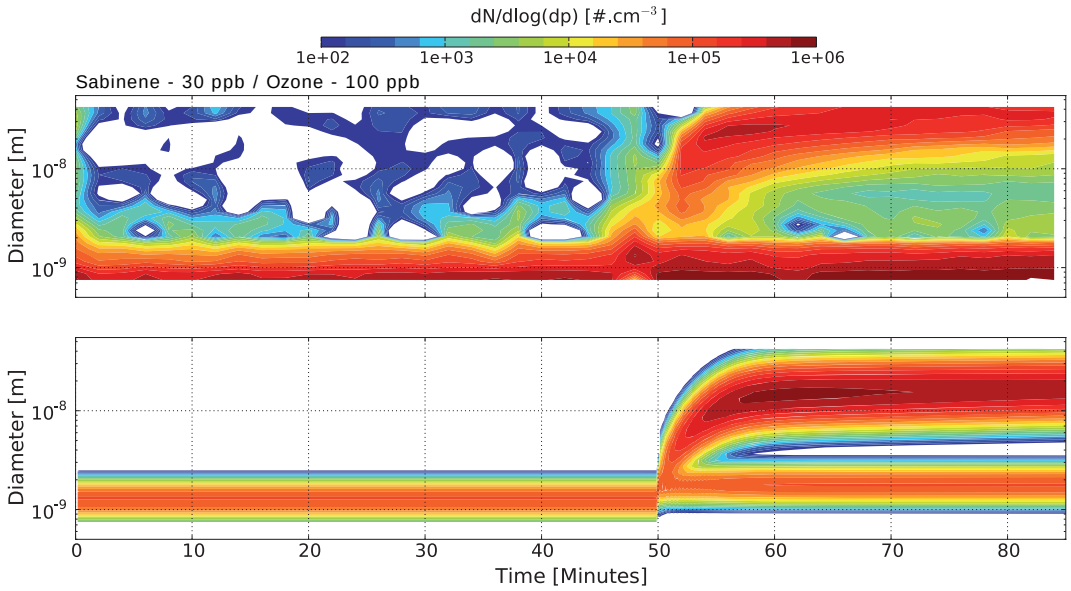

Figure 5.15: Comparison between measured and modelled time evolution of the particle size distribution during the sabinene 30 ppb dark ozonolysis.

As seen, the global dynamic of the nucleation experiment is well represented. However, strong differences are observed from the comparison of the real and simulated spectra: i- The growth rate and the particle formation rate are underestimated by the model during the first phase of the reaction (Tab. 5.4 at the end of this section) but also later (e.g. after 70 minutes of experiment, the modelled PSD do not grow anymore), ii- in the model, the clusters mode seem to have increase from 1.5 nm to 2 nm while this phenomenon is not observed on the experimental data. The analysis of the particle concentration time evolution highlights other discrepancies especially in the SMPS size ranges (Fig. 5.16). This latter difference is probably linked to the fact that the injected condensable vapor was calculated only with NAIS data and for the first step of the particle growth (from 1.3 to 7 nm) without any consideration of what happen at higher diameters.

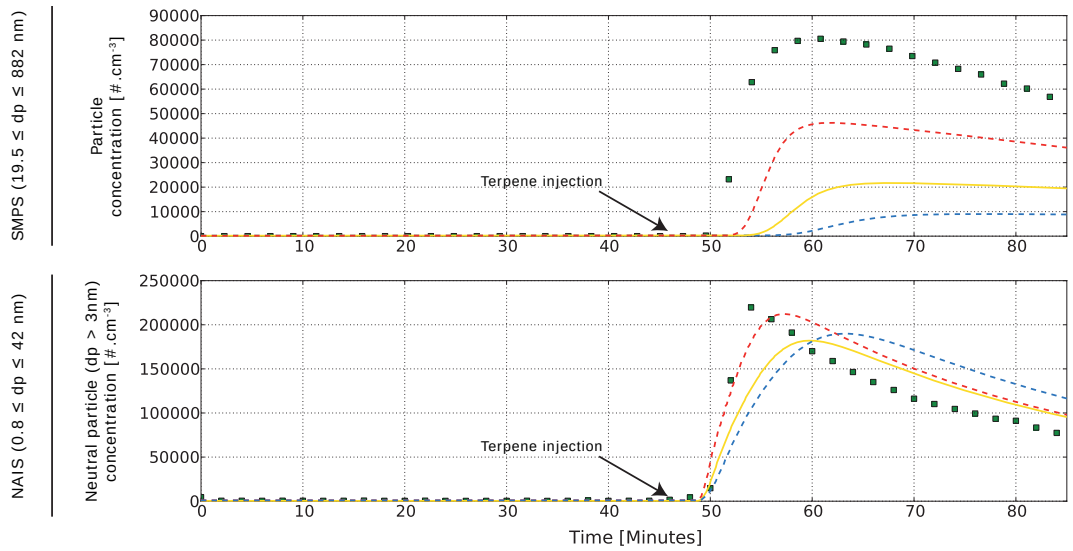

Figure 5.16: Comparison between measured and modelled time evolution of the particle concentration during the sabinene 30 ppb dark ozonolysis.

The first steps of the new particle formation from the sabinene dark ozonolysis are still well represented (see the comparison Tab. 5.4 at the end of this section) and provide new informations on the dynamic of the reaction. As seen, both simulated 3 nm-particle formation rate and growth rate are very similar to those measured in the chamber suggesting that the first steps of the new particle formation can be described by the simple condensation of the primary oxidative compounds of the sabinene ozonolysis (Tab. 5.4). However, this conclusion is based on the assumption that the inputted sub-3nm particles concentration is qualitatively and quantitatively relevant. Other experiments using an appropriate instrumentation for such particle measurements will be conducted in a near future to confirm (or not !) this assumption. In case that the neutral clusters are not as numerous as inputted, the nucleation of organics vapors will be necessary to describe the observed new particle formation rates.
Furthermore, in those simulations we used only one condensable vapor with several assumptions on its properties such as its molecular weight. As suggested by the results observed at higher size ranges, a more complete chemical scheme should be implemented to describe the particle growth until reaching climatic relevant sizes. For example, a sequence of different injections of condensable vapors in the model could represent a first approximation of the chemical evolution of oxidative products and thus could help to describe more accurately the growth process at larger sizes.

5.2.3.2 Pinene experiments

The simulation of the particle size distribution and concentration time evolutions of the α-pinene dark ozonolysis simulation are reported on figure 5.17 and 5.18. In this case, important differences between measured and simulated dynamic could be noticed even

during the first steps of the reaction. In fact, the condensational growth rate from pre-existing clusters is overestimated by a factor 2 and consequently the simulated particle formation rate was found to be more than 3 times higher than the one deduced from the NAIS data. However, for diameter higher than 7 nm, the growth rate seems to be significantly underestimated since the simulated PSD exhibits a lower geometric mean diameter. This discrepancy could be quenched by increasing the condensable vapor concentration by a factor 2 suggesting that the dynamic of the condensable vapors available is more complex than in the case of the sabinene based experiment as previously proposed (see the growth rate time dependence analysis, Fig. 5.13). The particle concentration evolutions confirm large differences between the simulation and the observation for all the size ranges.

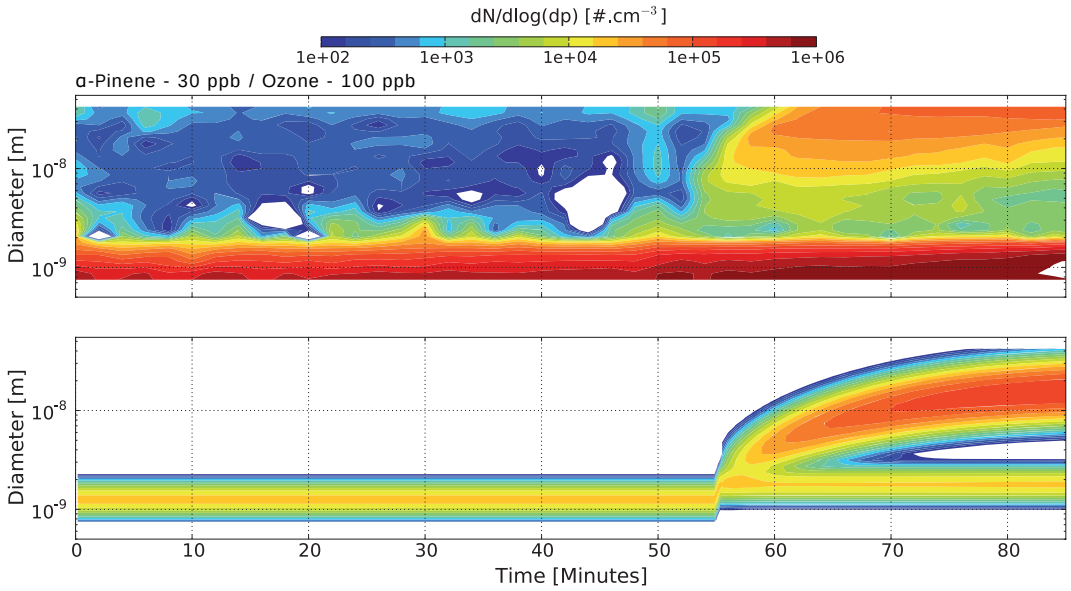

Figure 5.17: Comparison between measured and modelled time evolution of the particle size distribution during the α-pinene 30 ppb dark ozonolysis.

Large discrepancies between modelled and observed results come from the simplistic processes representations in the model. This suggest that the α-pinene ozonolysis can not only be described by the condensation/coagulation processes using a one single component condensing vapor. The time dependence analysis of the GR had already suggested that the dynamic of the condensable vapor species could be more complex than in the case of the sabinene ozonolysis. The simulations confirm that a sequence of injections of different condensable vapors during the simulation should be more appropriate to describe the PSD evolution in the chamber. A similar modelling approach had been already published by Tsimpidi et al. (2010) from the chemical point of view. Instead of size bins, authors built a model based of volatility bins hence it is only possible to predict a mass of particulate matter. Adapting this kind of chemical properties evolution in a physical-based approach by acting on the condensable vapor properties (molecular weight, volatility, partition coefficient...) could enhance the description of the

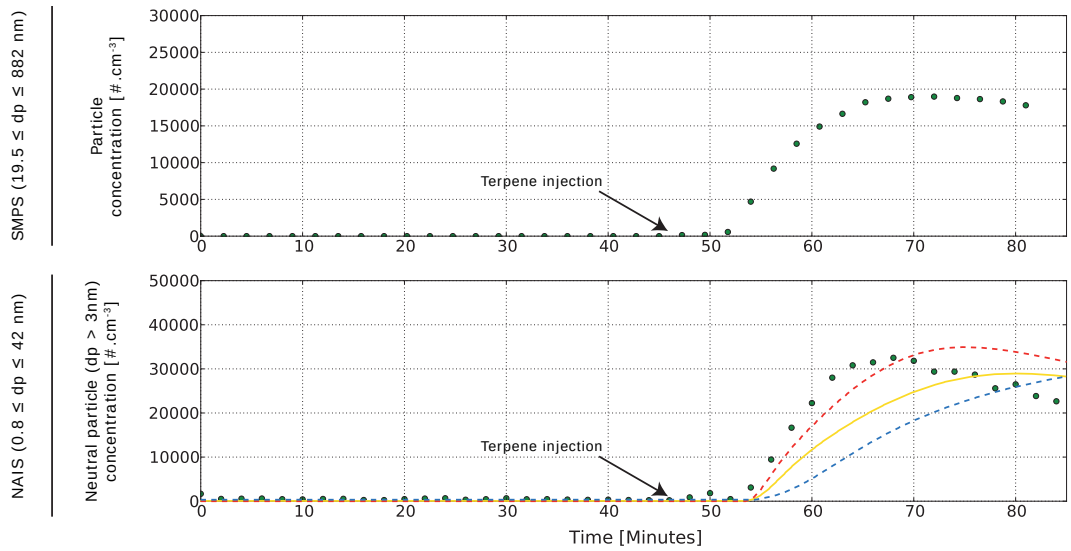

Figure 5.18: Comparison between measured and modelled time evolution of the particle size distribution during the α-pinene 30 ppb dark ozonolysis.

condensational growth.

Table 5.4: Summarize of *in-silico* experiments equivalent to sabinene and α-pinene dark ozonolysis (30 ppb).

SABINENE			
Observable	Simulation	Measurements	Relative error
sub-3nm particles [µg.m^{-3}]	1.3×10^{-05}	$13.3 \pm 3.3 \times 10^{-05}$	$\sim$ 10 (input)
$GR_{1.3-7}$ [nm.h^{-1}]	102	112	-9.8 %
J_3 [#.cm^{-3}.s^{-1}]	811	932	-13.0 %
max(SOA) [#.cm^{-3}]	45000	80540	-44.1 %

α-PINENE			
Observable	Simulation	Measurements	Relative error
sub-3nm particles [µg.m^{-3}]	0.2×10^{-05}	$14.5 \pm 4.2 \times 10^{-05}$	$\sim$ 60 (input)
$GR_{1.3-7}$ [nm.h^{-1}]	33	16	106.2 %
J_3 [#.cm^{-3}.s^{-1}]	172	40	330 %
max(SOA) [#.cm^{-3}]	5000	18980	-73.6 %

5.2.3.3 The cluster assumption

As mentioned above, during the simulation, the sub-3nm cluster concentration was assumed to be constant and constrained by the NAIS measurements. However, as previously demonstrated by Asmi et al. (2009), the NAIS overestimates particle with a diameter below 2 to 3 nanometers. Moreover, the overestimation is dependent of the particle concentration and on the atmospheric thermodynamical properties (T, P, RH). Consequently, we chose to run the simulations with an optimized sub-3nm clusters concentration constrained by the NAIS measurements. Values used as input in the simulations and NAIS

derived values are reported in the table 5.4. It can be noticed that for both terpenes, the implemented cluster concentration was lower than the measured one to decrease the misfits between simulation and observations.
Without more accurate data on the cluster concentration using another instrument such as a particle size magnifier, it is quite hard to conclude but some assumptions could be made. Based on previous conclusions, the α-pinene is the terpene which presents the lowest potential of nucleation, thus we can estimate the particle produced by nucleation in the case of sabinene experiment following the approach:

1- Hypothesis: The particle production by nucleation is negligible compared to the activation and condensational growth process in the case of α-pinene experiments.

   1a- $\Longleftrightarrow$ The particle number concentration could be accurately predicted using the model M4-NPF with the appropriate sub-3nm seeds input.

   1b- $\Longleftrightarrow$ The sub-3nm seeds input for α-pinene ozonolysis simulations is the closest to the sub-3nm seeds concentration in the smog chamber.

2- In the case of sabinene experiments, the nucleation of new particles seems to be non-negligible. Since the model do not represent such a process, freshly nucleated particles should be integrate in the sub-3nm seeds simulations input to allow a good representation of the particle number concentration during the reaction.

   2a- Considering the 1b point, its possible to estimate the particle production by nucleation following the relation (5.6).

$$N_{nuc,Sab.} = [\text{Sub-3nm seeds}]_{Sab.} - [\text{Sub-3nm seeds}]_{\alpha P.} \tag{5.6}$$

   where $N_{nuc,Sab.}$ is the particle formed from sabinene and/or its primary oxidative products nucleation and $Nnuc, Sab. \approx 10^{+04}$ #.cm^{-3} which represents 12.5 to 25 % of the total particle concentration.

Consequently, the 2-nm particle formation rates due to nucleation from the primary oxidative products of sabinene, $J_{3,Nuc,Sab.}$, was derived, $J_{3,Nuc,Sab.} \sim 150$ #.cm^{-3}.s^{-1}. According to the Metzger's formulation of the formation rate (Eq. 5.1), this imply that sulfuric acid concentration must be $\sim 3 \times 10^{+05}$ molec.cm^{-3} to explain the J_3 due to activation of seeds by organic vapors.

Those experiments have pointed out that the nucleation could be triggered from organic compounds derived from monoterpenes atmospheric oxidation. Particle formation rate parametrization were established in atmospheric relevant conditions for both sabinene and α-pinene ozonolysis (Eq. 5.5). Furthermore, different nucleation behavior have been revealed depending on the parent molecule. The sabinene have been found to exhibit a stronger nucleation potential when oxidized compared to the α-pinene oxidative

derived products which tend to condense on pre-existing particles rather than form new particles from gas to particle conversion. Moreover, the role of secondary and higher oxidative product generations were likely to be more important in the new particle formation process in case of α-pinene oxidation reactions while sabinene reactions dynamics seems to mainly depends on firsts oxidative products as revealed by the growth rate time evolutions (Fig. 5.13). We use a simple numerical tool to investigate the nucleation dynamics and results are in agreement with previous conclusions. Those simulations also highlights numerous improvements which are necessary to represent correctly the nucleation and growth of freshly formed secondary particles, especially the need to take into account the secondary (or higher) generation oxidation products and their physical properties (such as volatility or partition coefficient) evolution in a physical-based model approach. However, it is important to keep in mind that those conclusions are based on numerous assumptions and many of them are not trivial and need to be prooved. Consequently, further experiments are needed to test all hypotheses we've made during this work and experimental campaigns are already planed in a near future:

- to measure the impact of the gas composition on the NAIS cluster self production,
- to measure accurately the cluster population using a particle size magnifier,
- to test the sulfuric acid cleanliness,
- to investigate the nucleation an new particle formation at lower terpene initial concentrations,
- and to test the impact of the ozone concentration on the particle formation rate since all experiments were carried out under 100 ppb of ozone at the injection time.
- to investigate the impact of water on such systems.

Chapter 6

Conclusions and perspectives

During these three years of research experience as a PhD. student at the Laboratoire de Météorologie Physique, I had to investigate the "sources and properties of atmospheric particles". This wide topic was rapidly "reduced" (luckily!) to the study of the secondary particle formation, which is still quite large. The way we chose to tackle this issue was to focus on the very first steps of the new particle formation process: the nucleation. Current global climate models underestimate secondary particle production rates by many orders of magnitude and, once formed, these particles grow about ten times faster than can be explained. To try to better identify and understand the gaps in our understanding of these complex processes, we chose to base the thesis on two different complementary approaches: field observations and laboratory simulations, both analogical and numerical. The major outcomes of this thesis are related to (i) the vertical extend of the nucleation and growth events in the natural atmosphere, and (ii) the relative contributions of sulphuric acid and organic condensable vapors in the nucleation and growth processes.

On the vertical extend of the nucleation and growth events

The specific environment provided by the puy de Dôme area naturally lead us to investigate the nucleation process in background elevated environments, in the continuity of the work of Hervé Venzac. In the frame of the European Integrated project on Aerosol Cloud Climate and Air Quality Interaction, EUCAARI, we completed our experience of high altitude nucleation and new particle formation studies with long term measurements at the high alpine altitude research station of the Jungfraujoch, Switzerland (chapter 4, section 1). Results show that the nucleation frequency is globally not as high as at the puy de Dôme (1465 m a.s.l., Boulon et al., 2011), nor as at the Himalayan NCO-P station (5079 m a.s.l., Venzac et al., 2008). The frequency of nucleation and growth events is hence not a direct function of altitude. The vertical extend of nucleation and growth events was then studied in more details at the puy de Dôme station by using in situ measurements at two altitudes (chapter 4, section 2). Coupled with air parcel thermodynamic analysis and atmospheric back-scattering vertical profile measured by LIDAR, we studied the link between the planetary boundary layer extent and the nucleation process in a statistically relevant approach. This work provides a quite unique data-set and analysis which brings new information on the potential vertical scale of the nucleation process. It reveals that

nucleation and growth occurred twice as frequently at the high altitude site as in the lower planetary boundary layer site. It appeared that when nucleation and growth occurs at the high altitude station while not in low altitude station, the puy de Dôme lies a few hundreds of meters above the PBL detected by LIDAR. Hence, this increased frequency could either (i) take place in the whole free troposphere or (ii) could only be restricted to a thinner mixing interface between the PBL and the FT. In favor of the hypothesis (i), the events take place over large periods of time and show a clear continuous growth, indicating a large scale phenomenon which is unlikely to take place in a limited width portion of the atmosphere (e.g. Hamburger et al., 2010). In favor of the hypothesis (ii), as stated earlier, nucleation and growth frequency detected at the Jungfraujoch is lower than at the puy de Dôme, although the alpine station is more frequently located in the FT (e.g. Wehner et al., 2010; Crumeyrolle et al., 2010). More studies of the vertical extend of nucleation are then clearly needed, by combining ground based measurement with soundings or airborne studies.

On the role of sulphuric acid in the nucleation and growth events

Recent modelling studies assumed that the new particle formation can be described in the planetary boundary layer using an activation-type nucleation parametrization involving different condensable vapors (sulfuric acid and oxidized biogenic organic compounds). For free and upper tropospheric media, the nucleation is classically described in models using the binary homogeneous nucleation theory of the sulfuric acid–water system. Both at the JFJ and at the puy de Dôme, there were indications that sulfuric acid might not be as important as observed in the planetary boundary layer to trigger the new particle formation at high altitudes. We showed in this study that the activation type nucleation could also be better adapted for the low free troposphere. During spring 2010, a volcanic eruption in Iceland provided us a unique opportunity to investigate the relevance of a such a parametrization and provided in a sulfate-enriched environment.

On the 20th of March 2010, the Eyjafjallajokull volcano located in the south of Iceland entered in a major eruptive phase which was going to impact Europe for months. Over the 6 months of the eruptive phase, the volcanic plume was detected two times over Clermont-Ferrand. From the 18th to the 20th of May 2010, the volcanic plume reached the puy de Dôme research station (1465 m a.s.l.) where nucleation and growth events were observed and could be characterized by our instrumentation. The new particle formation events observed during the volcanic plume intrusion were clearly linked to the sulfuric acid produced from the volcanic emitted sulfur dioxide. Different nucleation models (BHN and THN) and parametrizations (activation and kinetic) were tested and it was found that neither the BHN nor the THN where able to simulate the observed

particle formation rate and underestimate it at least by 7 to 8 orders of magnitude. Activation or kinetic parametrizations gave overestimated but more relevant results. However these latter parametrizations do not account for temperature or relative humidity dependencies and use prefactors which can vary by up to 4 orders of magnitude, which as a consequence make their use very delicate. Those results highlight the lack of adequacy of the actual parametrizations for describing the nucleation and growth events observed in the natural atmosphere, even in sulfate-enriched environments and the need of new theoretical approaches to better represent the nucleation process in the global climate models. Volcanic induced new particle formation events were simulated using an aerosol dynamics model that does not include any nucleation scheme, but allow a source of cluster particles to grow. It was shown that, assuming a constant cluster source during the event, the condensation and coagulation processes applied at the cluster size scale could provide a good approximation of new particle formation and growth rates in an environment dominated by one type of condensable vapor. Hence, while parametrizations using sulphuric acid fail to explain the observed new particle formation rates, a modelling approach based on pre-existing clusters grown by sulphuric acid give a relatively good approximation of the observed new particle formation rate, although the growth is slightly underestimated. If this approach proved its relevance under normal conditions (i.e. outside a volcanic plume!), a climatology of the cluster concentration (neutral and charged) in various environments and altitudes would reveal to be extremely useful for feeding mesoscale models.

On the role of organics in the nucleation and growth events

Further understanding of the nucleation and growth processes was achieved in this work by conducting atmospheric smog chamber experiments on organic compounds. The goal was to determine the various parameters involved in new particle formation in the absence of sulfuric acid. Two different experimental campaigns were conducted during this PhD. Work (chapter 5, *Laboratory experiments: probing the nucleation process*). In the first experiment, emissions from a diesel engine were simulated using a sulfur-free fuel. After filtration with a post-treatment device, the formation of new clusters was detected and enhanced during the particle filter regeneration. When increasing the residence time of these clusters in the sample flow, they were found to grow at a rate of 21.2 $nm.s^{-1}$, showing that would reach the climate-relevant size of 50 nm after a residence time of 2.3 seconds in the atmosphere. Results obtained during those experiments highlight that the nucleation of new secondary particles derived from organic compound [incomplete] combustion products occur in exhausts, even without sulfuric acid. Parametrization of the nucleation and growth of organics were further

proposed from experiment conducted in a more relevant atmospheric conditions in a smog chamber, in collaboration with the Laboratoire Interuniversitaire des Systèmes Atmospheriques of Créteil, CNRS UMR 7583 (see the second section of the chapter 5). In this work, the new particle formation from the ozonolysis of two atmospheric relevant monoterpenes, the sabinene and the α-pinene, were studied. From those experiments 3 nm-particle formation rate parametrization were established for both terpenes and nucleation mechanisms were investigated through the particle size dynamics and numerical modelling. Strong differences were pointed out between the two monoterpenes based reactions. The sabinene-based reactions exhibit a stronger nucleation potential and the particle production in the NAIS size range seems to be mainly driven by the firsts generations of oxidative products. On the contrary, in case of the α-pinene ozonolysis reactions, it is likely that oxidative products rather condense on pre-existing clusters rather form new clusters by nucleation. Furthermore, the role of secondary generation products seems to be more important than during the sabinene-based experiments. All results obtained during this experimental work highlight the key role of the chemical and physical properties of the oxidative products in the new particle formation and growth and suggest the implementation of chemical considerations in the current aerosol dynamics models. This effort will allow to represent more accurately the nucleation of new particles and subsequently growth to climatic relevant size in such models.

On the future...

Numerous other questions are still suspended both on the fundamental mechanism of the nucleation and on its atmospheric occurrence. For example, no informations on the gas phase composition, relevant to the nucleation issue, were available during this work. However, accurate measurements of key species such as sulfuric acid and (even or) volatile organic compounds could significantly contribute to improve our understanding of the onset of new particle formation events at the daily but also seasonal time scale at the puy de Dôme station. As proposed by many, condensation of sulfuric acid often accounts for only a fraction of the observed growth while organics role become more and more relevant (e.g. Birmili et al., 2003; Fiedler et al., 2005; Smith et al., 2008; Riipinen et al., 2010). Therefore, the simultaneous characterization of the nanometric aerosol size distribution and of the chemical composition of the gas phase at the puy de Dôme station are still required and can be set-up in a near future. Such measurements would provide a unique data set to investigate the nucleation and growth processes at a remote altitude site.

Considering the very first steps of the nucleation process, i.e. the critical cluster formation and composition, our knowledge is limited to few measurements and theoretical considerations from quantum mechanic calculations since instrumental devices which

allow physical and chemical measurements at the cluster size scale are not numerous. However, the cluster representation is a central issue in the nucleation process-based modelling effort. In a recent paper, Smith et al. (2010) proved that aminium salts play a major role in the formation and growth of secondary particles. Such a result provide new field of investigation in the quest of an accurate numerical scheme of particle growth and vapor uptake. Consequently, a strong experimental effort has to be conducted in flowtube and smog chamber to explore the role of such species in the nucleation and particle growth processes.
Those few points are just examples of the work needed to contribute to the enhancement of our understanding of nucleation and growth events. Both latter issues will be the main preoccupations of my future work during my post-doctoral position.

To conclude, the last words, which are probably a bit arrogant or pretentious but strongly stimulating, of this PhD. thesis come from the great mathematician David Hilbert, who in a very positive and enthousiastic attitude stated:

Wir müssen wissen.
Wir werden wissen.

which is tranlated in english as:

We must know.
We will know.

Appendix A

Annexes

Contents

A.1 Characterization of the neutral cluster mode measurement of the NAIS: the filtering experiment results

Table A.1: Impact of filtration on particle concentration. T is for the concentration over the whole PSD measured with the NAIS ($0.8 - 42$ nm), C is for sub-3 nm particles, the * is for charged particles and ($\pm$) is for the polarity of the analyzer, i.e. $T^\star(+)$ is for the concentration of positively charged particle over the size range $0.8 - 42$ nm.

Mode	Ambient air	Ambient air + Filter
$T^\star(+)$	900 ± 473	34 ± 30
$C^\star(+)$	325 ± 267	23 ± 22
$T^\star(-)$	1243 ± 497	83 ± 73
$C^\star(-)$	257 ± 384	53 ± 62
$T(+)$	13625 ± 1592	3162 ± 6941
$C(+)$	932 ± 886	3116 ± 6941
$T(-)$	34882 ± 8650	8567 ± 21286
$C(-)$	16822 ± 8434	8437 ± 21287

A.2 Smog chamber experiments in CESAM

Table A.2: Experimental conditions and results of smog chamber experiments. The *code* is composed by the number of the experiment + the first letter of the injected terpene (S for sabinene and P for α-pinene) + the terpene concentration injected ppbv, *Pre-Clus* is the sub-3nm particles concentration when the terpene is injected and *SOA max* is the maximal total concentration measured by the SMPS)

Code	Time Inj. [min]	Time O_3 [min]	Pre-Clus. [$\times 10^{+05}$ #.cm^{-3}]	$N_2 : O_2$ [∅]	GR [nm.h^{-1}]	J_3 [#.s−1]	SOA max [#.cm^{-3}]
1S10	47	27	2.01	8.8	27	96.4	16310
1S15	56	34	2.24	10.1	45	172	26270
1S30	126	99	41.1	29.2	N.D.	N.D.	5060
2S30	83	53	5.67	15.4	51.1	386	78140
3S30	47	27	2.20	8.8	112	932	80540
4S30	41	20	2.19	8.0	116	1969	161860
1S50	75	45	4.60	13.6	44	366	53610
2S50	56	46	3.63	10.1	168	1691	181290
1S80	60	31	5.09	10.8	109	1948	222930
2S80	52	32	9.87	9.5	179	2851	173420
3S80	44	24	3.75	8.4	140	2208	302500
1S89	69	55	9.87	12.4	96	3377	N.D.
1P30	103	83	11.0	20.8	4	63	15920
2P30	49	27	3.09	9.1	16	40	18980
3P30	46	26	2.61	8.7	69	321	56660
1P72	71	44	2.67	12.8	47	371	N.D.
1P74	63	42	10.2	11.3	73	281	N.D.
1P80	46	25	2.78	8.6	51	108	37980
2P80	41	21	3.27	8.0	32	94	31940

A.3 Intercomparison of 11 air ion spectrometers

Atmos. Meas. Tech., 4, 805–822, 2011
www.atmos-meas-tech.net/4/805/2011/
doi:10.5194/amt-4-805-2011

Atmospheric Measurement Techniques

Intercomparison of air ion spectrometers: an evaluation of results in varying conditions

S. Gagné[1], K. Lehtipalo[1], H. E. Manninen[1], T. Nieminen[1], S. Schobesberger[1], A. Franchin[1], T. Yli-Juuti[1], J. Boulon[2], A. Sonntag[3], S. Mirme[4], A. Mirme[4], U. Hõrrak[4], T. Petäjä[1], E. Asmi[5], and M. Kulmala[1]

[1]Department of Physics, University of Helsinki, P. O. Box 64, 00014 Helsinki, Finland
[2]Laboratoire de Météorologie Physique, Blaise Pascal Univ., 63000 Clermont-Ferrand, France
[3]Leibniz Institute for Tropospheric Research, Permoserstrasse 15, 04303 Leipzig, Germany
[4]Institute of Physics, University of Tartu, Ulikooli 18, 50090 Tartu, Estonia
[5]Finnish Meteorological Institute, P. O. Box 503, 00101 Helsinki, Finland

Received: 16 November 2010 – Published in Atmos. Meas. Tech. Discuss.: 22 February 2011
Revised: 20 April 2011 – Accepted: 29 April 2011 – Published: 4 May 2011

Abstract. We evaluated 11 air ion spectrometers from Airel Ltd. after they had spent one year in field measurements as a part of the EUCAARI project: 5 Air Ion Spectrometers (AIS), 5 Neutral cluster and Air Ion Spectrometers (NAIS) and one Airborne NAIS (ANAIS). This is the first time that an ANAIS is evaluated and compared so extensively. The ion spectrometers' mobility and concentration accuracy was evaluated. Their measurements of ambient air were compared between themselves and to reference instruments: a Differential Mobility Particle Sizer (DMPS), a Balanced Scanning Mobility Analyzer (BSMA), and an Ion-DMPS. We report on the simultaneous measurement of a new particle formation (NPF) event by all 11 instruments and the 3 reference instruments. To our knowledge, it is the first time that the size distribution of ions and particles is measured by so many ion spectrometers during a NPF event. The new particle formation rates ($\sim$0.2 cm^{-3} s^{-1} for ions and $\sim$2 cm^{-3} s^{-1} for particles) and growth rates ($\sim$25 nm h^{-1} in the 3–7 nm size range) were calculated for all the instruments. The NAISs and the ANAIS gave higher concentrations and formation rates than the AISs. For example, the AISs agreed with the BSMA within 11 % and 28 % for negative and positive ion concentration respectively, whereas the NAISs agreed within 23 % and 29 %. Finally, based on the results presented here, we give guidelines for data evaluation, when data from different individual ion spectrometers are compared.

Correspondence to: S. Gagné
(stephanie.gagne@helsinki.fi)

1 Introduction

Air ions have been studied extensively in the past both because of their influence on aerosol particle processes and because charged particles are easier to detect than neutral ones. Ions in the atmosphere influence aerosol particles through their formation and growth mechanisms (Laakso et al., 2002; Lovejoy et al., 2004; Kulmala et al., 2004), through cloud processes (Harrison and Carslaw, 2003), and scavenging of particles (Andronache et al., 2006). In turn, aerosols affect the Earth's climate and the health of its inhabitants (Twomey, 1991; Lohmann and Feichter, 2005; Myhre et al., 2009; Stevens and Feingold, 2009).

Measurements of charged atmospheric particles (air ions) are the basis of several aerosol measurement techniques (e.g. Gerdien counters, ion spectrometers, air conductivity measurement techniques; see Hirsikko et al., 2010). The charge of the particles can be used for their detection, and their electrical mobility for size classification. Other techniques rely on bringing the particles to a known charge equilibrium, allowing for the retrieval of the total particle concentration by data inversion. An example is the well-known and extensively used Differential/Scanning Mobility Particle Sizer systems (DMPS/SMPS, e.g. Wang and Flagan, 1990).

The ion spectrometers evaluated in this work have been developed by Airel Ltd. (Tartu, Estonia) based on long-term measurements and instrumentation development made at the University of Tartu (Matisen et al., 1992). The Air Ion Spectrometer (AIS) was first released in 2003 and measures the mobility distributions of small atmospheric ions and charged particles (0.8–40 nm in mobility diameter at NTP, Mirme et al., 2007). Later, a second generation instrument

was released by the same company: the Neutral cluster and Air Ion Spectrometer (NAIS, Kulmala et al., 2007 and Manninen et al., 2009a). The NAIS can, in addition to the AIS operation modes (negative and positive ions), measure the total (neutral + charged) particle size distribution by using corona chargers to charge the particle population. An airtight and improved version of the NAIS, the Airborne NAIS (ANAIS, 2nd generation of NAIS, Mirme et al., 2010), was developed in 2007/2008 to allow measurements at different altitudes, including measurements on board an airplane. In this paper, results from all three different instrument types are presented.

New particle formation (NPF) and growth is an important phenomena and takes place frequently in different environments (see e.g. Kulmala et al., 2004). Previous measurements of NPF events were traditionally made using instruments capable of measuring only above 3 nm, while the first steps of nucleation occur below this limit. The use of instruments such as the AIS and NAIS allowed for the detection of naturally charged particles and total (neutral and charged) particles below 3 nm. This gives the possibility to observe the behavior of particles at the very first steps of nucleation (Kulmala et at., 2007).

The above mentioned ion spectrometers have been used in both field and laboratory measurements. They have been measuring, for example, on a trans-Siberian train (Vartiainen et al., 2007), indoors (Hirsikko et al., 2007), at a chamber experiment at CERN (Duplissy et al., 2010), on board an airplane (Mirme et al., 2010), and on field campaigns (see Hirsikko et al., 2010 and references therein). Between spring 2008 and spring 2009, the instruments were measuring at different EUCAARI stations (European Integrated Project on Aerosol Cloud Climate Air Quality Interactions; Kulmala et al., 2009; Manninen et al., 2010, Kerminen et al., 2010).

The first air ion spectrometer calibration workshop (Asmi et al., 2009) took place during January and February 2008 in Helsinki, Finland, where 10 instruments (5 AISs and 5 NAISs) were calibrated. The purpose of the first calibration workshop was to verify the accuracy of the instruments so that they can be compared after being deployed in different sites around the world. Another purpose was to help in the development of such instruments by thoroughly characterizing them. Asmi et al. (2009) performed mobility and concentration comparisons to reference instruments and compared the ion spectrometers to each other. They concluded that the 10 instruments were comparing well with each other and were accurate. They found that the theoretical transfer function used for data inversion was comparable to the one they measured for 1 AIS, and 3 NAISs. They also found that the ion spectrometers were slightly overestimating the mobility. Although they found that the NAISs showed larger concentrations than the AISs in ambient measurements, they did not find such a difference during calibrations.

One of the two main aims of the second air ion spectrometer calibration workshop (this work), was to investigate the repeatability of the measurements, after the instruments had spent about one year in varying weather conditions in different environments. The second aim was to compare the instruments to each other and to reference instruments more extensively using ion and particle concentrations that reflect the ones observed in the field, also during new particle formation events. The latter aims at producing guidelines for data analysis, especially when comparing ion spectrometers with each other.

In this paper, we present the calibration results for mobility and concentration, and discuss the differences and similarities to the first calibration workshop. We also discuss the results of the intercomparison as well as the comparison with other instruments: a Balanced Scanning Mobility Analyzer (BSMA, Tammet, 2006), a Differential Mobility Particle Sizer (DMPS, Aalto et al., 2001) and an Ion-DMPS (Laakso et al., 2007). We present the values obtained from NPF events and discuss the charged fraction measurements made with the different (A)NAISs. Thus we evaluate the performance of different instruments and provide guidelines for data analysis and interpretation of field and other measurements.

2 Ion spectrometers

All the ion spectrometers (AIS, NAIS, ANAIS) are based on the same principle and share the same mobility analyzer structure (Fig. 1). However, the models vary in their inlet part (including the chargers) and the air flow system (sampling and sheath air). It is to be noted that second generation NAIS models and the ANAIS have more than one blower. Each ion spectrometer is identified with an individual name which is built from the instrument type and its serial number (e.g. NAIS3, see Table 1 for a list). These names were used during the EUCAARI campaign as well as in this paper.

2.1 Air Ion Spectrometer (AIS)

The Air Ion Spectrometer (AIS, Mirme et al., 2007) measures the size distribution of charged particles with a high time resolution. The measured mobilities range between 3.2 and 0.0013 $cm^2\,V^{-1}\,s^{-1}$, corresponding to Stokes-Millikan mobility diameters (Mäkelä et al., 1996) between 0.8 and 42 nm in NTP conditions. The AIS has two identical differential mobility analyzers (DMA) functioning in parallel: one for negatively charged particles and the other for positively charged particles. Each analyzer has a flow rate of 90 lpm: 30 lpm of sample flow, and 60 lpm of closed loop sheath air flow. The sheath air is filtered for re-use by using a corona charger and an electrical filter. The sample air comes through a single inlet with a 60 lpm flow which is then divided into two (30 lpm for each polarity). The high flow rate allows for smaller diffusional losses, so that low concentrations of smaller ions can be detected with a reasonable signal to noise ratio. The high time resolution of the instrument is

Table 1. Tasks performed for each ion spectrometer. The signs + and – in the task represent positive and negative polarities, "–" means not done or not possible, and the "X" sign means that the task was performed. In the first two rows (standards and mobilities) the number of mobility standards used is shown on the left, and the number on the right expresses the total number of different mobility and concentration combinations.

	AIS1	AIS2	AIS3	AIS6	AIS7	NAIS1	NAIS2	NAIS3	NAIS4	NAIS5	A-NAIS
+ standards (nb. mob./conc.)	4/12	4/12	4/15	4/14	4/23	4/13	–/–	4/15	4/15	4/15	4/10
– mobilities (nb. mob./conc.)	–/–	4/10	4/8	4/10	4/9	4/8	4/10	4/9	4/8	4/10	4/8
+ HDMA silver	–	X	X	–	X	–	–	X	X	X	X
– HDMA silver	–	X	X	–	X	–	–	X	X	X	X
+ HAUKE silver	X	X	X	X	X	X	–	X	X	X	X
– HAUKE silver	X	X	X	X	X	X	X	X	X	X	X
Neutral HAUKE silver	–	–	–	–	–	X	X	X	X	X	X

due to the design of its analyzers, which detect all mobility classes simultaneously, rather than by scanning the mobility distribution like in the SMPS or DMPS systems. The analyzers consist of an inner cylinder with 4 isolated sections to which different voltages are applied. The outer cylinder has 21 isolated cylindrical electrometers piled up vertically. The charged particles pass between the cylinders, perpendicular to an electric field, and are thus directed to an electrometer according to their electrical mobility. Each electrometer corresponds to a mobility channel and measures the current transmitted by these charged particles, from which their concentration is derived. The time resolution is user-adjustable but a minimum of one minute has been found to work with good accuracy, depending on noise levels (Asmi et al., 2009).

An offset measurement is made between each ion concentration measurement. A unipolar corona charger charges the particles with ions of the opposite polarity to that measured in the analyzer, and the charged particles are partly removed with an electric filter. During this operation mode, the electric field in the DMA is the same as for the other modes. This procedure allows for the measurement of air free of positively or negatively charged particles (for the positive or negative DMA, resp.) and thus the zero drift of the electrometers can be assessed as well as the RMS noise and noise due to parasitic currents. The offset is subtracted from the signal in the data inversion process. The data is inverted using the instrument equation of the ion spectrometer and the transfer function of the channels (based on geometry, flows, voltages and losses), and converted to a mobility distribution over 28 mobility bins. The inverting software is provided by Airel Ltd. It is also possible to record the raw electrometer electrical signal.

2.2 Neutral cluster and Air Ion Spectrometer (NAIS)

The Neutral cluster and Air Ion Spectrometer is an improved version of the AIS (Manninen et al., 2009a, Fig. 1). An additional charging-filtering section was added in order to measure the total number distribution of particles (the particle mode module in Fig. 1). The sample (assumed to be at or close to the bipolar charge equilibrium) goes through a unipolar corona charger. The charged fraction of particles induced to the sampled air is known for all sizes (estimated from Fuchs theory, Fuchs and Sutugin, 1971). The corona ions (generally <2 nm depending on concentration, air composition, polarity, etc.) are removed by the electrical filters, leaving a confidence size range between 2 and 42 nm (Asmi et al., 2009). The NAIS measures, in turn, the mobility distribution of particles (from negative and positive DMAs, particle measurements), and of naturally negatively and positively charged particles and ions (ion measurements), and the offset (offset measurements). The NAIS is also capable of measuring in the so-called alternative measurement mode, during which extra charging units, with the opposite polarity to the main charger, are turned on. This mode of operation should allow the retrieval of the total number concentration of particles even if the charge distribution of the particles in the atmosphere was not at charge steady-state. The alternative measurement operation mode was not used during the workshop.

2.3 Airborne Neutral cluster and Air Ion Spectrometer (Airborne NAIS)

The Airborne Neutral cluster and Air Ion Spectrometer (ANAIS, Mirme et al., 2009) is a second generation NAIS. It was developed to measure at varying altitudes (and thus pressures and temperatures). This was done by implementing an automatic sheath air flow adjustment system that compensates for the change in particle electrical mobility due to the change in pressure and temperature. The ANAIS has 3 or 4 blowers, depending on the model, to control the flows separately (one for the sheath air of the mobility analyzer and one or two connected in series for the sampling line), whereas first generation NAISs had only one central blower. The data acquisition system was also upgraded to adjust to the conditions so that the data is always adjusted to NTP conditions. The charger current in the corona charger is controlled

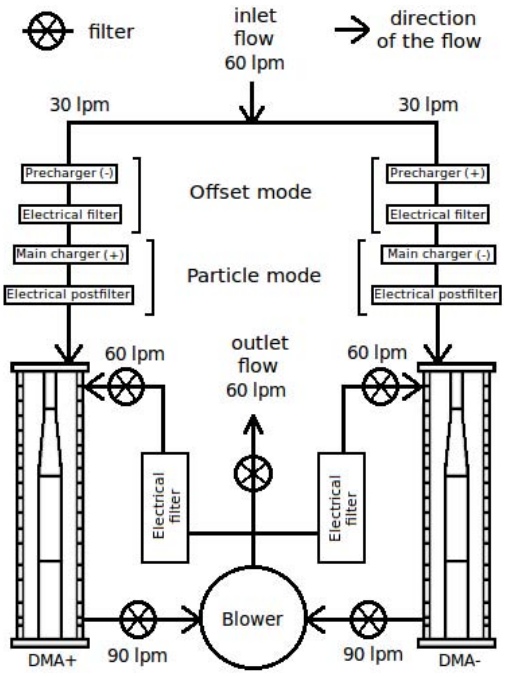

Fig. 1. Schematic figure of an NAIS. The inlet flow is 60 lpm split into two, 30 lpm for each polarity. The offset mode box is active only during the offset measurement mode; and the particle mode box is active only during the particle measurement mode. In the AIS, the particle mode box does not exist. The ANAIS has a different design with multiple blowers to control different parts of the flow.

to keep the efficiency of diffusion charging stable. All the changes were made to insure that the DMA parameters of the ion spectrometer remain constant and the same data inversion procedure can be used. A new, 2nd generation inversion program was also developed along with the instrument. This new version of the NAIS can be easily used in changing atmospheric conditions, and requires little maintenance.

3 Measurement setups and procedure

During the calibration period (25 May 2009–26 June 2009), we used mobility standards, silver ions and silver particles to investigate the measurements of mobility and concentration. The flows were also adjusted prior to the calibrations, to insure the accuracy of the comparison. In this section, we will describe the different experimental setups (or stations) used to calibrate the ion spectrometers. Four main stations can be distinguished: the flow adjustment station, the Hauke-type DMA station (4–40 nm particles), the High resolution DMA station (HDMA, <5 nm particles), and the intercomparison station. The high resolution DMA setup allows for two different sub-setups: using mobility selected silver ions and mobility standards (Ude and Fernández de la Mora, 2005).

The Airborne NAIS as well as the AIS 2, which had not been calibrated in the first calibration workshop but participated in the EUCAARI measurement campaign, were calibrated for the first time. The AIS 5, that was present in the first calibration workshop, was not available this time. The same mobility and concentration calibration were performed on 5 AISs, 5 NAISs and the Airborne NAIS (ANAIS). The calibration procedures that were performed are summarized in Table 1.

3.1 Flow adjustment setup

When the instruments arrived in Helsinki, they were thoroughly cleaned and sent to the flow adjustment station to ensure the best mobility and concentration measurements. The different parts of the flow system were adjusted while keeping the sampling flow at ∼60 lpm. In all ion spectrometers, except the ANAIS, five flows share one central blower (Fig. 1). Each of those five flows were measured through the pressure drop in Venturi tubes, and adjusted if required. The flow balance was verified for leaks in the same fashion as described by Asmi et al. (2009), before sending the ion spectrometer further to mobility and concentration calibration. All the pressure drops had been stable during the field campaign, provided that the Venturi tubes were unobstructed, and only small adjustments were made. This means that, if maintenance cleaning is done regularly, the instruments can perform well for long periods in diverse field conditions.

3.2 Hauke DMA

One of the purposes of this station was to compare the mobility diameter measured with the ion spectrometers with the mobility diameter selected with a Hauke-type DMA (10.9 cm in length, Winklmayr et al., 1991). Also, the concentrations given by the ion spectrometers was compared with a Condensation Particle Counter (CPC, TSI 3025, Stoltzenburg and McMurry, 1991) and an aerosol electrometer (TSI 3068A) as shown in Fig. 2a.

Polydisperse silver particles were produced with a tube furnace (Carbolite Furnaces MFT 12/388), then sent into a bipolar charger (^{241}Am) to get charged and then size selected with a DMA. The particle size varied between 4 and 40 nm. The sample flow in the DMA was 4 lpm and the sheath air flow was 20 lpm. To make up for the total sampling flow of the detection instrument (ion spectrometers 60 lpm, CPC: 1.5 lpm, and aerosol electrometer: 3 lpm), 63 lpm of diluting air was introduced after the DMA. The 50 % cut-off size of the CPC was 3 nm, while the electrometer, in principle, detects all ions and charged particles with a noise level of about ∼300 cm^{-3}.

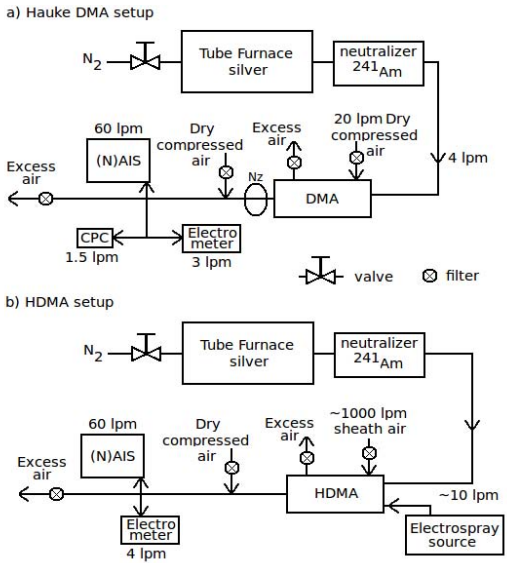

Fig. 2. Schematic figure of the setups used during the calibration procedure. The instruments and the most important flows are included for **(a)** Hauke setup, and **(b)** HDMA setup. The Hauke-setup includes a neutralizer (Nz) for calibrations in particle measurement mode. The HDMA setup can be operated either with the furnace or the electrospray, not both at the same time.

The ion spectrometers were operated in two or three of their operation modes: ions, particles (in the case of NAISs only) and offset mode. Concentration and mobility measurements were made when the concentration or the mobility was kept stable over several measurement cycles of the ion spectrometers. We also performed measurements of the ion spectrometer transfer function in which the mobility was scanned stepwise, each step spanning over one complete measurement cycle. The mobility range varied between 0.0014 and 0.13 $cm^2\,V^{-1}\,s^{-1}$ (∼4–40 nm) and was divided over 100 size bins.

3.3 High resolution DMA (HDMA)

The high resolution DMA, or Herrmann DMA (HDMA, Eichler, 1997; de Juan and Fernández de la Mora, 1998, Ude and Fernández de la Mora, 2005; Herrmann et al., 2000) was used in mobility standard and silver ion calibrations as well as for transfer function measurements. The very high mobility resolution of the HDMA, due to its high sheath flow rate (more than 1000 lpm), allows for the very precise selection of the mobility and the use of small particle sizes (<5 nm). The width of the DMA transfer function is much smaller than the resolution of the ion spectrometers. The HDMA was calibrated every day before starting the measurements, for establishing an accurate voltage to mobility conversion. The concentration was measured with an electrometer, in parallel with the ion spectrometers as shown in Fig. 2b.

3.3.1 Calibration with mobility standards

Mobility standards were used for mobility calibration at particle sizes smaller than 3 nm in diameter. For producing positive standards, we used THAB (tetra-heptyl ammonium bromide) and TMAI (tetra-methyl ammonium iodide), and for negative mobilities only THAB was used. Those compounds were electrosprayed, producing singly charged ions with known mass and mobility (Ude and Fernández de la Mora, 2005). Four such positive ions and four negative ions were selected using the HDMA. Each peak was measured at different concentrations.

The mobilities of the positively charged standards were 2.18 (TMAI derived TMA^+ ions), 0.97, 0.65 and 0.53 $cm^2\,V^{-1}\,s^{-1}$ (THAB derived THA^+, $(THAB)THA^+$ and $(THAB)_2THA^+$, resp.) at NTP. The standards used here are the same that were used in the first calibration workshop and their values are well established.

Four mobility peaks were selected from the negative THAB spectrum as well, even though their composition has not been verified by mass spectrometry and their stability is not known. The mobilities of the peaks that were used are: 2.45 (most probably Br^- ions), 1.48, 0.87 and 0.64 $cm^2\,V^{-1}\,s^{-1}$.

3.3.2 Calibrations with silver ions

The transfer function of the ion spectrometers for small particles was also measured using silver ions, mobility-selected with a HDMA. The silver particles were produced using a tube furnace and charged downstream with a bipolar charger (^{241}Am) before entering the HDMA. Below about 2 nm in mobility diameter, the particles were probably a mixture of ions produced in the charger and silver particles. For positively charged particles, we selected 81 logarithmically spaced mobilities between 0.09 and 1.10 $cm^2\,V^{-1}\,s^{-1}$ (∼1.4–4.8 nm). For negatively charged particles, the mobilities ranged between 0.38 and 1.48 $cm^2\,V^{-1}\,s^{-1}$ (∼1.2–2.3 nm) separated over 51 mobility bins.

3.4 Intercomparison

The intercomparison took place in a classroom at the University of Helsinki Kumpula campus. The room was situated on the 4th floor of the physics building “Physicum”. The room had a door leading to a large balcony and another one leading to a corridor with offices. The room’s surface was about 42 m^2 with a height of about 4 m. When the door to the balcony was opened, the particle concentration rose rapidly. The ion spectrometers were measuring in this room whenever they were not being calibrated, in cleaning, or in

repair. The ion spectrometers measured indoor air, or mixed indoor and outdoor air, and during new particle formation and growth. The NPF event was provoked by peeling citrus fruits in the middle of the room at approximately the same distance from each instrument. There was no additional fan system insuring that the air was well mixed, but all ion spectrometers were able to detect the new particle formation almost instantly and simultaneously. After each original event, secondary events always took place a few hours later in the same closed room.

3.4.1 Accompanying instruments

Three other instruments were measuring in the same room along with the AIS and NAIS ion spectrometers: a BSMA, a DMPS and an Ion-DMPS. In this section, we describe those three instruments.

The Balanced Scanning Mobility Analyzer (BSMA, Tammet 2006) measures the number size distribution of cluster ions and naturally charged particles in the size range 0.7–7 nm (Stokes-Millikan mobility diameters). The BSMA consists of two parallel plane-type DMAs for negative and positive ion classification and one common electrical amplifier as a detector. Here, the detector measures the electrical currents of air ions. The BSMA measures negative and positive ion spectra one after the other – not simultaneously. Due to high electrometer sensitivity, high flow rates and small wall losses, the BSMA is typically used as a reference for small ion concentrations. The BSMA agrees well with other instruments (see e.g. Hirsikko et al., 2005; Kulmala et al., 2007; Manninen et al., 2009a and Ehn et al., 2010), .

The Differential Mobility Particle Sizer (DMPS, Aalto et al., 2001) measured the atmospheric aerosol particle number size distribution between 10 and 300 nm in diameter. The DMPS consisted of a Hauke-type DMA (length 28.0 cm) in closed loop sheath flow arrangement (Jokinen and Mäkelä 1996), a CPC (TSI 3025, Stolzenburg and McMurry 1991) as a particle detector and a radioactive C-14 alpha neutralizer (370 MBq). Sampled particles were charged in an alpha-active bipolar charger and classified according to their electrical mobility in the DMA. Subsequently, the classified particles were counted by a particle detector (CPC), and the total concentration was retrieved after standard DMPS inversion. The DMPS was not calibrated, but the transfer function of the DMA and the CPC cut off size were known from earlier calibration measurements.

The Ion-DMPS (Laakso et al., 2007) is identical to a DMPS, with the exceptions that its bipolar charger can be switched on or off and the voltage applied to the DMA can be either positive or negative. The Ion-DMPS thus measured in four modes: positively charged particles neutralized (1. + neu.) or ambient (2. + amb.); negatively charged particles neutralized (3. − neu.) or ambient (4. − amb.). During the intercomparison, the Ion-DMPS was measuring particles between 2.2 and 11.5 nm in mobility diameter. The calibration curves of the instrument can be found in Laakso et al. (2007). This instrument was used as a reference instrument to compare the charged fraction, the fraction of particles that are charged in the particle distribution. The Ion-DMPS is designed to measure the charge ratio: the ratio of the ambient, "naturally" charged particle concentration to the neutralized (electrical bipolar steady-state) ion concentration. This quantity is equivalent to the ratio of the ambient charged fraction to the neutralized charged fraction. The NAIS measures the charged fraction: the ratio of the ion concentration to the total particle concentration. The neutralized charged fraction in the bipolar steady-state is known (Wiedensohler, 1988) so the charged fraction at ambient can be calculated from the Ion-DMPS charge ratio and compared to the charged fraction derived with the NAISs.

4 Results and discussion

The performance of the 11 ion spectrometers (5 AISs, 5 NAISs, one Airborne NAIS) was tested against reference devices and compared to each other (Table 1), after a one-year field measurement campaign. Also, all the instruments measured a NPF event simultaneously for the first time. In this section, we discuss the results from mobility and concentration calibrations as well as the intercomparison and the new particle formation event.

4.1 Mobility, mobility standards and concentration calibrations

All 11 ion spectrometers measured electrospray-generated mobility standards according to the method described in Sect. 3.3.1. Results from three examples of mobility standards of each polarity are presented in Fig. 3. The AISs and NAISs alike detected the mobility of the concentration peak almost accurately and compare well with each other. A shift can be observed with the TMA^+ ion (the smallest positive standard) and with negative standards. Part of the inaccuracies could result from clustering or fragmentation of the ions after mobility selection. All inaccuracies for negative standards point to an underestimation of the mobility, thus an overestimation of the size. Another observation that can be made on Fig. 3 is that the AISs display a sharper peak than the NAISs. This was also seen in the previous workshop, as shown by Asmi et al. (2009). The fact that normalized concentration peaks are broader for NAISs than for AISs could suggest that the NAISs detect small concentrations also in other size bins, in the ion measurement mode, that contribute to the total concentration. It could also be due to more turbulent flows in the NAISs than in the AISs, making particles land on the neighboring electrometers.

Figure 4 shows the results from the calibrations done with silver particles with the HDMA setup (<5 nm) and the Hauke-DMA setup (4–40 nm). In the first column, we

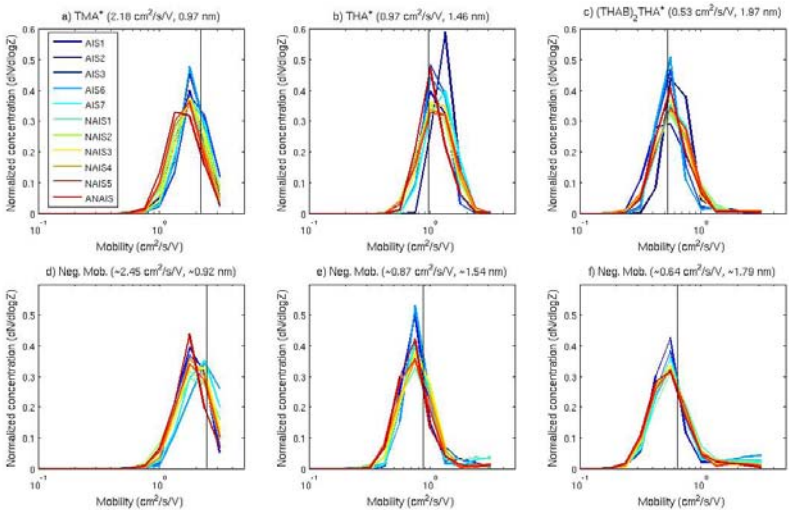

Fig. 3. Examples of mobility standards measurements. Panels **(a)**, **(b)** and **(c)** show the response of the ion spectrometers (normalized mobility distribution) for 3 positively charged mobility standards, and panels **(d)**, **(e)** and **(f)** for 3 negative mobilities. The black vertical lines represent the mobility that was selected through the HDMA. The mobility and size of the standards are above each plot. TMAI is tetra-methyl ammonium iodide and THAB is tetra-heptyl ammonium bromide.

compare the mobilities detected by the ion spectrometers (the peak of the mobility distribution) and the mobilities selected by the DMAs. In the second column, the concentrations seen by the ion spectrometers and the reference instruments are compared. Finally, in the third column, the ratio of the concentrations detected by the ion spectrometers and the reference instruments is shown as a function of the mobility. The first and second rows show the negative and positive ions, respectively. Background measurements are presented in Fig. 5. We used the DMA as a filter by applying a zero voltage so that the ion spectrometers were measuring particle-free air. In the following analysis, we will first focus on the ion data (first two rows in Fig. 4), then we will discuss the results from the particle mode (third row in Fig. 4).

In the ion measurement mode of the ion spectrometers, the peak mobilities were detected very accurately. In the positive mode at small diameters, however, the mobility was slightly overestimated. This was also observed by Asmi et al. (2009). In the second column of Fig. 4, the concentrations are compared to those measured with an electrometer. The concentration detection is rather good, but the NAISs overestimate the concentrations, and this is especially noticeable for the positive polarity. The concentration for the ion spectrometers in Fig. 4 is the total concentration integrating the whole size range of the instrument. In the third column, the ratio of the concentrations detected with the ion spectrometers to the electrometer concentration is shown as a function of mobility. The AISs and NAISs behaved similarly at larger diameters (smaller mobilities) but the NAISs overestimated the concentration at smaller diameters. The Airborne NAIS generally followed the behavior observed in first generation NAISs. One should note that the two setups cover different size ranges (Hauke DMA: $\sim$4–40 nm = 0.0014–0.13 $cm^2\,V^{-1}\,s^{-1}$; HDMA: $<\sim$5 nm = $>$0.083 $cm^2\,V^{-1}\,s^{-1}$). Hence, we have a gap for negative ions (the voltage supply only allowed for a smaller mobility range) and double lines for positive ions (the methods overlap on a small mobility range). The two methods are not in perfect agreement. This may be explained by that, at small sizes, the transfer function of the Hauke DMA is wider and the concentration of silver particles available is smaller. Thus the losses (and corrections) are more important in the Hauke setup than in the HDMA setup. One can see in the third column that the concentrations are overestimated more as the diameter decreases for both setups. Part of this overestimation can be due to the setup, since the ratio falls back to one when the setup changes from the Hauke DMA to the Herrmann DMA. However, despite corrections for losses in the experimental setups, the trend remains. In the left column of Fig. 5, one can see the background of the ion spectrometers in ion measurement mode as a function of diameter. The median total background concentration was 13.6 (23.5) cm^{-3} for AISs and 71.7 (53.2) cm^{-3} for NAISs for negative (and positive) ions. The background could partly be caused by ionization through radioactive decay or cosmic rays in the inlet of the instrument.

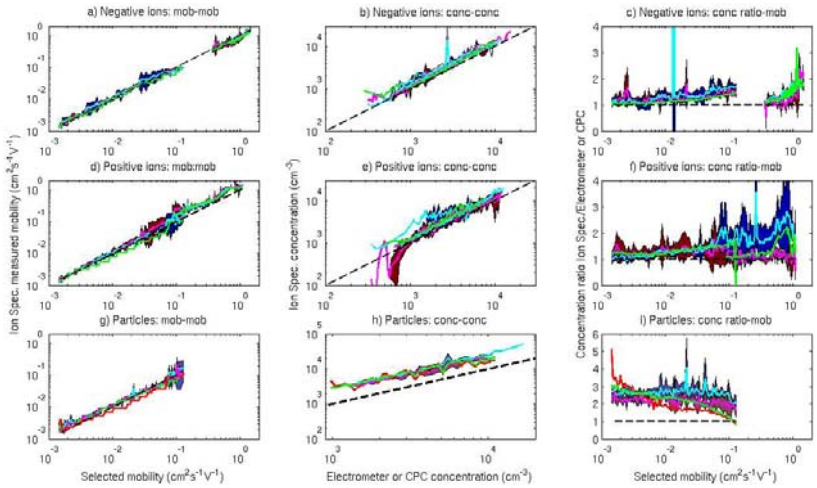

Fig. 4. Comparison of the ion spectrometers to reference instruments. **(a)**, **(b)**, **(c)**: negative polarity; **(d)**, **(e)**, **(f)**: positive polarity; **(g)**, **(h)**, **(i)**: total particles (charged+neutral, NAISs only). Panels **(a)**, **(d)** and **(g)** display the mobility measured by the ion spectrometers as a function of the mobility selected by the DMA. Panels **(b)**, **(e)** and **(h)** display the total concentration measured by the ion spectrometers as a function of the concentration measured with reference instruments. Panels **(c)**, **(f)** and **(i)** display the ratio of the ion spectrometer concentration to the concentration of the reference instrument as a function of the particle mobility. In panels **(a)** to **(f)**, the AISs are represented by magenta lines and red filling (standard deviation between instruments), the NAISs by cyan lines and blue filling, and the ANAIS by a green line. The electrometer is the reference instrument in these two lines. In panels **(g)**, **(h)** and **(i)**, the total particles, cyan lines and blue fillings correspond to the negative DMAs of the ion spectrometers; magenta lines and red fillings correspond to the positive DMAs of the ion spectrometers. The green and red lines represent the negative and positive DMAs of the ANAIS, respectively. The reference instrument is the CPC in this line. The black dashed lines are the ideal values. All the points in this figure were obtained from calibration with silver particles.

In the particle measurement mode of the ion spectrometers, the peak mobility was detected accurately. In the case of the Airborne NAIS, the positive polarity DMA was underestimating the mobility while its negative polarity DMA was accurate. This can either be due to a temporary malfunction of the instrument (e.g. changes in flows) or to a difference between the positive and negative DMA data inversion. The large variation between the instruments for smaller particles is most probably due to corona ions being detected up to about 5 nm ($0.08\,cm^2\,V^{-1}\,s^{-1}$), making the maximum of the measured mobility distribution difficult to find.

In the case of the particle measurement mode, the total concentration was calculated from 3.4 nm ($0.18\,cm^2\,V^{-1}\,s^{-1}$) instead of calculating the total concentration between 0.8 and 42 nm. This was done in an attempt to avoid including most of the background corona ions (see Fig. 5). The smallest size selected with the Hauke DMA was 4 nm, the DMA had a transmission width of 0.3 nm. To avoid the corona ions completely, we changed the minimum size integrated in the total concentration from 3.4 to 5.6 nm, but the overestimation of the concentration by the ion spectrometers remained. The concentration ratio with the reference instrument was still between 2 and 3 for first generation NAISs, although it decreased by about 0.2 compared to the ratio presented in ratio presented in Fig. 4i. This means that, even when avoiding corona ions, the NAISs seem to overestimate the concentration, especially in particle measurement mode. The concentration ratio does not vary much as a function of particle size for the NAISs. However, the Airborne NAIS overestimated the concentrations more significantly at bigger sizes than at smaller sizes. This is most likely due to a different inversion program provided by the manufacturer with the second generation models. The background concentration in particle mode is presented on the right side of Fig. 5. Most of the background is probably corona ions from the chargers. The median total background was $1.6 \times 10^5\,cm^{-3}$ for the negative DMA and $2.5 \times 10^6\,cm^{-3}$ for the positive DMA. When we applied the same minimum size of 3.4 nm to avoid corona ions, the background became much smaller with medians of $71.9\,cm^{-3}$ and $86.5\,cm^{-3}$ for the negative and positive DMA respectively. It is important to note that the background varies with the particle concentration. When there are particles in the sample air, part of the corona ions charge the particles and do not contribute to the background anymore. It is thus difficult to evaluate what fraction of the concentration is imputable to the background.

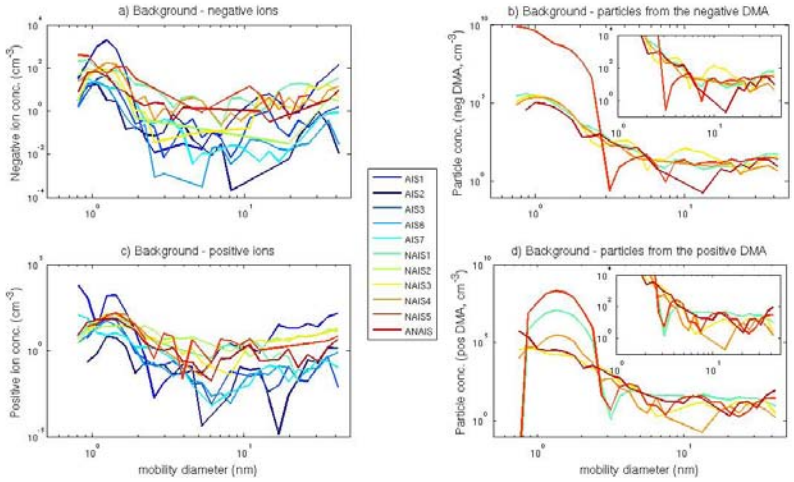

Fig. 5. The background concentrations is presented as a function of particle diameter. The total background concentration in ion measurement mode (**a** and **c**) was generally below 30 cm^{-3} for AISs and in the 30–150 cm^{-3} concentration range for NAISs. In particle measurement mode (**b** and **d**), the median total background concentration was 1.6×10^5 cm^{-3} and the median total background concentration above 3.4 nm was 86.5 cm^{-3}. In these background measurements we used the Hauke DMA as a filter (by applying a zero voltage) to provide the ion spectrometers with particle-free air.

Concentration calibrations have shown that the efficiency of the ion spectrometers does not depend on the concentration, so that the ratio of the ion spectrometer concentration to a reference instrument concentration remains the same as a function of the concentration. This was observed both by detecting 15 nm particles at varying concentrations and by plotting the concentration ratios presented in Fig. 4 as a function of concentration.

4.2 Intercomparison

The intercomparison period lasted roughly 20 days between 31 May 2009 and 22 June 2009. During that time, the instruments were measuring in the intercomparison room as described in Sect. 3.4, unless they were being calibrated, cleaned, fixed, or malfunctioning. The days on which most of instruments were measuring uninterruptedly in the room were on 6–7 and 13–14 June 2009.

4.2.1 Indoor and outdoor air measurements

On the 6 June 2009, the instruments were measuring indoor air (Fig. 6a–d) and on the 7 June 2009, the instruments were measuring outdoor air through an opened door giving on a balcony on the highest floor of the building (Fig. 6e–h). Here, we present the median concentration and current for each size channel. In both cases, if the median was a negative value, the value was replaced by 1×10^{-2} cm^{-3} for the concentrations and by 0.03 fA for the currents in order to facilitate visualization in logarithmic scale. The detection limit of the electrometers due to the noise is considered to be around 0.03 fA.

In the case of indoor air (Fig. 6a–d), the median concentration varied between about 0.01 and 10 000 particles per cm^3 per size channel (logarithmically spaced). The concentrations agree well from one instrument to another within the same instrument type, especially for negatively charged particles. However, once again, the NAISs display concentrations sometimes an order of magnitude bigger than the AISs depending on the particle diameter. This difference is also observed when looking at the raw electrometer signal on the right panels. The problem is bigger at small currents or concentration. In the case of outdoor air (Fig. 6e–h), the median concentration varied between about 1 and 2000 particles per cm^3 per size channel. The instruments agree well with each other, although a difference of about an order of magnitude can be seen between instrument types at certain diameters. At concentrations approaching the detection limit, the difference can be explained by the difference in background concentrations. Again, the agreement is better for negatively charged particles than for positively charged particles. One can notice that the concentration of small particles is bigger in the indoor air, while the concentration of large particles (>10 nm) is bigger in outdoor air. This is probably due to coagulation of smaller particles onto the numerous larger particles found in outdoor air.

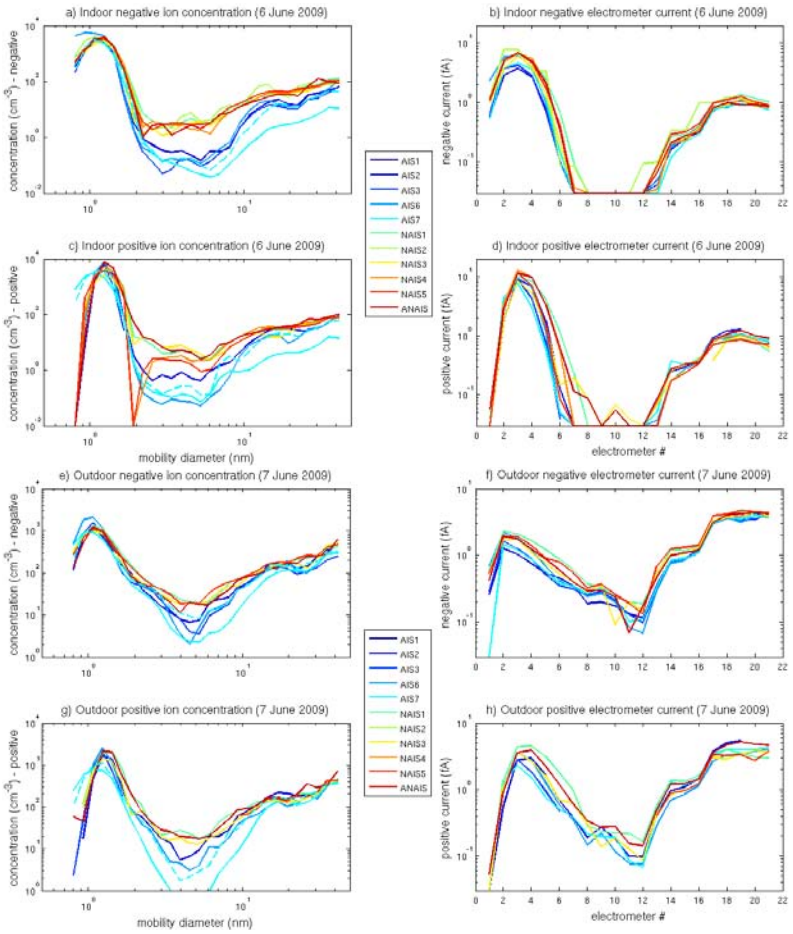

Fig. 6. Median concentration size distribution and electrometer current size distribution for indoor air (negative: **(a)**, **(b)**; positive: **(c)**, **(d)**, measured on 6 June 2009 and for outdoor air (negative: **(e)**, **(f)**; positive: **(g)**, **(h)**, measured on 7 June 2009. The AIS7 re-inverted concentrations are represented by the dashed line of the same color.

As can be seen from Fig. 6, the current of the AIS7 behaves like all other AISs, however, its concentrations are smaller than the other AISs is certain size ranges. The difference between the AIS7 and the others was caused by that the AIS7 was using different inverters, and had a much shorter measurement cycle. The AIS7 cycle was about 10 times shorter than the other AISs. This made noise levels more important in respect to the concentration, leading to the smaller concentrations. We re-inverted the currents using an inversion matrix that takes into account the shorter measurement cycle time. The new concentrations are presented in Figure 6 as dashed lines. One can see that the re-inverted output is much closer to the other AISs. Hence, we would like to point out the importance of using the appropriate inverters and upgrade the software in order to be comparable with other (N)AIS. This also shows that longer cycles are recommendable to allow better noise control leading to a better signal to noise ratio, and a better inversion of the currents.

4.2.2 Mean diameter and concentration comparison

The mean concentrations and diameters of ions and particles detected during the intercomparison workshop were calculated and are presented in Fig. 7. In general, all instruments showed similar concentrations and diameters, for both

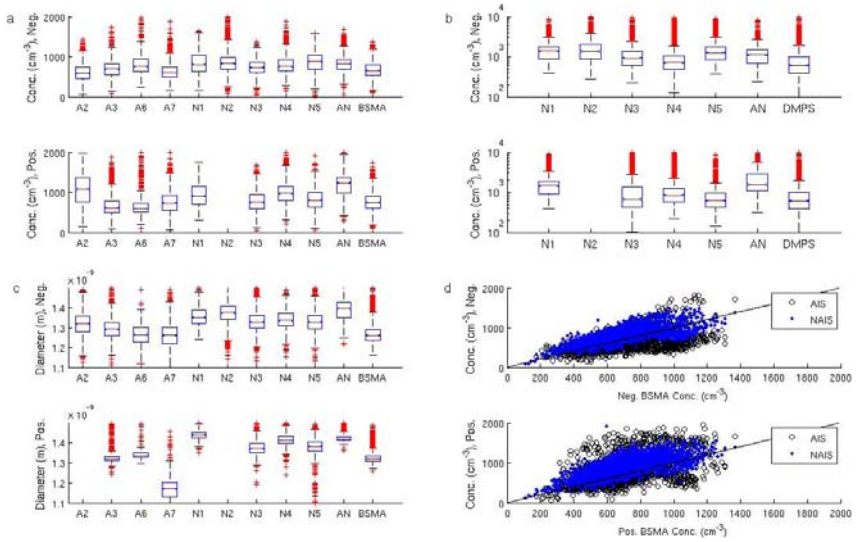

Fig. 7. Performance during the intercomparison period (7 June–25 June 2009). **(a)** Concentration of ions for AISs, NAISs and the BSMA (size range: 3–7 nm). **(b)** Concentration of particles for NAISs and the DMPS (size range: 10–40 nm). **(c)** Mean diameter for AISs, NAISs and the BSMA (0.8–3 nm). The red lines are the median value, the blue boxes are the 25-th and 75-th percentile, whiskers are 10-th and 90-th percentiles and red crosses are outliers. For readability purposes, the AISs are coded "A" and the NAISs, "N". The ANAIS is coded AN. **(d)** The total ion concentration of the ion spectrometers in the 3–7 nm size range is compared to the BSMA concentration. The AISs are represented by black circles and the NAISs by blue diamonds.

polarities, and also for neutral particles. However, in the case of negatively charged particles, measured with the ion measurement mode of the spectrometers, the AISs showed slightly smaller concentrations than the NAISs (Fig. 7a), consistent with the calibration results and the measurements of indoor and outdoor air. The BSMA, the reference instrument in this figure, agrees better with the AISs. For positively charged particle, the median concentrations varied more than for negatively charged particles. It is thus impossible to say whether the NAISs are overestimating the concentration for positively charged particles in this figure. As can be seen from Fig. 7d, the NAISs tend to measure higher concentrations than the AISs, at least for negatively charged particles at all concentrations. In general, the BSMA and the ion spectrometers agree well with each other.

The concentrations measured with the NAISs in the particle measurement mode can be compared to the DMPS as a reference instrument (Fig. 7b). The concentrations measured by the ion spectrometers were all in the same range. Once again, the negative analyzers agreed better with each other than the positive analyzers. For both polarities, the DMPS yielded smaller concentrations, suggesting that the NAISs may be overestimating the concentrations. The only differences between the AISs and NAISs are the extra charging modules found in the NAISs (causing a more turbulent flow) and a slightly different inversion process that takes into account the diffusional losses happening in these extra modules. The cause for the different concentrations, in this case, is most likely due to the differences in the flow turbulence and the data inversion process.

The size of small ions, smaller than ∼3 nm, is influenced by air composition, temperature, pressure and sink due to aerosol particles (see e.g. Luts and Parts, 2002; Parts and Luts, 2004). The mean mobility or size of small ions has thus been reported in the literature (see Hirsikko et al., 2010 and references therein). During the intercomparison period, the diameter distribution of the <3 nm particles varied from one instrument to another (Fig. 7c). The NAISs systematically had larger median diameters than the AISs, and the BSMA measured smaller diameters than the ion spectrometers in general. The median diameter of small ions varied between 1.25 and 1.45 nm with the exception of the AIS 7's positive mode and AIS 1's negative mode. Since the NAISs also detect different concentrations, and the diffusional losses are more important for smaller particles, it is probable that in the case of polydisperse particle distributions, the size distribution has been skewed. This difference in mobility diameter detection was not observed for monodisperse distributions (Fig. 3). Ehn et al. (2011) found that the size distribution from the BSMA compared well to the ion mass distribution

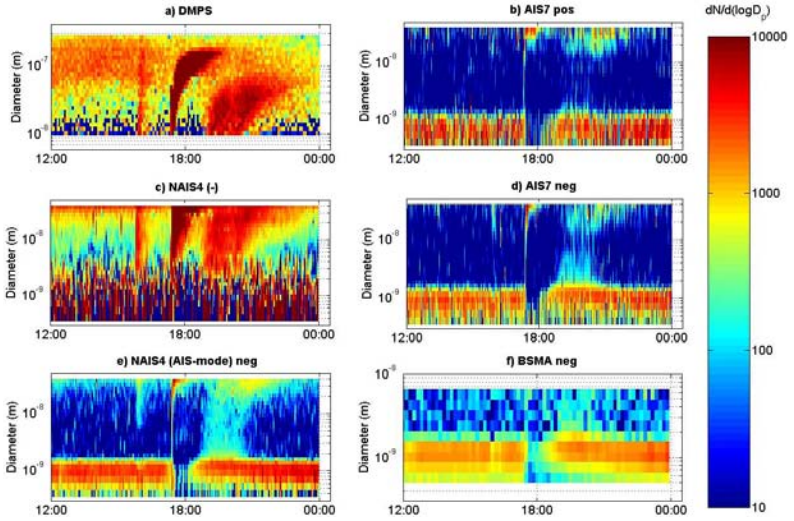

Fig. 8. Size distribution during the NPF event (12 June 2009) for a range of instruments. **(a)** DMPS, total concentration of aerosol particles, **(b)** AIS, positive air ions, **(c)** NAIS concentration of particles in particle operation mode (from the negative analyzer), **(d)** AIS negative air ions, **(e)** NAIS negative air ions, **(f)** BSMA negative air ions.

measured with the APi-TOF, whereas a shift towards larger sizes was observed when comparing AIS and APi-TOF. The median size of small ions is expected to differ according to their chemical composition.

4.2.3 Measurements during a NPF event

Three NPF events were provoked in the room during the intercomparison: on the 10, 12 and 14 June 2009. The NPF events were provoked by peeling citrus fruits in the middle of the room. The clearest event, with the most instruments monitoring it, was on 12 June 2009 and a sample of the results is presented in Fig. 8. What may look like a burst at ca. 15:30 is only due to briefly opening the door giving on the outside air. The fruits were peeled only at the start of the first burst at ca. 17:20. Secondary, weaker events started after the main one at 18:50 and 20:00. The core of the analysis will focus on the first secondary event, starting at 18:50.

The first event was very strong and fast, so that it was impossible to calculate the growth and formation rates accurately. After this event, the population of small ions was almost completely depleted. This is probably partly due to the high coagulation sink of the newly formed particles and partly to the activation of these small ions into new particles. The small ion population slowly rebuilt allowing the formation and growth of new particles (2nd and 3rd events). The concentration of small ions returned to normal levels once new particles had ceased to form, indicating the activation of small air ions during the event.

The charged fraction, which is the fraction of particles that are electrically charged, can be calculated for the NAIS data. It is presented for 12 June 2009 in Fig. 9. The charged fraction is the ratio of the concentration of charged particles (negatively + positively charged particles in the ion measurement mode) divided by the concentration of particles (NAIS particle measurement mode) for corresponding size ranges. Figure 9 shows the charged fraction of negatively (panels a–f) and positively (panels g–l) charged particles for 6 SIZE channels corresponding to 6 size channels of the Ion-DMPS. Since the NAISs provide two different measurements of the particle measurement mode (one for each DMA), the charged fraction was calculated for each DMA i.e. negative (positive) charged fraction = negative (positive) ion concentration ÷ particle concentration from the negative (positive) DMA. The charged fractions calculated from malfunctioning channel/polarity were removed from the figure.

The charged fractions measured with the NAISs were compared to the ones measured with the Ion-DMPS. The Ion-DMPS charged ratio was calculated as the ratio of the ambient mode concentration to the neutralized mode concentration (at steady-state charged fraction). The charged ratio was then multiplied by the steady state charging probability for the appropriate diameter (Wiedensohler, 1988) to get the charged fraction of the particles. The charged fraction derived from the Ion-DMPS data agrees with the range of charged fractions calculated with the different NAIS data. Based on calibration results, the charged fraction provided by the NAIS should be underestimated (because the particle

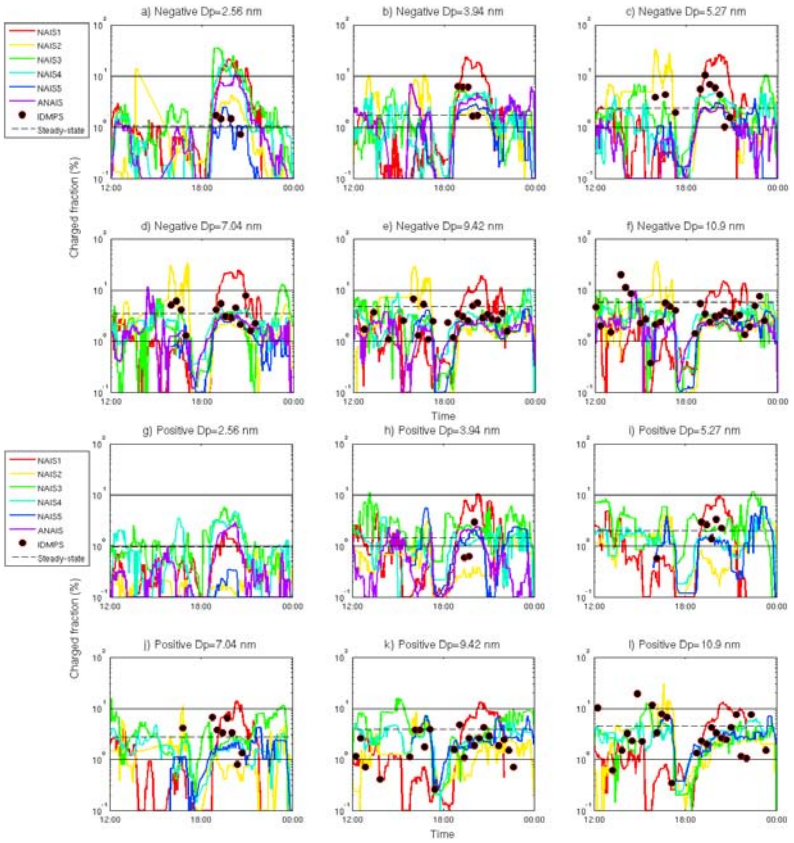

Fig. 9. Negative (**a** to **f**) and positive (**g** to **l**) charged fraction (fraction of charged particles, in percents) at 6 different diameters per polarity as a function of time for all NAISs on 12 June 2009. The charged fraction retrieved by the Ion-DMPS is shown as black circles and the steady-state charged fraction is marked with a black dashed line.

concentration is overestimated, and the ion concentration is not overestimated as much). However, the charged fraction corresponds well to that of the Ion-DMPS. It is possible that the NAISs overestimate the total concentration in particle operation mode when the charged fraction of the aerosol sample is much bigger than the equilibrium of the unipolar charger (overcharged situations). The aerosol sample used in calibrations in the particle operation mode was neutralized by a bipolar charger so the sample should not have been in an overcharged state. In most field situations strong overcharging seems to be rare (see Manninen et al. (2010) and references therein), however the subject requires further investigation. It is not clear why the charged fraction corresponded so well to the Ion-DMPS.

Particle formation rates at 2 nm (Manninen et al., 2009b) were calculated from each instrument during the second event on 12 June. The formation rate is the rate at which new particles are formed and appear in a given size range, in our case, at 2 nm (Kulmala et al., 2007). Values are shown in Table 2 for all modes and instruments for which it was possible to get a value. One has to bear in mind that the formation and growth rates calculated with the method of using the methods of Manninen et al. (2009b) can be trusted within a factor 2, and that using different methods may cause an even bigger difference. The new particle formation events were mostly driven by negatively charged particles as is often observed in other environments, in laboratory experiments and in quantum chemistry calculations (see e.g. Vana et al., 2006; Gagné 2010; Winkler et al., 2008; Kurtén et al., 2009). For that reason, it was impossible to calculate the formation rate in the

Table 2. Analysis of the 2nd new particle formation event of 12 June 2009 (18:50) by different instruments and ions spectrometers (see Fig. 8 for details). J_2 is the formation rate at 2 nm for negative and positive ions, and for total particles. GR is the growth rate of particles negative or positive (−/+) in different size ranges: 2–3, 3–7 and 7–20 nm. The mean and standard deviation for the AISs and NAISs are shown in the last two rows.

Instrument	J_2 ($cm^{-3}\,s^{-1}$)			GR ($nm\,h^{-1}$)					
	negative	positive	particle	2–3 nm (−/+)		3–7 nm (−/+)		7–20 nm (−/+)	
AIS 1	–	–	–	–	–	–	–	–	–
AIS 2	0.13	–	–	12.3	–	24.5	–	34.9	–
AIS 3	0.18	–	–	12.8	–	22.6	–	33.8	–
AIS 6	–	–	–	–	–	–	–	–	–
AIS 7	0.15	–	–	16.3	–	33.8	–	37.7	–
NAIS 1	0.21	0.08	2.2 (weak)	15.2	13.3	21.4	23.4	39.6	39.3
NAIS 2	0.23	–	–	9.6	–	27.5	–	37.1	–
NAIS 3	0.20	–	3.9	11.2	–	27.1	–	34.6	–
NAIS 4	0.21	0.07	1.6 (weak)	13.7	10.8	22.7	19.1	37.3	36.2
NAIS 5	0.24	0.09	1.3 (weak)	15.8	12.2	22.9	25.1	34.9	38.9
A-NAIS	0.20	0.08	4.7	16.2	13.2	25.3	22.0	38.1	–
DMPS	–	–	1.1	–	–	–	–	37 (10–20 nm)	
BSMA	0.27	–	–	11.4	–	23.0	–	–	
AIS (mean and st. dev.)	0.15 ± 0.03	–	–	13.8 ± 2.2	–	27.0 ± 7.0	–	35.5 ± 2.0	
NAIS (mean and st. dev.)	0.22 ± 0.02	0.08 ± 0.01	2.7 ± 1.5	13.6 ± 2.7	12.4 ± 1.2	24.5 ± 2.5	22.4 ± 2.5	38.1 ± 1.7	

positive mode for all AISs and some NAISs. The formation rates calculated from the AISs' negative mode were smaller than those calculated from the NAISs' same mode. This is consistent with the finding that NAISs seem to overestimate the ion concentration, especially at small diameters where the formation rates were calculated. The formation rate of ions calculated based on the BSMA was higher than those of the other ion spectrometers, closer to the NAISs than the AISs. During the intercomparison, the BSMA agreed better with the AISs because small ions (<2 nm) were dominating the size distribution. However, during the NPF event, the concentration of small ions decreased and the concentration of larger particles increased. The BSMA agrees better with the NAISs in the larger size range.

The formation rate in the particle mode was calculated in the case of NAISs using the same method as for ions. The formation rate of particles at 2 nm was also calculated from the DMPS. Due to the measurement range of the DMPS, the formation rate was first calculated at 10 nm and then scaled back to 2 nm using the formula described by Kerminen and Kulmala (2002) to be comparable to those calculated with the ion spectrometers. The formation rate J_2 of ions was found to be around 0.1–0.3 ($cm^{-3}\,s^{-1}$). The BSMA gave the highest rate ($0.27\,cm^{-3}\,s^{-1}$) while the AISs and the NAISs gave an average of $0.15\,cm^{-3}\,s^{-1}$ and $0.22\,cm^{-3}\,s^{-1}$ respectively. The difference between the AISs and the NAISs is not a surprise since the NAISs seem to have a tendency to overestimate the concentrations. In particle mode, the DMPS gave a formation rate of $1.1\,cm^{-3}\,s^{-1}$ while the NAIS average was $2.7\,cm^{-3}\,s^{-1}$, again this is not too surprising given the results given in Figs. 4g–i and 7b.

Also, the growth rates of particles were calculated for the AISs, NAISs DMPS and BSMA. The growth rate is the rate at which particles in a given size range grow. The results are presented in Table 2. Due to the small concentrations in the positive mode, it was impossible to calculate them for all the instruments. The growth rates were calculated in 3 different size ranges: 2–3 nm, 3–7 nm and 7–20 nm. As observed before, the growth is slower at small diameters and faster at bigger diameters (Hirsikko et al., 2007; Yli-Juuti et al., 2009). The AISs gave an average growth rate of 13.8, 27.0 and $35.5\,nm\,h^{-1}$ in each size range, respectively. The NAISs, on the other hand showed growth rates of 13.6, 24.5, $38.1\,nm\,h^{-1}$ for the negative polarity and slightly smaller values for the positive polarity. The BSMA yielded a growth rate of $11.4\,nm\,h^{-1}$ in the 2–3 nm size range and 23.0 in the 3–7 nm range. The DMPS gave a growth rate of $37\,nm\,h^{-1}$ in the 10–20 nm size range. No clear difference between the AISs and the NAISs was observed in the determination of the growth rate. This result can be explained by an accurate detection of the mobility for both types of instruments as shown in Figs. 3 and 4.

5 Conclusions

In this work, we inspected 11 ion spectrometers that had been deployed in field measurements during the EUCAARI project in 2007–2009. Three types of ion spectrometers were characterized and compared: 5 AISs, 5 NAISs and one second generation NAIS that is called an Airborne NAIS (ANAIS). We evaluated the response of the instruments regarding mobility (particle size) and concentration using mobility standards and silver particles in two experimental setups covering a size range between roughly 1 and 40 nm (the measurements performed are resumed in Table 1). We also had all the ion spectrometers and three reference instruments (BSMA, DMPS, ion-DMPS) measuring ambient indoor and outdoor air during the workshop, and compared their response. In addition, we provoked a new particle formation event in the room air that was monitored by all ion spectrometers side by side with the reference instruments. The formation and growth rates as well as the charged fraction were calculated and compared for all ion spectrometers and relevant reference instruments.

Based on the results presented in this paper, we present a number of results to keep in mind while performing analysis of air ion spectrometer data and evaluating results from different instruments:

1. The mobility detection can be trusted for AISs and NAISs, provided that the instrument is clean and the flows are not obstructed.
2. The growth rates calculated from the ion spectrometer data are reliable (as a consequence of conclusion 1 and the analysis of a NPF event).
3. The concentration can vary from one individual instrument to the other by up to 10 % within the same instrument type.
4. In ion measurement mode, the NAISs give higher concentrations than the AISs, the AISs agreed better with the BSMA.
5. The NAISs can overestimate the concentration by a factor of 2–3 in particle measurement mode (based on calibration results and comparison with a DMPS).
6. The formation rates vary from one individual instrument to the other (based on conclusion 3; it is also important to note that formation rates can be trusted within a factor 2 with the method described by Manninen et al., 2009).
7. The formation rates calculated from NAISs are higher than those calculated from AISs in ion measurement mode. However, the BSMA agreed better with the NAISs.
8. The formation rates of particles calculated from NAISs (in particle measurement mode) are higher than the reference instrument (based on conclusion 5 and on the analysis of a NPF event where it was compared to a DMPS).
9. The charged fraction calculated from NAISs is still considered unreliable even though it compared well with the reference instrument in this work (based on the analysis of a NPF event where it was compared to an Ion-DMPS).

The ion spectrometers proved to be good mobility detectors in ion measurement mode (Fig. 3). In particle measurement mode, some NAIS models had better accuracy than others (Fig. 4). The concentration measurements were in good agreement with the reference instruments for AIS models (Figs. 4 and 7). The ion spectrometers seemed to overestimate the concentrations as the particle size decreases. This can be partly explained by uncertainties with the different experimental setups, but a general tendency remains (Fig. 4). The NAIS models also detected the concentration well, but slightly overestimated the concentration compared to the AISs and the reference instruments. This was observed both in calibration measurements (Fig. 4) and in ambient measurements (Figs. 6 and 7a). Moreover, the NAISs had bigger background concentrations than the AISs (Fig. 5). In particle measurement mode, the NAISs overestimated the concentration by a factor 2 to 3, again both in calibration (Fig. 4) and in ambient measurements (Fig. 7b). The overestimation in the particle measurement mode seemed to be independent of the mobility for all NAISs except for the Airborne NAIS (Fig. 4). This was attributed to the different inversion process that the ANAIS and second generation NAISs use. At smaller particle sizes, the concentration of the ANAIS data seemed to be closer to the reference values, whereas the concentration was overestimated at bigger particle sizes.

A new particle formation event was detected by all the ion spectrometers as well as a BSMA, a DMPS and an Ion-DMPS. The formation rate J_2 of ions was found to be around 0.1–0.3 ($cm^{-3}\,s^{-1}$). The BSMA gave a rate of $0.27\,cm^{-3}\,s^{-1}$, the highest rate of all instruments. The AISs gave an average of $0.15\,cm^{-3}\,s^{-1}$ and the NAISs (including the ANAIS) an average of $0.22\,cm^{-3}\,s^{-1}$. It is not surprising to get higher formation rates from the NAISs than from the AISs given that the NAISs show higher concentrations than the AISs. In particle measurement mode, the formation rate at 2 nm scaled back from the DMPS measurements was $1.1\,cm^{-3}\,s^{-1}$ while the average for NAISs was $2.7\,cm^{-3}\,s^{-1}$. We thus recommend that this result be kept in mind when calculating formation rates from an NAIS, especially if compared with an AIS or with a DMPS/SMPS system.

The differences between the calculated formation rates may also have an effect on the ion-induced fraction, which has been previously calculated as the ratio of the ion formation rate to the particle formation rate (see e.g. Manninen et al., 2009b, 2010). Our results in Fig. 4 suggest that the overestimation is more important in particle measurement mode

than in ion measurement mode. Thus the ratio of the ion and particle formation rates, representing a part of the ion-induced fraction calculated from NAIS data, may be slightly underestimated (this does not affect the recombination part of the calculations). However, the charged fraction itself does not seem to be affected too greatly by this difference in formation rates (Fig. 9), probably because the charged fraction was not too high. The charged fraction calculated with the Ion-DMPS data was generally slightly higher than the one calculated with the NAISs data. The Ion-DMPS and the ion spectrometers yielded a similar behavior for the charged fraction, especially at larger diameters where the Ion-DMPS is more reliable, suggesting that the charged fraction obtained from the NAISs is a good estimation, at least at larger sizes (>9 nm).

The growth rates, presented in Table 2, were similar for all the ion spectrometers, regardless of whether they were AISs or NAISs, and agreed well with the reference instruments. This is a direct result of the high performance of the instruments regarding mobility detection. The growth rates were about 14, 25, 35 nm h^{-1} in the 2–3, 3–7, 7–40 nm size range, respectively.

The ion spectrometers evaluated in this paper performed well, despite having spent a year in varying weather conditions. They proved to be reliable and enduring instruments, although they need to be cleaned regularly to insure the quality of the data. Some systematic differences between the AISs and NAISs were observed, as well as minor differences between the first and second generation of NAISs. The reasons behind the overestimation of the concentration by NAISs did not become clear during the calibration workshop. Additionally, the inversion processes may need some improvements, especially in particle measurement mode. A measurement-based data inversion could be a replacement solution to the present theory-based data inversion of the air ion spectrometers.

Acknowledgements. Jani Hakala, Jyri Mikkilä and Joonas Vanhanen are acknowledged for their help in various tasks throughout the workshop. Ella-Maria Kyrö and Anna Frey are acknowledged for their help in preparing the instruments for calibration. This research was supported by the Academy of Finland Center of Excellence program (project number 1118615), the European Commission 6th Framework program project EUCAARI, contract no 036833-2 (EUCAARI) and the Estonian Science Foundation, grant number 8342. The work of A. Franchin and S. Schobesberger was supported by the European Commission under the 7th Framework Programme (grant agreement number 215072: Marie Curie Initial Training Network, CLOUD-ITN).

Edited by: J. Curtius

References

Aalto, P., Hämeri, K., Becker, E., Weber, R., Salm, J., Mäkelä, J. M., Hoell, C., O'Dowd, C. D., Karlsson, H., Hansson, H.-C., Väkevä, M., Koponen, I. K., Buzorius, G., and Kulmala, M.: Physical characterization of aerosol particles during nucleation events, Tellus, 53B, 344–358, 2001

Andronache, C., Grönholm, T., Laakso, L., Phillips, V., and Venäläinen, A.: Scavenging of ultrafine particles by rainfall at a boreal site: observations and model estimations, Atmos. Chem. Phys., 6, 4739–4754, doi:10.5194/acp-6-4739-2006, 2006.

Asmi, E., Sipilä, M., Manninen, H. E., Vanhanen, J., Lehtipalo, K., Gagné, S., Neitola, K., Mirme, A., Mirme, S., Tamm, E., Uin, J., Komsaare, K., Attoui, M., and Kulmala, M.: Results of the first air ion spectrometer calibration and intercomparison workshop, Atmos. Chem. Phys., 9, 141–154, doi:10.5194/acp-9-141-2009, 2009.

Duplissy, J., Enghoff, M. B., Aplin, K. L., Arnold, F., Aufmhoff, H., Avngaard, M., Baltensperger, U., Bondo, T., Bingham, R., Carslaw, K., Curtius, J., David, A., Fastrup, B., Gagné, S., Hahn, F., Harrison, R. G., Kellett, B., Kirkby, J., Kulmala, M., Laakso, L., Laaksonen, A., Lillestol, E., Lockwood, M., Mäkelä, J., Makhmutov, V., Marsh, N. D., Nieminen, T., Onnela, A., Pedersen, E., Pedersen, J. O. P., Polny, J., Reichl, U., Seinfeld, J. H., Sipilä, M., Stozhkov, Y., Stratmann, F., Svensmark, H., Svensmark, J., Veenhof, R., Viisanen, Y., Wagner, P. E., Wehrle, G., Weingartner, E., Wex, H., Wilhelmsson, M., and Winkler, P. M.: Results from the CERN pilot CLOUD experiment, Atmos. Chem. Phys., 10, 1635–1647, doi:10.5194/acp-10-1635-2010, 2010.

Eichler, T.: A Differential Mobility analyzer for ions and nanoparticles: Laminar flow at high Reynolds numbers, Senior Graduation Thesis presented to Fachhochschule Offenburg, Germany, May 1997.

Ehn, M., Junninen, H., Schobesberger, S., Manninen, H., Franchin, A., Sipilä, M., Petäjä, T., Kerminen, V.-M., Tammet, H., Mirme, A., Mirme, S., Hõrrak, U., Kulmala, M., and Worsnop, D. R.: An instrumental comparison of mobility and mass measurements of atmospheric small ions, Aerosol Sci. Technol., 45, 522–532, 2011.

Fuchs, N. A. and Sutugin, A. G.: Highly dispersed aerosols, Vol H of In Topics in Current Aerosol Research, Pergamon Press, New York, 19439, 1971.

Gagné, S., Nieminen, T., Kurtén, T., Manninen, H. E., Petäjä, T., Laakso, L., Kerminen, V.-M., Boy, M., and Kulmala, M.: Factors influencing the contribution of ion-induced nucleation in a boreal forest, Finland, Atmos. Chem. Phys., 10, 3743–3757, doi:10.5194/acp-10-3743-2010, 2010.

Harrison, R. G. and Carslaw, K. S.: Ion-aerosol-cloud processes in the lower atmosphere, Reviews of Geophysics, 41, 1012, 2003.

Herrmann,W., Eichler, T., Bernardo, N., and Fernández de la Mora, J.: Turbulent transition arises at Re 35 000 in a short Viennatype DMA with a large laminarizing inlet, Abstract to the annual conference of the AAAR, St. Louis, MO, 6–10 October, 2000.

Hirsikko, A., Laakso, L., Hõrrak, U., Aalto, P.P., Kerminen, V.-M., and Kulmala, M.: Annual and size dependent variation of growth rates and ion concentrations in boreal forest, Boreal Environ. Res., 10, 357–369, 2005.

Hirsikko, A., Yli-Juuti, T., Nieminen, T., Vartiainen, E., Laakso, L., Hussein, T., and Kulmala, M.: Indoor and outdoor air ion and

aerosol particles in the urban atmosphere of Helsinki: characteristics, sources and formation, Boreal Environ. Res., 12, 295–310, 2007.

Hirsikko, A., Nieminen, T., Gagné, S., Lehtipalo, K., Manninen, H. E., Ehn, M., H˜rrak, U., Kerminen, V.-M., Laakso, L., McMurry, P. H., Mirme, A., Mirme, S., Petäjä, T., Tammet, H., Vakkari, V., Vana, M., and Kulmala, M.: Atmospheric ions and nucleation: a review of observations, Atmos. Chem. Phys., 11, 767–798, doi:10.5194/acp-11-767-2011, 2011.

Jokinen, V. and Mäkelä, J.: Closed loop arrangement with critical orifice for DMA sheath/excess flow system, J. Aerosol Sci., 28, 643–648, 1996.

de Juan, L. and Fernández de la Mora, J.: Size analysis of nanoparticles and ions: Running a Vienna DMA of near optimal length at Reynolds numbers up to 5000, J. Aerosol Sci., 29, 617–626, 1998.

Kerminen, V.-M. and Kulmala, M.: Analytical formulae connecting the "real" and the "apparent" nucleation rate and the nuclei number concentration for atmospheric nucleation events, J. Aerosol Sci., 33, 609–622, 2002.

Kerminen, V.-M., Petäjä, T., Manninen, H. E., Paasonen, P., Nieminen, T., Sipilä, M., Junninen, H., Ehn, M., Gagné, S., Laakso, L., Riipinen, I., Vehkamäki, H., Kurten, T., Ortega, I. K., Dal Maso, M., Brus, D., Hyvärinen, A., Lihavainen, H., Leppä, J., Lehtinen, K. E. J., Mirme, A., Mirme, S., Hõrrak, U., Berndt, T., Stratmann, F., Birmili, W., Wiedensohler, A., Metzger, A., Dommen, J., Baltensperger, U., Kiendler-Scharr, A., Mentel, T. F., Wildt, J., Winkler, P. M., Wagner, P. E., Petzold, A., Minikin, A., Plass-Dülmer, C., Pschl, U., Laaksonen, A., and Kulmala, M.: Atmospheric nucleation: highlights of the EUCAARI project and future directions, Atmos. Chem. Phys., 10, 10829–10848, doi:10.5194/acp-10-10829-2010, 2010.

Kulmala, M., Laakso, L., Lehtinen, K. E. J., Riipinen, I., Dal Maso, M., Anttila, T., Kerminen, V.-M., Hõrrak, U., Vana, M., and Tammet, H.: Initial steps of aerosol growth, Atmos. Chem. Phys., 4, 2553–2560, doi:10.5194/acp-4-2553-2004, 2004a.

Kulmala, M., Vehkamäki, H., Petäjä, T., Dal Maso, M., Lauri, A., Kerminen, V.-M., Birmili, W., and McMurry, P. H.: Formation and growth of ultrafine atmospheric particles: a review of observations, J. Aerosol Sci., 35, 143–176, 2004b.

Kulmala, M., Riipinen, I., Sipilä, M., Manninen, H., Petäjä, T., Junninen H., Dal Maso, M., Mordas, G., Mirme, A., Vana, M., Hirsikko, A., Laakso, L., Harrison, R. M., Hanson, I., Leung, C., Lehtinen, K. E. J., and Kerminen, V.-M.: Toward Direct Measurement of Atmospheric Nucleation, Science, 318, 89–92, doi:10.1126/science.1144124, 2007.

Kulmala, M., Asmi, A., Lappalainen, H. K., Carslaw, K. S., Pöschl, U., Baltensperger, U., Hov, Ø., Brenquier, J.-L., Pandis, S. N., Facchini, M. C., Hansson, H.-C., Wiedensohler, A., and O'Dowd, C. D.: Introduction: European Integrated Project on Aerosol Cloud Climate and Air Quality interactions (EUCAARI) – integrating aerosol research from nano to global scales, Atmos. Chem. Phys., 9, 2825–2841, doi:10.5194/acp-9-2825-2009, 2009.

Kurtén, T., Ortega, I. K., and Vehkamäki, H.: The sign preference in sulfuric acid nucleation, Journal of Molecular Structure: THEOCHEM, 901, 169–173, 2009.

Laakso, L., Mäkelä, J. M., Pirjola, L., and Kulmala, M.,: Model studies on ion-induced nucleation in the atmosphere, J. Geophys. Res.–Atmos., 107, 4427, doi:10.1029/2002JD002140, 2002.

Laakso, L., Gagné, S., Petäjä, T., Hirsikko, A., Aalto, P. P., Kulmala, M., and Kerminen, V.-M.: Detecting charging state of ultra-fine particles: instrumental development and ambient measurements, Atmos. Chem. Phys., 7, 1333–1345, doi:10.5194/acp-7-1333-2007, 2007.

Lohmann, U. and Feichter, J.: Global indirect aerosol effects: a review, Atmos. Chem. Phys., 5, 715–737, doi:10.5194/acp-5-715-2005, 2005.

Lovejoy, E. R., Curtius, J., and Froyd, K. D.: Atmospheric ion-induced nucleation of sulfuric acid and water, J. Geophys. Res., 109, D08204, doi:10.1029/2003JD004460, 2004.

Luts, A. and Parts, T.-E.: Evolution of negative small air ions at two different temperatures, J. Atmos. Sol.-Terr. Phys., 64, 763–774, 2002.

Manninen, H. E., Petäjä, T., Asmi, E., Riipinen, I., Nieminen, T., Mikkilä, J., Hõrrak, U., Mirme, A., Mirme, S., Laakso, L., Kerminen, V.-M., and Kulmala, M.: Long-term field measurements of charged and neutral clusters using Neutral cluster and Air Ion Spectrometer (NAIS), Boreal Environ. Res., 14, 591–605, 2009a.

Manninen, H. E., Nieminen, T., Riipinen, I., Yli-Juuti, T., Gagné, S., Asmi, E., Aalto, P. P., Petäjä, T., Kerminen, V.-M., and Kulmala, M.: Charged and total particle formation and growth rates during EUCAARI 2007 campaign in Hyytiälä, Atmos. Chem. Phys., 9, 4077–4089, doi:10.5194/acp-9-4077-2009, 2009b.

Manninen, H. E., Nieminen, T., Asmi, E., Gagné, S., Hkkinen, S., Lehtipalo, K., Aalto, P., Vana, M., Mirme, A., Mirme, S., Hõrrak, U., Plass-Dülmer, C., Stange, G., Kiss, G., Hoffer, A., Törő, N., Moerman, M., Henzing, B., de Leeuw, G., Brinkenberg, M., Kouvarakis, G. N., Bougiatioti, A., Mihalopoulos, N., O'Dowd, C., Ceburnis, D., Arneth, A., Svenningsson, B., Swietlicki, E., Tarozzi, L., Decesari, S., Facchini, M. C., Birmili, W., Sonntag, A., Wiedensohler, A., Boulon, J., Sellegri, K., Laj, P., Gysel, M., Bukowiecki, N., Weingartner, E., Wehrle, G., Laaksonen, A., Hamed, A., Joutsensaari, J., Petäjä, T., Kerminen, V.-M., and Kulmala, M.: EUCAARI ion spectrometer measurements at 12 European sites – analysis of new particle formation events, Atmos. Chem. Phys., 10, 7907–7927, doi:10.5194/acp-10-7907-2010, 2010.

Matisen, R., Miller, F., Tammet, H. and Salm, J.: Air ion counters and spectrometers designed in Tartu University, Acta et Comm. Univ. Tartuensis, 947, 60–67, 1992.

Mirme, A., Tamm, E., Mordas, G., Vana, M., Uin, J., Mirme, S., Bernotas, T., Laakso, L., Hirsikko, A., and Kulmala, M.: A widerange multi-channel Air Ion Spectrometer, Boreal Environ. Res., 12, 247–264, 2007.

Mirme, S., Mirme, A., Minikin, A., Petzold, A., Hõrrak, U., Kerminen, V.-M., and Kulmala, M.: Atmospheric sub-3 nm particles at high altitudes, Atmos. Chem. Phys., 10, 437–451, doi:10.5194/acp-10-437-2010, 2010.

Myhre, G., Berglen, T. F., Johnsrud, M., Hoyle, C. R., Berntsen, T. K., Christopher, S. A., Fahey, D. W., Isaksen, I. S. A., Jones, T. A., Kahn, R. A., Loeb, N., Quinn, P., Remer, L., Schwarz, J. P., and Yttri, K. E.: Modelled radiative forcing of the direct aerosol effect with multi-observation evaluation, Atmos. Chem. Phys., 9, 1365–1392, doi:10.5194/acp-9-1365-2009, 2009.

Mäkelä, J. M., Riihelä, M., Ukkonen, A., Jokinen, V., and Keskinen, J.: Comparison of mobility equivalent diameter with Kelvin-Thomson diameter using ion mobility data, J. Chem. Phys., 105,

1562–1571, 1996.

Parts, T.-E. and Luts, A.: Observed and simulated effects of certain pollutants on small air ion spectra: I. Positive ions, Atmos. Environ., 38(9), 1283–1289, 2004.

Stevens, B. and Feingold, G.: Untangling aerosol effects on clouds and precipitation in a buffered system, Nature, 461, 607–613, 2009.

Stolzenburg, M. R. and McMurry, P. H.: An Ultrafine Aerosol Condensation Nucleus Counter, Aerosol Sci. Technol., 14, 48–65, 1991.

Tammet, H.: Continuous scanning of the mobility and size distribution of charged clusters and nanometer particles in atmospheric air and the Balanced Scanning Mobility Analyzer BSMA, Atmos. Res., 82, 523–535, 2006.

Twomey, S.: Aerosols, clouds and radiation, Atmos. Environ., 25A, 2435–2442, 1991.

Ude, S. and Fernández de la Mora, J.: Molecular monodisperse mobility and mass standards from electrosprays of tetra-alkyl ammonium halides, J. Aerosol Sci., 36, 1224–1237, 2005.

Vana, M., Tamm, E., Hõrrak, U., Mirme, A., Tammet, H., Laakso, L., Aalto, P., and Kulmala, M.: Charging state of atmospheric nanoparticles during the nucleation burst events, Atmos. Res., 82, 536–546, 2006.

Vartiainen, E., Kulmala, M., Ehn, M., Hirsikko, A., Junninen, H., Petäjä, T., Sogacheva, L., Kuokka, S., Hillamo, R., Skorokhod, A., Belikov, I., Elansky, N., and Kerminen, V.- M.: Ion and particle number concentrations and size distributions along the Trans-Siberian railroad, Boreal Environ. Res., 12, 375–396, 2007.

Wang, S. C. and Flagan, R. C.: Scanning electrical mobility spectrometer, Aerosol Sci. Technol., 13, 230–240, 1990.

Wiedensohler, A.: An approximation of the bipolar charge distribution for particles in the submicron size range, J. Aerosol Sci., 19, 387–389, 1988.

Winkler, P. M., Steiner, G., Virtala, A., Vehkamäki, H., Noppel, M., Lehtinen, K. E. J., Reischl, G. P., Wagner, P. E., and Kulmala, M.: Heterogeneous Nucleation Experiments bridging the scale from molecular ion clusters to nanoparticles, Science, 319, 1374, doi:10.1126/science.1149034, 2008.

Winklmayr, W., Reischl, G. P., Lindner, A. O., and Berner, A.: A new electromobility spectrometer for the measurement of aerosol size distributions in the size range from 1 to 1000 nm, J. Aerosol Sci., 22, 289–296, 1991.

Yli-Juuti, T., Riipinen, I., Aalto, P. P., Nieminen, T., Maenhaut, W., Janssens, I. A., Claeys, M., Salma, I., Ocskay, R., Hoffer, A., Imre, K., and Kulmala, M.: Characteristics of new particle formation events and cluster ions at K-puszta, Hungary, Boreal Environ. Res., 14, 683–698, 2009.

Bibliography

Aitken, J.: On dust, fogs, and clouds, Proc. R. Soc. Edinb., 9, 14–18, 1880a. (Cited page 3.)

Aitken, J.: On dust, fogs, and clouds, Nature, 14, 384–385, 1880b. (Cited page 3.)

Aitken, J.: On the number of dust particles on the atmosphere of certain places in Great Britain and on the continent, with remarks on the relation between the amount of dust and meteorological phenomena, Trans. Royal Soc. Edin., 37, 621–693, 1885. (Cited page 4.)

Aitken, J.: On the number of dust particles in the atmosphere, Nature, 37, 187–206, 1888. (Cited pages 3 and 4.)

Aitken, J.: On improvement in the apparatus for counting the dust particles in the atmosphere, Proc. R. Soc. Edinb., 16, 135–172, 1889. (Cited page 3.)

Aitken, J.: On a simple pocket dust counter, Proc. R. Soc. Edinb., 18, 39–52, 1891a. (Cited page 3.)

Aitken, J.: On the solid and liquid particles in clouds, Nature, 44, 279, 1891b. (Cited page 4.)

Albrecht, B.: Aerosols, cloud microphysics and fractional cloudiness, Science, 245, 1227–1230, 1989. (Cited page 10.)

Andreas, E. L.: A new sea spray generation function for wind speed up to 32 m s^{-1}, J. Phys. Oceanogr., 28, 2175–2184, 1998. (Cited page 11.)

Aplin, K., Harrison, R., and Bennett, A.: Effect of the troposphere on surface neutron counter measurements, Adv. Space Res., 35, 1484–1491, doi:10.1016/j.asr.2005.02.055, 2005. (Cited page 49.)

Arnold, F.: Multi-ion complexes in the stratosphere – implications for trace gases and aerosol, Nature, 284, 610–611, 1980. (Cited pages 27 and 53.)

Arnold, F., Pirjola, L., Aufmhof, H., Schuck, T., Lahde, T., and Hameri, K.: First gaseous sulfuric acid measurements in automobile exhaust: Implications for volatile nanoparticle formation, Atm. Env., 40, 7097–7105, 2006. (Cited page 96.)

Asmi, E., Sipilä, M., Manninen, H. E., Vanhanen, J., Lehtipalo, K., Gagné, S., Neitola, K., Mirme, A., Mirme, S., Tamm, E., Uin, J., Komsaare, K., Attoui, M., and Kulmala, M.: Results of the first air ion spectrometer calibration and intercomparison workshop, Atmos. Chem. Phys., 9, 141 – 154, doi:10.5194/acp-9-141-2009, 2009. (Cited pages 31, 32, 97, 104 and 116.)

Asmi, E., Frey, A., Virkkula, A., Ehn, M., Manninen, H. E., Timonen, H., Tolonen-Kivimäki, O., Aurela, M., Hillamo, R., and Kulmala, M.: Hygroscopicity and chemical composition of Antarctic sub-micrometre aerosol particles and observations of new particle formation, Atmos. Chem. Phys., 10, 4253–4271, doi:10.5194/acp-10-4253-2010, 2010. (Cited page 12.)

Atkinson, R. and Arey, J.: Atmospheric Degradation of Volatil Organic Compounds, Chem. Rev., 103, 4605–4638, 2003. (Cited page 107.)

Aumont, B., Szopa, S., and Madronich, S.: Modelling the evolution of organic carbon during its gas-phase tropospheric oxidation: development of an explicit model based on a self generating approach, Atmos. Chem. Phys., 5, 2497–2517, doi:10.5194/acp-5-2497-2005, 2005. (Cited page 39.)

Auzout, A.: Lettre a Monsieur l'Abbe Charles, Journal des savants, pp. 21–24, 1666. (Cited page 1.)

Baltensperger, U., Gäggeler, H. W., Jost, D. J., Lugauer, M., Schwikowski, M., Seibert, P., and Weingartner, E.: Aerosol climatology at the high-alpine site Jungfraujoch, Switzerland, J. Geophys. Res., 102, 19 707 – 19 715, 1997. (Cited page 47.)

Baltensperger, U., Schwikowski, M., Jost, D. T., Nyeki, S., Gäggeler, H. W., and Poulida, O.: Scavenging of atmospheric constituents in mixed phase clouds at the high-altitude alpine site Jungfraujoch part I: Basic concept and aerosol scavenging by clouds, Atm. Env., 32, 3975–3983, 1998. (Cited page 53.)

Baron, P. A. and Willeke, K., eds.: Aerosol Measurement - Principles, Techniques, and Applications., Wiley - Interscience, 2001. (Cited pages 4 and 5.)

Barsanti, K. C., McMurry, P. H., and Smith, J. N.: The potential contribution of organic salts to new particle growth, Atmos. Chem. Phys., 9, 2949–2957, doi:10.5194/acp-9-2949-2009, 2009. (Cited page 92.)

Birmili, W., Berresheim, H., Plass-Dülmer, C., Elste, T., Gilge, S., Wiedensohler, A., and Uhrner, U.: The Hoenpeissenberg aerosol formation experiment (HAFEX): a log term sutdy including size-resolved aerosol, H_2SO_4, OH and monoterpenes measurements, Atmos. Chem. Phys., 3, 361–376, doi:10.5194/acp-3-361-2003, 2003. (Cited page 122.)

Bolton, D.: The Computation of Equivalent Potential Temperature, Mon. Weather Rev., 108, 1046 – 1053, 1980. (Cited page 74.)

Bonn, B. and Moortgat, G. K.: New particle formation during α- and β-pinene oxydation by O_3, OH and NO_3, and the influence of water vapour: particle size distribution studies., Atmos. Chem. Phys., pp. 183–196, doi:10.5194/acp-2-183-2002, 2002. (Cited pages 13 and 95.)

Bonn, B., Schuster, G., and Moortgat, G. K.: Influence of Water Vapor on the Process of New Particle Formation during Monoterpene Ozonolysis, J. Phys. Chem. A, 106, 2869–2881, doi:10.1021/jp012713p, 2002. (Cited pages 13, 102 and 110.)

Bonn, B., Kulmala, M., Riipinen, I., Sihto, S.-L., and Ruuskanen, T. M.: How biogenic terpenes govern the correlation between sulfuric acid concentrations and new particle formation, J. Geophys. Res., 113, D12 209, doi:10.1029/2007JD009327, 2008. (Cited page 102.)

Boulon, J., Sellegri, K., Venzac, H., Picard, D., Weingartner, E., Wehrle, G., Collaud Coen, M., Bütikofer, R., Flückiger, E., Baltensperger, U., and Laj, P.: New particle formation and ultrafine aerosol climatology at a high altitude site in the Alps (Jungfraujoch, 3580m a.s.l., Switzerland), Atmos. Chem. Phys., 10, 9333 – 9349, 2010. (Cited pages 66, 67, 72, 74, 82 and 83.)

Boulon, J., Sellegri, K., Hervo, M., Picard, D., Pichon, J.-M., Fréville, P., and Laj, P.: Investigation of nucleation events vertical extent: a long term study at two different altitude sites, Atmos. Chem. Phys. Discuss., 11, 5625–5639, doi:10.5194/acp-11-5625-2011, 2011. (Cited pages 52, 56, 87, 88 and 119.)

Brooks, I. M.: Finding Boundary Layer Top: Application of a Wavelet Covariance Transform to Lidar Backscatter profiles, J. Atmos. Oceanic Technol., 20, 1092–1105, 2003. (Cited page 38.)

Brown, C. W. and Keeling, C. D.: The concentration of atmospheric carbon dioxide in Antarctica, J. Geophys. Res., 70, 6077–6085, doi:10.1029/JZ070i024p06077, 1965. (Cited pages 5 and 6.)

Brushby, B., Fernandes, A., Wallace, D., and Kibblewhite, M.: Determination of trace organic micropollutants in atmospheric deposition, Sci. Total Environ., 135, 81–94, 1993. (Cited page 8.)

Byrd, R. H., Schnabel, R. B., and Shultz, G. A.: A trust region algorithm for nonlinearly constrained optimization, Siam J. Num. Anal., 24, 1152 – 1170, 1987. (Cited page 36.)

Camredon, M., Hamilton, J. F., Alam, M. S., Wyche, K. P., Carr, T., White, I. R., Monks, P. S., Rickard, A. R., and Bloss, W. J.: Distribution of gaseous and particulate organic composition during dark α-pinene ozonolysis, Atmos. Chem. Phys., 10, 2893–2917, 2010. (Cited page 39.)

Carltonn, A. G., Wiedinmyer, C., and Kroll, J. H.: A review of Secondary Organic Aerosol (SOA) fromation from isoprene, Atmos. Chem. Phys., 9, 4987–5005, doi:10.5194/acp-9-4987-2009, 2009. (Cited page 102.)

Charlson, R. J., Harrison, H., and Witt, G.: Aerosol concentrations: Effects on planetary temperatures, Science, 175, 95–96, 1972. (Cited page 6.)

Charlson, R. J., Langner, J., Andreae, M. O., and Warren, S. G.: Perturbation of the northern hemisphere radiative balance by backscattering from anthropogenic sulfate aerosols, Tellus, Ser. A Ser. B, 43, 152–163, 1991. (Cited pages 6 and 8.)

Charlson, R. J., Schwartz, S. E., Hales, J. M., Cess, R. D., Coakley, J. A., Hansen, J. E., and Hofmann, D. J.: Climate forcing by anthropogenic aerosols, Science, 255, 423–430, 1992. (Cited page 8.)

Collaud Coen, M., Weingartner, E., Nyeki, S., Cozic, J., Henning, S., Verheggen, B., Gehrig, R., and Baltensperger, U.: Long-term trend analysis of aerosol variables at the high-alpin site Jungfraujoch, J. Geophys. Res., 112, D13 213, 2007. (Cited page 46.)

Covert, D. S., Kapustin, V. N., Quinn, P. K., and Bates, T. S.: New particle formation in the marine boundary layer, J. Geophys. Res., 97, 20 581–20 589, 1992. (Cited page 20.)

Crumeyrolle, S., Manninen, H. E., Sellegri, K., Roberts, G., Gomes, L., Kulmala, M., Weigel, R., Laj, P., and Schwarzenboeck, A.: New particle formation events measured on board the ATR-42 aircraft during the EUCAARI campaign, Atmos. Chem. Phys., 10, 6721–6735, doi:10.5194/acp-10-6721-2010, 2010. (Cited pages 63, 83 and 120.)

Dal Maso, M., Kulmala, M., Lehtinen, K. E. J., Mäkelä, J., Aalto, P., and O'Dowd, C.: Condensation and coagulation sinks and formation of nucleation mode particles in coastal and boreal forest boundary layer, J. Geophys. Res., 107 (D19), 8097, doi:10.1029/2001JD001053, 2002. (Cited pages 37, 55 and 88.)

Dal Maso, M., Kulmala, M., Riipinen, I., Wagner, R., Hussein, T., Aalto, P., and Lehtinen, K. E. J.: Formation and growth of fresh atmospheric aerosols: eight years of aerosol size distribution data from SMEAR II, Hyytiälä, Finland, Bor. Env. Res., 10, 323 – 336, 2005. (Cited page 34.)

Deshler, T., Hofmann, D. J., Johnson, B. J., and Rozier, W. B. R.: Balloonborne measurments of the Pinatubo aerosol size distribution and volatility at Laramie, Wyoming, during the summer of 1991, Geophys. Res. Lett., 19, 199–202, doi:10.1029/91GL02787, 1992. (Cited page 87.)

Donahue, N. M., Epstein, S. A., Pandis, S. N., and Robinson, A. L.: A two-dimensional volatility basis set: 1. organic-aerosol mixing thermodynamics, Atmos. Chem. Phys., 11, 3303–3318, 2011. (Cited page 112.)

Draxler, R. R. and Rolph, G. D.: HYSPLIT (Hybrid Single-Particle Lagrangian Integrated Trajectory) Model access via NOAA ARL READY website

(http://www.arl.noaa.gov/ready/hysplit4.html), NOAA Air Resources Laboratory, Silver Spring, MD, 2003. (Cited pages 47 and 68.)

Du, H. and Yu, F.: Nanoparticle formation in the exhaust of vehicles running on ultra-low sulfur fuel, Atmos. Chem. Phys., 8, 4729–4739, 2006. (Cited page 96.)

Dunn, M. J., Jiménez, J.-L., Baumgardner, D., Castro, T., McMurry, P. H., and Smith, J. N.: Measurements of Mexico City nanoparticle size distributions: Observations of new particle formation and growth, Geophys. Res. Lett., 31, L10 102, doi:10.1029/2004GL019483, 2004. (Cited page 12.)

Duplissy, J., Enghoff, M. B., Aplin, K. L., Arnold, F., Aufmhoff, H., Avngaard, M., Baltensperger, U., Bondo, T., Bingham, R., Carslaw, K., Curtius, J., David, A., Fastrup, B., Gagné, S., Hahn, F., Harrison, R. G., Kellett, B., Kirkby, J., Kulmala, M., Laakso, L., Laaksonen, A., Lillestol, E., Lockwood, M., Mäkelä, J., Makhmutov, V., Marsh, N. D., Nieminen, T., Onnela, A., Pedersen, E., Pedersen, J. O. P., Polny, J., Reichl, U., Seinfeld, J. H., Sipilä, M., Stozhkov, Y., Stratmann, F., Svensmark, H., Svensmark, J., Veenhof, R., Verheggen, B., Viisanen, Y., Wagner, P. E., Wehrle, G., Weingartner, E., Wex, H., Wilhelmsson, M., and Winkler, P. M.: Results from the CERN pilot CLOUD experiment, Atmos. Chem. Phys., 10, 1635–1647, doi:10.5194/acp-10-1635-2010, 2010. (Cited page 13.)

Eichel, C., Kramer, M., Schultz, L., and Wurzler, S.: The water-soluble fraction of atmospheric aerosol particles and its influence on cloud microphysics, J. Geophys. Res., 101, 29 499–29 510, 1996. (Cited page 9.)

Fiedler, V., Dal Maso, M., Boy, M., Aufmhoff, H., Hoffmann, J., Schuck, T., Birmili, W., Hanke, M., Uecker, J., Arnold, F., and Kulmala, M.: The contribution of sulfuric acid to atmospheric particle formation and growth: a comparison between boundary layers in Northern and Central Europe, Atmos. Chem. Phys., 5, 1773–1785, doi:10.5194/acp-5-1773-2005, 2005. (Cited page 122.)

Flentje, H., Clause, H., Eltse, T., Gilge, S., Köhler, U., Plaß-Dülmer, C., Steinbrecht, W., Thomas, W., Werner, A., and Ficke, W.: The Eyjafjallajökull eruption in April 2010 – detection of volcanic plume using in-situ measurements, ozone sondes and lidar-ceilometer profiles, Atmos. Chem. Phys., 10, 10 085–10 092, doi:10.5194/acp-10-10085-2010, 2010. (Cited pages 85 and 86.)

Flückiger, E. O. and Bütikofer, R.: Swiss neutron monitors and cosmic ray research at Jungfraujoch, Adv. Space Res., 44, 1155–1159, 2009. (Cited page 46.)

Forrer, J., Rüttimann, R., Schneiter, D., Fischer, A., Buchmann, B., and Hofer, P.: Variability of trace gases at the high-Alpin site Jungfraujoch caused by meteorological transport process, J. Geophys. Res., 105, 12 241–12 251, 2000. (Cited page 48.)

Fuchs, N. A.: The Mechanics of Aerosols, Pergamon, New York, rev. ed. edn., 1964. (Cited pages 5 and 42.)

Fuchs, N. A. and Sutugin, A.: Topics in Current Aerosol Research, chap. Highly dispersed aerosol, Pergamon, New York, 1971. (Cited pages 24 and 25.)

Gäggeler, H. W., Jost, D. T., Baltensperger, U., and Schwikowski, M.: Radon and thoron decay product and ^{210}Pb measurements at Jungfraujoch, Switzerland, Atm. Env., 29, 607–616, 1995. (Cited page 49.)

Gagné, S., Lehtipalo, K., Manninen, H. E., Nieminen, T., Schobesberger, S., Franchin, A., Yli-Juuti, T., Boulon, J., Sonntag, A., Mirme, S., Mirme, A., Hõrrak, U., Petäjä, T., Asmi, E., and Kulmala, M.: Intercomparison of air ion spectrometers: an evaluation of results in varying conditions, Atm. Meas. Tech., 4, 805–822, 2011. (Cited pages 32, 33 and 97.)

Griffin, R. J., Cocker, D. R., Flagan, R. C., and Seinfeld, J. H.: Organic aerosol formation from the oxidation of biogenic hydrocarbons, J. Geophys. Res., 104, 2555–3567, 1999. (Cited page 13.)

Guenther, A., Kerl, T., Harley, P., Wiedinmyer, C., Palmer, P., and Geron, C.: Estimates of global terrestrial isoprene emissions using MEGAN (Model of Emission of Gases and Aerosols from Nature), Atmos. Chem. Phys., 6, 3181–3210, doi:10.5194/acp-6-3181-2006, 2006. (Cited page 102.)

Hõrrak, U., Salm, J., and Tammet, H.: Diurnal variation in the concentration of air ions of different mobility classes in a rural area, J. Geophys. Res., 108(D20), 4653, doi:10.1029/2002JD003240, 2003. (Cited page 49.)

Hamburger, T., McMeeking, G., Minikin, A., Birmili, W., Dall'Osto, M., O'Dowd, C., Flentje, H., Henzing, B., Junninen, H., Kristensson, A., de Leeuw, G., Stohl, A., Burkhart, J. F., Coe, H., Krejci, R., and Petzold, A.: Overview of the synoptic and pollution situation over Europe during the EUCAARI-LONGREX field campaign, Atmos. Chem. Phys., 11, 1065–1082, doi:10.5194/acp-11-1065-2011, 2010. (Cited pages 63 and 120.)

Hämeri, K., Kulmala, M., Aalto, P., Leszczynski, K., Visuri, R., and Hämekoski, K.: The investigations of aerosol particle formation in urban background area in Helsinki, Atm. Res., 41, 281–298, 1996. (Cited page 12.)

Hansen, J. E., Wang, W.-C., and Lacis, A. A.: Mount Agung eruption provides test of a global climatic perturbation, Science, 199, 1065–1068, doi:10.1126/science.199.4333.1065, 1978. (Cited page 6.)

Hao, L. Q., Yli-Pirilä, P., Romakkaniemi, S., Vaattovaara, P., Kajos, M. K., Rinne, J., Heijari, J., Kortelainen, A., Miettinen, P., Kroll, J. H., Holopainen, J. K., Smith, J. N., Joutsensaari, J., Kulmala, M., Worsnop, D. R., and Laaksonen, A.: New particle formation from the oxidation of direct emissions of pine seedlings, Atmos. Chem. Phys., 9, 8121–8137, doi:10.5194/acp-9-8121-2009, 2009. (Cited page 13.)

Harrington, D. Y. and Kreidenweis, S. M.: Simulations of sulfate aerosol dynamics – I. Model description, Atm. Env., 32, 1691–1700, 1998. (Cited page 27.)

Harrison, R. G., Grenfell, J. L., Savage, N., Allen, A., Clemitshaw, K. C., Penkett, S., Hewitt, C. N., and Davison, B.: Observations of new particle production in the atmosphere of a moderatly polluted site in eastern England, J. Geophys. Res., D105, 17 819–17 832, 2000. (Cited page 12.)

Highwood, E. J. and Stevenson, D. S.: Atmospheric impact of the 1783-1784 Laki Eruption: Part II Climatic effect of sulphate aerosol, Atmos. Chem. Phys., 3, 1177–1189, doi:10.519/acp-3-1177-2003, 2003. (Cited page 87.)

Hirsikko, A., Laakso, L., Hõrrak, U., Aalto, P., Kerminen, V.-M., and Kulmala, M.: Annual and size dependant variation of growth rates and ion concentrations in boreal forest, Bor. Env. Res., 10, 357–369, 2005. (Cited pages 35 and 36.)

Hirsikko, A., Bergman, T., Laakso, L., Dal Maso, M., Riipinen, I., Hõrrak, U., and Kulmala, M.: Identification and classification of the formation of intermediate ions measured in boreal forest, Atmos. Chem. Phys., 7, 201–210, 2007. (Cited page 34.)

Hoppel, W. A., Frick, G. M., and Fitzgerald, J. M.: Marine boundary layer measurements of new particle formation and the effect of non precipitating clouds have on aerosol size distribution, J. Geophys. Res., 99, 14 443–14 495, 1994. (Cited page 20.)

Husar, R. B.: Chapter in: History of Aerosol Science, chap. Atmospheric Aerosol Science Before 1900., Vienna: Verlag der Österreichischen Akademie der Wissen-schaften, 2000. (Cited page 2.)

Idso, S. B. and Brazel, J.: Planetary radiation balance as a function of atmospheric dust: Climatological consequences, Science, 198, 731–733, 1977. (Cited page 6.)

Idso, S. B. and Brazel, J.: Atmospheric dust: Climatological consequences, Science, 201, 378–379, 1978. (Cited page 6.)

Iida, K., Stolzenburg, M., McMurry, P. H., Dunn, M. J., Smith, J. N., Eisele, F., and Keady, P.: Contribution of ion-induced nucleation to new particle formation: Methodology and its application to atmospheric observations in Boulder, Colorado, J. Geophys. Res., 111, D23 201, doi:10.1029/2006JD007167, 2006. (Cited page 67.)

IPCC: Climate Change 2007 – The physical science basis: Contribution of working group I to the fourth Assessment report of the IPCC, Cambridge: Cambridge University Press, 2007. (Cited pages 8, 9 and 10.)

Jacobson, M. C., Hansson, H.-C., Noone, K. J., and Charlson, R. J.: Organic atmospheric aerosols: Review and state of the science, Rev. Geophys., 38, 267–294, 1998. (Cited pages 7 and 8.)

Jaecker-Voirol, A. and Mirabel, P.: Heteromolecular nucleation in the sulfuric acid-water system, Atm. Env., 23, 2053–2057, 1989. (Cited page 20.)

Kanakidou, M., Seinfeld, J. H., Pandis, S. N., Barnes, I., Dentener, F. J., Facchini, M. C., Van Dingenen, R., Ervens, B., Nenes, A., Nielsen, C. J., Swietlicki, E., Putaud, J. P., Balkanski, Y., Fuzzi, S., Horth, J., Moortgat, G. K., Winterhalter, R., Myhre, C. E. L., Tsigaridis, K., Vignati, E., Stephanou, E. G., and Wilson, J.: Organic aerosol and global climate modelling: a review, Atmos. Chem. Phys., 5, 1053–1123, doi:10.5194/acp-5-1053-2005, 2005. (Cited pages 102 and 106.)

Kazil, J. and Lovejoy, E. R.: Tropospheric ionization and aerosol production: A model study, J. Geophys. Res., 109, D19 206, doi:10.1029/2004JD004852, 2004. (Cited page 46.)

Kerminen, V.-M. and Kulmala, M.: Analytical formulae connecting the "real" and the "apparent" nucleation rate and the nuclei number concentration for atmospheric nucleation events, J. Aerosol Sci., 33, 609–622, 2002. (Cited page 37.)

Kerminen, V.-M., Petäjä, T., Manninen, H. E., Paasonen, P., Nieminen, T., Sipilä, M., Junninen, H., Ehn, M., Gagné, S., Laakso, L., Riipinen, I., Vehkamäki, H., Kurten, T., Ortega, I. K., Dal Maso, M., Brus, D., Hyvärinen, A., Lihavainen, H., Leppä, J., Lehtinen, K. E. J., Mirme, A., Mirme, S., Hõrrak, U., Berndt, T., Stratmann, F., Birmili, W., Wiedensohler, A., Metzger, A., Dommen, J., Baltensperger, U., Kiendler-Scharr, A., Mentel, T. F., Wildt, J., Winkler, P. M., Wagner, P. E., Petzold, A., Minikin, A., Plass-Dülmer, C., Pöschl, U., Laaksonen, A., and Kulmala, M.: Atmospheric nucleation: highlights of the EUCAARI project and future directions, Atmos. Chem. Phys., 10, 10 829–10 848, doi:10.5194/acp-10-10829-2010, 2010. (Cited page 68.)

Kittelson, D. B., Watts, W. F., and Johnson, J. P.: On-road and laboratory evaluation of combustion aerosols – Part1: Summary of diesel engine results, J. Aerosol Sci., 37, 913–930, 2006. (Cited page 96.)

Koch, S., Winterhalter, R., Uherek, E., Kolloff, A., Neeb, P., and Moortgat, G. K.: Formation of new particles in the gas-phase ozonolysis of monoterpenes, Atm. Env., 34, 4031–4042, 2000. (Cited pages 13, 102 and 107.)

Köhler, H.: The nucleus in the growth of hygroscopic droplets, Trans. Faraday Soc., 32, 1152–1161, 1936. (Cited page 25.)

Komppula, M., Lihavainen, H., Hatakka, J., Paatero, J., Aalto, P., Kulmala, M., and Viisanen, Y.: Observations of new particle formation and size distributions at two different heights and surroundings in subarctic area in northern Finland, J. Geophys. Res., 108, 4295, 2003. (Cited page 63.)

Korhonen, H., Lehtinen, K. E. J., and Kulmala, M.: Multicomponent aerosol dynamics model UHMA: model development and validation, Atmos. Chem. Phys., 4, 757–771, doi:10.5194/acp-4-757-2004, 2004. (Cited pages 13 and 39.)

Korhonen, P., Kulmala, M., Laaksonen, A., Viisanen, Y., McGraw, R., and Seinfeld, J. H.: Ternary nucleation of the H_2SO_4, NH_3 and H_2O in the atmosphere, J. Geophys. Res., 104, 26 349–26 353, 1999. (Cited pages 21 and 89.)

Kuang, C., McMurry, P. H., McCormick, A. V., and Eisele, F. L.: Dependence of nucleation rates on sulfuric acid vapor concentration in diverse atmospheric locations, J. Geophys. Res., 113, D10 209, 2008. (Cited pages 27 and 91.)

Kuang, C., Riipinen, I., Sihto, S.-L., Kulmala, M., McCormick, A. V., and McMurry, P. H.: An improved criterion for new particle formation in diverse atmospheric environments, Atmos. Chem. Phys., 10, 8469–8480, doi:10.5194/acp-10-8469-2010, 2010. (Cited page 92.)

Kulmala, M. and Kerminen, V.-M.: On the formation and growth of atmospheric nanoparticles, Atm. Res., 90, 132 – 150, doi:10.1016/j.atmosres.2008.01.005, 2008. (Cited page 49.)

Kulmala, M. and Laaksonen, A.: Binary nucleation of water-sulfuric acid system: Comparison of classical theories with different H_2SO_4 saturation vapor pressures, J. Chem. Phys., 93, 696–701, 1990. (Cited pages 18 and 19.)

Kulmala, M., Kerminen, V.-M., and Laaksonen, A.: Simulations on the effect of sulfuric acid formation on atmospheric aerosol concentrations, Atm. Env., 29, 377–382, 1995. (Cited page 13.)

Kulmala, M., Korhonen, P., Vesala, T., Hansson, H.-C., Noone, K. J., and Svenningsson, B.: The effect of hygroscopicity on cloud droplet formation, Tellus, 48B, 347–360, 1996. (Cited page 9.)

Kulmala, M., Pirjola, L., and Mäkelä, J. M.: Stable sulfate clusters as a source of new atmospheric particles, Nature, 404(6773), 66 – 69, 2000. (Cited page 60.)

Kulmala, M., Dal Maso, M., Mäkelä, J. M., Pirjola, L., Väkevä, M., Aalto, P., Miikkulainen, P., Hämeri, K., and O'Dowd, C. D.: On the formation, growth and composition of nucleation mode particles, Tellus B, 53, 479 – 490, 2001a. (Cited page 25.)

Kulmala, M., Hämeri, K., Aalto, P. P., Mäkelä, J. M., Pirjola, L., Nilsson, E. D., Buzorius, G., Rannik, U., Dal Maso, M., Seidl, W., Hoffmann, T., Janson, R., Hansson, H.-C., Viisanen, Y., Laaksonen, A., and O'Dowd, C. D.: Overview of the international project on biogenic aerosol formation in the boreal forest (BIOFOR), Tellus B, 54, 324–343, doi:10.1034/j.1600-0889.2001.530402.x, 2001b. (Cited page 21.)

Kulmala, M., Korhonen, P., Napari, I., Karlsson, A., Berresheim, H., and O'Dowd, C. D.: Aerosol formation during PARFORCE: Ternary nucleation of H_2SO_4, NH_3, and H_2O, J. Geophys. Res., 107, 8111, doi:10.1029/2001JD000900, 2002. (Cited page 21.)

Kulmala, M., Kerminen, V.-M., Anttila, T., Laaksonen, A., and O'Dowd, C. D.: Organic aerosol formation via sulfate cluster activation, J. Geophys. Res., 109, D04 205, doi:10.1029/2003JD003961, 2004a. (Cited pages 22, 25, 89 and 95.)

Kulmala, M., Vehkamäki, H., Petäjä, T., Dal Maso, M., Lauri, A., Kerminen, V.-M., Birmili, W., and McMurry, P.: Formation and growth rates of ultrafine atmospheric particles: a review of observations, J. Aerosol Sci., 35, 143 – 176, 2004b. (Cited pages 12 and 15.)

Kulmala, M., Lehtinen, K. E. J., and Laaksonen, A.: Cluster activation theory as an explanation of the linear dependence between formation rate of 3 nm particles ans sulfuric acid concentration, Atmos. Chem. Phys., 6, 787 – 793, 2006. (Cited pages 25 and 60.)

Kulmala, M., Riipinen, I., Sipilä, M., Manninen, H. E., Petäjä, T., Junninen, H., Dal Maso, M., Mordas, G., Mirme, A., Vana, M., Hirsikko, A., Laakso, L., Harrison, R., Hanson, I., Leung, C., Lehtinen, K. E. J., and Kerminen, V.-M.: Towards direct measurements of atmospheric nucleation, Science, 318a, 89 – 92, 2007. (Cited page 37.)

Laaksonen, A., Korhonen, P., Kulmala, M., and Charlson, R. J.: Modification of the Köhler equation to include soluble trace gases and slightly soluble substances, J. Atmos. Sci., 55, 853–862, 1998. (Cited page 25.)

Laaksonen, A., Kulmala, M., O'Dowd, C. D., Joutsensaari, J., Vaattovaara, P., Mikkonen, S., Lehtinen, K. E. J., Sogacheva, L., Dal Maso, M., Aalto, P., Petäjä, T., Sogachev, A., Yoon, Y. J., Lihavainen, H., Nilsson, D., Facchini, M.-C., Cavalli, F., Fuzzi, S., Hoffmann, T., Arnold, F., Hanke, M., Sellegri, K., Umann, B., Junkermann, W., Coe, H., Allan, J. D., Alfarra, M. R., Worsnop, D. R., Riekkola, M.-L., Hyötyläinen, T.,

and Viisanen, Y.: The role of VOC oxidation products in continental new particle formation, Atmos. Chem. Phys., 8, 2657 – 2665, 2008. (Cited page 53.)

Lähde, T., Rönko, T., Virtanen, A., Schuk, T. J., Pirjola, L., Hämeri, K., Kulmala, M., Arnold, F., Rothe, D., and Keskinen, J.: Heavy duty diesel engine exhaust: Aerosol particle and ion measurements, Environ. Sci. Technol., 43, 163–168, 2009. (Cited page 96.)

Laj, P., Drummey, S. M., Spencer, M. J., Palais, J. M., and Sigurdsson, H.: Depletion of H_2O_2 in a Greenland ice core: implications for oxydation of volcanic SO_2, Nature, 346, 45–48, 1990. (Cited page 86.)

Lane, T. E., Donahue, N. M., and Pandis, S. N.: Simulating secondary organic aerosol formation using the volatility basis-set approach in a chemical transport model, Atm. Env., 42, 7439–7451, 2008. (Cited page 39.)

Lanz, V. A., Henne, S., Staehelin, J., Hueglin, C., Vollmer, M. K., Steinbacher, M., Buchmann, B., and Reimann, S.: Statistical analysis of anthropogenic non-methan VOC variability at a European background loaction (Jungfraujoch, Switzerland), Atmos. Chem. Phys., 9, 3445–3459, doi:10.5194/acp-9-3445-2009, 2009. (Cited page 57.)

Lauri, A.: Theoritical and computational approaches on heterogeneous nucleation., Ph.D. thesis, University of Helsinki, 2006. (Cited page 26.)

Lazaridis, M., Kulmala, M., and Gorbunov, B. Z.: Binary heterogeneous nucleation at a non-uniform surface, J. Aerosol Sci., 23, 457–466, 1992. (Cited page 22.)

Lehtinen, K. E. J. and Kulmala, M.: A model for particle formation and growth in the atmosphere with molecular resolution in size, Atmos. Chem. Phys., 3, 251–257, 2003. (Cited page 39.)

Lehtinen, K. E. J., Dal Maso, M., Kulmala, M., and Kerminen, V.-M.: Estimating nucleation rates from apparent particle formation rates and vice versa: Revised formulation of the Kerminen-Kulmala equation, J. Aerosol Sci., 38, 988–994, doi:10.1016/j/jaerosci.2007.06.009, 2007. (Cited pages 37 and 67.)

Lehtipalo, K., Kulmala, M., Sipilä, M., Petäjä, T., Vana, M., Ceburnis, D., Dupuy, R., and O'Dowd, C.: Nanoparticles in boreal forest and coastal environment: a comparison of observations and implications of the nucleation mechanism, Atmos. Chem. Phys., 10, 7009 – 7016, 2010. (Cited page 60.)

Leppä, J., Kerminen, V.-M., Laakso, L., Korhonen, H., Lehtinen, K. E. J., Gagné, S., Manninen, H. E., Nieminen, T., and Kulmala, M.: Ion-UHMA: a model for simulating the dynamics of neutral and charged aerosol particles, Bor. Env. Res., 14, 559–575, 2009. (Cited pages 13 and 39.)

Lihavainen, H., Komppula, M., Kerminen, V.-M., Järvinen, H., Viisanen, Y., Lehtinen, K. E. J., Vana, M., and Kulmala, M.: Size distribution of atmospheric ions inside clouds and in cloud-free air at a remote continental site, Bor. Env. Res., 12, 337 – 344, 2007. (Cited page 50.)

Lovejoy, E., Curtius, J., and Froyd, K.: Atmospheric ion-induced nucleation of sulfuric acid and water, J. Geophys. Res., 109, D08 204, doi:10.1029/2003JD004460, 2004. (Cited page 26.)

Lugauer, M., Baltensperger, U., Furger, M., Gäggeler, H. W., Jost, D. J., Nyeki, S., and Schwikowski, M.: Influences of vertical transport and scavenging on aerosol particle surface area and radon decay product concentrations at the Jungfraujoch (3454 m above the sea level), J. Geophys. Res., 105, 19 869 – 19 879, 2000. (Cited page 47.)

Mäkelä, J. M., Riihelä, M., Ukkonen, A., Jokinen, V., and Keskinen, J.: Comparison of mobility equivalent diameter with Kelvin-Thomson diameter using ion mobility data, J. Chem. Phys., 105, 1562–1571, 1996. (Cited page 30.)

Mäkelä, J. M., Aalto, P., Jokinen, V., Pohja, T., Nissinen, A., Palmroth, S., Markkanen, T., Seitsonen, K., Lihavainen, H., and Kulmala, M.: Observations of ultrafine particle formation and growth in boreal forest, Geophys. Res. Lett., 24, 1219 – 1222, 1997. (Cited page 12.)

Manninen, H. E., Nieminen, T., Riipinen, I., Yli-Juuti, T., Gagné, S., Asmi, E., Aalto, P. P., Petäjä, T., Kerminen, V.-M., and Kulmala, M.: Charged and total particle formation and growth rates during EUCAARI 2007 campaign in Hyytiälä, Atmos. Chem. Phys., 9, 4077 – 4089, 2009. (Cited pages 54 and 56.)

Manninen, H. E., Nieminen, T., Asmi, E., Gagné, S., Häkkinen, S., Lehtipalo, K., Aalto, P., Kivekäs, N., Vana, M., Mirme, A., Mirme, S., Hõrrak, U., Plass-Dülmer, C., Stange, G., Kiss, G., Hoffer, A., Moerman, M., Henzing, B., Brinkenberg, M., Kouvarakis, G. N., Bougiatioti, K., O'Dowd, C., Ceburnis, D., Arneth, A., Svenningsson, B., Swietlicki, E., Tarozzi, L., Decesari, S., Sonntag, A., Birmili, W., Wiedensohler, A., Boulon, J., Sellegri, K., Laj, P., Baltensperger, U., Laaksonen, A., Joutsensaari, J., Petäjä, T., Kerminen, V.-M., and Kulmala, M.: EUCAARI ion spectrometer measurements at 12 European sites - analysis of new-particle formation events, Atmos. Chem. Phys., 10, 7907 – 7927, doi:10.5194/acp-10-7907-2010, 2010. (Cited pages 52, 54, 55, 56, 66, 67 and 82.)

Manninen, H. E., Franchin, A., Schobesberger, S., Hirsikko, A., Hakala, J., Skromulis, A., Kangasluoma, J., Ehn, M., Junninen, H., Mirme, A., Mirme, S., Sipilä, M., Petäjä, T., Worsnop, D. R., and Kulmala, M.: Characterization of corona-generated ions used in a Neutral cluster and Air Ion Spectrometer (NAIS), Atm. Meas. Tech. Discussions, 4, 2099–2125, doi:10.5194/amtd-4-2099-2011, 2011. (Cited page 105.)

Maricq, M. M.: On the elctrical charge of motor vehicle exhaust particles, J. Aerosol Sci., 37, 858–874, 2006. (Cited page 96.)

McCormick, R. A. and Ludwig, J. H.: Climate modification by atmospheric aerosols, Science, 156, 1358–1359, 1967. (Cited page 5.)

McMurry, P. H.: The history of condensation nucleus counters, Aerosol Sci. Technol., 33, 297–322, 2000. (Cited page 3.)

Merikanto, J., Napari, I., Vehkamäti, H., Anttila, T., and Kulmala, M.: New parametrization of sulfuric acid-ammonia-water ternary nucleation rates at tropospheric conditions, J. Geophys. Res., 112, D15 207, doi:10.1029/2006JD007977, 2007. (Cited pages 21 and 27.)

Merikanto, J., Napari, I., Vehkamäti, H., Anttila, T., and Kulmala, M.: Correction to "New parametrization of sulfuric acid-ammonia-water ternary nucleation rates at tropospheric conditions", J. Geophys. Res., 114, D09 206, 2009. (Cited page 27.)

Metzger, A., Verheggen, B., Dommen, J., Duplissy, J., Prevot, A. S., Weingartner, E., Riipinen, I., Kulmala, M., V., S. D., Carslaw, K. S., and Baltensperger, U.: Evidence for the role of organics in aerosol particle formation under atmospheric conditions, P. Natl. Acad. Sci. USA, 107, 6646–6651, doi:10.1073/pnas.0911330107, 2010. (Cited pages 13, 53, 60, 67, 95, 102, 103 and 109.)

Mirme, A., Tamm, A., Mordas, G., Vana, M., Uin, J., Mirme, S., Bernotas, T., Laakso, L., Hirsikko, A., and Kulmala, M.: A wide range multi-channel Air Ion Spectrometer, Bor. Env. Res., 12, 247 – 264, 2007. (Cited pages 31 and 65.)

Mirme, S., Mirme, A., Minikin, A., Petzold, A., Hõrrak, U., Kerminen, V.-M., and Kulmala, M.: Atmospheric sub-3 nm particles at high altitudes, Atmos. Chem. Phys., 10, 437 – 451, 2010. (Cited page 55.)

Mitchell, J. M.: A preliminary evaluation of atmospheric pollution as a cause of the global temperature fluctuation of the past century., pp. 139–155, S. F. Singer, 1970. (Cited page 6.)

Morh, M., Lehmann, U., and Margaria, G.: ACEA programme on the emissions of fine particulates from passenger cars (2). Part 1. Particle characterization of a wide range of engine technologies, SAE Technical Paper, 2003-01-1889, 2003a. (Cited page 96.)

Morh, M., Lehmann, U., and Margaria, G.: ACEA programme on the emissions of the fine particulates from passenger cars (2). Part 2. Effect of sampling conditions and fuel sulphur content on the particle emission, SAE Technical Paper, 2003-01-1890, 2003b. (Cited page 96.)

Müller, L., Reining, M.-C., Hayen, H., and Hoffmann, T.: Characterization of oligomeric compounds in secondary organic aerosol using liquid chromatography coupled to electrospray ionization Fourier transform ion cyclotron resonance mass spectrometry, Rapid Commun. Mass Spectrom., 23, 971–979, 2009. (Cited page 113.)

Nadykto, A. B. and Yu, F.: Formation of binary ion clusters from polar vapours: Effect of the dipole-charge interaction, Atmos. Chem. Phys., 4, 385–389, 2004. (Cited page 26.)

Napari, I., Noppel, M., Vehkamäki, H., and Kulmala, M.: Parametrization of ternary nucleation rates for H_2SO_4−NH_3−H_2O vapors, J. Geophys. Res., 107, 4381, doi:10.1029/2002JD002132, 2002. (Cited page 21.)

Nieminen, T., Paasonen, P., Manninen, H. E., Kerminen, V.-M., and Kulmala, M.: Parameterization of ion-induced nucleation rates based on ambient observations, Atmos. Chem. Phys., 10, 21 697–21 720, doi:10.5194/acpd-10-21697-2010, 2010. (Cited page 68.)

Nilsson, E. D. and Kulmala, M.: The potential for atmospheric mixing processes to enhance the binary nucleation rate, J. Geophys. Res., 103(D1), 1381–1389, doi:10.1029/97JD02629, 1998. (Cited page 63.)

Nilsson, E. D., Rannik, U., Kulmala, M., Buzorius, G., and O'Dowd, C. D.: Effects of continental boundary layer evolution, convection, turbulence and entrainment, on aerosol formation, Tellus B, 53B, 441–461, 2001. (Cited page 63.)

Nishita, C., Osada, K., Kido, M., and Matsunaga, K.: Nucleation mode particles in upslope valley winds at Mount Norikura, Japan: Implications for the vertical extent of new particle formation events in the lower troposphere, J. Geophys. Res., 113, D06 202, doi:10.1029/2007JD009302, 2008. (Cited pages 12 and 56.)

O'Dowd, C. D., Geever, M., Hill, M. K., Smith, M. H., and Jennings, S. G.: New particle formation: Nucleation rates and spatial scales in the clean marine coastal environment, Geophys. Res. Lett., 25, 1661–1664, 1998. (Cited page 12.)

O'Dowd, C. D., McFiggans, G., Greasey, D. J., Pirjola, L., Hoell, C., Smith, M. H., Allan, B., Plane, J. M. C., Heard, D. E., Lee, J. D., Pilling, M. J., and Kulmala, M.: On the photochemical production of new particles in the coastal boundary layer, Geophys. Res. Lett., 26, 1707 – 1710, 1999. (Cited page 21.)

O'Dowd, C. D., Facchini, M. C., Cavalli, F., Ceburnis, D., Mircea, M., Decesari, S., Fuzzi, S., Yoon, Y. J., and Putaud, J.-P.: Biogenically driven organic contribution to marine aerosol, Nature, 431(7009), 676–680, 2004. (Cited page 95.)

Paasonen, P., Sihto, S.-L., Nieminen, T., Vuollekoski, H., Riipinen, I., Plaß-Dülmer, C., Berresheim, H., Birmili, W., and Kulmala, M.: Connection between new particle

formation and sulfuric acid at Hohenpeissenberg (Germany) including the influence of organic compounds, Bor. Env. Res., 14, 616 – 629, 2009. (Cited page 53.)

Paasonen, P., Nieminen, T., Asmi, E., Manninen, H. E., Petäjä, T., Plaß-Dülmer, C., Flentje, H., Birmili, W., Wiedensohler, A., Hõrrak, U., Metzger, A., Hamed, A., Laaksonen, A., Facchini, M.-C., Kerminen, V.-M., and Kulmala, M.: On the roles of sulfuric acid and low-volatility organic vapors in the initial steps of atmospheric new particle formation, Atmos. Chem. Phys., 10, 11 223–112 242, doi:10.5194/acp-10-11223-2010, 2010. (Cited pages 88 and 102.)

Pales, J. C. and Keeling, C. D.: The concentration of atmospheric carbon dioxide in Hawaii, J. Geophys. Res., 70, 6053–6076, doi:10.1029/JZ070i024p06053, 1965. (Cited pages 5 and 6.)

Petäjä, T., Mauldin, III, R. L., Kosciuch, E., McGrath, J., Nieminen, T., Boy, M., Adamov, A., Kotiaho, T., and Kulmala, M.: Sulfuric acid and OH concentrations in a boreal forest site, Atmos. Chem. Phys., 9, 7435 – 7448, doi:10.5194/acp-9-7435-2009, 2009. (Cited pages 53, 67, 86 and 89.)

Petersen, D., Ortner, R., Vrtala, A., Wagner, P. E., Kulmala, M., and Laaksonen, A.: Soluble-Insoluble Transition in Binary Heterogeneous Nucleation, Phys. Rev. Lett., 87, 225 703, doi:10.1103/PhysRevLett.87.225703, 2001. (Cited page 26.)

Peterson, T. C., Connolley, W. M., and Fleck, J.: The myt of the 1970s global cooling scientific consensus, Bull. Am. Meteorol. Soc., 89, 1325–1337, doi:10.1175/2008BAMS2370.1, 2008. (Cited page 5.)

Pinto, J., Turco, R., and Toon, O.: Self-limiting Physical and Chemical Effects in Volcanic Eruption Clouds, J. Geophys. Res., 94, 11 165–11 173, doi:10.1029/JD094iD08p11165, 1989. (Cited page 86.)

Pirjola, L., Kulmala, M., Wilck, ., Bischoff, A., Stratmann, F., and Otto, E.: Formation of sulphuric acid aerosols and cloud condensation nuclei : An expression for significant nucleation and model comparison, J. Aerosol Sci., 30, 1079–1094, 1999. (Cited pages 13, 24, 72 and 86.)

Podzimek, J.: John Aitken's contribution to atmospheric and aerosol sciences: Ones hundred years of condensation nucleai counting, Bull. Am. Meteorol. Soc., 70, 1538–1545, 1989. (Cited page 3.)

Prospero, J. M., Charlson, R. J., Mohnen, V., Jaenicke, R., Delany, A., Moyers, J., Zoller, W., and Rahn, K.: The Atmospheric Aerosol System: An Overview, Rev. Geophys. Space Phys., 21, 1607–1629, 1983. (Cited page 7.)

Rafinesque, C.: Thoughts on atmospheric dust, Am. J. Sci., 1, 397–400, 1819. (Cited pages 1 and 2.)

Ramaswamy, V., Ramachandran, S., Stenchikov, G., and Robock, A.: A model study of the effect of Pinatubo volcanic aerosols on stratospheric temperature, Chapter 6 of Frontiers of Climate modeling., Cambridge Univ. Press, New York, 2006. (Cited page 87.)

Rasool, S. I. and Schneider, S. H.: Atmospheric carbon dioxide and aerosols: Effects of large increases on global climate, Science, 173, 138–141, 1971. (Cited page 6.)

Rasool, S. I. and Schneider, S. H.: Aerosol concentrations: Effect on planetary temperatures, Science, 175, 96, 1972. (Cited page 6.)

Reck, R. A.: Aerosols and polar temperature change, Science, 188, 728–730, 1975. (Cited page 6.)

Riipinen, I., Pierce, J. R., Yli-Juuti, T., Nieminen, T., Häkkinen, S., Ehn, M., Junninen, H., Lehtipalo, K., Petäjä, T., Slowik, J., Chang, R., Shantz, N. C., Abbatt, J., Leaitch, W. R., Kerminen, V.-M., Worsnop, D. R., Pandis, S. N., Donahue, N. M., and Kulmala, M.: Organic condensation: a vital link connecting aerosol formation to cloud condensation nuclei (CCN) concentrations, Atmos. Chem. Phys., 11, 3865–3878, doi:10.5194/acp-11-3865-2011, 2010. (Cited page 122.)

Rodriguez, S., González, Y., Cuevas, E., Ramos, R., Romero, P. M., Abreu-Afonso, J., and Redondas, A.: Atmospheric nanoparticle observations in the low free troposphere during upward orographic flows at Izaña Mountain Observatory, Atmos. Chem. Phys., 9, 6319–6335, doi:10.5194/acp-9-6319-2009, 2009. (Cited page 12.)

Rohr, A. C., Weschler, C. J., Koutrakis, P., and Spengler, J. D.: Generation and quantification of ultrafine particles through terpene/ozone reaction in a chamber setting, Aerosol Sci. Technol., 37, 65–78, doi:10.1080/02786820390112597, 2003. (Cited pages 13 and 102.)

Sassen, K., Zhu, J., Webley, P., Dean, K., and Cobb, P.: Volcanic ash plume identification using polarization lidar: Augustine eruption, Alaska, Geophys. Res. Lett., 34, L08 803, doi:10.1029/2006GL027237, 2007. (Cited page 85.)

Schmidt, A., Carslaw, K. S., Mann, G. W., Wilson, M., Breider, T. J., Pickering, S. J., and Thordarson, T.: The impact of the 1783-1784 Laki eruption on global aerosol formation processes and cloud condensation nuclei, Atmos. Chem. Phys., 10, 6025–6041, doi:10.5194/acp-10-6025-2010, 2010. (Cited page 87.)

Schneider, S. and Mass, C.: Volcanic dust, sunspots, and temperature trends, Science, 190, 741–746, 1975. (Cited page 6.)

Seinfeld, J. H. and Pandis, S. N.: Atmospheric Chemistry and Physics : From Air Pollution to Climate Change., Wiley, 1998. (Cited pages 16, 17, 19, 20 and 23.)

Sellegri, K., Laj, P., Venzac, H., Boulon, J., Picard, D., Villani, P., Bonasoni, P., Marinoni, A., Cristofanelli, P., and Vuillermoz, E.: Seasonal variations of aerosol size distributions based on long-term measurements at the high altitude Himalayan site of Nepal Climate Observatory-Pyramid (5079 m), acp, 10, 10 679–10 690, doi:10.5194/acp-10-10679-2010, 2010. (Cited page 60.)

Shaw, G. E.: Aerosols at a mountain top observatory in Arizona, J. Geophys. Res., 112, D07 206, doi:10.1029/2005JD006893, 2007. (Cited pages 12 and 56.)

Sihto, S.-L., Kulmala, M., Kerminen, V.-M., Dal Maso, M., Petäjä, T., Riipinen, I., Korhonen, H., Arnold, F., Janson, R., Boy, M., Laaksonen, A., and Lehtinen, K. E. J.: Atmospheric sulphuric acid and aerosol formation: implications from atmospheric measurements for nucleation and early growth mechanism, Atmos. Chem. Phys., 6, 4079–4091, 2006. (Cited pages 27 and 91.)

Smith, J. N., Dunn, M. J., Van Reken, T. M., Iida, K., Stolzenburg, M. R., McMurry, P. H., and Huey, L. G.: Chemical composition of atmospheric nanoparticles formed from nucleation in Tecamac, Mexico: evidence for an important role for organic species in nanoparticles growth, Geophys. Res. Lett., 4, L04 808, doi:10.1029/2007GL032523, 2008. (Cited page 122.)

Smith, J. N., Barsanti, K. C., Friedli, H. R., Ehn, M., Kulmala, M., Collins, D. R., Scheckman, J. H., Williams, B. J., and McMurry, P. H.: Observations of aminium salts in atmospheric nanoparticles and possible climatic implications, P. Natl. Acad. Sci. USA, 107, 6634–6639, doi:10.1073/pnas.0912127107, 2010. (Cited pages 92 and 123.)

Sogacheva, L., Dal Maso, M., Kerminen, V.-M., and Kulmala, M.: Probability of nucleation events and aerosol particle concentration in different air mass types arriving at Hyytiälä, southern Finland based on back trajectories analysis, Bor. Env. Res., 10, 479 – 491, 2005. (Cited pages 57 and 58.)

Spurny, K. R.: Methods for aerosol measurement before the 1960s, Aerosol Sci. Technol., 29, 327–349, 1998. (Cited page 3.)

Stanier, C. O., Khlystov, A., Y., and Pandis, S. N.: Nucleation events during the Pittsburgh air quality study: Description and relation to key meteorological, gas phase, and aerosol parameters, Aerosol Sci. Technol., 38, 253–264, 2004. (Cited page 12.)

Stratmann, F., Siebert, H., Spindler, G., Wehner, B., Althausen, D., Heintzenberg, J., Hellmuth, O., Rinke, R., Schmieder, U., Seidel, C., Tuch, T., Uhrner, U., Wiedensohler, A., Wandinger, U., Wendisch, M., Schell, D., and Stohl, A.: New-particle formation

events in a continental boundary layer: first results from the SATURN experiment, Atmos. Chem. Phys., 2, 1445–1459, doi:10.5194/acp-3-1445-2003, 2003. (Cited page 63.)

Suni, T., Kulmala, M., Hirsikko, A., Bergman, T., Laakso, L., Aalto, P. P., Leuning, R., Cleugh, H., Zegelin, S., Hughes, D., van Gorsel, E., Kitchen, M., Vana, M., Hõrrak, U., Mirme, S., Mirme, A., Sevanto, S., Twining, J., and Tadros, C.: Formation and characteristics of ions and charged particles in an native Australian Eucalypt forest, Atmos. Chem. Phys., 8, 129 – 139, doi:10.5194/acp-8-129-2008, 2008. (Cited page 12.)

Tammet, H. and Kulmala, M.: Simulation tool for atmospheric aerosol nucleation bursts, J. Aerosol Sci., 36, 173 – 196, 2005. (Cited pages 13 and 37.)

Tsimpidi, A. P., Karydis, V. A., Zavala, M., Lei, W., Molina, L., Ulbrich, I. M., Jimenez, J. L., and Pandis, S. N.: Evaluation of the volatility basis-set approach fro the simulation of organic aerosol formation in the Mexico City metropolitan area, Atmos. Chem. Phys., 10, 525–546, doi:10.5194/acp-10-525-2010, 2010. (Cited pages 39 and 115.)

Tunved, P., Nilsson, E. D., Hansson, H.-C., Ström, J., Kulmala, M., Aalto, P., and Viisanen, Y.: Aerosol characteristics of air masses in norther Europe: Influences of location, transport, sinks, and sources, J. Geophys. Res., 110, D07 201, doi:10.1029/2004JD005085, 2005. (Cited page 47.)

Twomey, S.: Pollution and planetary albedo, Atm. Env., 8, 1251–1256, 1974. (Cited pages 6 and 10.)

Usoskin, I. G. and Kosvaltsov, G. A.: Cosmic rays and climate of the Earth: Possible connection ?, C. R. Geoscience, 340, 441–450, 2008. (Cited page 49.)

Vehkamäki, H., Kulmala, M., Napari, I., Lehtinen, K. E. J., Timmreck, C., Noppel, M., and Laaksonen, A.: An improved parametrization for sulfric acid-water nucleation rates for tropospheric and stratospheric conditions, J. Geophys. Res., 107(D22), 4622, 2002. (Cited page 27.)

Venzac, H.: Étude des processus de nucléation dans l'atmosphère., Ph.D. thesis, École Doctorale des Sciences Fondamentales - Université Blaise Pascal, Clermont-Ferrand, France., 2008. (Cited pages 32 and 56.)

Venzac, H., Sellegri, K., and Laj, P.: Nucleation events detected at the high altitude site of the Puy de Dôme research station, France, Bor. Env. Res., 12, 345–359, 2007. (Cited pages 12, 48, 49, 50, 56, 65, 66, 72 and 75.)

Venzac, H., Sellegri, K., Laj, P., Villani, P., Bonasoni, P., Marioni, A., Cristofanelli, P., Calzolari, F., Fuzzi, S., Decesari, S., Facchini, M.-C., Vuillermoz, E., and Verza, G.-P.:

High frequency new particle formation in the Himalayas, P. Natl. Acad. Sci. USA, 105, 15 666 – 15 671, 2008. (Cited pages 32, 46, 48, 49, 52, 56, 66 and 119.)

Venzac, H., Sellegri, K., Villani, P., Picard, D., and Laj, P.: Seasonal variation of aerosol size distributions in the free troposphere and residual layer at the puy de Dôme station, France, Atmos. Chem. Phys., 9, 1465 – 1478, doi:10.5194/acp-9-1465-2009, 2009. (Cited pages 12, 42, 65, 70 and 74.)

Vignati, E., Wilson, J., and Stier, P.: M7: An efficient size-resolved aerosol microphysics module for large-scale aerosol transport models, J. Geophys. Res., 109, D22 202, 2004. (Cited pages 40 and 41.)

Wang, J., Doussin, J.-F., Perrier, S., Perraudin, E., Katrib, Y., Pangui, E., and Picquet-Varrault, B.: Design of a new multi-phase experimental simulation chamber for atmospheric photosmog, aerosol and cloud chemistry research, Atm. Meas. Tech. Discussions, 4, 315–384, doi:10.5194/amtd-4-315-2011, 2011. (Cited pages 103 and 112.)

Weber, R. J., McMurry, P. H., Eisele, F. L., and Tanner, D. J.: Measurements of expected nucleation precursor species and 3 to 500 nm diameter particles at Mauna Loa Observatory, Hawaï, J. Atmos. Sci., 52, 2242–2257, 1995. (Cited page 12.)

Weber, R. J., Marti, J. J., McMurry, P., Eisele, F. L., Tanner, D. J., and Jefferson, A.: Measurements of new particle formation and ultrafine particle growth rates at a clean continental site, J. Geophys. Res., 102(D4), 4375 – 4385, 1997. (Cited page 12.)

Weber, R. J., Orsini, D., Wang, B., Scheuer, E., Talbot, R. W., Dibb, J. E., Seid, G. K., DeBell, L., Mauldin, R. L., Koschiuch, E., Cantrell, C., and Eisele, F.: Investigation into free tropospheric new particle formation in the central Canadian arctic during the winter/spring transition as part of TOPSE, J. Geophys. Res., 108(D4), doi:10.1029/2002JD002239, 2003. (Cited page 12.)

Wehner, B., Siebert, H., Ansmann, A., Ditas, F., Seifert, P., Stratmann, F., Wiedensohler, A., Apituley, A., Shaw, R. A., Manninen, H. E., and Kulmala, M.: Observation of turbulence-induced new particle formation in the residual layer., Atmos. Chem. Phys., doi:10.5194/acp-10-4319-2010, 2010. (Cited pages 63, 84 and 120.)

Weingartner, E., Nyeki, S., and Baltensperger, U.: Seasonal and diurnal variation of aerosol size distributions ($10 < D < 750$nm) at a high-alpin site (Jungfraujoch, 3580m a.s.l.), J. Geophys. Res., 104, 26 809 – 26 820, 1999. (Cited pages 48 and 49.)

Wexler, A. S., Lurmann, F. W., and Seinfeld, J. H.: Modelling urban and regional aerosols – I. Model development, Atm. Env., 28, 531–546, 1994. (Cited page 20.)

Whitby, E. R. and McMurry, P. H.: Modal aerosol dynamic modeling, Aerosol Sci. Technol., 27, 673–688, 1997. (Cited page 40.)

Wiedensohler, A.: An approximation of the bipolar charge distribution for particles in the submicron size range, J. Aerosol Sci., 19, 387–389, 1988. (Cited page 31.)

Woo, K. S., Chen, D. R., Pui, D. Y. H., and McMurry, P. H.: Measurements of Atlanta aerosol size distributions: Observations of ultrafine particle events, Aerosol Sci. Technol., 34, 75–87, 2001. (Cited page 12.)

Yu, F.: Chemiions and nanoparticle formation in diesel engine exhaust, Geophys. Res. Lett., 28, 4191–4194, 2001. (Cited page 96.)

Yu, F.: Altitude variations of cosmic ray induced production of aerosols: Implications for global cloudiness and climate, J. Geophys. Res., 107, 10.1029/2001JA000 248, 2002. (Cited page 46.)

Yu, F.: Effect of ammonia on new particle formation: A kinetic $H_2SO_4-H_2O-NH_3$ nucleation model constrained by laboratory measurements, J. Geophys. Res., 111, D01 204, 2006. (Cited pages 27 and 91.)

Yu, F.: Improved quasi-unary nucleation model for binary $H_2SO_4-H_2O$ homogeneous nucleation, J. Chem. Phys., 127, 054 301, 2007. (Cited page 87.)

Yu, F.: Updated $H_2SO_4-H_2O$ binary homogeneous nucleation look-up tables, J. Geophys. Res., 113, D24 201, 2008. (Cited pages 27 and 91.)

Yu, F. and Turco, R. P.: From molecular clusters to nanoparticles: Role of ambient ionization in tropospheric aerosol formation, J. Geophys. Res., 106, 4797–4814, 2001. (Cited pages 27 and 53.)

Yu, F., Wang, Z., Luo, G., and Turco, R. P.: Ion-mediated nucleation as an important global source of tropospheric aerosols, Atmos. Chem. Phys., 8, 2537–2554, doi:10.5194/acp-8-2537-2008, 2008. (Cited pages 55 and 82.)

Zellweger, C. ammann, M., Buchmann, B., Hofer, P., Lugauer, M., Rüttimann, R., Streit, N., Weingartner, E., and Baltensperger, U.: Summertime NO_y speciation at the Jungfraujoch, 3580 m above the sea level, Switzerland, J. Geophys. Res., 105, 6655 – 6667, 2000. (Cited page 47.)

Zhang, Y., Seigneur, C., Seinfeld, J. H., Jacobson, M. Z., and Binkowski, F. S.: Simulation of aerosol dynamics: A comparative review of algorithms used in air quality models, Aerosol Sci. Technol., 31, 487–514, 1999. (Cited page 40.)

Zhang, Y., McMurry, P. H., Fangqun, Y., and Jacobson, M. Z.: A comparative study of nucleation parametrizations: 1. Examination and evaluation of the formulations, J. Geophys. Res., 115, D20 212, 2010. (Cited pages 27, 87 and 92.)

Zhao, J., Turco, R., and Toon, O.: A model simulation of Pinatubo volcanic aerosols in the stratosphere, J. Geophys. Res., 100, 7315–7328, doi:10.1029/94JD03325, 1995. (Cited page 87.)

Approche multi-échelle de la formation des particules secondaires

Résumé : À venir dans la version finale...
Dans le cadre de l'étude de l'évolution du système climatique terrestre, comprendre la composition gazeuse et particulaire de l'atmosphère est un enjeu majeur dans notre compréhension de la Terre et de son atmosphère, de son passé et de son évolution à venir. Les aérosols secondaires, i.e. formés par nucléation, représentent la source la plus importante en nombre des aérosols atmosphériques mais prédire où, quand et en quelle proportion ces aérosols sont formés dans l'atmosphère demeure à ce jour un exercice peu fiable. C'est dans ce contexte que cette étude s'est attachée à compléter nos connaissances des processus conduisant à la formation et à la croissance des particules atmospheriques secondaires. Des études réalisées à partir de mesures de terrain à long terme sur différents sites d'altitude en Europe ont permis de mettre en évidence différentes speciations verticales de la nucleation démontrant que ce phénomène semble être jusqu'à deux fois plus fréquents à la frontière avec la basse troposphère libre que dans la couche limite planétaire. D'autre part ces mêmes études ont pu mettre en évidence que les mécanismes conduisant à la nucléation de nouvelles particules se diffŕencient avec l'altitude implicant un rôle plus important de la voie de formation induite par les ions ainsi que des composés organiques volatils. La contribution de cette dernière famille de composés à la nucleation a été également testée durant plusieurs campagnes d'expŕimentation en système réactifs ainsi qu'en chambre de simulation atmosphérique. Différents comportements et paramétrisation de la nucléation selon la nature chimique du composé parent ont pu être mis en évidence. Enfin, des études numériques réalisées à partir de données de terrain et d'expérimentation ont permis d'explorer, d'infirmer, de confirmer et de proposer différentes approches numériques afin de simuler les évènements de formation des aérosols secondaires.

Mots clés : Nucléation, aérosols secondaire, chambre de simulation atmospherique, modelisation des processus.

Multi-scale approach of the atmospheric new secondary particle formation

Abstract: As part of the study of the evolution of Earth's climate system, understanding the composition of gaseous and particulate atmospheric matter is a major issue in our understanding of Earth and its atmosphere, its past and its evolution. The secondary aerosols, i.e. formed from nucleation, represents the largest source in a number concentration of atmospheric particles but predicting, where, when and in what proportion these aerosols are formed in the atmosphere are still challenging. It is in this context that this study focused to complete our understanding of the process leading to the formation and growth of atmospheric secondary particles. Investigations conducted from long term field measurements at different altitude sites across Europe have made possible to highlight different vertical speciation of the nucleation process and that this phenomenon seems to be occur two times more frequently at the interface between the planetary boundary layer and the free troposphere than in the low planetary boundary layer. In addition these studies have been able to show that different nucleation path are enhanced according to the altitude, implicant a greater role in the process of formation induced by ions and volatile organic compounds at altitude sites. The contribution of this last family of compounds to the nucleation has also been examinated through numerous experimenal campaigns using reactive system as well as smog chambers experiments. Different behaviors of the new particle formation and nucleation parametrization depending on the chemical nature of the parent compound were pointed out. Finally, numerical studies based on both field and smog chamber experiments were conducted to confirm or explore, different numerical approaches to simulate the new secondary aerosol formation.

Keywords: Nucleation, organic aerosols, VOCs, smog chambers, process-based modelling.